Summer 8-2024

Methionine Restriction Counteracts Age- and Diet-Related Metabolic Dysfunction in Mice

Marissa McGilvrey
University of Maine, marissa.mcgilvrey@maine.edu

METHIONINE RESTRICTION COUNTERACTS AGE- AND DIET-RELATED METABOLIC DYSFUNCTION IN MICE

By

Marissa Irene McGilvrey

B.S. Biomedical Science, Northern Arizona University, 2013

A DISSERTATION

Submitted in Partial Fulfillment of the

Requirements for the Degree of

Doctor of Philosophy

(in Biomedical Science)

The Graduate School of Biomedical Science and Engineering

The University of Maine

May 2024

Advisor Committee:

Lucy Liaw, Faculty Scientist III, MaineHealth Institute for Research, Advisor

Robert Koza, Faculty Scientist III, MaineHealth Institute for Research, Chair

Aaron Brown, Faculty Scientist II, MaineHealth Institute for Research

Karen Houseknecht, Professor of Pharmacology, University of New England

Dorothy Klimis-Zacas, Professor of Clinical Nutrition, University of Maine

METHIONINE RESTRICTION COUNTERACTS AGE- AND DIET-RELATED METABOLIC DYSFUNCTION IN MICE

By

Marissa Irene McGilvrey

B.S. Biomedical Science, Northern Arizona University, 2013

A DISSERTATION
Submitted in Partial Fulfillment of the
Requirements for the Degree of
Doctor of Philosophy
(in Biomedical Science)
May 2024

The leading cause of death worldwide is cardiovascular disease (CVD), and the risk of developing CVD increases with metabolic dysfunction. Metabolic dysfunction of adipose tissue can lead to obesity, and this can affect the adipose depot that surrounds blood vessels and contributes directly to vascular health. This unique adipose depot is called perivascular adipose tissue (PVAT) and like other adipose depots, PVAT is susceptible to both age- and diet-related metabolic dysfunction. Developing therapies that counteract age- and diet-related adipose dysfunction is crucial to effectively treat metabolic dysfunction and associated excess adiposity that contribute to increased risk of CVD. Methionine restriction (MR) has been found to counteract age-related pathologies, extend lifespan, and increase health span primarily. Many of these benefits are associated with changes in liver and adipose function, such as hepatokine and adipokine secretion. However, it is not known what durations of MR are necessary to obtain metabolic benefits or if the benefits of MR extend to PVAT and associated vasculature. Furthermore, there are several pathways reported to mediate the effects of MR that are important for the ability of PVAT to modulate vascular response.

Therefore, we hypothesize that MR will induce beneficial effects that can modulate age- and diet-related alterations in metabolism and these benefits will extend to the vasculature and associated PVAT.

To test this hypothesis, we employ morphometric and molecular techniques to assess if an 80% MR influences overall metabolic health in male mice *in vivo*, as well as morphological, molecular, and proteomic techniques to measure changes in the thoracic aorta, associated PVAT, and additional adipose depots. This approach was applied to study the effects of long-term MR in age-related metabolic decline in three different aged cohorts, young, middle-age and old mice. This was also applied to study the effects of short-term MR in diet-related metabolic dysfunction in obese mice for 3-10 days. Additionally, an *in vitro* model was developed to study cellular effects of MR on PVAT-derived pre-adipocytes and adipocytes, as well as test proteomic targets of MR in PVAT. The data discussed provides evidence that MR counteracts age-related and diet-related metabolic dysfunction, and for the first time that MR induces lean phenotype in thoracic PVAT. This lean phenotype was simulated in our novel *in vitro* model of MR in PVAT-derived adipocytes. Proteomic analysis of PVAT reveals a transient metabolic signature, hallmarked by reductions in lipogenic pathways and increase in understudied lysosomal protease. Proteomic analysis of thoracic aorta reveals vascular remodeling signature; however, no morphological changes were observed.

With these studies, we provide evidence that MR has even greater potential to reduce risk of cardiovascular and metabolic disease by impacting thoracic PVAT and aorta. These findings have potential to increase the utility of MR to improve cardiometabolic health in three adult life phases as well as for short durations.

DEDICATION

This thesis is dedicated to my family who have been incredibly supportive of my scientific career.

To my mother, Beth Saltzman, my siblings, Leslie, Elizabeth and Jennifer and the rest of my family for your unconditional love and understanding, even when I have moved far away to pursue education and scientific endeavors.

To my husband, Trevor McGilvrey, for being my number one fan and being just as committed as I am to this life path. For the countless cups of tea that have kept me alert and motivated to keep writing. Your support is invaluable to me.

To my stepson, Mason Ramirez, for your patience and understanding while we have lived great distances away and worked to become better parents to you.

To my cat, Echo, for keeping my lap warm, day and night, while I worked tirelessly to complete my dissertation. To my dogs, Charlie and Sophie, for reminding me that fresh air, consistent meals and regular movement are non-negotiable activities.

This thesis is also dedicated in loving memory to dear family members who are no longer able to witness this educational accomplishment.

To my great aunt, Emma Louise Weigman, for setting an example of working hard to become a PhD educated woman and playing even harder.

To my uncle, Edwin Junior Saltzman, for always demonstrating deep appreciation of love, faith, and science. As well as supplying a balanced perspective on life, in how meaningful or meaningless it can be in this ever-growing universe.

To my father, Dennis Leroy Saltzman, for supporting me through everything I have ever done, from reading, to sports, to learning from my mistakes, and delivering the perfect joke at the right moment.

ACKNOWLEDGEMENTS

First, I would like to acknowledge my mentor, Dr. Lucy Liaw, who has helped form me into a more empowered and confident researcher. Dr Liaw's extraordinary mentorship, advocacy and leadership abilities have provided me with countless opportunities and skills to become a successful researcher.

I would like to acknowledge the Orentreich Foundation for the Advancement of Science for setting up this research path. Especially, Dr. Gene Ables and Diana Cooke for their extensive work on this project and for being exemplary collaborators.

I owe many thanks to the entire Liaw Laboratory, both past and present, for being incredibly supportive. For those who have directly contributed to this project's success; a special thank you to Bethany Fortier, Larisa Rhyzhova, Abigail Kaija, Benjamin Tero, Christian Potts, and Maryam Mahdi.

My committee members Dr. Robert Koza (MHIR), Dr. Aaron Brown (MHIR), Dr. Karen Houseknecht (UNE), and Dr. Dorothy Klimis-Zacas (UMaine) have been incredible resources of knowledge, inspiration, and support throughout my time in this program and will continue to inspire me moving forward.

Special recognition to the many core facilities at MHIR that have contributed many hours to the success of this project, including the Proteomics and Lipidomics Core (Drs. Calvin Vary and Carlos Gartner) for the acquisition of our proteomic data, to the Histopathology Core (Dr. Volkhard Lindner

and Armie Mangoba) for tissue processing and histology, and to the Molecular Phenotyping Core (Michele Karolak and Chad Doucette) for qualifying many RNA isolates.

I would like to recognize several individuals within my program, GSBSE, and my home institution, MHIR. The individuals from administration who have been supportive over the past five years are many, but some of the most important are Jennifer Chiarell (GSBSE), Zhen Zhang (GSBSE), Dr. Clarissa Henry (GSBSE), Dr. Gregory Cox (GSBSE), Elisabeth Bergst (MHIR), and Christine Ellis (MHIR). My peers have also been a wonderful support system throughout this journey- special thank you to Abigail Kaija, Carolina Cora, Katie Ellis, Connor Murphy, Audrie Langlais, John Butts, and Samantha Costa.

I would like to acknowledge all those who encouraged me to pursue a scientific career and further my education; Julie Anderson, Christopher Allender, Dr. Paul Keim, Dr. Patrick Pirrotte, and Dr. Khyatiben Pathak. Without your attention and encouragement, I would not be where I am now.

Additionally, I would like to acknowledge the countless animals that have given their lives to advance scientific understanding and medical practice. Many lives have been saved because of your sacrifice.

Finally, I would like to acknowledge all the incredible humans, including educators, scientists, engineers, and doctors, who have come before me that have made science what it is today. Without your knowledge, dedication, passion, as well as both successes and failures- this work would not be accessible to me.

SOURCES OF FUNDING

This work is supported by National Institutes of Health (NIH) grant from the National Heart, Lung, and Blood Institute, R01 2R01HL141149 (Liaw PI), and American Heart Association Predoctoral Fellowship 23PRE1022890 (M.McGilvrey). Our institutional Histopathology Core Facility is supported by NIH/NIGMS award 1P20GM12130 to Lucy Liaw and NIH/NIGMS award U54GM115516 (C. Rosen and G. Stein, principal investigators). Supplemental funding was received from the Graduate School of Biomedical Science and Engineering (GSBSE) and Maine Economic Improvement Fund (MEIF).

TABLE OF CONTENTS

LIST OF TABLES

LIST OF FIGURES

CHAPTER 1: INTRODUCTION

1.1. Define Disease Pathologies of Interest

Cardiovascular disease (CVD) describes a group of conditions that involve the heart (cardio) and/or blood vessels (vasculature). Since the heart is responsible for pumping blood throughout the entire body by way of blood vessels, dysfunctions of the cardiovascular system are diverse, complex and result in various health complications. These dysfunctions range from arrhythmia, hypertension, coronary artery disease, peripheral artery disease, veinous thrombosis, heart disease, heart failure, and cerebrovascular disease [1]. Anatomical region of the dysfunction determines the type of CVD that manifests in an individual, but the defining characteristic of CVD is insufficient or complete loss of blood flow through the system [1]. Blood flow can be affected by narrowing of the blood vessels in your heart, other organs or throughout the body, irregular heart rhythms, dysfunction in valves of the heart, or an abnormality that was present at birth [2].

Metabolic syndrome describes a range of interrelated risk factors of metabolic origin that appear to directly promote development of CVD [3], which is why some of these complications will be referred to as cardiometabolic in nature. The most recognized defining characteristics of metabolic syndrome are abdominal obesity, dyslipidemia, hyperglycemia, inflammation and hypertension [4].

1.1.1. Prevalence of Cardiovascular Disease is Increasing

CVD is the leading causes of death worldwide [1]. According to the annual report from the American Heart Association, which is based on data from the National Institute of Health, it is estimated that about 127.9 million Americans (48.6%) have CVD [5]. With nearly half of adults ≥20 years of age in the United States living with at least one form of CVD, it is a major

cause of concern given that heart disease has continued to be the leading cause of death in the United States since 1921 [6]. Excluding hypertension, about 28.6 million American adults (9.9%) have some type of CVD [5], thus most CVD is related to increased blood pressure, however the root causes of hypertension are diverse in nature.

1.1.1.1. Pathophysiology of Cardiovascular Disease

As the highest contributor to the burden of CVD, hypertension is classified as systolic blood pressure ≥130 mmHg or diastolic blood pressure ≥ to 80 mmHg, or currently taking medication to lower high blood pressure [7]. Sustained increase in blood pressure is facilitated by increased constriction and reduced dilation of major blood vessels, like the aorta which comes directly off the heart [8], and this creates increased friction or shearing force on endothelial cells that line blood vessel walls and come into direct contact with blood [9]. If this increased shearing force continues for prolonged periods, this injures endothelial cells (Figure 1.1B), leading to endothelial dysfunction, and the evolution of atherosclerotic plaques [9]. As the primary characteristic of CVD, atherosclerosis, is the development of lesions within the aorta and other arteries that can decrease blood flow and lead to secondary consequences [10]. Atherosclerosis involves a cascade of events following endothelial dysfunction and continues with immune cell activation, arterial inflammation, lipid deposition, platelet activation and accumulation of extracellular matrix [9, 11]. Vessel anatomy and the cascade of events leading the atherosclerotic plaque is depicted in figure 1.1 Many of the initiating events, such as endothelial cell activation are mediated by nitric oxide, prostacyclin, plasminogen activator, thrombomodulin, among others [12]. Contributing factors to atherosclerosis are irritative stimuli such as hypertension, dyslipidemia, or pro-inflammatory mediators like hyperglycemia [13, 14].

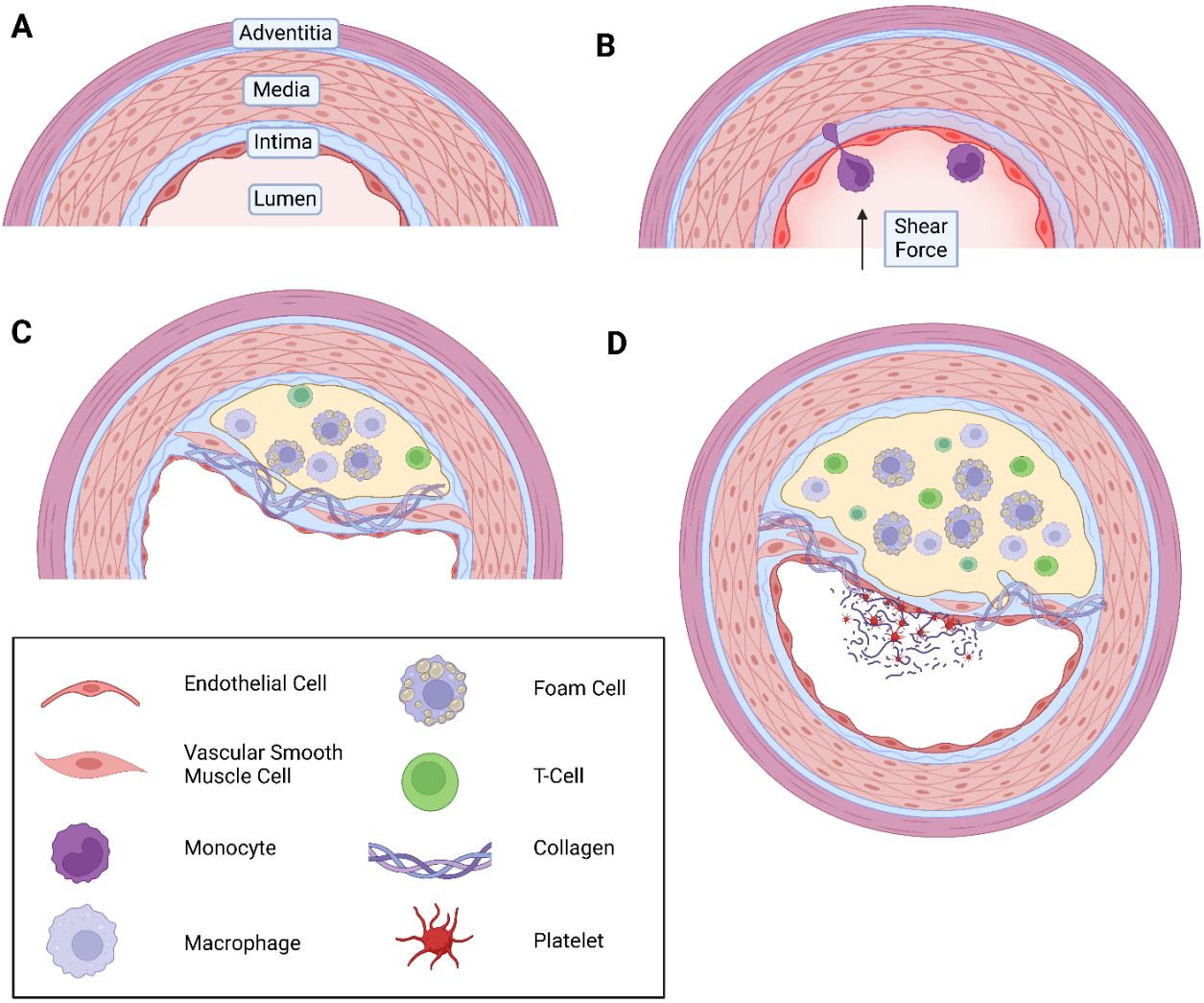

Figure 1.1: Pathophysiology of Cardiovascular Disease Development of atherosclerotic plaques in blood vessels. **A.)** Layers of blood vessels; Tunica Adventitia – contains fibrous tissue to maintain vessel shape, Tunica Media – contains vascular smooth muscle cells to regulate vessel contraction, Tunica Intima – contains endothelial cell to sense shear force as primary regulator of vessel dilation, Lumen – space in vessel that blood flows through [11]. **B.)** Prolonged increase in shear force leads to endothelial cell activation, monocyte adherence, endothelial permeability, and monocyte infiltration into the intima layer **C.)** Monocyte maturation, T-cell recruitment, and uptake of lipids, yielding foam cells. Vascular smooth muscle cell migration and proliferation, and collagen deposition initiate fibrous cap formation. **D.)** Fibrous cap rupture, platelet activation, thrombosis formation and potential to rupture vessel (aneurysm).
Created with Biorender.com

1.1.2. Prevalence of Metabolic Syndrome is Increasing

Among adults in the United States, the rate of metabolic syndrome has steadily risen from 25% in 1994, to 34% in 2012, to 42% in 2018 [15, 16]. More than a third of US adults have met the international criteria for metabolic syndrome of having at least three components of elevated waist circumference, elevated triglycerides, reduced high-density lipoprotein cholesterol, high blood pressure, and elevated fasting blood glucose [16]. Among adolescents in the United States, metabolic syndrome is also steadily increasing [17, 18], which is of concern because the association of metabolic syndrome and CVD is greater when the age of onset occurs at a younger age [19].

1.1.2.1. Pathophysiology of Metabolic Syndrome

The interrelated metabolic risk factors that make up metabolic syndrome are abdominal or visceral obesity, insulin resistance or hyperglycemia, dyslipidemia, and hypertension. Individuals with characteristics of metabolic syndrome commonly manifest a prothrombotic and inflammatory state [3], which correlate to increased risk for CVD. Inflammation and oxidative stress can originate from adipose tissue dysfunction which can further impair insulin signaling, promote endothelial dysfunction and trigger the atherosclerotic cascade [20]. Reactive oxygen species that cause oxidative stress can inhibit bioavailability of nitric oxide, which can promote hypertension and furthermore endothelial dysfunction [4]. As the constellation of issues associated with metabolic syndrome are diverse and interrelated, it is difficult to determine the initiating factor in metabolic dysfunction. However along with CVD, there are several lifestyle factors that have been identified to increase disease risk.

1.2. Factors that Determine Disease Risk

There are several factors that contribute to increased risk of cardiovascular and metabolic dysfunction which include but are not limited to lifestyle, sex, age, and obesity.

1.2.1. Lifestyle

Decreased physical activity and increased sedentary behavior are explanations for increased metabolic syndrome and associated cardiovascular issues [21]. Fewer than one-fourth (24.2%) of US adults meet national recommendations for physical activity [5]. Participating in physical activity just 1-2 times per week has been shown to reduce all cause, CVD and cancer mortality risk [22].

Tobacco use is a major contributor to the incidence of CVD and metabolic syndrome as it induces vascular inflammation [23]. A few examples of tobacco-induced effects are chemical damage to blood vessels, narrowing blood vessels, or making the blood more likely to clot [24].

Socioeconomic factors, such as education, employment status, income, food, and housing insecurity have also been shown to impact risk for CVD and metabolic syndrome [25]. Family income to poverty ratio has been associated with increased risk for CVD [26]. Rates of metabolic syndrome is above 55% for populations with low educational attainment [15]. For adolescents, the prevalence of metabolic syndrome is higher among those who come from households with food insecurity [18]. People can live in obesogenic environments and have generally poor health due to limited access to exercise facilities, healthful food, and opportunities to change their environment [27, 28].

1.2.2. Sex

While CVD is the leading cause of death for both male and females, sex-specific disease patterns have been observed, where generally women have lower incidence of disease due to delayed onset and higher resistance to multisystem diseases [29]. In 2017, hypertension prevalence was higher among men (51.0%) than women (39.7%) [5]. Estrogen has been shown to have protective effects from CVD and the hormonal imbalance that occurs in women experiencing menopause contributes to increased CVD later in life [3, 30]. Additionally, testosterone influences lipid uptake into visceral adipose tissue in males, so loss testosterone will increase abdominal obesity [31]. Metabolic syndrome appears to have higher prevalence in males, both adult and adolescents [17]. The prevalence of hypertension between men and women is consistently higher in men in all age groups [32].

1.2.3. Age

Cancer, CVD, and neurodegeneration are the most prevalent diseases in developed countries and the primary risk factor is age [33]. According to the National Health and Nutrition Examination Survey, hypertension significantly increases with age in both sexes, as the average prevalence in the 18–39 year age group is 22.4%, 40-59 age group is 54.5%, and 60 and over age group is 74.5% [7, 32]. As demonstrated in the previous section, age in an important factor for women in CVD risk, as the average age of menopause onset is 51 [34]. There are several physiological processes that decline with age including cardiac output, glucose and drug metabolism, mitochondrial function, bone density and muscle mass [35, 36].

1.2.4. Obesity

Central obesity, also referred to as abdominal or visceral adiposity, has already been demonstrated to be a major contributor to CVD progression and is one of the inclusion criteria

for metabolic syndrome. Increased body weight can be initiated by environmental conditions, such as obesogenic chemical exposure [37], genetic factors, and by energy imbalance when energy intake exceeds energy expenditure [38]. Increased obesity is also associated with age and the prevalence of obesity will increase as life expectancy increases [39]. It is a major public health interest to reduce the burden of obesity. However, there are a multitude of interacting factors that contribute to the rise in obesity and related dysfunctions.

1.3. Optimizing Metabolic Health for Overall Wellness

Dedicating efforts to improve individual metabolic health will improve overall wellness. There are several lifestyle aspects that can help individuals prevent or recover from metabolic distress. The American Heart Association's "Life's Essential 8" include core health behaviors (smoking, physical activity, sleep, diet, and weight) and measurable health factors (cholesterol, blood pressure, and glucose control) that contribute to cardiovascular health [5, 40]. Good nutrition is essential to preserve the health of current and future generations across entire lifespans. The National Center for Chronic Disease Prevention and Health Promotion, which is a part of the Centers for Disease Control, emphasizes that a healthy diet in childhood will help children to grow and develop properly while also reducing their risk of chronic diseases. Also, maintaining a healthy diet throughout adulthood will help individuals to live longer and have lower risk of obesity, heart disease, type 2 diabetes, and certain cancers. Randomized clinical trial of medically tailored meal program showed to reduce hospital and skilled nursing admissions and lower medical spending [41]. However, these lifestyle behaviors may not be available due to socioeconomic disparities in accessibility to healthy food and low stress levels. Improving accessibility to diagnostic tools and therapies is important to reduce the disease burden.

1.4. Define Need for Effective Therapies for Patients

While overall wellness is ideally important to prevent metabolic dysfunction and lifestyle-related CVD, there is a strong need to provide therapies to help patients achieve this. Many patients, despite trying to lose weight or reduce lifestyle habits that contribute to disease incidence are unable to do so. Obesity might lead to disability, lower productivity, early retirement or unemployment, reduced quality of life and social disadvantages [42]. While there is a need to improve healthy eating behaviors and physical activity on a population level through public policy and societal practice [43], obesity is a complex condition and has high inter-individual variability. Recommendations to reduce obesity rely on the fundamental idea of energy imbalance causing obesity, however interventions that aim to reduce calorie intake and increase energy expenditure are often unsuccessful long-term. There is a strong need and desire to develop accessible therapies that help individuals manage metabolic insufficiencies that may be driving obesogenic tendencies. Therefore, it is critical to identify underlying biological mechanisms that support or prevent obesity and related metabolic issues for patients and at-risk individuals.

1.5. Targeting Excess Adiposity to Reduce Disease Incidence

Excess adiposity is a risk factor for both metabolic dysfunction and CVD. Researchers and clinicians aim to modulate adipose tissue function to reduce disease incidence [44]. There are several adipose tissues with distinct locations in the body and are generally separated by phenotype and function, some of which are depicted in Figure 1.2. White adipose tissue (WAT) is the predominant type of adipose and is called such due to the white like appearance and associated lipid-storing function. There is also the less abundant brown adipose tissue (BAT) which is brown like in appearance due to rich mitochondrial content and functions

to generate heat via non-shivering thermogenesis. These two types of adipose tissue with opposing functions are targeted in equally opposite ways to reduce disease incidence. Excess adiposity that occurs in obese individuals typically occurs in WAT depots as shown in Figure 1.2 and can be associated with tissue dysfunction. Before discussion of ways in which adipose tissues can become dysfunctional, an understanding of baseline adipose function is necessary.

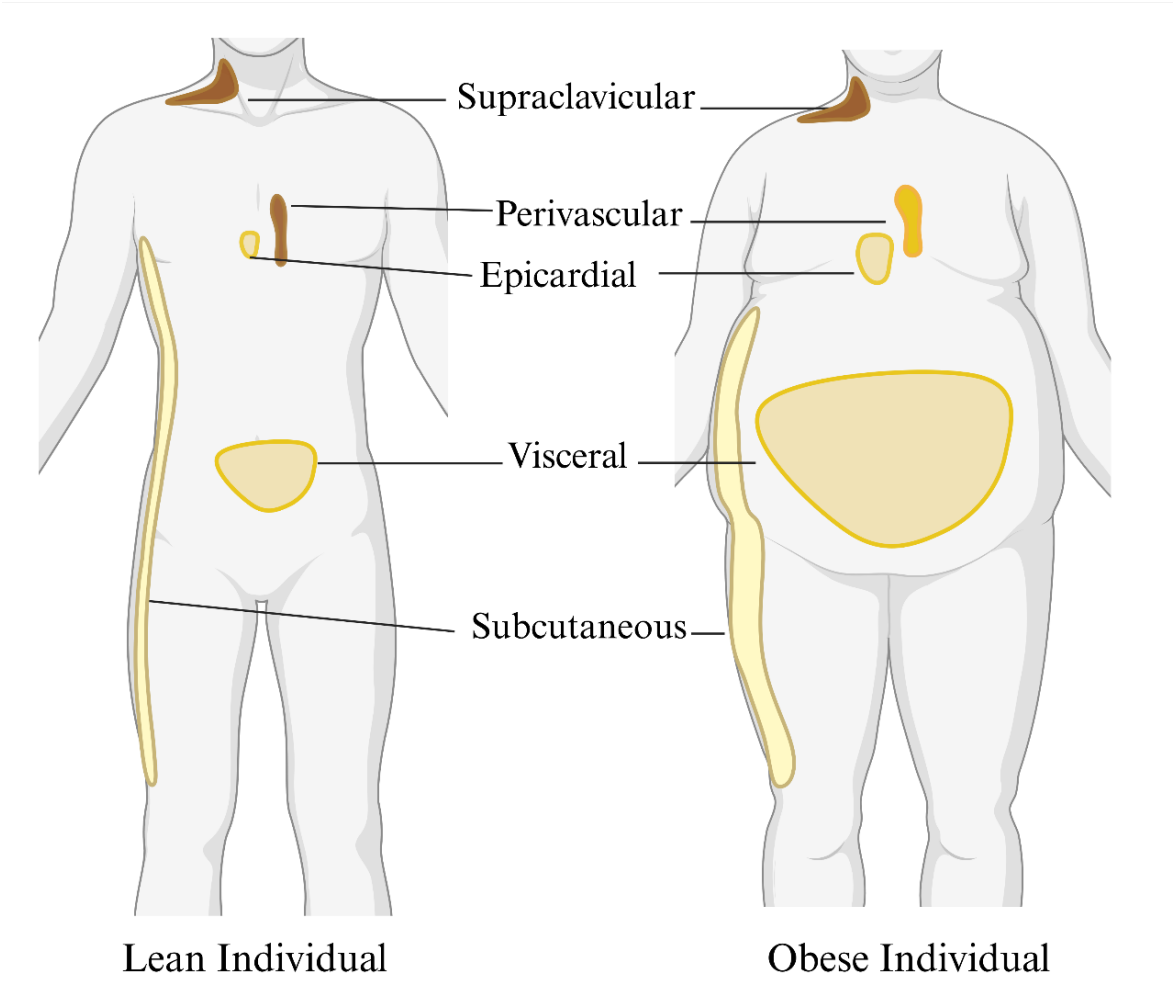

Figure 1.2: Obesity Results from Expansion of Multiple Adipose Depots. Anatomical representation of a select adipose tissues in lean state vs obese state. Supraclavicular adipose tissue sits along the neck and the clavicle. Perivascular adipose tissue sits on the outside of most blood vessels. Epicardial adipose tissue develops on the exterior of the heart. Visceral adipose tissue surrounds abdominal organs. Subcutaneous adipose tissue is located underneath the skin throughout the body. Tissues are present in the lean individual and have expanded in the obese individual. *Created with BioRender*.com Adapted from Huang, E. (2022). Adipose Tissue Depots. https://app.biorender.com/biorender-templates/figures/all/t-62050c4ceb716f00a565d765-adipose-tissue-depots

1.5.1. Heterogeneous Composition of Adipose Tissues

Adipose tissues are composed of a heterogeneous population of cell types including but not limited to adipocytes, preadipocytes, fibroblasts, immune cells, neurons, and endothelial cells. There are multiple types of adipocytes and while all adipocytes are derived from mesenchymal stem cell lineages, this is where similarities between types of adipocytes diverge (Figure 1.3). There are multiple types of adipocytes; white, brown, and beige/brite adipocytes are discussed in detail below.

Most adipose tissues are comprised of a dominant type of adipocyte based on the anatomical location of the depot. Comprised of primarily white adipocytes, subcutaneous adipose tissue is located under the skin and visceral adipose depots surround most abdominal organs (Figure 1.2). Supraclavicular adipose tissue is made up of brown adipocytes and is in the neck and along the clavicle. The perivascular adipose tissue (PVAT) depot surrounds blood vessels the predominate adipocyte type depends on the vessel location and is a mixture of brown and white adipocytes.

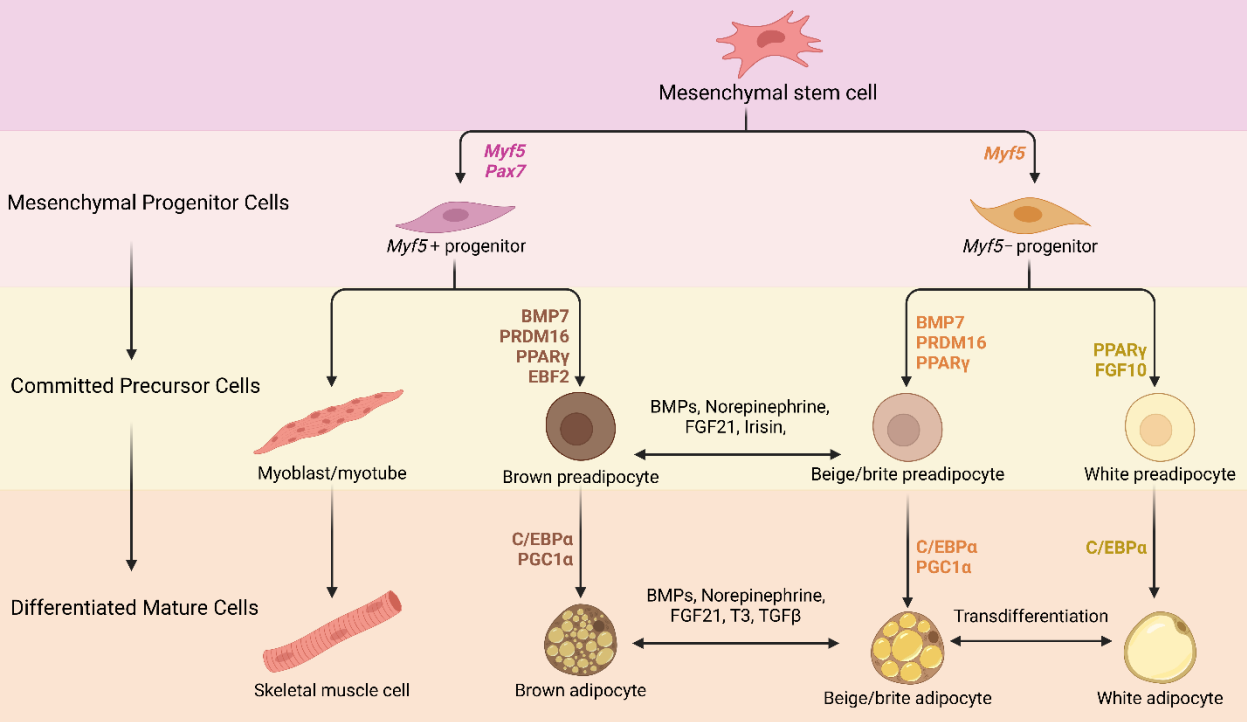

Figure 1.3: Multiple Types of Adipocytes Results in Heterogeneity of Adipose Tissue. Mesenchymal stem cells are progenitor cells for several different cell types, including adipocytes. Cellular fate for adipocyte type diverges with these progenitor cells. The majority of brown preadipocytes arise from *Myf5*+ and *Pax7*+ progenitors, while white and beige preadipocytes arise from *Myf5*- progenitors [45, 46]. Preadipocytes are committed from progenitor cells via transcriptional regulation of *Bmp7*, *Prdm16, Pparγ*, and *Ebf2* for brown/beige preadipocytes or *Pparγ*, and *Fgf10* for white preadipocytes. Preadipocytes are then differentiated through transcriptional regulation of *Cebpa* and *Pgc1a* to result in mature brown or beige adipocytes or only *Cebpa* for white adipocytes. White adipocytes can be bidirectionally transdifferentiated into beige adipocytes. Thermogenic capacity can also be further regulated in response to catecholamine neurotransmitter norepinephrine, or endocrine factors such as FGF21, irisin, T3, and BMPs. *Created with BioRender.com.* Adapted from Huang, E. (2022). Adipocyte Lineage. https://app.biorender.com/profile/eunice_huang/templates/620659243208cc00a62c9bff

1.5.1.1. Brown Adipocytes: Non-Shivering Thermogenesis

Mature brown adipocytes are unique in lineage, phenotype, and function. They derived from a distinctive mesenchymal stem progenitor that is myogenic factor 5 positive (*Myf5*+) and paired box protein 7 positive (*Pax7*+) [45, 47]. Brown preadipocytes require activation of PRD1-BF1-RIZ1 homologous domain containing 16 (PRDM16) or B cell factor 2 (EBF2) to transcriptionally bind to peroxisome proliferator-activated receptor-γ (PPARγ) and

CCATT enhancer-binding proteins (C/EBP α) to differentiate into classical brown adipocytes. [46-49]. These classical brown adipocytes are characterized by high mitochondrial content and distinct multilocular lipid droplets (Figure 1.3). The high mitochondrial content is pertinent to their primary function of non-shivering thermogenesis, which is where energy stored in lipid droplet is metabolized through the electron transport chain and uncoupled from ATP synthesis to dissipate energy as heat. This function is driven by high expression of mitochondrial uncoupling protein 1 (UCP1). Thermogenic capacity of brown adipocytes can be further activated through biochemical action of catecholamine neurotransmitter norepinephrine, or endocrine factors such as fibroblast growth factor 21 (FGF21), irisin, triiodothyronine (T3), as well as bone morphogenic proteins (BMPs) and transforming growth factor-β (TGFβ) [46]. These factors can be physiologically released via cold exposure, exercise, and stress.

1.5.1.2. White Adipocytes: Energy Storage

White adipocytes are the most abundant adipocytes in the body and arise from cells that are negative for myogenic factor 5 (*Myf5*-) expression. Differentiation in white adipocytes also utilizes transcriptional regulation of PPARγ and C/EBP [50]. White adipocytes have a characteristic unilocular lipid droplet phenotype that represents their primary function to store excess energy in a lipid reservoir (Figure 1.3). To store excess energy as lipid, white adipocytes receive fatty acids from triglyceride-containing lipoproteins in circulation with the assistance of lipoprotein lipase and cluster of differentiation 36 (CD36) or are stimulated by insulin to uptake glucose via glucose transporter (GLUT4) [51]. Once inside the adipocyte, glucose undergoes lipogenesis to make glycerol which serves as a backbone for the esterification of lipid derived fatty acids to form triacylglycerol and contained within the lipid droplet pool. The process of *de novo* lipogenesis is another form of lipogenesis and that synthesizes another form of fatty acids

from acetyl-coenzyme A (acetyl-CoA), with assistance from acetyl-CoA carboxylase 1 (ACC1 or ACACA) and fatty acid synthase (FAS) [51].

Under physiological conditions, such as fasting or exercise, when energy demand is high and metabolic fuel is low, white adipocytes also undergo lipolysis to mobilize their stored triglycerides. Lipolysis occurs through the action of adipocyte triglyceride lipase (ATGL), hormone sensitive lipase (HSL) and monoacylglycerol lipase (MGL) [51]. Lipolysis is controlled by hormones and the sympathetic nervous system through cyclic adenosine monophosphate (cAMP) mediated activation of protein kinase A (PKA) and inhibited by AMP-activated protein kinase (AMPK). Perilipin-1 (PLIN1) is a lipid droplet associated protein that is important for regulating lipolysis [52] by protecting the lipid droplet surface from interacting with lipases. In states of metabolic dysfunction, white adipocytes become insulin resistant leading to reduced ability to assimilate excess calories through lipogenic hypertrophic expansion.

1.5.1.3. Beige Adipocytes: Transformed Phenotype

Beige adipocytes display characteristics of both white and brown adipocytes. They can arise from existing white adipocytes via transdifferentiation (Figure 1.3) or they can arise directly from *Myf5*- progenitors [46] that is initiated by different physiological inputs, such as cold exposure, exercise, and dietary changes [51, 53, 54]. Meaning that while these adipocytes appear to have brown characteristics, they are a distinct population and can be transdifferentiated into white adipocytes [55]. Just like brown adipocytes, beige adipocytes can burn metabolic fuels and generate heat utilizing UCP1 mediated protein leak [46] however this occurs within depots that are traditionally exhibit white phenotype.

1.5.2. Obesity Results from Adipose Tissue Expansion

Adipose tissue expansion is a normal physiological process that occurs during development and in response to excess calories, however the mechanism in which adipose expands is an important determinant in downstream adipose function or dysfunction. Obesity is defined as the excess expansion of adipose tissue and as mentioned previously this is often thought to be a result of energy imbalance. Adipose tissue expansion occurs in two ways, either hyperplasia or hypertrophy (Figure 1.4). Hyperplasia occurs through induction of mesenchymal stem cells conversion to preadipocytes that then differentiate into adipocytes [56]. This results in greater adipocyte number, and the more adipocytes that are present the greater insulin sensitivity and adiponectin secretion. Hypertrophy is where adipose tissue expands through existing mature adipocytes increasing in size. Individual adipocytes can expand by increasing lipid storage which is beneficial in the short-term to restore energy balance, however there is a threshold in which individual adipocytes can grow and eventually they will become resistant to insulin and no longer be able to store lipid. Hypertrophy can occur in concert with hyperplasia, however when hypertrophy is the dominant strategy for adipose tissue expansion, adiponectin secretion will be lower.

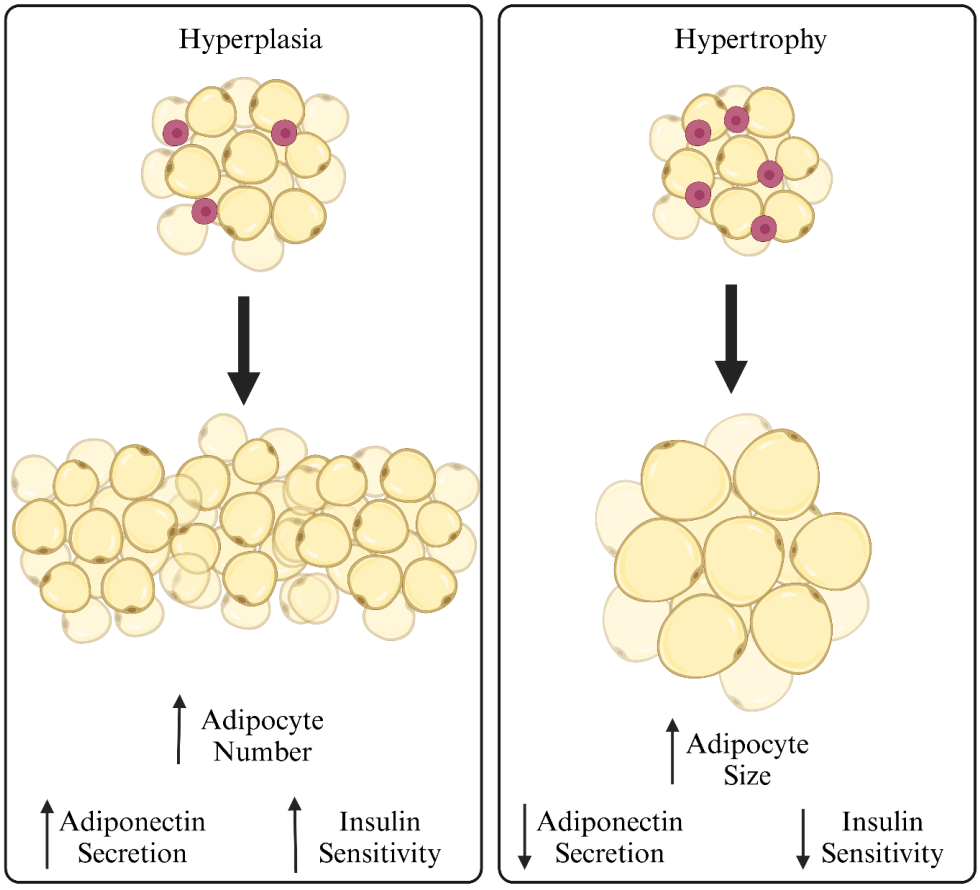

Figure 1.4: Expansion of Adipose Tissue Occurs through Hyperplasia and Hypertrophy. Adipose tissue adaptations in lipid storage capacity are necessary to respond to excess energy. Yellow cells are adipocytes and pink cells are pre-adipocytes. Hyperplastic expansion of adipose tissue occurs through differentiation of pre-adipocytes to adipocyte resulting in a greater number of adipocytes, which produce more adiponectin collectively and are more insulin sensitive. Hypertrophic expansion of adipose tissue occurs due to increased size of mature adipocytes and results in large adipocytes that produce less adiponectin collectively and are less insulin sensitive.

1.5.3. Adipose Tissue Physiology During Disease

Adipose tissue is constantly in flux based on food intake and utilization. When calories are in excess this leads to lipogenesis, adipocyte hypertrophy and adipose tissue remodeling that expand the tissue to support increased lipid storage. Remodeling of adipose tissue requires adipocyte turnover, a process of cell death and recruitment from resident progenitor pool. As dietary stress continues, such as in the case of a high fat diet, the newly

formed adipocytes support a new adipose phenotype that is pathogenic in nature. This phenotype is dominated by altered inflammatory factors and adipokine secretion, as well as changes in lipolysis, thermogenesis, and autophagy (Figure 1.5).

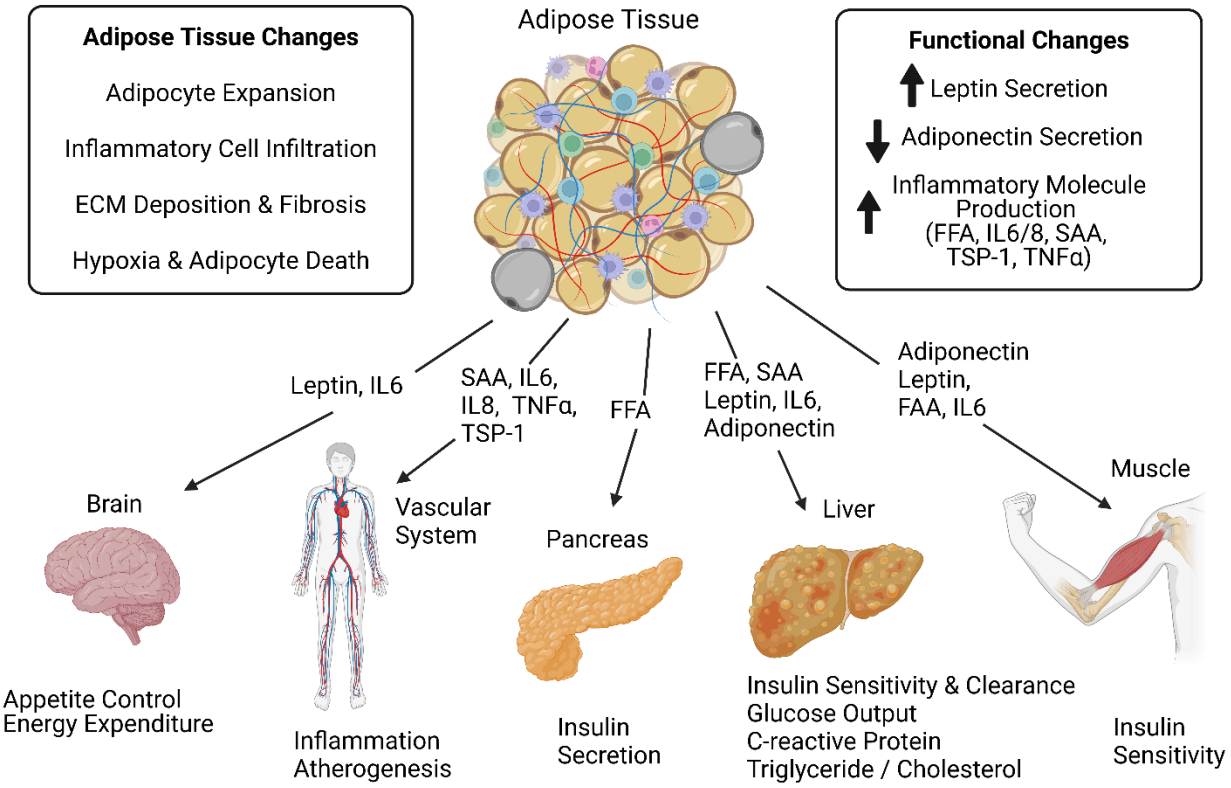

Figure 1.5: Pathophysiology of Obesity. Dysfunctional adipose tissue begins with hypertrophic adipocyte expansion and infiltration of immune cells. This modifies adipocyte release of adipokines, cytokine and free fatty acids, which impact the brain, vascular system, pancreas, liver and muscle and associated functions, such as insulin resistance. Chronic adipocyte expansion alters crosstalk among adipocytes, macrophages and other cells which promotes further inflammation, high cellular turnover, ECM remodeling. If unable keep up with cellular turnover, high cell death and inflammation lead to fibrosis in the adipose tissue. ECM – Extracellular matrix FFA- free fatty acids, IL6 – interleukin-6, SAA- serum amyloid A, TSP-1- thrombospondin-1, CRP– C-reactive protein, TNFα- tumor necrosis factor alpha, Adapted from Lee et al [57] *Created with BioRender.com*

1.5.3.1. Metabolic Fuel Utilization is Reduced During Disease

Metabolic dysfunction in obesity is partially related to impaired fatty acid storage in adipose tissue, and this can be caused by systemic insulin resistance as well adipocyte reaching

lipid storage capacity after continuous hypertrophy [58]. Chronic overeating and continuous hypertrophy disrupt normal regulation of WAT lipid metabolism through elevated lipolysis, where stored fatty acids are released beyond energy demand and are redirected to the liver which promotes hepatic lipid accumulation [59]. Furthermore, catecholamine-induced lipolysis and non-shivering thermogenesis is suppressed in people with obesity [60, 61]. Deficiencies in non-shivering thermogenesis have potential to be an inherited trait and not a consequence of obesity [61]. Taken together, lipolytic and non-shivering thermogenic abnormalities are important physiological components of obesity pathophysiology.

1.5.3.2. Secreting Signaling Factors are Altered in Disease State

There are several adipose-secreted factors that act as important signaling factors throughout the body, here we summarize some of a most meaningful adipocyte hormones, which are commonly referred to as adipokines. Leptin is an important adipokine that is positively associated with percentage of body fat [62, 63]. Leptin acts on the brain to regulate food intake and energy expenditure (Figure 1.5). Leptin is considered pro-inflammatory and pro-atherogenic, as excessive production of leptin is a consequence of resistance in target organs, and associated with increased BMI, insulin resistance and C-reactive protein[63, 64].

Adiponectin is an adipokine that is documented to be important for insulin sensitivity, as well as having atheroprotective and anticoagulant function [65]. Decreased secretion of adiponectin decrease as a function of increasing fat mass in both rodents and humans with obesity [51, 66]. Adiponectin has beneficial effects in the liver, where it protects against metabolic dysfunction and metabolic dysfunction-associated steatotic liver disease (MASLD) [51]. It also appears to play an important role in regulating skeletal muscle development, regeneration and maintaining mass [67]. Additionally, adiponectin has cardioprotective functions

by stimulating AMPK signaling which leads to the suppression of myocyte hypertrophy and apoptosis, as well as stimulating COX-2 expression which results in reduced cardiac inflammation [68].

1.5.3.3. Inflammation is Increased in Disease State

In a healthy adipose tissue, CD4+ T-cells and M2 macrophages are present and function in part to restrict inflammation. The ratio of CD8+/CD4+ T-cells increases when adipocytes undergo hypertrophy, which helps to recruit macrophages [69]. As adipose tissue expansion continues, high adipocyte death contributes to an inflammatory phenotype that begins to form by infiltration of macrophages that have adopted a proinflammatory M1 phenotype. As adipocytes continue to turnover and remodel the adipose tissue, blood flow might be restricted leading to hypoxia and further stimulate cytokine production and further complicate adipocyte dysfunction [69].

1.5.3.4. Cellular Material Recycling is Altered in Disease State

A component of obesity pathophysiology that is often overlooked is autophagy, where unnecessary or dysfunctional cellular machinery is recycled through lysosomal degradation. Lysosomes contain several types of hydrolytic enzymes, including proteases such as cathepsins. Lysosomal dysfunction is associated with obesity [70, 71] and when this occurs there is reduced ability to support proper cellular needs as well as to clear dead or dying adipocytes, which further contributes to cytokine release and adipocyte dysfunction. A family of lysosomal proteases, cathepsins, are altered in subcutaneous adipose tissue of obese and overweight humans [72]. Whether this is dysfunction caused by obesity or a protective mechanism to slow adipocyte turnover remains to be answered.

1.5.4. Effects of Different Adipose Depots on Health

Obesity is generally described as an increase in adiposity; however, it is important to distinguish between which adipose depots have expanded as metabolic consequences of obesity vary by adipose distribution [73]. Adverse cardiometabolic consequences are associated with visceral and ectopic adipose accumulation, gluteal-femoral adipose accumulation is inversely associated with adverse consequences [73]. Differences between these two distinct WAT depots are hypothesized to be in the expansion mechanism as well as tissue-specific secreted factors [57]

1.5.4.1. Visceral: Strong Association with Disease Risk

Excess intra-abdominal adipose tissue is often termed visceral obesity. Age-adjusted visceral adiposity has been found to be a reliable parameter for assessing mortality risk [74]. Waist circumference combined with plasma triglyceride concentrations, named "hypertriglyceridemic waist" has been shown to be predictive of glucose intolerance, type 2 diabetes, and coronary artery disease [75-77]. Accumulation of visceral adiposity is accelerated in women following the menopause transition which contribute to the increase of CVD in post-menopausal women [78]. There are numerous reports detailing the relationship between visceral adiposity and increased disease risk.

1.5.4.2. Subcutaneous: Weak Association with Disease Risk

Subcutaneous adipose tissue is located under the skin (Figure 1.2) in arms, legs, and abdominal regions of the body. These tissues have a white adipose phenotype and expansion of the specific subcutaneous depots have been found to be protective from metabolic dysfunction. Larger subcutaneous thigh adipose depot has been reported to be independently associated with desirable lipid levels in both males and females, as well as favorable glucose levels in men [79].

Interestingly, abdominal subcutaneous adipose tissue, just as visceral adiposity, is associated with insulin resistance [80], therefore protective effects of subcutaneous adipose tissue is location and sex dependent.

1.5.4.3. Perivascular: Unique Junction Between Adipose and the Vasculature

Perivascular adipose tissue (PVAT) is the adipose tissue that surrounds most blood vessels in the body. This unique depot has emerged as an active and important component of the vasculature by regulating vasodilative abilities as well as the pathogenesis of atherosclerosis [81]. The phenotype of PVAT is dependent on the location within the body. PVAT that sits on the carotid, femoral and mesenteric arteries display a white phenotype, whereas the PVAT that sits on the thoracic aorta is a mostly brown and thermogenic phenotype. PVAT has been shown to influence vascular reactivity, and as such thoracic PVAT is of particular interest because it is located on the largest vessel in the body coming right off the heart and can change blood flow dynamics for the entire system. PVAT can change vasoreactivity by adipokine secretion that is common among other adipose depots, however due to the proximity to the vessel, the effects on blood coagulation, endothelial function and inflammation are magnified (Figure 1.6) [81]. PVAT also secretes gaseous molecules like nitric oxide and hydrogen sulfide and that signal the vasculature to relax. PVAT inflammation can initiate macrophage infiltration which alters cytokine release and increases reactive oxygen species in the vasculature. Further research is necessary to fully understand the role of PVAT in hypertension and progression of CVD. Given the location of PVAT, it is primarily studied in patients already undergoing surgical intervention related to the cardiovascular system and thus is particularly difficult to assess in healthy individuals.

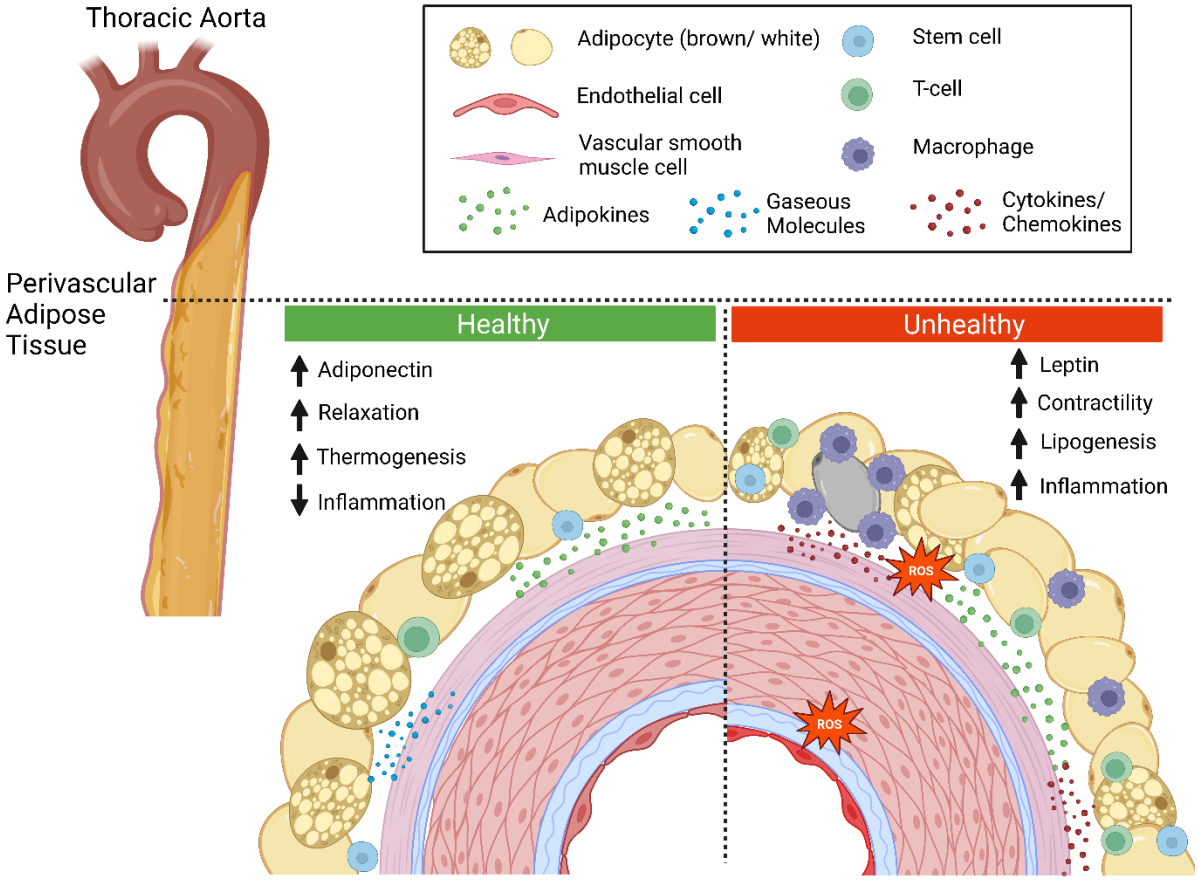

Figure 1.6: Perivascular Adipose Tissue is Uniquely Positioned to Influence Vascular Function. PVAT is the outmost layer of the blood vessel. A healthy PVAT phenotype contains a mix of white and thermogenic brown adipocytes, which secrete vasoprotective adiponectin as well as gaseous molecules (Nitric Oxide, Hydrogen Sulfide) that promote vasodilation. An unhealthy PVAT phenotype is dominated by white adipocytes due to increased lipogenesis, which secretes proinflammatory leptin and macrophage infiltration. High adipocyte turnover increases adipocyte death where macrophages accumulate in "crown like structures" around dead adipocytes. T-cells and macrophages secrete chemokines and adipokines that contribute to inflammatory ROS production in both PVAT and local vasculature. Unhealthy PVAT also has reduced secretion of vasodilatory factors and increased vasocontractile factors that in combination, increase blood pressure. These pathological factors have been observed to precede endothelial activation. *Created with BioRender.com*

1.5.5. Strategies to Attenuate Negative Effects of Adiposity on Cardiometabolic Health

There are several strategies to influence adipose tissue in hopes of reducing obesity, cardiometabolic dysfunction, and thus CVD risk. Targeted strategies for either brown, white, or beige adipocytes are detailed below.

1.5.5.1. Activating Brown Adipocytes

Studies have shown that there is an inverse association between BMI and BAT, and targeting BAT as a putative treatment for obesity and related pathologies is an ongoing endeavor [82, 83]. As mentioned previously, cold exposure can increase thermogenic activity of brown adipocytes, thus increasing heat production BAT. This results from cold temperature and activation of β-adrenergic receptors by way of norepinephrine and G-protein coupled receptors [84, 85] and is associated with increased expression of peroxisome proliferator-activated receptor gamma coactivator 1α (PGC1α), a co-activator of PPARγ and upregulates UCP1-mediated thermogenesis [86]. This can also be induced by chemical agonists of β-adrenergic receptors [53, 87-89].

1.5.5.2. Activating White Adipocytes

The primary therapeutic strategy to activate white adipocytes is to improve insulin sensitivity and ability to remove excess glucose and lipids from the blood stream. Increasing insulin sensitivity of white adipocytes is possible through treatment with thiazolidinediones which stimulates adipogenesis particularly in subcutaneous white adipose tissue (WAT) [90-92]. This results in increased hyperplasia by acting as a PPARγ agonist as well as increasing adiponectin expression and plasma levels and improves metabolic dysfunction in white adipocytes [93, 94]. Thus, patients treated with thiazolidinediones have improved glucose metabolism by increasing WAT storage of excess calories, however patients continue to gain excess adiposity despite improved metabolism. As discussed in section 1.5.3.4, a cellular dysfunction often seen in obesity is lysosomal dysfunction [70, 71]. A possible therapeutic target that is not as commonly is recovering lysosomal dysfunction to improve overall tissue and cellular function [95].

1.5.5.3. Activating Beige Adipocytes

Given that beige adipocytes arise within WAT, targeting beige adipocytes is an additional strategy to improve metabolism of WAT. Increasing energy expenditure in WAT through transdifferentiation of white adipocytes into beige adipocytes or induction of beige adipocytes from precursor cells, would help take metabolic pressure off needing to store excess calories as lipid and instead burning them through non-shivering thermogenesis [96]

1.5.6. Dietary Strategies to Attenuate Negative Effects of Adiposity on Cardiometabolic Health

Diet and exercise cause preferential fat loss from visceral adiposity over subcutaneous adiposity, supporting the utility of these lifestyle behaviors modulating disease risk [97]. There are several targeted dietary approaches that will improve metabolism and allow a person to achieve their physical goals. General dietary approaches include modifying macronutrient content and/or micronutrient content, as well as modifying total calorie intake or the timing of when food is consumed. The approaches summarized below have various levels of efficacy, which is dependent on an individual's genetics, environments, and lifestyles.

1.5.6.1. Modifying Macronutrient Content

Modifying macronutrient content of an individual's diet requires precise monitoring of food consumed and nutritional content. Macronutrients contained in food are protein, carbohydrates, and fat.

1.5.6.1.1. Protein

Adequate protein consumption is critical for muscle maintenance during growth and aging [98]. High protein diets are commonly utilized by individuals seeking to build or maintain muscle mass especially during weight loss [99] however this effect has been reported to only occur when coupled with weight training [100]. However, multiple long-term prospective and

retrospective clinical trials have shown that dietary protein intake is correlated with rates of multiple age-related diseases in humans, including cancer, CVD, and diabetes as well as increased mortality in those under 65 years of age [101]. To counteract these age-related health problems, many adopt a low protein diet or modify quality of protein consumed [102-105].

1.5.6.1.2. Carbohydrates

Carbohydrates have been shown to impact hyperglycemia and insulin sensitivity [106]. For patients with type 2 diabetes and obesity, low carb diets can be recommended that result in decreased insulin secretion and improved insulin sensitivity [107-109]. However, for healthy lean patients a low carb diet has been shown to induce insulin resistance and metabolic acidosis [110]. Very low carb diet (<40%) as well as very high carb diet (>70%) are associated with increased mortality [111]. Exchanging highly refined carbohydrates (white bread, white rice, sweetened cereal/desserts) for unprocessed carbohydrates (whole grain, sweet potato, vegetables) has been shown to induce many of the same health benefits of limited carb diets.

1.5.6.1.3. Fat

Consumption of a diet high in fat has become common in the standard American diet, both intentionally and unintentionally. A familiar message is that diets high in fat and cholesterol are damaging to the cardiovascular system, brain and metabolic health [112-118], however the widespread adoption of low-fat diets have also shown to be damaging [119]. While a diet high in fat can occur if there is not special attention paid towards dietary consumption, there are a multitude of reasons why a diet high in fat has become an intentional practice for many. When pairing low-carb with high-fat, known as ketogenic diets, this combination can be therapeutic. Typically following a macronutrient ratio, 70-75% of calories from fat, 20-25% from protein, 5-10% from carbohydrates, the intentional consumption of low carb and moderate

protein seeks to force the body into a state of nutritional ketosis, as the body adapts to primarily utilize fat-derived ketones as a source of energy. The diet was originally developed as a treatment for epilepsy but has gained popularity for various health goals, including weight loss, athletic performance, improved metabolic health, as well as cognitive and neurological conditions [21, 120-124]. A ketogenic diet can be particularly difficult to manage and requires careful monitoring of blood ketones to ensure nutritional adequacy and prevent ketoacidosis. However, in the right context and consistent practice there are many potential benefits from adopting a ketogenic diet.

There are other strategies that allow moderate consumption of dietary fat which focus on the type of fat that is consumed. Exchanging saturated fats for mono/polyunsaturated fats has been a common strategy to improve cardiovascular health [112], however depending on the metabolic complications that affect patients with metabolic syndrome, there are variations in efficacy [125].

1.5.6.2. Modifying Micronutrient Content

A diet rich in micronutrient diversity is important to promote cardiovascular health, however targeted supplementation may be supportive in specific conditions. Micronutrients that have shown various levels of efficacy in randomized controlled trials for cardiovascular risk are L-arginine, L-citrulline, α-lipoic acid, coenzyme Q10, n-3 fatty acid, n-6 fatty acid, folic acid, vitamin D, magnesium, zinc, melatonin, catechin, curcumin, flavanol, genistein, and quercetin [126]. Specifically, n-3 fatty acid has been shown to decrease CVD mortality, myocardial infarction, and coronary heart disease events [127].

1.5.6.3. Modfying Calorie Intake

Another dietary strategy to improve cardiometabolic health and lose weight is to reduce the total amount of calories either completely (fasting) or partially (calorie restriction) [128]. In obese participants, 3-days of very-low calorie diet (<600 kcal/day) improves fat metabolism, body weight and composition and vascular stiffness [129]. However, adoption of new lifestyle behaviors, like regular physical activity, fasting or calorie restriction is difficult to implement in the general population due to psychological and social-behavioral limitations. Some studies have reported that short-term fasting decreases vitality and positive emotions while increasing negative emotions [130-134]. Alternative strategies to replicate the net-calorie intake of calorie restriction utilize intermittent fasting and time-restricted eating which focus on timing and frequency of meals [135].

1.5.6.4. Mimicking Fasting and Calorie Restriction

To improve adherence to therapeutic diets, several molecules and fasting mimicking diets have been developed and have been shown to be feasible, safe, and effective in reducing biomarkers for age-related disease [136, 137]. Conventional calorie restriction mimetic molecules like resveratrol, metformin and rapamycin have been shown to activate autophagy improve physiological function and extend lifespan, however, often have adverse side effects such as increase incidence of diabetes [137-140]. The fasting mimicking diet is low in calories, sugar, and protein but high in unsaturated fats and utilizes an intermittent strategy of consuming the diet for five consecutive days per month for a duration of 3 months [141]. Reduction of cancer, multiple sclerosis, Type 1 and Type 2 diabetes, modulation of immune response, and reversal of inflammatory bowel disease pathology have been observed in both rodent and human studies [136, 141, 142]. This fasting mimicking diet has also been shown to reverse

accumulation of adiposity induced by high-fat, high calorie, while increasing cardiac function and preventing hyperglycemia, hyperleptinemia, hypercholesterolemia, and improve glucose and insulin intolerance [141, 142]. The goal of fasting mimicking diets is to reduce risk of age-related disease without drastic dietary behaviors.

1.6. Dietary Methionine Restriction as a Mimetic for Calorie Restriction

Another dietary strategy to mimic calorie restriction without decreasing calorie consumption is methionine restriction, which has been extensively studied and has many proven benefits. These benefits will be discussed in sections 1.9 – 1.13 and are governed by the role of methionine in cellular functions discussed below.

1.6.1. Methionine as an Essential Amino Acid

Amino acids are building blocks of proteins, and to be an essential amino acid it means that it must be obtained in the diet because it cannot be sufficiently synthesized in the body to meet the body's demands. To obtain amino acids, foods that contain protein must be eaten. There are nine essential amino acids, and methionine is one of them. Methionine is classified as a sulfur-containing amino acid, as is cysteine, cystine, homocysteine, and taurine. Sulfur is the third most abundant mineral in the body [143], and the sulfur-amino acids contribute significantly to maintenance and integrity of cellular systems by influencing protein structure, redox state, and the ability to detoxify toxic compounds and reactive oxygen species [144]. Methionine is the precursor for a multitude of metabolic intermediates that contribute to a wide array of cellular functions such as polyamine synthesis, epigenetic regulation, redox balance, ATP and DNA synthesis [145].

1.6.2. Methionine Metabolic Cycle

The methionine metabolic cycle, also known as the methionine cycle, is a crucial biochemical pathway that is involved in synthesis and regulation of various important molecules in the body. As depicted in Figure 1.8, this pathway starts with methionine, which is primarily obtained externally from the diet, activated by adenosine triphosphate (ATP), catalyzed by methionine adenosyl transferase (MAT1A or MAT2A), and converted to S-adenosyl methionine (SAM or AdoMet) [144]. SAM is condensed with glycine, releasing a methyl group and sarcosine, which is catalyzed by glycine N-methyltransferase (GNMT) or other methyltransferases. This forms S-Adenosyl-L-homocysteine (SAH or AdoHys) which is catalyzed by S-Adenosyl-L-homocysteine hydrolase (SAHH or AHCY) to cleave off adenosine forming homocysteine. From here, homocysteine has multiple fates and can be directed to the transsulfuration pathway to form cystathionine through cystathionine β-synthase (CBS) requiring serine and α-ketoglutarate, followed by conversion to cysteine and α-ketobutyrate through cystathionine γ lyase (CGL) and requiring glutamate and B6. Depending on cellular need and substrate availability, CGL can also reconvert cystathionine back into homocysteine and α-ketobutyrate. The dipeptide formed (γ-Glu-Cys) by cysteine and glutamate is a precursor to glutathione (GSH) which can be oxidized to form glutathione disulfide (GSSG) and then reduced back to GSH by glutathione reductase. Cysteine is also a precursor to hydrogen sulfide [146]. Cysteine can also undergo a series of oxidation events to form intermediates that eventually form taurine. Another fate of homocysteine is re-methylation by betaine homocysteine methyltransferase, requiring choline, or 5-methyltetrahydrofolate (5-MTHF) and conversion back to methionine, which utilizes vitamin B12 as a cofactor, and catalyst methionine synthase. The methyl group transferred from 5-

MTHF to homocysteine during methionine synthesis is derived from dietary folate or from the conversion of serine to glycine and results in the formation of tetrahydrofolate (THF) and then dihydrofolate (DHF). The reconversion back to 5-MTHF is mediated by the enzyme methylenetetrahydrofolate reductase (MTHFR) and requires vitamin B2 as a cofactor. While this reaction is vital to folic acid homeostasis, it does not contribute significantly to the regeneration of methionine, which is why methionine is characteristically an essential amino acid. Methionine can also be recycled through the methionine salvage pathway, through a by-product of SAM in the synthesis of polyamines (including putrescine, spermidine, and spermine). This by-product 5'-methylthioadenosine (MTA) which is then further processed by enzyme methylthioadenosine phosphorylase (MTAP) to generate adenine (a purine nucleotide) and methionine [147].

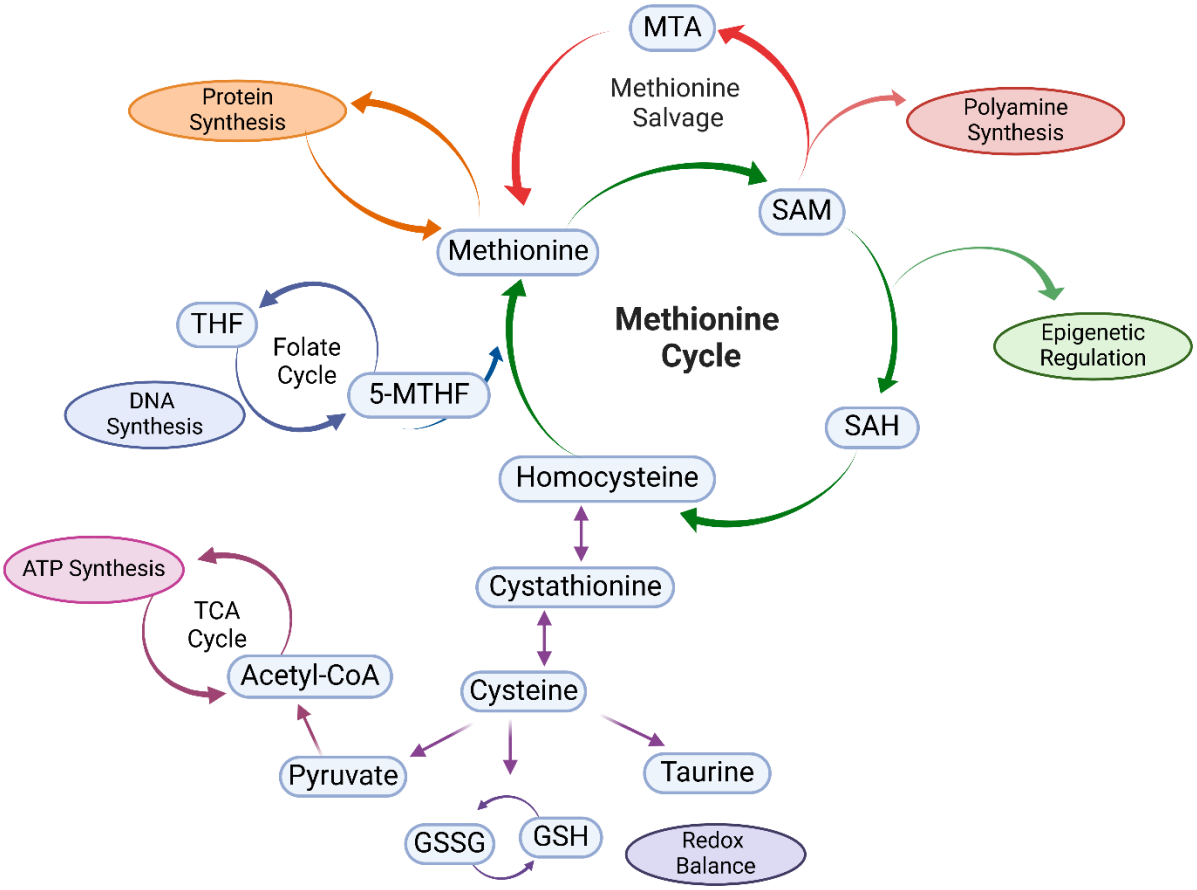

Figure 1.7. Methionine Metabolic Cycle Controls Important Cellular Functions
The methionine cycle starts with exogenous methionine derived from the diet, which contributes directly to protein synthesis (orange) and indirectly to polyamine synthesis (red), epigenetic regulation (green), redox balance (purple), TCA cycle/ ATP synthesis (pink), folate cycle/DNA synthesis (blue). Methionine is recycled by completing the entire methionine cycle or through the methionine salvage pathway. SAM- S-adenosyl methionine, SAH- S-Adenosyl-L-homocysteine, MAT2A- methionine adenosyl transferase, TCA – tricarboxylic acid cycle, ATP- adenosine triphosphate, GSH- glutathione, GSSG – glutathione disulfide, Acetyl-CoA- Acetyl coenzyme A, 5-MTHF- 5-methyltetrahydrofolate, THF – tetrahydrofolate, DNA – deoxyribonucleic acid. *Adapted from Sanderson et al [147] and Lauinger et al [145]. Created with BioRender.com*

1.6.2.1. Methionine: The Initiating Amino Acid in Protein Synthesis

Start codon in protein synthesis for most proteins is AUG, which encodes for methionine. This means that methionine is the initiating amino acid in protein synthesis, which is true for virtually all eukaryotic proteins [148]. Protein synthesis can also be controlled by methionine through the synthesis of polyamines (Figure 1.7) which promote the assembly of ribosomes and facilitate the initiation of translation. Methionine restriction has bene shown to reduce protein synthesis [149, 150].

1.6.2.2. Methionine: Important for Epigenetic Regulation

Epigenetic regulation is controlled by methionine as SAM is responsible for epigenetic regulation by donating methyl groups to acceptor molecules such as DNA, proteins, lipids and neurotransmitters. As mentioned in section 1.6.2, a methyl group is released by the conversion of SAM to SAH. Regulating the amount of SAH by SAHH is important to control the availability of methyltransferases and thus the rate of methylation reactions. Transcriptional activity can also be controlled by polyamines by binding to nucleic acids and stabilizing their chromatin structure and protecting them from degradation.

1.6.2.3. Methionine: Balancing Redox Potential and Inflammation

As described in section 1.6.2, the transsulfuration pathway which converts homocysteine to cysteine and downstream to either taurine or GSH is critical to support redox balance within the cell. The recycling system between GSH and GSSG helps to maintain the pool of reduced glutathione which supports the cellular antioxidant capacity. Hydrogen sulfide plays an active role in the production of glutathione by enhancing cysteine and cystine transport into cells [146, 151]. Glutathione and taurine possess properties that scavenge free radicals and reactive oxygen species, which are by-products of normal cellular metabolism and can cause

oxidative damage to proteins, lipids and DNA and result in inflammation [152]. The redox status also plays a role in regulating signaling pathways and gene expression. Namely, ratio of GSH/GSSH can influence the activity of redox-sensitive transcription factors such as nuclear factor-κB, which control inflammation, apoptosis, and cellular proliferation [153]. Furthermore, glutathione acts as a co-factor for enzymes involved in Phase II detoxification reactions, which help to make harmful compounds more water-soluble and assist excretion [154].

1.6.2.4. Methionine: Contributes to Energy Production

Cysteine contributes to the production of ATP in two ways. The first of which is through hydrogen sulfide which can donate electrons to the electron transport chain and fuel ATP synthesis [155]. The second way is by synthesis of pyruvate which is converted to acetyl-CoA, enters the TCA cycle and drives ATP generation [155].

1.6.2.5. Methionine: Controls Cell Cycle Progression and Proliferation

There are multiple metabolic outputs from the methionine cycle that impact cell cycle progression and ultimately cellular proliferation. Fundamental building blocks of DNA are synthesized through the folate cycle through participation in one-carbon metabolism. Folate contributes to the pool of one-carbon units that are necessary for *de novo* synthesis of both purine (adenine and guanine) and pyrimidine (cytosine and tyrosine) nucleotides [156]. While the folate cycle is not the only pathway that synthesizes these nucleotides, without nucleotides the cell would not be able to synthesize DNA. Methionine controls the flux of one-carbon units through the folate cycle, which regulates the contribution of folate metabolism to one-carbon metabolism [157]. Furthermore, reduction in SAM leads to cell cycle arrest at the G1/S transition, by blocking DNA replication [145, 158]. Methionine deprivation blocks cells from progressing into the G1 phase [159]. Polyamines are also involved in regulating progression from G1 phase [160],

as mutations in regulatory genes that mediate polyamine synthesis result in S phase and G1/M arrest [161].

1.7. Abnormalities in Methionine Metabolism and Health Consequences

Expansion in newborn screening programs has led to increased detection of inborn errors in metabolism and more information is now known about disorders in methionine metabolism [162]. There are various enzymatic reactions in methionine metabolism that have critical co-factors and if a diet is deficient in one or more of these co-factors the reactions will not be completed [144]. Clinical symptoms vary based on which part of the methionine cycle is experiencing a bottle neck. Once the metabolic deficiency is identified there are numerous dietary strategies including targeted supplements that can be implemented to prevent symptoms from forming or worsening.[163]. Conditions and associated symptoms that result from abnormalities or deficiencies within the methionine or related pathways are discussed below.

1.7.1. Hypermethioninemia

Hypermethioninemia refers to an excess of methionine in the blood and can occur from multitude of origins including excessive dietary intake of methionine-enriched foods, and it can also occur in combination with other metabolic disorders such as homocystinuria. The improper metabolism of methionine can also result from mutations in MAT1A, GNMT or AHCY. Variants in one of these genes result in a deficiency of the resulting enzyme that is involved in breaking down methionine and leads to a buildup of methionine. Hypermethioninemia can also result from liver disease, B12 deficiency or from medications that impact methionine metabolism. Symptoms are not observed often in patients with hypermethioninemia; however, some individuals exhibit intellectual disability and other neurological problems [164]; delays in motor skills (walking or standing) [165]; sluggishness,

muscle weakness; liver injury [166] and hepatocellular carcinoma [167], unusual facial features; and they exhibit a smell similar to boiled cabbage in their breath, sweat or urine [168]. Depending on the cause, hypermethioninemia can be counteracted with B12 supplementation [169].

1.7.2. Hyperhomocysteinemia

Hyperhomocysteinemia refers to elevated levels of homocysteine in the blood and can result from various factors, including genetic mutations affecting enzymes involved in homocysteine metabolism, deficiencies in vitamins such as B6, B12, and B6 (folate), or impaired renal function [170-172]. Hyperhomocysteinemia can be categorized into re-methylation defects (due to deficiencies in enzymes like MTHFR) or transsulfuration defects (due to deficiencies in enzymes like CBS). Hyperhomocysteinemia is associated with an increased risk of CVD, such as hypertension, atherosclerosis, and coronary artery disease [173-181]. Interestingly, a vascular phenotype observed that is distinctive in animals with hyperhomocysteinemia is endothelial dysfunction, which promotes inflammation and thrombosis, and impairs vascular function [182]. Endothelial impairment manifests by decreased nitric oxide derived from the endothelium and may be mediated by either accelerated oxidative inactivation of nitric oxide or inhibition of nitric oxide production caused by the endogenous nitric oxide synthase inhibitor, asymmetric dimethylarginine [182, 183]. This phenotype is present *in vitro* with bovine endothelial cells [184], Wistar rats [185, 186] and non-human primates [187] and humans [188]. Numerous studies have shown a correlation between hyperhomocysteinemia and abdominal obesity, suggesting that here may be a collective effect on the risk of metabolic syndrome and CVD mortality [189-194].

1.7.3. Homocystinuria

Homocystinuria refers to the accumulation of homocysteine and its metabolites in blood and urine. The most common manifestation is classical homocystinuria caused by CBS deficiency, but it can also be caused by other transsulfuration defects (CGL) and remethylation defects (MTHFR). While homocystinuria has similar genetic origins to hyperhomocysteinemia, is it differentiated by unique clinical symptoms such as intellectual disability [195], psychiatric symptoms, vison issues, skeletal abnormalities [196, 197], and vascular issues (stroke, thromboembolism) [198]. It has also been found that patients with homocystinuria and alterations in choline metabolism commonly have reduced fat mass [199].

1.7.4. Cystathioninuria

Cystathioninuria is characterized by elevated levels of cystathionine in the urine due to deficiencies in enzymes in the transsulfuration pathway, such as CGL or CBS, or enzymes that catalyze conversion of homocysteine back into methionine, such as MTHFR [200]. This can also be caused by deficiencies of reaction cofactors, serine or B6 or in substrates, methionine, and homocysteine. Thus, this condition can accompany other defects in the methionine cycle. There are no significant clinical symptoms or health effects observed in individuals with cystathioninuria.

1.7.5. Cystinuria

Cystinuria is caused by defects in the transport of cystine across the renal tubules and gastrointestinal tract, due to mutations in genes encoding specific transport proteins (SLC3A1 and SLC7A9) [201]. These mutations predispose patients to the formation of cystine stones in the urinary tract, leading to recurrent kidney stones and potentially other complications [202].

1.8. Methionine Supplementation

Following thorough description of various inborn defects or diet-related abnormalities in methionine cycle metabolism and how those abnormalities result in the toxic accumulation of different substrates. This leads to the contemplation of what reasons might there be to supplement methionine. Methionine supplementation has been shown to improve liver function to support detoxification pathways and protect against liver damage caused by toxins, medications, or alcohol consumption [203-205]. Supplementation provides support for individuals with hair loss, brittle nails to increase keratin production in hair and nails [206]. The recommended daily allowance (RDA) for methionine in adults is 15 mg/kg/day [207] and some diets such as plant-based diets can lead to an insufficiency of methionine, which could make supplementation necessary to prevent deficiency. Methionine is also important to maintain healthy microbiome populations [208], as well as contribute to inheritable stress behaviors [209] Since methionine has such an important role in protein synthesis, performance athletes may be motivated to supplement methionine to support muscle recovery, and promote overall athletic performance [210] however there is limited evidence to support this practice.

With any food or supplement, moderation is key because excessive levels of methionine can have potential adverse effects on health. With excessive levels of methionine, those undesired effects can manifest in the form of early reduced cardiac function, atherosclerosis, atherothrombosis, gastrointestinal issues, impaired liver function, increased oxidative stress, alteration of protein synthesis, kidney stones, toxicity (headache, nausea, vomiting, diarrhea) and neurological symptoms such as Alzheimer's [204, 211-220]. The upper limit of methionine intake without observed adverse effects is 46 mg/kg/day [221]. Historically, methionine is sourced using petrochemical feedstocks by a reaction between methanol and

hydrogen sulfide, however this practice has become less prevalent due to environmental and cost concerns. Modern techniques to synthesize methionine utilize microbial fermentation of natural sources of glucose substrates [222, 223]. Increased demand for meat products and growing global population is driving increased use of synthetic methionine in livestock feed, which has potential to shape industrial food production and change diet-related health outcomes [224]. Due to the increasing rate of use, more research is needed to understand if synthetic methionine production can alter aspects of cellular metabolism in humans [224, 225]

1.9. Dietary Methionine Restriction Extends Lifespan and Counteracts Age-Related Pathologies

The first studies of methionine restriction were conducted by Dr. Norman Orentreich of the Orentreich Foundation for the Advancement of Science and reported life extension in rats and have since been replicated in yeast, *Drosophila*, *Caenorhabditis elegans*, mice and rats [101, 226-239]. Additionally, methionine restriction prevents accelerating aging in progeroid mice [229]. Lifespan extension by methionine restriction has been shown to delay senescence and suppress senescence-associated secretory phenotypes [240]. Furthermore, age-associated cognitive decline and oxidative stress is improved by methionine restriction [239, 241-248]. There are several age-related pathologies that are counteracted by methionine restriction and thus increase lifespan. Reduced methionine diets for dogs have been patented in hopes of reducing age-related pathologies and extending canine companion lifespan [225, 249, 250].

1.10. Dietary Methionine Restriction is Utilized as a Treatment for Cancer

Methionine restriction is currently being implemented in humans to reduce cancer progression and improve therapeutic response. Cancer cells have been shown to have an increased dependence on methionine [147, 159, 251-253]. Combining methionine restriction with chemotherapy is shown to have increased efficacy in treating cancer [254-260]. As

previously described, the impact of methionine and downstream biomolecules influence epigenetic regulation, which is an important factor in cancer development [147]. Interestingly, methionine supplementation has been shown to reduce liver tumor aggressiveness [261] demonstrating the relationship of methionine with cancer is highly complex.

1.11. Dietary Methionine Restriction Improves Risk Factors for Cardiovascular Disease

High methionine diets have been associated with vascular remodeling and reduced cardiac output [220]. Downstream of methionine, taurine has been shown to have potential vasodilatory effects that modulate cardiac contractility, regulate blood pressure, protect against arrhythmias that reduce hypertension and CVD [262]. High circulating levels of methionine have also been as well as associated with insulin resistance, fatty liver, BMI, and adiposity in overweight and obese participants [263]. Methionine restriction reduces fat accumulation, systemic inflammation and improves cardiac function in obese mice [264-267]. The effect on adipose has been reported to have distinct associations with different adipose depots [268]. This diet has shown to be effective in obese participants to increase fat oxidation [269]. Furthermore, methionine restriction is reported to improve cardiac function through hydrogen sulfide production [266]. Interesting, while hyperhomocysteinemia been associated with cardiovascular disease, methionine restriction has been shown to increase homocysteine while either not influencing or improving cardiac function [266, 270]. There is a lack of research to understand the effects of methionine restriction on vascular function.

1.12. Dietary Methionine Restriction is Utilized to Improve Insulin Sensitivity and Glucose Metabolism

As previously demonstrated, methionine restriction heavily influences adipose tissue, which is a primary site for insulin resistance. This effect is partially due to upregulated secretion of adiponectin from adipose tissue. This diet also influences liver, renal, and muscular

functions to improve insulin sensitivity and glucose metabolism. Fibroblast growth factor 21 (FGF21) is a hepatokine that mediates thermogenesis and insulin effects and is consistently upregulated in studies of methionine restriction [270-275]. Another hepatokine consistently impacted by methionine restriction is insulin growth factor-1 (IGF-1) [232, 276, 277]. Due to structural similarity, IGF-1 can modulate insulin signaling by activating similar pathways and receptors as insulin such as Phosphoinositide 3-Kinase (PI3K) and Mitogen-Activated Protein Kinase (MAPK) but can change the downstream effects differently than if activated through insulin. Furthermore, methionine restriction increased glutathione production [239] and hepatic glutathione enhances insulin signaling [273]. There are many ways in which methionine restriction influences insulin sensitivity and glucose metabolism.

1.13. Dietary Methionine Restriction Improves Mitochondrial Function and Muscle Strength

Similar to the effects of methionine restriction on insulin signaling there are many ways in which the diet influences mitochondrial function, including repairing damage from oxidative stress and reducing ROS production to prevent further damage [248, 278, 279]. Methionine restriction also enhances metabolic flexibility by increasing energy expenditure though uncoupled respiration in both fed and fasted states [280, 281]. While these effects appear to be independent of FGF21 [281], mitochondrial biogenesis appears to be driven by FGF21 [282]. Furthermore, hydrogen sulfide also alters mitochondrial electron transport and inhibits oxidative phosphorylation triggering glucose uptake into muscle and glycolytic ATP production. Interestingly, while methionine restriction results in smaller body size and less muscle mass when accompanied by with physical activity there is improved skeletal muscle [283] and extended wire hang and running wheel activities compared to control fed mice [284]. These

effects can be partially attributed to increased skeletal muscle mitochondrial activity as well as intrinsic bone strength [285].

1.14. Durations of Methionine Restricted Diets

A critical factor when discussing the studies on methionine restricted diets is the duration in which the diet was implemented. There have been several studies that look at the effects over moderate to long time periods. In rodents, there have been studies that range from long-term for 1.5 years [286], 1 year [284, 287], to moderate term for 14 weeks [270, 275, 288], 8 weeks [281], 6 weeks [289], with 14 weeks being the most common duration. Intermittent methionine restriction has also been studied, where methionine restriction is consumed 3 days a week for 6.5 weeks [276, 290], many of the same benefits are maintained. In human clinical studies, 16 weeks [269], 4 weeks [291], and 1 week [292]. There is a need to expand studies of methionine restriction over short-term durations.

1.15. Different Approaches to Induce Methionine Restriction

While methionine restriction has been studied for several decades, there are several approaches to induce this diet. The approaches to these diets will be discussed in the following section.

1.15.1. Percent Decrease in Dietary Methionine

Due to the essential nature of methionine, it cannot be depleted from the diet without inducing essential amino acid deprivation and large amounts of cell death as demonstrated in section 1.10. An important study identified upper and lower thresholds of methionine restriction where metabolic responses are optimal [293]. The primary metabolic outcome measured was maximal reduction in adiposity without sacrificing lean muscle mass. To do this, mice were fed diets containing between 0.34% - 0% methionine for 8 weeks. Utilizing food formulated to

contain 0.86% methionine for a control diet or 0.17% methionine for a restricted diet, body weight and adiposity were reduced, accompanied by increased food and water intake in mice. This effect was lost when methionine was above 0.25% and restriction beyond 0.12% methionine containing diet resulted in rapid weight loss and food aversion consistent with essential amino acid deprivation [293]. Improved cardiac function observed with 80% methionine restriction is lost with 40% restriction. These studies illustrate that the amount of methionine restriction is crucial to gaining specific benefits.

1.15.2. Methionine Content in Food

Methionine is inherently present in food containing protein; therefore, animal studies of methionine restriction utilize diets that do not contain whole protein sources and supplement in individual amino acids expect methionine. Clinical studies have utilized an isolated amino acid protein replacement drink that is free from methionine [291, 292, 294, 295]. Diets containing oxidized protein sources such as casein have also been utilized to implement methionine restriction [250, 296]. However, while it is difficult to implement, methionine restriction is possible through consumption of whole foods only.

The amount of methionine in different foods groups varies quite widely. A list of commonly consumed foods is shown in table 1.1. This list is organized into food groups and within each food group there are color coded categories that represent the methionine concentration which corresponds to the legend in bottom right corner. Within each category, the food items appear in alphabetical order. This list is prepared from the USDA National Nutrient Database for Standard Reference - Composition of Foods Raw, Processed, Prepared [297, 298]. This table can be used as a guide to build a meal plan that is enriched in foods that are low in methionine.

Table 1.1 Methionine Content in Foods Source: USDA National Nutrient Database for Standard Reference Release 28 [297, 298]

Vegetables	Weight (g)	Met (mg)
Asparagus	180	50
Green beans	125	29
Beets	170	32
Broccoli	91	35
Cabbage	150	9
Carrots	128	26
Cauliflower	107	21
Celery	101	5
Chard, swiss	175	35
Collards	36	12
Cucumber	104	6
Eggplant	99	9
Endive	50	8
Kale	67	18
Kohlrabi	135	18
Leeks	124	12
Lettuce	40	7
Mushrooms	156	34
Okra	160	32
Onions	210	23
Parsley	60	25
Pepper, sweet	149	9
Pumpkin	245	20
Radicchio	40	3
Radishes	116	12
Seaweed	26	38
Spinach	30	16
Squash	205	23
Taro	132	9
Tomatoes	149	9
Tomato sauce	245	17
Turnips	156	14
Watercress	34	7
Yam	136	27
Zucchini	124	22
Brussels sprouts	155	54
Potatoes, white	148	56
Spinach	180	99
Sweet potato	200	74
Corn, sweet	165	112
Peas	145	119

Fruits	Weight (g)	Met (mg)
Apples	125	1
Apricots	65	10
Bananas	225	18
Blueberries	148	18
Cantaloupe	177	21
Cherimoya	160	34
Cranberries	110	3
Dates	147	32
Figs	64	4
Gogi berries	28	24
Grapefruit	230	16
Grapes	92	19
Guava	165	26
Honeydew	170	8
Kiwi	180	43
Limes	67	1
Mango	165	13
Nectarines	143	8
Olives	15	2
Orange	180	36
Papaya	145	3
Peach	154	15
Pear	140	3
Persimmons	25	2
Pineapple	165	20
Plantains	148	25
Plums	165	13
Raisins	165	35
Strawberries	152	3
Tangerines	195	4
Watermelon	154	9
Avocado	150	57
Figs, dried	149	51
Jackfruit	165	56

Legumes	Weight (g)	Met (mg)
Black-eyed peas	165	74
Hummus	60	48
Miso	17	22
Soy sauce	18	30
Soy milk, fortified	243	39
Fava beans	170	105
Lima beans	170	116
Pigeon peas,	168	128
Tofu, soft	120	101
Veggie sausages	50	126
Adzuki beans	230	182
Chickpeas	164	190
Cowpeas	171	188
Kidney beans	177	200
Lentils	198	152
Lupins	166	183
Mung beans	202	170
Refried beans	238	155
Split peas	196	167
Black turtle beans	185	228
Black beans	172	229
Edamame	155	215
Navy beans	182	201
Pink beans	169	230
Veggie/Soy burgers	70	204
Tempeh	166	290
Tofu, firm	126	266
White beans	179	261
Soybeans, mature	172	385
Soy nuts, roasted	93	497

Grains	Weight (g)	Met (mg)
Hominy	160	50
Tapioca	38	1
Barley	157	68
Buckwheat groats	168	74
Cornmeal	39	64
Pasta, wheat	124	79
Pasta, corn	140	77
Soba Noodles	114	82
Sorghum grain	48	81
Rice, white	158	100
Amaranth	48	109
Millet	174	122
Oats	39	122
Oat bran	219	109
Pasta, rice	169	134
Rice, brown	202	117
Spelt	44	112
Wheat bran	58	136
Wheat, hard	48	111
Wheat, sprouted	108	125
Quinoa	185	178
Kamut	172	167
Wild rice	164	195
Teff	252	315

Nuts & Seeds	Weight (g)	Met (mg)
Acorns	28.35	39
Almonds	28.35	44
Almond butter	16	20
Cashew butter	16	50
Chestnuts	28.35	33
Coconut, fresh	80	50
Macadamia nuts	28.35	7
Coconut milk	240	86
Hazelnuts	28.35	63
Pecans	28.35	54
Pine nuts	28.35	59
Peanuts	28.35	82
Tahini	15	88
Walnuts	28.35	67
Cashews	28.35	103
Flaxseeds	28.35	105
Pistachio nuts	28.35	102
Sunflower seeds	28.35	119
Chia seeds	28.35	167
Pumpkin seeds	28.35	171
Sesame seeds	28.35	159
Hempseeds	28.35	264
Brazil nuts	28.35	319

Animal Products	Weight (g)	Met (mg)
Eggs	33	132
Brie	28.35	168
Gouda	28.35	204
Milk, 1%	245	215
Milk, 3.25%	244	203
Yogurt, low fat	170	219
Parmesan	28.35	272
Yogurt, skim	170	287
Beef, lean	85	648
Chicken breast	85	675
Crab	134	730
Fish, cod	85	448
Fish, salmon	85	640
Fish, tuna	85	733
Ham	85	435
Lobster	145	689
Pork	85	609
Shrimp	85	565
Turkey	85	670

Methionine Content
0-50 mg
51-100 mg
101-150 mg
151-200 mg
201-250 mg
251-300 mg
301+ mg

1.15.3. Plant-Based Diets

As seen in table 1.1, the food group that is most prevalent in high levels of methionine are animal products, such as dairy and meat. Without a doubt, a methionine restricted diet would need to be dominated by plant-based foods. Methionine restriction has been hypothesized to be responsible for beneficial effects of vegetarian and vegan diets, as these diets are inherently low in methionine due to the proportion of protein being low in plants [299, 300]. The vegan diet has shown to have several beneficial outcomes that are similar to methionine restriction, such as reducing obesity, diabetes, CVD, and cancer, and has potential to increase life expectancy [301-305], while vegetarians share a few of these benefits [305]. However, while amino acid intake differs between meat eaters, vegetarians, and vegans, according to a cross-sectional metabolomic study of 379 men in the EPIC-Oxford cohort, plasma methionine levels are generally highest in fish eaters and vegetarians, followed by meat eaters and vegans [306, 307]. This suggests that different amino acid intakes between meat eaters, vegetarians, and vegans does not directly translate to lower methionine levels in the plasma.

Interestingly, due to disparities in the digestibility and bioavailability of protein between plant and animal sources, vegan diets have been further theorized to be a feasible strategy to implement methionine restriction [300]. Thus, the low methionine content of plant foods would be further restricted due to even less methionine being utilized from plant foods than animal foods. While this concept is based on physiological reality, there are several other differences that could account for the benefits of vegan and vegetarian diets, such as high levels of fiber, bioactive phytochemicals [308] and unsaturated fats [309, 310] and low levels of saturated fats and protein [311]. It has also been argued that protein dietary reference intakes (DRI) may be inadequate for vegetarians and vegans and that due to the decreased bioavailability

of plant protein and associated nutrient inadequacy, the DRI for protein should be increased for those eating diets low or devoid of animal protein [312]. While plant-based diets are in theory low in methionine, they may not be the optimal strategy for implementing methionine restriction due to restriction of other key nutrients.

1.15.3.1. Reduction of Methionine Influences Utilization of Other Amino Acids

As stated above, protein intake is a concern with predominantly plant-based diets, and this is based off the nutritional concept of protein quality in foods. It is well established in nutrition that different sources of protein are either high-quality or low-quality (complete or incomplete) [313]. The quality of a protein source is based on the amino acid composition, where a complete protein contains sufficient amount of all nine essential amino acids and an incomplete protein does not contain sufficient amounts of certain essential amino acids when consumed alone. Sufficiency is based on the protein requirements to stimulate cellular protein synthesis, and this is dependent on the amino acid composition. Animal proteins are known to be complete proteins, which most plant protein sources are considered incomplete (except soybeans and quinoa). Once any of the nine essential amino acids in the plant protein have been used up, protein synthesis is unable to continue. This all-or-nothing principle explains that either all the essential amino acids are available, or none can be used [314]. A different way to illustrate this principle is with Liebig's law of minimum, which was developed in agricultural science by Carl Sprengel in 1840 and later popularized by Justus von Liebig. The law states that growth is dictated not by total resources available, but by the scarcest resource which acts as the limiting factor. When one nutrient is low, other nutrients will only be utilized in equal amounts. The law of minimum was applied to human nutrition in 1935 by William Cumming Rose to discover unknown essential amino acids and daily requirements of essential amino acids for

optimal growth [315] and was also later confirmed in 1947 [316]. This concept depicts why is important to consume complementary plant-based proteins that have opposite amino acid profiles that balance each other out and allow for amino acids to be utilized in their full capacity. As depicted in table 1.1, vegetables and legumes are low in methionine and thus methionine is the limiting factor in these food groups. Complementary protein groups for vegetables or legumes are either nuts and seeds or grains, which are limited in lysine. Examples of common pairings of these complementary groups are green beans and almonds, or tomatoes and pasta, or beans and rice.

The law of minimum can be applied to methionine restriction and how it can mimic calorie restriction and plant-based diets. Perhaps methionine acts as a limiting factor and prevents utilization of other amino acids to stimulate protein synthesis. In Figure 1.9, the law of minimum is illustrated by a wooden barrel, where each stave of the barrel is one of the nine essential amino acids, and the shortest stave is the limiting factor in holding water in the barrel, where the water level is the amount of protein synthesis that can occur from amino acids available. In Figure 1.8A, methionine levels are the highest and represent a diet that is rich in methionine where the amount of protein synthesis is at the highest level possible. Figure 1.8B shows a diet that is depleted of methionine and can only hold a very small amount of water, or unable to synthesize protein. Figure 1.8C depicts a methionine restricted diet that holds an intermediate amount of water and thus allows for protein synthesis without being in excess. Alternatively, it has been argued that the benefits of plant-based diets over omnivorous diets are due to reduction in total protein, not amino acid composition [317]. Interestingly, restriction of threonine [318-320], tryptophan [321, 322], branched chain amino acids- leucine, isoleucine and

valine [323-327]- have shown to have similar benefits to methionine restriction in increasing lifespan and healthspan [328].

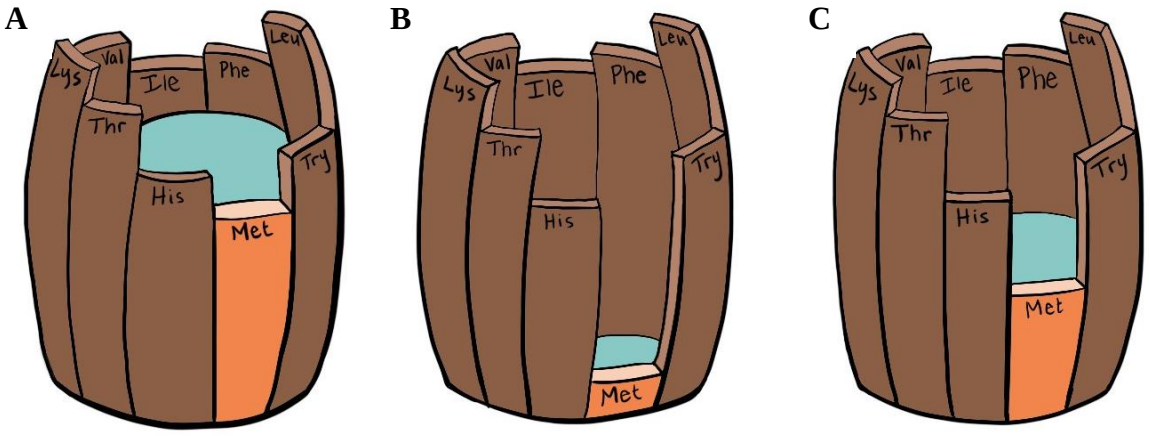

Figure 1.8. Methionine as a Limiting Factor in Amino Acid Utilization: Liebig's Law of Minimum Illustrates a barrel that is filled with water, and the staves of the barrel represent the nine essential amino acids (Histidine, Threonine, Lysine, Valine, Isoleucine, Phenylalanine, Leucine, Tryptophan, Methionine). The shortest stave of the barrel represents the limiting amino acid (orange), and the water level (blue) represents the amount of total amino acids that are utilized to stimulate protein synthesis. A.) Methionine-Rich Diet B.) Methionine Depleted Diet C.) Methionine Restricted Diet. *Adapted from Einarsson et al.[329]*

1.15.4. Methioninase Treatment

It has been shown that methionine restriction does not need to be introduced with a reduced methionine diet, and that the same effects can be introduced using recombinant methioninase. This recombinant L-methionine α-deamino-γ-mercaptomethane lyase (rMETase) is produced from *Pseudomonas putida* and has been cloned and produced in *Escherichia coli (E.coli)* (AntiCancer, Inc., San Diego, CA, USA) and purified for treatment applications. Numerous therapeutic benefits have been reported with rMETase use including sensitivity in human xenografts of lung, colon, kidney, brain, prostate, and melanoma *in vitro* and *in vivo* [330-336]. Evidence for use of rMETase as tumor-selective anticancer therapy is further supported by the finding that normal cells were insensitive to rMETase treatment, no toxicity was observed *in vivo* with effective doses [330], and there is increased efficacy of

chemotherapeutic drugs when in combination with rMETase [255, 331, 332].

Furthermore, rMETase has been shown to counteract obesity, diabetes, and non-alcoholic fatty liver disease in C57Bl/6 mice on high-fat diet [337-339]. Specifically, 8-week-old mice on 60% HFD treated with rMETase twice daily for 25 days had rapid reductions in plasma methionine which resulted in significant prevention of weight gain without restricting calorie intake [337]. Additionally, 8-week-old mice on 60% HFD treated with rMETase twice daily for 56 days had significant improvements in fasting glucose and glucose tolerance paired with loss of weight and visceral adiposity [339]. High-fat diet induced changes in the liver were also prevented by twice daily rMETase treatment over 56 days [338]. These studies show that there is potential for methionine restriction to be achieved with non-dietary approaches and still result in desired outcomes for metabolic health.

1.15.5. Probiotics Engineered to Metabolize Methionine

Due to the need to develop improved treatment options for people with homocystinuria, there have been efforts to develop an orally available approach that lowers the burden of dietary methionine that is capable of degrading methionine, and thus homocysteine. This has been achieved through use of a non-pathogenic member of the *E.coli* family, Escherichia coli Nissle 1917 (EcN) that is commonly consumed as a probiotic to treat various gastrointestinal conditions. EcN has been genetically modified to create SYNB1353 that degrades dietary methionine to prevent it from being absorbed in the gastrointestinal tract and successfully simulates dietary methionine restriction [340]. SYNB153 modifications utilize methionine decarboxylase which catalyzes the conversion of methionine into 3-methylthiopropylamine (3-MTP). SYNB153 efficacy was studied in male C57Bl/6J mice, male cynomolgus monkeys as well as male and female healthy human volunteers. Immediate

reduction of plasma methionine and homocysteine were observed within 2 hours of treatment in mice along with increased urinary and plasma 3-MTP. Mouse weight was not changed over 28-day treatment with SYNB153. Single dose of SYNB153 administered to non-human primates had similar results to mice for plasma and urinary assessment of methionine, homocysteine and 3-MTP. In a double-blind, placebo-controlled phase 2 study, healthy volunteers were administered with increasing doses of SYNB153 for 7 days. Without any serious adverse events, patients had 25-26% reduction in plasma methionine, 4-13% reduction in plasma homocysteine, and increased 3-MTP excretion in urine. This proof-of-concept study demonstrates the activity of SYNB153 in metabolizing methionine in the gastrointestinal tract, and evidence of efficacy in healthy volunteers [340]. This concept was originally developed for other amino acid disorders, including phenylketonuria [341-343]. A similar approach has been used to administer rMETase-producing *E. coli* twice daily in obese C57Bl/6 mice 12-18 months of age. The rMETase-producing *E. coli* reversed old-age induced obesity and significantly reduced weigh by 14 days of treatment [344]. These studies are another example of a non-dietary approach to attaining methionine restriction, however while the evidence in mice does not consistently produce beneficial effects on weight, further investigations of this engineered probiotic on weight and metabolic outcomes are necessary.

1.16. Project Goal: Determine the Effects of Dietary Methionine Restriction on Age- and Diet-Related Dysfunctions in Metabolism and Perivascular Adipose Tissue

Based on the existing body of work, methionine restriction (MR) is a powerful metabolic therapy that can improve cardiometabolic parameters by heavily influencing adipose tissue while also extending lifespan. However, there are limited studies that compare effects of MR between different age groups and for short durations. Furthermore, there are several pathways reported to mediate the effects of MR that are important for the ability of PVAT to

modulate vascular response. We aim to examine if an 80% MR diet can induce beneficial changes in cardiometabolic dysfunctions in male mice and whether PVAT is impacted by these metabolic improvements. Therefore, the objectives of this work are to evaluate circulating metabolic parameters, adipose tissues including PVAT, and thoracic aorta morphology in response to MR. We implemented these experimental objectives in two different cohorts: an age cohort with three different age phases, and a diet cohort with high fat diet induced obesity. The age study utilizes a long-term MR diet, and the diet study utilizes a short-term MR diet. We hypothesize that MR will induce beneficial effects that can modulate age- and diet-related alterations in metabolism and PVAT. With these studies, we provide evidence that MR has even greater potential to reduce risk of cardiovascular and metabolic disease by impacting thoracic PVAT.

CHAPTER 2

EXPERIMENTAL METHODS

2.1. *In vivo* methods

All methods described under Section 2.1 pertain to *in vivo* experiments utilized within this study. Methods employed were approved by the Institutional Animal Care and Use Committee of the Orentreich Foundation for the Advancement of Science.

2.1.1.1. Long-Term Study

Mice were weight and age matched, and then separated into two groups, one group was fed a control diet (CD, 10% fat/0.86% methionine; A14040402, Research Diets - New Brunswick, New Jersey), and the other group 80% methionine restricted diet (MR, 10% fat/0.12% methionine; A14040401, Research Diets). These diets were custom formulated, see table 2.1 for additional nutritional information for these diets. Food was exchanged twice a week; and was weighed prior to placement in the animal cage as well as after time had elapsed. The difference in food from prior to after was considered the amount of food eaten by the single-housed animal. The reporting of amount of food consumed during that time period was divided by the number of days elapsed and multiplied by the amount of kilocalories per gram of food. Mice were divided into three cohorts and were as follows: young mice were entered into the study at approximately 2 months (8 weeks) of age, consuming either the control or MR diet for 52 weeks (young; n = 8/diet group); a second cohort of middle-aged mice was entered at 12 months (52 weeks) of age, fed either the control or MR diet for 52 weeks (middle-aged; n = 8/ diet group); and a third cohort of old-aged mice was entered at 23.5 months (102 weeks) of age, fed either the control or MR diet for 15 weeks (old; 5/ control diet and 7/ MR diet). These age groups were chosen to model different phases within the mature mouse lifespan: young adult,

middle-aged adult, and old adult. These experimental groups are referred to based on the age of initiation of the diet: young, middle-aged, or old. See Figure 3.1 for the experimental timeline.

2.1.1.2. Short-Term Study

To induce obesity, 10-week-old WT mice were fed a very high fat diet (60% kilocalories from fat, D12492, Research Diets) for 15 weeks. All mice were weight matched and divided into two groups that were fed either high fat diet (HFD, 60% fat/0.86% methionine; A14032002, Research Diets) or an 80% methionine restricted high fat diet (HFD-MR, 60% fat/0.12% methionine; A14032001, Research Diets). These diets were custom formulated, see table 2.1 for additional nutritional information for these diets. The HFD-MR group was further split into 3 groups, where the HFD-MR was administered for three different durations, 10 days (7/group), 5 days (8/group), and 3 days (8/group), while the HFD control group contained 8 animals. Animals were permitted food and water ad libitum for the duration of the experiment. Food was exchanged twice a week; and was weighed prior to placement in the animal cage as well as after time had elapsed. The difference in food from prior to after was considered the amount of food eaten by the single-housed animal. The reporting of amount of food consumed during that time period was divided by the number of days elapsed and multiplied by the amount of kilocalories per gram of food. See figure 4.1 for a diagram of the experimental timeline.

2.1.1. Genotype

Seven-week-old mice male C57BL/6J mice (WT, JAX#000664) were purchased from the Jackson Laboratory (Bar Harbor, Maine). While this mouse strain is one of the most commonly used strains, it was selected because they are susceptible to the development of diet-induced obesity and diabetes [345]. This is mostly due to the missense mutation in nicotinamide nucleotide transhydrogenase (*Nnt*), and results in impaired glucose tolerance and age-related decline in mitochondria function [346-348]. Both of the *in vivo* studies that are included were

performed on male mice, thus we do not address potential variations in response based on sex differences. This is further addressed in section 6.7.1.

2.1.2. Housing

Mice were single housed and maintained at 20°C± 2°C with 50% ± 10% relative humidity, and they had a 12-hour light/12-hour dark photoperiod with water and standard chow diet (Laboratory Rodent Diet 5001, PMI Nutrition International, Brentwood, MO) provided *ad libitum* for 1 week. Cage locations and animal numbers were randomized to reduce confounding variables between diet groups. Cages were replaced and cleaned weekly by animal technicians.

2.1.3. Dietary Intervention

Rodent diets utilized in this study were custom formulated by Research Diets. See table 2.1 for full nutritional components of all diets used in this study.

Table 2.1. Nutritional Content of Methionine Restricted Diets										
Diet Abbreviation	CF		MR		HFD		HFD-control		HFD-MR	
Product #	A14040402		A14040401		D12492		A14032002		A14032001	
	10% fat, 0.86% Met		10% fat, 0.12% Met		60% fat, whole protein		60% fat, 0.86% Met		60% fat, 0.12% Met	
	gm%	kcal%	gm%	kcal%	gm%	kcal%	gm%	kcal%	gm%	kcal%
Protein	13	14	13	14	26.2	20	15	13	17	13
Carbohydrate	74	76	74	76	26.3	20	31	28	36	28
Fat	4	10	4	10	34.9	60	30	60	35	60
total		100		100		100		100		100
kcal/gm	3.9		3.9		5.24		4.5		5.3	
Ingredient	gm	kcal	gm	kcal	gm	kcal	gm	kcal	gm	kcal
Casein	0	0	0	0	200	800	0	0	0	0
L-Arginine	11.2	45	11.2	45	0	0	11.2	45	11.2	45
L-Histidine-HCL-H20	3.3	13	3.3	13	0	0	3.3	13	3.3	13
L-Isoleucine	8.2	33	8.2	33	0	0	8.2	33	8.2	33
L-Leucine	11.1	44	11.1	44	0	0	11.1	44	11.1	44
L-Lysine	14.4	58	14.4	58	0	0	14.4	58	14.4	58
DL-Methionine	**8.86**	**35**	**1.24**	**5**	0	0	**6.5**	**26**	**0.9**	**4**
L-Phenylalanine	11.6	46	11.6	46	0	0	11.6	46	11.6	46
L-Threonine	8.2	33	8.2	33	0	0	8.2	33	8.2	33
L-Tryptophan	1.8	7	1.8	7	0	0	1.8	7	1.8	7
L-Valine	8.2	33	8.2	33	0	0	8.2	33	8.2	33
L-Glutamic Acid	**27.83**	**111**	**35.5**	**142**	0	0	**20.4**	**82**	**25.9**	**104**
Glycine	23.3	93	23.3	93	0	0	23.3	93	23.3	93
L-Cystine	0	0	0	0	3	12	0	0	0	0
Sucrose	150	600	150	600	68.8	275.2	150	262	150	262
Dextrose	50	200	50	200	0	0	50	200	50	200
Maltodextrin	125	500	125	500	125	500	65.6	600	65.6	600
Corn Starch	424.5	1698	424.5	1698	0	0	0	0	0	0
Cellulose	50	0	50	0	50	0	50	0	50	0
Lard	0	0	0	0	245	2205	219	1971	219	1971
Corn Oil	46	414	46	414	0	0	46	414	46	414
Soybean Oil	0	0	0	0	25	225				
Mineral Mix S10001	35	0	35	0	0	0	35	0	35	0
Mineral Mix S10026	0	0	0	0	10	0	0	0	0	0
Vitamin Mix V10001	10	40	10	40	10	40	10	40	10	40
Choline Bitartrate	2	0	2	0	2	0	2	0	2	0
Dicalcium Phosphate	0	0	0	0	13	0	0	0	0	0
Calcium Carbonate	0	0	0	0	5.5	0	0	0	0	0
Potassium Citrate	0	0	0	0	16.5	0	0	0	0	0
Red Dye #40	0	0.025	0	0	0	0	0.05	0	0.025	0
Yellow Dye #5	0	0.025	0	0	0	0	0	0	0.025	0
Blue Dye #1	0	0	0.05	0	0.05	0	0	0	0	0
Total	1030.54	4004	1030.59	4004	773.85	4057	884.05	4000	755.75	4000

2.1.4. Measurement of Body Weight

For long-term study, the body weight of mice was measured twice weekly for the duration of the study. For the short-term study, to ensure obesity had been achieved within the 15 weeks of HFD, the body weight of mice was measured twice weekly until mice were greater than 45 grams. Mice weight was also recorded for the remainder of the study.

2.1.5. Tissue Collection

Upon completion of the long-term dietary intervention with CD and MR diets; young, middle-aged, and old mice were fasted for 4 hours, anesthetized with isoflurane (Patterson Vet, Cat#07-893-1389), and euthanized with cervical dislocation. Blood glucose was measured from a tail nick using a FreeStyle glucometer and test strips (Abbott). Blood was collected by retroorbital bleeding, processed for plasma separation, and stored in -80deg. Mice were perfused with phosphate buffered saline (PBS). Tissues collected were liver, inter-scapular brown adipose tissue (BAT), inguinal white adipose tissue (iWAT), retroperitoneal white adipose tissue (rpWAT), perigonadal adipose tissue (gWAT), and thoracic aorta with intact perivascular adipose tissue (PVAT). Tissues were collected for either fixation in 10% formalin or freezing at -80deg.

Upon completion of the short-term dietary intervention with HFD and HFD-MR diets, ~27-week-old-mice were fasted for 4 hours, anesthetized with isoflurane (Patterson Vet, Cat#07-893-1389) and euthanized with cervical dislocation. Blood glucose was measured from a tail nick using a FreeStyle glucometer and test strips (Abbott). Blood was collected by retroorbital bleeding, processed for plasma separation, and stored in -80deg. Mice were perfused with PBS. The tissues collected were BAT, iWAT, gWAT, liver and thoracic aorta with intact PVAT. See figure 1.3 for a diagram of tissue locations. The lymph nodes were removed from

male iWAT tissues during collection. The surrounding WAT was cleared from the BAT lobes prior to storage and processing. For PVAT and associated aorta samples, 5-6mm segments of the thoracic aortae were excised from below the ascending arch, PVAT separated from aorta, Tissues were collected for either fixation in 10% formalin or freezing at -80deg. Frozen tissues were processed for either protein or RNA analysis. We were limited by the size of PVAT and were unable to obtain sufficient tissue for all analytical endpoints.

2.1.6. Assays on Circulating Analytes

Blood glucose was measured in fresh blood using a handheld Abbott® Freestyle glucometer and test strips. Plasma was used enzyme-linked immunosorbent assay (ELISA) kits were used to measure insulin (ALPCO Diagnostics, Salem, New Hampshire), leptin, insulin like growth factor 1 (IGF-1), adiponectin (R&D Systems, Minneapolis, Minnesota), and FGF21 (Millipore, Billerica, Massachusetts). Colorimetric assays were used to determine plasma triglyceride (TG), total cholesterol (TC) (Thermo Fisher Scientific, Middletown, Virginia), and aspartate aminotransferase (AST) and alanine aminotransferase activity (Abcam, Waltham, Boston). Homeostatic Model Assessment for Insulin Resistance (HOMA-IR) was calculated from the fasting blood glucose (mmol/L) x fasting plasma insulin (uU/ml) divided by 22.5 [288]. All assay details are available in table 2.2.

Table 2.2. Assays to Detect Blood Analytes			
Blood Analyte	**Product Name**	**Vendor**	**Catalog Number**
Total Triglyceride	Infinity Triglyceride	Thermo Scientific	TR22421
	Triglyceride standard	Pointe Scientific	T7531STD
Total Cholesterol	Matrix Plus Cholesterol Reference Kit	Verichem Laboratories	9550
	Infinity Cholesterol	Thermo Scientific	TR13421
FGF21	Rat / Mouse FGF-21 ELISA Kit	EMD Millipore	EZRMFGF21-26K
Adiponectin	Mouse Adiponectin/Acrp30 Quantikine ELISA Kit	R&D Systems	MRP300
IGF-1	Mouse/Rat IGF-I/IGF-1 Quantikine ELISA Kit	R&D Systems	MG100
Leptin	Mouse/Rat Leptin Quantikine ELISA Kit	R&D Systems	MOB00B
Insulin	Mouse Ultrasensitive Insulin ELISA	Alpco	80-INSMSU-E01
Glucose	FreeStyle glucometer and test strips	Abbott	7157975
AST	Aspartate Aminotransferase Activity Assay Kit	Abcam	ab105135
ALT	Alanine Transaminase Activity Assay kit	Abcam	ab105134

2.1.7. Gene Expression

2.1.7.1. RNA Isolation & RT-qPCR

Frozen tissues, stored at -80°C, were ground with pre-chilled mortar and pestle with liquid nitrogen. Tissues were homogenized in 1mL of TRIzol Reagent (Invitrogen, Cat#15596026) and mixed several times with 1mL sterile syringe with 20G needle. 1-Bromo-3-chloropropane was added to samples, followed by incubation at RT and centrifugation at 4°C. Aqueous layer was carefully collected and 70% ethanol was added. Isolated RNA was then cleaned using RNeasy Mini Kit (Qiagen, Cat#74104) and eluted in RNAse-free water. Sample concentration and chemical purity were quantified with NanoDrop 1.000 Spectrophotometer (ThermoScientific) and RNA quality was assessed by 2100 Bioanalyzer Instrument (Agilent Technologies). cDNA was synthesized using AzuraQuant cDNA Synthesis kit (Azura Genomics, Cat#AZ-1996). RT-qPCR was performed on a CFX Connect Real-Time System (BioRad) using AzuraQuant Green Fast qPCR Mix LoRox (Azura Genomics, Cat#AZ-2105) to assess gene expression of selected transcripts according to manufacturer's instructions. Primer sets were designed or obtained from Harvard Primer Bank (https://pga.mgh.harvard.edu/primerbank/),

synthesized through Integrated DNA Technologies and validated prior to assessing adipose tissues and cell lines. See table 2.3 for primer sequences.

Table 2.3: Primer Sequences for Gene Expression		
Target	**Forward: 5'-> 3'**	**Reverse: 5'-> 3'**
Acyp2	TGCTCAAGTCTGTGGACTACGA	CAGCCAGGACTTCATGGCATC
Adipoq	TGACGACACCAAAAGGGCTCAG	CAGGATGTCCTGGGATGCCTG
Atgl1 (Pnpla2)	CAACGCCACTCACATCTACGG	GGACACCTCAATAATGTTGGCAC
aSMA (Acta2)	GGCACCACTGAACCCTAAGG	ACAATACCAGTTGTACGTCCAGA
Cd36	GGAGCCATCTTTGAGCCTTCA	GAACCAAACTGAGGAATGGATCT
Cebpa	AGTCGGTGGACAAGAACAGC	GTCACTGGTCAACTCCAGCA
Cidea	CTCGGCTGTCTCAATGTCAA	GGGATGGCTGCTCTTCTGTA
CoxIV	ATTGGCAAGAGAGCCATTTCTAC	CACGCCGATCAGCGTAAGT
Ctsz (Catz)	GGCCAGACTTGCTACCATCC	ACACCGTTCACATTTCTCCAG
Fabp4	CATGAAAGAAGTGGGAGTGGGC	AAGTACTCTCTGACCGGATGGT
Fasn	GGCTCTATGGATTACCCAAGC	CCAGTGTTCGTTCCTCGGA
Pgc1a	GTCAACAGCAAAAGCCACAA	TCTGGGGTCAGAGGAAGAGA
Plin1	TCAGGATAAGCTCTATGTCTCGTG	CCTGATCTTGAATGTTCTGTGGT
Ppara	CATACTCGCGGGAAAGACCA	CAAGCGTCTTCTCGGCCATA
Pparg	GCTCCAAGAATACCAAAGTGCG	CCTTGCATCCTTCACAAGCATG
Scd1	CCCACATGCTCCAAGAGAT	AAATCCCGAAGAGGCAGGTG
Ucp1	GGGCCCTTGTAAACAACAAA	GTCGGTCCTTCCTTGGTGTA

2.1.7.2. Quantification

Quantification of RT-qPCR results is done by the traditional relative gene expression 2(-ΔΔ(Cq)) method [349].

2.1.8. Immunoblot

2.1.8.1. Protein Isolation and SDS-PAGE

Frozen PVAT tissues were mechanically lysed with a tube pestle in radioimmunoprecipitation assay (RIPA) buffer (150mM NaCl, 2mM EDTA, 1% Igepal, 0.5% sodium deoxycholate, 0.1% sodium dodecyl sulfate [SDS], and 50mM Tris HCl, pH 7.4) with 1x protease/phosphatase inhibitor cocktail (Cell Signaling Technology) on ice. Lysates were sonicated and centrifuged at 11,000g for 10 minutes at 4°C. Proteins were precipitated using 4-volume ice cold 100% acetone and incubated at 20°C overnight. Proteins were pelleted by

centrifugation at 10,000g for 10 minutes at 4°C, washed two times in 70% acetone, and air dried. Pellets were resuspended in RIPA lysis buffer supplemented with 1% SDS and 1x protease/phosphatase inhibitor cocktail (Cell Signaling Technology), sonicated, and stored at 20°C. Protein was quantified using the Pierce BCA protein assay; followed by the addition of Laemmli sample buffer with 100mM dithiothreitol and incubated at 95°C for 15 minutes. SDS-polyacrylamide gel electrophoresis (PAGE) was performed using BioRad TGX FastCast gels between 10% and 12% (#1610173, #1610175) and 45 to 50 µg of protein per lane. Gels were transferred to polyvinylidene fluoride membranes (PVDF) with 0.2µm pore size and blocked using 5% milk/0.1% Tween in 1X phosphate buffered saline (PBS-T). Primary antibodies were diluted in 5% milk, added to PVDF membrane and incubated overnight at 4°C. Chemiluminescent signal was detected using Immobilon Forte Western HRP substrates (Millipore #WBLUF0500). Cell cycle markers were measured by western blot using fluorescent secondary antibodies, Revert™ 520 Total Protein Stain, and measured with LI-COR Odyssey in 520nm, 700nm, and 800nm channel. Additional information on antibodies is provided in Table 2.4. Due to the small tissue size of mouse PVAT we were limited in the number of PVAT immunoblots performed.

2.1.8.2. Quantification

Band intensity was measured by collecting Raw Integrated Pixel Density in ImageJ and normalized to total protein by Ponceau stain of PVDF membrane. Cell cycle markers were normalized to total protein by Revert™ 520 stain of PVDF membrane and quantified with Empiria Studio® (LI-COR).

Table 2.4. Antibodies to Detect Protein Abundance				
PRIMARY ANTIBODIES				
IB = Immunoblot, IHC = Immunohistochemistry, WC = Working Concentration				
Target Antigen	Vendor	Catalog #	IB WC (mg/mL)	IHC WC (mg/mL)
ACYP2	Abnova	H00000098-M06	0.0005	0.002
αSMA	Abcam	ab7817	-	0.5
CATZ	RnD Systems	AF1033	0.0005	0.002
C/EBPa	Cell Signaling	cs8178	0.000014	-
COXIV	Cell Signaling	cs4850	0.000716	0.2983
COXIV	Cell Signaling	cs4850	0.00078	0.2983
FABP4	Cell Signaling	ab23693	0.00011	-
GRP75	Santa Cruz Biotechnology	sc133137	0.00007	0.571
Histone 3	Cell Signaling	9715	0.00001	-
HES5	Abcam	ab194111	0.00025	6.22
IgG isotype control, rabbit	Cell Signaling	cs3900	-	matched
IgG1 isotype control, mouse	Cell Signaling	cs5415	-	matched
IgG isotype control, goat	R&D Systems	AB-108-C	-	matched
p53	Cell Signaling	9282	0.00002	-
PCNA	Santa Cruz Biotechnology	sc-25280	0.0002	-
PGC1a	Abcam	ab54481	0.0002	-
PLIN1	Cell Signaling	cs9349	0.000151	0.03775
PPARG	Cell Signaling	cs2435	0.00006	-
Puromycin	Millipore	MABE343	0.001	-
RAB10	Cell Signaling	8127T	-	0.00125
TIM17a	Abcam	ab192246	-	0.0058
TOM20	Abcam	ab186735	-	0.048
UCP1	Cell Signaling	cs14670	0.0050	0.1
SECONDARY ANTIBODIES				
Target Antigen	Vendor	Catalog #	IB Titer	IHC Titer
Goat anti-mouse, HRP-linked	Cell Signaling	cs7076	0.00002	-
Goat anti-rabbit, HRP-linked	Cell Signaling	cs7074	0.00001	-
Donkey anti-goat, HRP-linked	R&D Systems	HAF109	0.00001	-
Goat anti-mouse, IRDye 800CW	LI-COR	827-08364	0.00007	-
Goat anti-rabbit, IRDye 680CW	LI-COR	926-68171	0.00007	-
Goat anti-mouse, AlexaFluor488	Invitrogen	A11001	-	2
Goat anti-rabbit, AlexaFluor488	Invitrogen	A11034	-	2
Donkey anti-goat, AlexaFluor 488	Molecular Probes	A-11055	-	2
Goat anti-mouse, AlexaFluor594	Invitrogen	A11005	-	2
Goat anti-rabbit, AlexaFluor594	Invitrogen	A11037	-	2
Chicken anti-rabbit, AlexaFluor647	Invitrogen	A21443	-	2

2.1.9. Histology

Fixed PVAT/Aorta tissues were paraffin embedded, sectioned, and stained by the MHIR Histopathology Core Facility for either immunostaining or routing histology.

2.1.9.1. Hematoxylin and Eosin

Deparaffinization-Rehydration: Sections were cut at 5μm thickness and incubated at RT in Clear-Rite3 (Epredia, Cat #6915) for 10 minutes, 3 times. Slides were transferred to incubate at RT in 100% ethyl alcohol for 2 minutes, 2 times. Slides were then incubated in 95% ethyl alcohol for 1 minute. Slides were rinsed with water for 5 minutes. At each change, every slide was dipped in the solution 10-20 times. Between changes, slides were drip-dried. Staining: Slides were incubated at RT in Hematoxylin (Richard Alan, Cat #7231) for 5 minutes. Post incubation, slides were rinsed clear with water then placed in 5% acetic acid for 1 minute. Post washing with water, slides were incubated for 2 minutes in Bluing Agent (Righard Alan, Cat #7301). Following a wash, the slides were transferred to ethanol for 1 minute. Slides were incubated in Eosin Y (Richard Alan, Cat #711) for 2 minutes. Slides were then rinsed in 95% ethanol for 30 seconds, two times. Dehydrating: Slides were incubated 3 times in 100% ethanol and followed by 3 incubations in clear agent, once for 3 minutes and twice for 2 minutes. Coverslip Mounting: Slides were mounted with a coverslip using Permount Mounting Medium (Fisher Chemical, Cat #SP15-100) and allowed to dry for 48 hours. Resulting color stains are nuclei = blue, cytoplasm/structures = pink, and erythrocytes, collages, muscle cytoplasm = shades of pink. Stained PVAT sections were imaged with Zeiss Axioscope 40 microscope equipped with a Canon EOS 90D camera, 4x objective (ACHROPLAN- 4x/0,10NA) and 40X objective (Ph2 Plan-NEOFLUAR 40x/0,75NA), at least 5 images per animal were obtained.

2.1.9.2. Perivascular Adipose Lipid Quantification

An ImageJ protocol developed in our lab for PVAT was utilized to measure accumulated lipid [350]. Two independent raters were used to quantify lipid and these values were averaged to ensure unbiased results. These results are reported as percent lipid area out of total PVAT area.

2.1.9.3. Thoracic Aorta Area Quantification

Total area was determined by outlining the external wall of the vessel, lumenal area was determined by outlining the internal vessel wall, and medial area was determined by subtracting the lumenal area from the total area. Tracing utilized a Wacom sketching pad (Wacom, Intuos Pro) and area was measured in ImageJ (FIJI).

2.1.10. Immunofluorescence

2.1.10.1. Staining

For immunofluorescence staining, slides were deparaffinized; this was followed by heated antigen retrieval (0.01M sodium citrate buffer, pH 6.0; Agilent Technologies) for 25 minutes and permeabilization (Tris-buffered saline - TBS + 0.1% Triton-X) for 10 minutes. Sections were blocked in TBS with 5% goat serum and 1% bovine serum albumin (BSA) for 2 hours. For mouse monoclonal antibodies, sections were incubated with M.O.M. Blocking Reagent (Vector Laboratories) for 30 minutes and then washed. Primary antibodies were diluted in TBS supplemented with 1% BSA and 0.1% Tween (TBS-T) and slides were incubated overnight at 4degC and washed with TBS-T. For immunofluorescence, samples were incubated with Alexa Fluor-conjugated secondary antibody in 1% BSA/TBS-T for 2 hours. Sections were washed and then incubated with TrueVIEW Autofluorescence Quenching Kit (Vector Laboratories) for 2 minutes. After washing, slides were cover-slipped using Vectashield HardSet Antifade Mounting Medium with DAPI (Vector Laboratories). Slides were imaged

using a Leica TCS SP8 confocal microscope on Lieca DMI6000 inverted equipped with 20X dry objective (HC PL APO CS2 20x /0.75NA Dry) and 63X objective (HC PL APO CS2 63x/1.4NA Oil). Mounted tissue sections were imaged with 488nm (Argon), 561nm (DPSS), or 633 (HeNe) lasers using LAS AF SP8 software.

For translocase of outer mitochondrial membrane 20 (TOM20) immunostaining, slides were deparaffinized, followed by heated antigen retrieval (0.01M sodium citrate buffer, pH 6.0) for 30 minutes. Sections were blocked in phosphate-buffered saline (PBS) with 5% goat serum and 1% BSA for 1 hour, and primary antibody was incubated in PBS supplemented with 1% BSA and 0.1% Tween overnight at 4degC. Sections were washed with PBS-T and incubated with Avidin/Biotin Blocking solution (Vector Laboratories, #SP-2001). Samples were then incubated with biotinylated secondary antibody for 2 hours (Jackson Immunoresearch). Slides were incubated with Avidin/Biotinylated Conjugated Enzyme Peroxidase System (ABC Elite, Vector Laboratories, #PK-6100). Sections were reacted with diaminobenzidine for 5 minutes, quenched and counterstained with hematoxylin nuclear stain, and cover-slipped using Permount Mounting Medium (Fisher Scientific, #SP15). Additional information on antibodies is provided in table 2.4.

2.1.10.2. Quantification

Fluorescence was quantified with ImageJ, measuring integrated density of separate channels, and subtracting baseline fluorescence of IgG isotype control. Average intensity from at least 3 images per animal was calculated for final values and displayed as relative intensity to equimolar IgG controls.

2.1.11. Mass Spectrometry

All samples submitted for mass spectrometry were prepared for data acquisition and analysis by the MaineHealth Institute for Research Proteomic and Lipidomic Core Facility. Procedures for data acquisition and analysis were provided by Proteomic and Lipidomic Core Facility in accordance with their operational procedures.

2.1.11.1. Data Acquisition

Separate ~5mg segments of PVAT or aorta were denatured 8M Urea/50mM Tris-HCL with phosphatase and protease inhibitors (Roche), reduced with 8mM dithiothreitol (DTT) and alkylated with 20mM iodoacetamide. The samples were digested overnight with 10µg sequencing grade trypsin (Promega, Trypsin Protease, MS Grade). Samples were cleaned using Pierce C18 Spin Columns (ThermoFisher Scientific) and fractionated with an Agilent1100 HPLC system was used to resolve samples over a Jupiter 5µm C18 300A 250mm x 4.6mm chromatography column (Phenomenex) with a 22 min increasing acetonitrile gradient. Twenty-one fractions were collected and merged into seven, dried using vacuum centrifugation ready for mass spectrometry.

Tryptic peptides were re-suspended in 0.1% formic acid and loaded onto a reverse phase C18 nano column (40 cm length, 75 µm ID) packed with Reprocil Pur C18,1.9µm (Dr Maisch, Ammerbuch, Germany) and resolved by an increasing acetonitrile gradient over 120 min at a flow rate of 220 nL/min. Samples were injected into a Sciex TripleTOF 5600 mass spectrometer using a Dionex Ultimate 3000 (RSLCnano) chromatography system. The mass spectrometer was operated using data-dependent acquisition (DDA) to create a spectral ion library and data-independent acquisition (DIA) to create Sequential Window Acquisition of all THeoretical spectra (SWATH) for relative quantitation. For both modes of operation (DDA and

SWATH) the mass spectrometer used an ion spray voltage floating (ISVF) of 2400 V, curtain gas (CUR) 25 PSI, interface heater temperature (IHT) 150 °C, ion source gas 1 of 6 PSI and a declustering potential (DP) 100 V

All data acquired in DDA mode used a high-resolution MS scan from 350-1500 m/z to select the 50 most intense ions prior to MS/MS analysis using CID (Collision Induced Dissociation). Other parameters include charge states 2-5, exclusion time 30 seconds accumulation time of 250ms for TOF MS and 50ms for TOF MS2, cycle time 2.8 seconds. Unique SWATH parameters included 1 TOF MS scan with an accumulation time of 96ms followed by 100 variable scan windows from 350 to 1500m/z, accumulation time of 89.9ms, cycle time 9.1 seconds. Identical chromatography parameters were used for SWATH and DDA analysis.

Liquid Chromatography Gradient. Buffer A: 97% water, 2.5% acetonitrile, 0.1% formic acid. Buffer B: 80% acetonitrile, 20% water, 0.1% formic acid. All solvents used are LCMS grade.From 0-9 minutes the sample is loaded on to a C18 trap column (Thermo Scientific) at a flow rate of 3µl/min. At 9 minutes a switching valve was used to switch the C18 trap column in line with the gradient pump. From 0-1 minutes buffer B increases from 0-1% at a flow rate of 220nl/min (using the gradient pump), from 1-104 minutes buffer B increases from 10-35%, from 104-108 minutes buffer B increases from 35-95%, from 108-118 minutes buffer B remains at 95%, from 118-119 minutes buffer B decreases from 95-2%, from 119-120 minutes buffer B remains at 2%.

2.1.11.2. Data Normalization and Analysis

The TripleTOF raw data was searched against a human UniProt database using ProteinPilot software (Version 5.0.2, Sciex) with the Paragon algorithm for the creation of a

protein library. Each peptide used for protein identification met specific Protein Pilot parameters i.e. only peptide scores that corresponded to a peptide confidence of greater than 99% were accepted and quantified. The database search parameters tryptic digestion, fixed modification of cysteine alkylation (57.02146) with an emphasis on Biological variable modifications were used. Spectral alignment and targeted data extraction of DIA samples were performed with the SWATH Processing Micro App in PeakView (Version 2.2.0, Sciex) using the reference spectral library generated earlier. The data was imported into MarkerView (Version 1.2.1, Sciex), where three technical replicates of each sample were averaged, normalized, groups compared by principal component analysis (Unsupervised with Autoscaling) and mined for significant differences (T-Test, fold change). Significant differences between individual MR timepoints and HFD control were used to determine significantly differentially expressed proteins. Significance threshold for pvalue ≤ 0.05 and fold change ≥ 2 or ≤ -2 was employed. The proteomic data were analyzed comparing MR3, 5, & 10 days to HFD control after log transformation to achieve normality. To understand the general functional impact of MR on PVAT and aorta, Gene Ontology (GO) biological process and cellular component annotations were retrieved from Uniprot.org using ViSEAGO and GOSemSim was also used to calculate semantic similarity between enriched GO terms [351-353]. PVAT and Aorta proteomic datasets will be available at Proteome Xchange, under Project Name “LC-MS/MS of thoracic aorta and perivascular adipose tissue following short-term dietary methionine restriction” and Accesion # PXD051504.

2.2. *In vitro* methods

All methods described under Section 2.2 pertain to in vitro experiments utilized within this study.

2.2.1. Primary Cell Line Isolation

For isolation of adipose progenitor cells (APC), thoracic PVAT of both male and female 8 week old mice was freshly excised (n= 3 per sex), washed with HBSS with antibiotic/antimycotic solution (Corning, #30-004-Cl), finely minced and digested in collagenase B (Roche, Purchased from Sigma), centrifuged, and stromal vascular fraction was cultured on gelatinized plate for several days.

2.2.2. Clonal Expansion and Maintenance

Primary cell isolates were lifted from culture plates with 0.05% trypsin (450000-660, Corning#25-052-Cl) and expanded in the following incubation conditions: 37°C, 5% CO2, 95% humidity. Growth media was made with DMEM/ Ham's F12 50/50 Mix (45000-350, Corning#10-092-CV), Fetal Bovine Serum (FBS, R&D Systems #S11550H), and recombinant murine FGF-2 (Peprotech #450-33). Additional details on media components available in table 2.5

Table 2.5. Nutritional Components of Cell Culture Mediums				
	DMEM/F12 (50/50)	Methionine Depleted	Induction	Maintenance
Heat Inactivated Fetal Bovine Serum	1X	1X	1X	1X
Penicillin-Streptomycin	1X	1X	1X	1X
mouse Fibroblast Growth Factor	0.01µg/mL	0.01µg/mL	-	-
Insulin	-	-	170nM	170nM
T3	-	-	2nM	2nM
Rosiglitazone	-	-	1µM	1µM
IBMX	-	-	0.5mM	-
Dexamethasone	-	-	5µM	-
Indomethacin	-	-	125µM	-
TGFβ RI Kinase Inhibitor VI (SB)	-	-	5µM	5µM
L-Ascorbic acid 2-phosphate sesquimagnesium salt hydrate (AA2P)	-	-	50µg/mL	50µg/mL
Inorganic Salts	mg/L	mg/L		
CaCl2 (anhydrous)	116.65	116.65		
FeSO4	0.417	0.417		
Fe(NO3)3	0.05	0.05		
KCl	311.8	311.8		
CuSO4 (anhydrous)	0.0008	0.0008		
KH2PO4	--	--		
MgSO4 (anhydrous)	84.95	84.95		
NaCl	7,000	7,000		
NaH2PO4, H2O	62.5	62.5		
Na2HPO4, (anhydrous)	71	71		
Na	--	--		
NaHCO3	2,438	2,438		
ZnSO4	0.4315	0.4315		
Amino acids	mg/L	mg/L		
L-Alanine	4.45	4.45		
L-Arginine	147.5	147.5		
L-Asparagine	7.5	7.5		
L-Aspartic	6.65	6.65		
L-Cysteine	17.56	--		
L-Cystine	31.285	--		
L-Glutamic	7.35	7.35		
L-Alanyl-L-glutamine	--	--		
L-glutamine	365.1	365.1		
Glycine	18.75	18.75		
L-Histidine	31.48	31.48		
L-Isoleucine	54.37	54.37		
L-Leucine	58.95	58.95		
L-Lysine	91.35	91.35		
L-Methionine	17.24	--		
L-Phenylalanine	35.48	35.48		
L-Proline	17.25	17.25		
L-Serine	26.25	26.25		
L-Threonine	53.55	53.55		
L-Tryptophan	9.02	9.02		
L-Tyrosine, 2H2O	55.815	55.815		
L-Tyrosine,free	--	--		
L-Valine	52.85	52.85		

Table 2.5. Nutritional Components of Cell Culture Mediums (Continued)		
Vitamins	mg/L	mg/L
Biotin	0.00365	0.00365
D-Ca-Pantothenate	2.24	2.24
Choline Chloride	8.98	8.98
D-Calcium	--	--
Choline	--	--
Folic acid	2.65	2.65
i-Inositol	12.61	12.61
Nicotinamide	2.0185	2.0185
Pyridoxine	2.031	2.031
Riboflavin	0.219	0.219
Thiamine	2.17	2.17
Vitamin B12	0.68	0.68
Other	mg/L	mg/L
Dextrose	3,151	3,151
D-Glucose	--	--
Hypoxanthine,	2.385	2.385
DL-Thioctic	0.105	0.105
Methyl Lineoleate	0.044	0.044
Phenol Red	8.1	8.1
Putrescine*2HCl	0.08	0.08
Sodium Pyruvate	110	110
Thymidine	0.365	0.365
HEPES	3574.8	3574.8
Succinic acid	--	--

2.2.3. Cell Line Authentication

Following multiple passages of clonal expansion, APC exhibited an increase in proliferative capacity. To test if APC cell lines had spontaneously immortalized and to rule out contamination with another highly prolific adipose derived cell line, we submitted samples for short tandem repeat (STR) profiling through ATCC Cell Line Authentication Service (www.atcc.org). To do this, early and late passages of PVAT APC along with another highly prolific cell line were cultured, counted, spotted onto Whatman FTA cards, dried and mailed into ATCC. ATCC takes the DNA from dried samples and performs multiplexed amplification of 20 select loci with ABI Prism 3500xl Genetic Analyzer. Fragment sizes from submitted samples are compared to an allelic ladder from internal standard using Gene Mapper ID-X v1.2 software (Applied Biosystems). This analysis process is described in the National Institute of Standards

and Technology (NIST) U.S. patent (No. 9,556,482). Allelic profiles are then compared to a mouse database using the Tanabe matching algorithm to compare the number of shared alleles between the submitted sample profile and the reference profile, and results are reported as a percentage [354]. Detailed allelic profiles from STR Profiling of PVAT-APC early and late passages are shown in table 5.1

2.2.4. Custom Formulation Methionine Depleted Media

Custom formulated media free of sulfur-amino acids- methionine, cystine and cysteine, was manufactured by Corning and acquired through VWR. Depleted media was prepared with antibiotic-antimycotic solution (45000-616, Corning#30-0040-Cl), dialyzed FBS (R&D Systems #S12850), supplemented with L-methionine (Sigma, #M9625) and L-cystine (Sigma, #C7602). Nutritional components of the medias used for cell culture are shown in table 2.5

2.2.5. Induction of Adipogenesis in Adipocyte Progenitor Cells

Growth media containing DMEM/F12, FBS, antibiotic-antimycotic and murine FGF was used to expand cell populations clonally. Differentiation medium contains insulin (Cell Applications #128-100), 3,3,5-triiodo-L-thyronine sodium salt (T3, Sigma #T6397), rosiglitazone (Sigma #R2408), indomethacin (Sigma #I8280), dexamethasone (Sigma #D4902), 3-isobutyl-1-methylxanthine (IBMX, Sigma #I5879), L-ascorbic acid 2-phosphate sesquimagnesium sale hydrate (AA2P, Sigma #A8960) and SB431542 TGFβ R1 Kinase Inhibitor (Sigma #616461) and is previously formulated for robust induction of adipogenesis [355]. Concentrations for induction and maintenance media can be seen in table 2.5. Cells were incubated in induction media for 3 days followed by maintenance media for 4 days. Media was replaced every other day.

2.2.6. Lipid Accumulation Staining

To quantify intracellular lipid that accumulated during adipogenesis, mature adipocytes were fixed in 10% formalin, dehydrated with 60% isopropanol, and stained with Oil Red O solution (ORO, Sigma #O-0625). Cells were washed to remove residual stain and imaged with Zeiss Axioscope 40 microscope equipped with a Canon EOS 90D camera and 40X objective (Ph2 Plan-NEOFLUAR 40x/0,75NA). ORO stain was eluted from cells using 100% isopropanol, and absorbance of eluates was measured at 490 nm with BioTek Epoch microplate spectrophotometer and compared to an ORO standard curve in 300-12.5 ug/mL range. To normalize ORO values by cell count, nuclei were stained with Crystal Violet (CV, Harleco #192), eluted in 1% SDS and absorbance was read at 560 nm and compared to standard curve in 16-0.5 ug/mL range. Results are reported as percent lipid, which is amount of ORO relative to amount of CV.

2.2.7. DNA Synthesis Assay

APC were seeded on glass coverslips, cell proliferation was measured with Click-iT EdU Imaging kit (Invitrogen, #C10337), according to manufacturer's instructions. Proliferating cells were labeled with 10μm Edu dissolved in DMSO for 2 hours. Cells were fixed with 10% formalin at room temperature and denatured in 0.5% Triton X-100 for 20 minutes. Incorporated EdU was fluorescently labeled with Click-iT reaction containing Alexa Fluor azide (488) and total DNA was stained with Hoechst 33342. Imaging was performed with Keyence BZ-X800 fluorescent microscope and acquired 10 images per condition, with both DAPI and GFP channels. Image analysis was performed with Image J. Results are reported as a percent EdU labeled cells relative to total DAPI labeled cells.

2.2.8. Protein Synthesis Assay

To measure protein synthesis, we employed the surface sensing of translation (SUnSET) assay following a published protocol [356]. Cells were incubated with 1uM puromycin (Sigma #540411) for 30 minutes, collected with lysis buffer containing 1% SDS. Following protein quantification, denaturation and gel electrophoresis process described in immunoblot section above, protein isolates were probed with anti-puromycin antibody (Millipore Sigma, MABE343). Chemiluminescent signal was detected using Forte Western HRP substrate (Millipore). Normalized to total protein by Revert™ 520 Total Protein Stain (LI-COR, 926-10010). Imaged with Odyssey M (LI-COR) and Empiria Studio® Software was used to normalize puromycin protein incorporation to total protein. Results are reported as relative intensity (Puromycin/Total Protein).

2.2.9. Treatment with Drug Inhibitor

Cathepsin X inhibitor (Compound Z9, MedChemExpress, HY-146985) was solubilized in DMSO. Inhibitor was added to either induction media or maintenance media that was added to differentiating APC.

2.2.10. Statistics

Two-way ANOVA with Tukey's multiple comparisons test was used for longitudinal body weight in both long- and short-term studies. Unpaired student's t-tests with multiple comparisons were used for comparisons in long-term study. One-way ANOVA with Tukey's multiple comparisons test was used for short-term study. Data is represented graphically and described in results as percent difference, mean and standard error of mean (SEM). PRISM GraphPad V. 10.2.0 was used to run statistical tests and BioRender.com was used to create several figures and indicated in figure legends.

CHAPTER 3
LONG-TERM METHIONINE RESTRICTION AFFECTS CARDIOMETABOLIC HEALTH AND ADIPOSE DEPOTS IN DIFFERENT AGED MALE MICE

3.1. Overview

Methionine Restriction (MR) has been shown to extend lifespan, induce beneficial effects on metabolism and has influence over adipose tissue. Recently, we showed that MR is effective at multiple ages though out the lifespan of C57Bl/6J male mice. Age is acknowledged as a risk factor for cardiovascular and cardiometabolic disease as discussed in section 1.2.3. *The data presented within Chapter 3 are from a manuscript that was published in Obesity (Silver Spring) in January 2023 [287].*

To determine the effects of a MR diet on cardiometabolic health and other physiological features that correlate with the adipose tissue phenotype during different age phases, we studied three cohorts of C57BL/6 male mice fed a standard 0.86% methionine diet (control) or a 0.12% methionine diet (MR). The three cohorts are modeled to represent young, middle-aged, and old mice. The young cohort of mice initiated the diet at 8 weeks (2 months) of age for a duration of 52 weeks; the middle-aged cohort ("middle") initiated the diet at 52 weeks (12 months) of age for a duration of 52 weeks; and the old cohort initiated the diet at 102 weeks (23.5 months) of age for a duration of 15 weeks. The experimental timeline is depicted in Figure 3.1A.

3.2. Long-Term Methionine Restriction Prevents Age-Related Weight Gain Without Calorie Restriction in Young, Middle-Aged and Old Male Mice

Age-related weight gain was observed between the young, middle-aged, and old mice used in this study and this effect was prevented by MR intervention in all three ages. Within the first year of life, young adult mice on the control diet gained weight up to 40 weeks of age and

after that weight gain slowed until 60 weeks of age (Figure 3.1C, young). MR reduced body weight significantly compared with controls ($p < 0.05$) in the young cohort after 3 weeks of MR, which persisted throughout the end of 1 year. Middle-aged mice at 52 weeks of age had significantly higher body weight compared with 8-week-old mice ($p <0.0001$). In the middle-aged mice with MR starting at 52 weeks of age, there was a significant difference in body weight starting at 2 weeks of the intervention, compared with the control diet (Figure 3.1C, middle). The starting body weight of old mice at 102 weeks of age was also significantly greater than the middle-aged mice at 52 weeks of age ($p=0.005$). For this oldest cohort of mice, those on the MR diet had significantly lower weight than their controls after 3 weeks of dietary intervention. In all age cohorts, MR significantly reduced weight gain regardless of the age at which the MR diet was initiated (Figure 3.1C). Since young mice are still in the growth phase of their adult life, the young mice gained weight along with their control fed counterparts, however when compared to their controls, young mice MR mice experienced an 60% decrease in body mass which was significant ($p<0.0001$) (Figure 3.1D). Middle-aged MR mice experienced significant weight loss at an 139% decrease compared to the control middle-aged mice ($p<0.0001$) (Figure 3.1D). Old MR mice experienced significant weight loss at a 261% decrease compared to the control old mice ($p=0.0004$) (Figure 3.1D). These data are evidence that MR diets are effective at reducing age-related weight gain at all life stages of mice, and importantly that this weight loss occurs without modification in kilocalories consumed. Significant weight loss with MR occurred at all age phases despite mice consuming the same number of calories on average (Figure 3.1B), demonstrating that these mice are not calorie deficient. Mean food consumption was calculated in kilocalories per day with 14.8kcal±0.5 in young control mice and 14.5kcal±0.2 in young MR mice ($p=0.64$), 14.9kcal±0.4

in middle controls and 14.2kcal±0.3 in middle MR (p=0.197), and 13.5kcal±0.3 in old controls and 14.4kcal±0.4 in old MR mice (p=0.132) (Figure 3.1B).

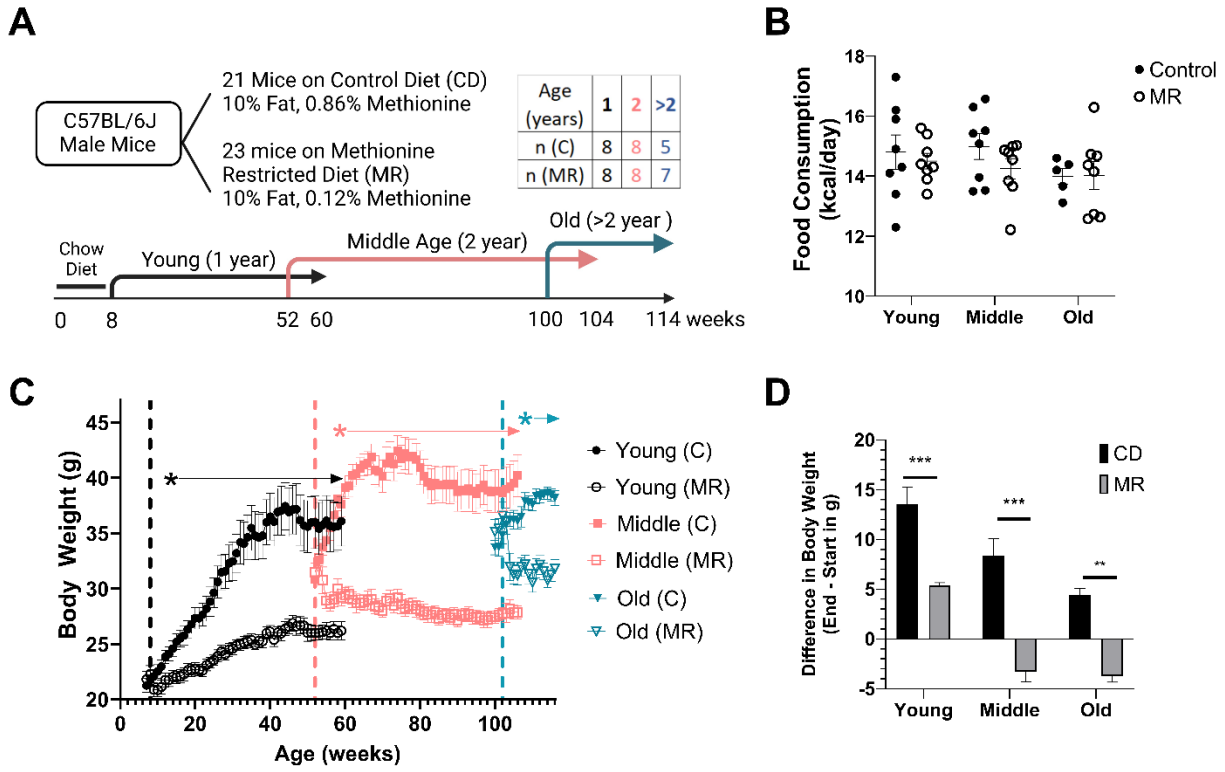

Figure 3.1. Long-Term Methionine Restriction Prevents Age-Associated Weight Gain Young, Middle-Aged and Old Male Mice Without Calorie Restriction A.) Experimental Timeline (young and middle-aged groups, n = 8/diet/age, old group, control n = 5 and MR n = 7) B.) Food consumption expressed as average kilocalories per day, graphed are mean ± SEM C.) Body weight (BW) of C57BL/6J male mice fed a control or MR diet over a 52- or 15-week period. First significant comparisons are depicted with asterisks and continue throughout duration of experiment and is depicted with arrow. Asterisk and arrow colors correspond to age group. D.) Change in BW over the course of dietary intervention. Values shown are mean ± SEM, with only significant p values indicated as * = p <0.05, ** = p<0.005, *** = p<0.0001

3.3. Long-Term Methionine Restriction Improves Metabolic Health at All Ages

Metabolic dysfunction is increasing in prevalence and an important underpinning of a myriad of health conditions. Analysis of fasting plasma shows that at all ages MR mice displayed an improved metabolic profile compared to controls. There are significant improvements in glucose homeostasis after MR, shown by glucose, insulin, and HOMA-IR (Figure 3.2A,B,C). In

young mice, fasting blood glucose was 116mg/dL±13 for control and 93mg/dL±14 for MR fed groups, a decrease of 19% with p =0.006. In middle-aged mice, fasting blood glucose was 116mg/dL±21 for control and 102mg/dL±12 for MR fed groups, a decrease of 12% however, was not significant with p=0.143. In old mice, fasting blood glucose was 111 mg/dL±9 for control and 91mg/dL ±11 for MR fed groups, a decrease of 17% with p=0.009 (Figure 3.2A).

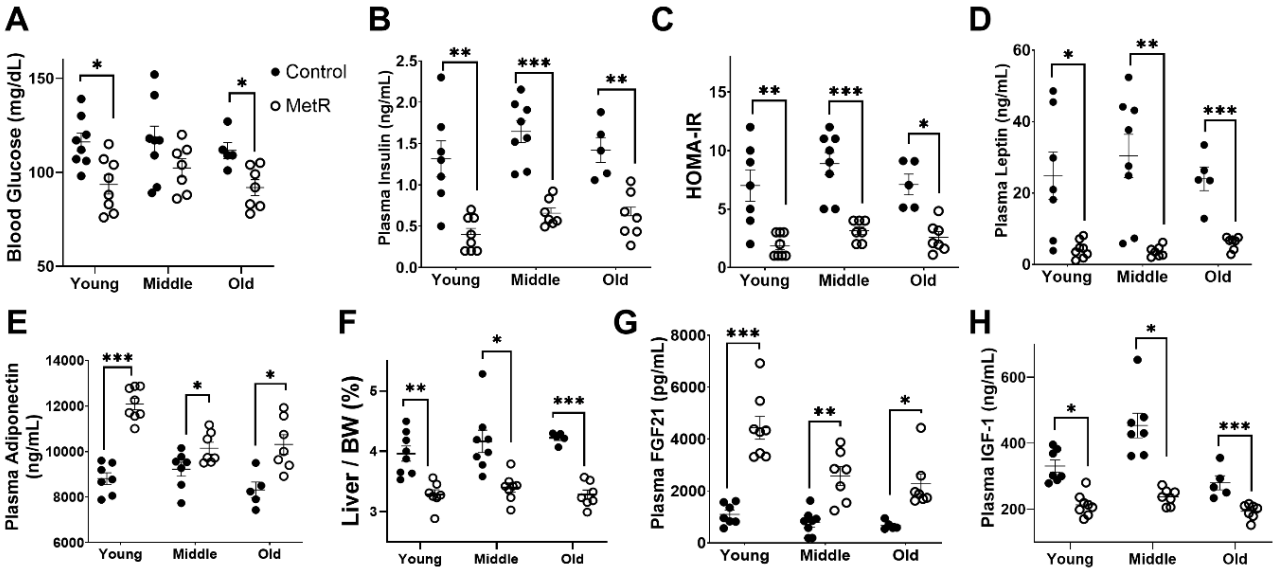

Figure 3.2. Long-Term Methionine Restriction Promotes Metabolic Health at All Ages A.) Fasting Blood Glucose (mg/dL) B.) Fasting Plasma Insulin (ng/mL) C.) Homeostatic Model Assessment for Insulin Resistance (HOMA-IR) D.) Fasting Plasma Leptin (ng/mL) E.) Plasma Adiponectin (ng/mL) F.) Liver weight divided by body weight (BW), represented as a percentage G.) Plasma Fibroblast growth factor (FGF21) (pg/mL) H.) Plasma Insulin-like growth factor (IGF-1) (ng/mL) Young & middle-aged groups, n = 8/diet/age, old group, control n = 5 and MR n = 7. Values shown are mean ± SEM, with only significant p values indicated as * = p <0.05, ** = p<0.005, *** = p<0.0001

For fasting plasma insulin, young mice had levels of 1.3ng/mL±0.2 for control and 0.4ng/mL±0.07 for MR fed groups, a decrease of 68% with p=0.001. In middle-aged mice, plasma insulin was 1.6ng/mL ±0.13 for control and 0.6ng/mL±0.06 for MR fed groups, a decrease 60% with p <0.0001. In old mice, plasma insulin was 1.4ng/mL±0.15 for control and 0.6ng/mL±0.1 for MR fed groups, a decrease of 55% with p=0.001 (Figure 3.2B). HOMA-IR

particularly shows that on average all three cohorts experience improved insulin sensitivity upon MR diet. For HOMA-IR young mice had a ratio of 7.0±1.3 for control and 1.8 ±0.3 for MR fed groups, a decrease of 73% with p =0.0001. In middle-aged mice, HOMA-IR was 8.8±0.9 for control and 3.1 ±0.3 for MR fed groups, a decrease of 66% with p =0.0001. In old mice, HOMA-IR was 7.0±0.8 for control and 2.5±0.4 for MR fed groups, a decrease of 63% with p =0.0006 (Figure 3.2C). These data together suggest that mice fed long-term MR diet experience significantly improved glucose homeostasis in young, middle, and old age.

Improved weight levels, specifically adiposity, is reflected in the significantly decreased leptin levels (Figure 3.2D) There is a wide range of leptin in control animals, which suggests that the level of adiposity varies greatly between mice in the same cohort. This variability is greatly reduced by MR diet and shows the ability of MR diet to regulate hunger suppression through leptin. For plasma leptin, young mice had levels of 24ng/mL±6.6 for control and 4.2ng/mL ±0.8 for MR fed groups, an 82% decrease with p =0.005. In middle-aged mice, plasma leptin was 30ng/mL ±6.0 for control and 3.6ng/mL ±0.5 for MR fed groups, an 87% decrease with p =0.001. In old mice, plasma leptin was 23ng/mL ±3.3 for control and 6.0ng/mL ±0.6 for MR fed groups, a 74% decrease with p <0.0001 (Figure 3.2D).

Adiponectin is another adipokine reflective of overall metabolism, which acts on many different organ systems to control energy expenditure, lipid and glucose metabolism and more. The significant increase in adiponectin after long-term MR diets in all ages, is another reflection of the metabolic therapeutic potential of this diet (Figure 3.2E). For plasma adiponectin, young mice had levels of 8811ng/mL±253 for control and 12087ng/mL±250 for MR fed groups, an increase of 37% with p <0.0001. In middle-aged mice, plasma adiponectin was 9222ng/mL±310 for control and 10148ng/mL±258 for MR fed groups, an increase of 10%

with p =0.04. In old mice, plasma adiponectin was 8315ng/mL±346 for control and 10312ng/mL±428 for MR fed groups, an increase of 24% with p =0.006 (Figure 3.2E).

Liver mass was increased with age and significantly decreased by MR compared with age-matched controls and this trend continued when in proportion to total body weight (Figure 3.2F). In young mice, there was a 41% decrease in absolute liver mass with MR; with 3.9±0.12 percent liver mass to body weight for control and 3.2%±0.08 for MR fed groups, with p <0.0001. In middle-aged mice, there was also a 41% decrease in absolute liver mass with MR; with 4.1±0.18 percent liver mass to body weight for control and 3.4%±0.07 for MR fed groups, with p = 0.001. In old mice, there was a 35% decrease in absolute liver mass with MR; with 4.2±0.04 percent liver mass to body weight for control and 3.2%±0.07 for MR fed groups, with p < 0.0001. In all age groups, secretion of FGF21 (Figure 3.2G) was significantly increased with MR and IGF-1 (Figure 3.2H) was significantly decreased with MR. In young mice, mean FGF21 was increased by 304% by MR, with 1096pg/mL±154 for control and 4431pg/mL±437 for MR fed groups (p <0.0001). In middle-aged mice, mean FGF21 was increased by 230% by MR 778pg/mL±166 for control and 2573pg/mL±367 for MR fed groups (p = 0.0004). In old mice, mean FGF21 was increased 239% by MR, with 668pg/mL±74 for control and 2270pg/mL±380 for MR fed groups (p = 0.005). In young mice, IGF-1 was 330ng/mL±18 for control and 213ng/mL±12 for MR fed groups, a 35% decrease with p=0.0001. In middle-aged mice, IGF-1 was 453ng/mL±37 for control and 237ng/mL±9 for MR fed groups, a decrease of 47% with p = 0.0001. In old mice, IGF-1 was 279ng/mL±21 for control and 193ng/mL±8 for MR fed groups, a decrease of 30% with p =0.001.

3.4. Early Initiation of Methionine Restriction Induces Browning of White Adipose Tissues of Young Mice

Due to the drastic improvements in metabolic markers, specifically adipokines -leptin and adiponectin, we chose to investigate the impact on adipose depots. White adipose depots have the potential to increase in thermogenic capacity, or to beige. We studied two of these adipose depots, inguinal white adipose tissue (iWAT) and retroperitoneal adipose tissue (rpWAT), using the young cohort that was fed the MR diet until 60 weeks of age. Immunoblot of iWAT (Figure 3.3A,B) showed a 9-fold increase in levels of the thermogenic marker UCP1 and 3.5-fold increase in levels of COXIV in MR mice compared with controls, indicative of an improved metabolic phenotype in a depot able to undergo beiging [357]. Indicative of a change in lipogenic/lipolytic balance in mature adipocytes, PLIN1 was 50% lower in MR (8.2±2.3) iWAT compared with controls (16.4±1.7, $p = 0.02$), which suggests a reduction in adiposity common with MR. Activation of the Notch signaling pathway was previously identified by our lab to induce a whitening phenotype in PVAT, thus members of this pathway were further explored in these depots [358]. Notch1 was 70% lower in MR (1.5±0.36) iWAT compared with controls (4.9±0.58, $p < 0.001$) and hes family bHLH transcription factor 5 (HES5) was 28% lower in MR (16.6±1.5) iWAT compared with controls (22.85±1.5, $p=0.01$).

In rpWAT, immunoblot (Figure 3.3 C,D) showed a similar trend in decrease in whitening marker PLIN1, which was 76% lower in rpWAT from MR (0.008±0.002) mice compared with controls (0.03±0.0007, $p<0.001$). Another hallmark of whitened adipose is immune cell infiltration and a marker that is often associated with the involvement of monocytes/ macrophages is cluster of differentiation 68 (CD68). CD68 was 80% lower in rpWAT from MR fed mice (0.0003±3x10-5) diet compared with controls. (0.001±2x10-4, $p<0.001$). Members of

the Notch family responded similarly to MR in rpWAT with Notch2 79% lower in the MR group (0.0004±0.00004) compared with controls (0.002±0.0003, $p<0.001$), however changes in Notch1 and HES5 were not statistically significant between groups.

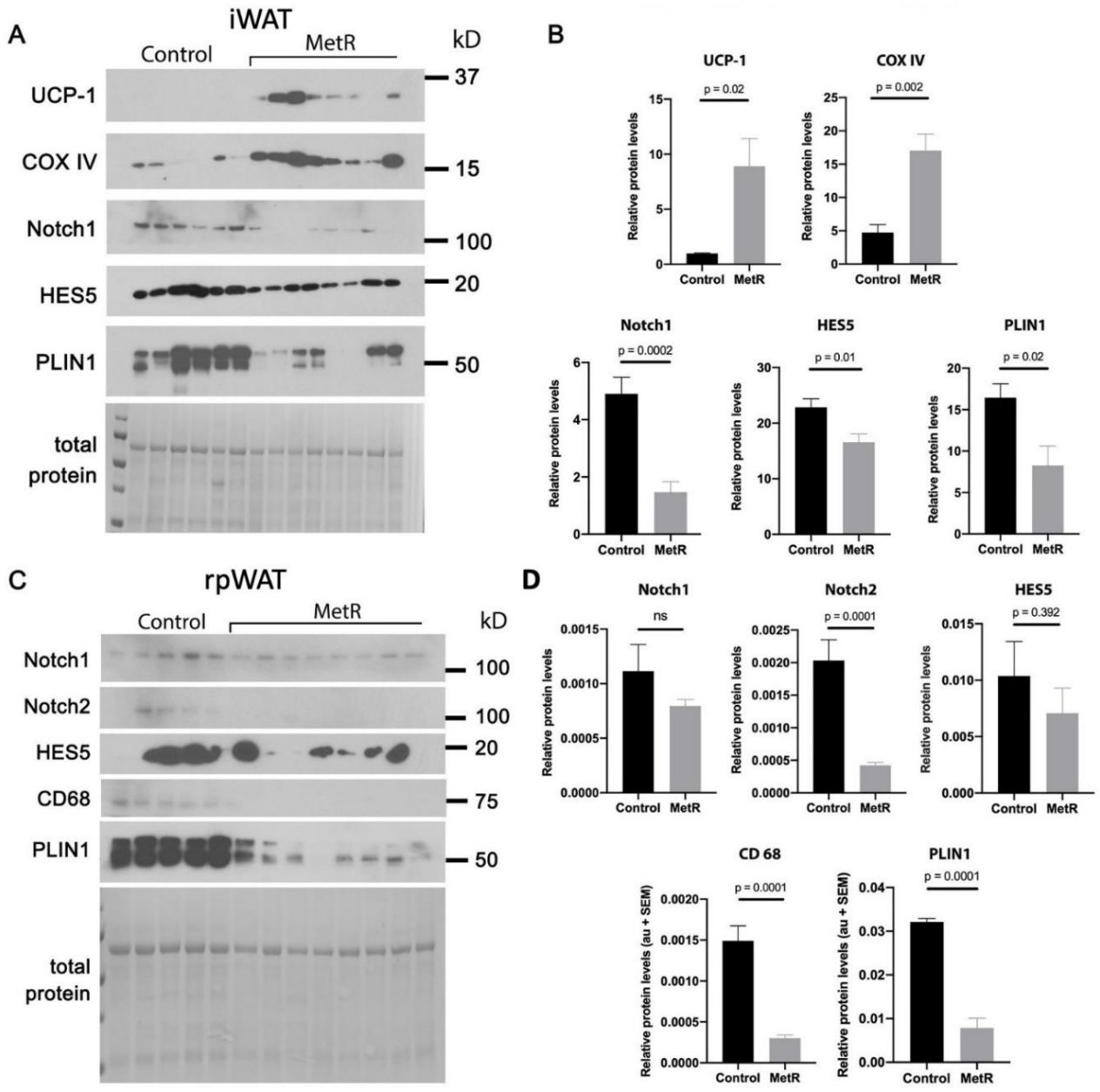

Figure 3.3. Early Initiation of Long-Term Methionine Restriction in Young Mice Increases White Adipose Tissue Capacity to Beige Immunoblot analysis was used to quantify thermogenic markers and Notch signaling components in the young cohort from tissues collected at 60 weeks of age from (A, B) inguinal white adipose tissue (iWAT) or (C, D) retroperitoneal white adipose tissue (rpWAT) derived from control or MR mice (n = 8/group). Band intensities were normalized to total protein and represented as relative difference between experimental groups. Values graphed are mean ± SEM, with p values indicated, ns - not significant;. CoxIV, cytochrome c oxidase subunit IV; HES5, hes family bHLH transcription factor 5; PLIN1, perilipin-1; UCP1, uncoupling protein 1

3.4.1. Early Initiation of Methionine Restriction Increases Thermogenic Proteins and Decreases Adipogenic Proteins in Divergent Adipose Depots

Since MR is known to increase adipose tissue browning, we examined several markers associated with thermogenic function in adipose. We chose to assess these markers in both perigonadal adipose tissue (gWAT) and interscapular brown adipose tissue (BAT), which are recognized to exhibit opposite phenotypes and contribute to pathology in different manners. There was no difference between control and MR groups for PGC1α, the master regulator of mitochondrial biogenesis. PGC1α was undetectable in gWAT which demonstrates stark contrast to BAT (Figure 3.4A,B). UCP1 demonstrated a significant increase ($p=0.016$) in BAT from MR mice when compared with controls, and to further display contrast between the two depots, as with PGC1α, UCP1 was similarly absent in all gWAT samples. COXIV, the terminal enzyme of the mitochondrial electron transport chain, demonstrated depot-specific expression similar to PGC1α. There was no significant difference in MR BAT or gWAT compared with their respective controls; however, COXIV levels were negligible in gWAT samples in comparison to BAT. In MR mice, GRP75 increased by 25% although not significant ($p=0.066$) in comparison to controls. Conversely, GRP75 expression was 35% less than controls in MR gWAT (Figure 3.4C,D).

Assessment of adipogenic markers in BAT and gWAT displayed expected characteristic protein expression profiles. Peroxisome proliferator-activated receptor gamma (PPARγ) and CCAAT/enhancer-binding protein alpha (C/EBPα) are important regulators of adipogenesis. PPARγ was unchanged in gWAT while BAT from MR mice demonstrated a 26% increase in controls however this was not statistically significant. C/EBPα trended upward in gWAT of MR mice, and 33% lower in BAT of MR mice, a significant decrease ($p=0.015$) when

compared with controls (Figure 3.4C,D). PLIN1 showed a significant reduction (p=0.048) in BAT of MR mice, with a decrease of 27% compared with controls. A decrease of 16% in PLIN1 was seen in gWAT of MR mice compared with controls, however it did not reach statistical significance. Interestingly, levels of PLIN1 in BAT were higher in both control and MR than gWAT. Fatty acid-binding protein 4 (FABP4) showed no significant difference in either BAT or gWAT for MR mice compared with controls, However, FABP4 demonstrated differences between depots and as expected was substantially higher in gWAT (Figure 3.4 C,D). We also examined markers associated with the inflammatory phenotype of adipose that are positively correlated with body mass. Cluster of differentiation molecule 11b (CD11b), also known as Mac-1, integrin alpha-M (ITGAM), and complement receptor type 3 (CR3), is frequently used as a macrophage marker and indicator of inflammation. When compared with controls, gWAT of MR mice showed a significant decrease of 65% (p=0.001) in CD11b. In contrast, levels of CD11b were undetectable in either control or MR BAT (Figure 3.4 E,F). Of the Notch signaling pathway, both Notch1 and Notch2 levels in BAT from mice on the MR diet were significantly less than controls, at 42% decrease (p=0.014) and 37% decrease (p=0.008), respectively (Figure 3.4 E,F). Interestingly, the opposite effect was seen in gWAT, with Notch1 demonstrating a significant 4-fold increase (p=0.038) with MR compared with controls and Notch 2 trending upward with a 1.8-fold increase which was not statistically significant. Consistent with Notch1 and Notch2 results, downstream Notch signaling pathway member HES5 slightly increased in both BAT and gWAT with MR (6% and 4%, respectively) when compared with controls. Again, indicative of a depot-specific response, levels of all Notch signaling pathway members were consistently higher in gWAT compared with BAT.

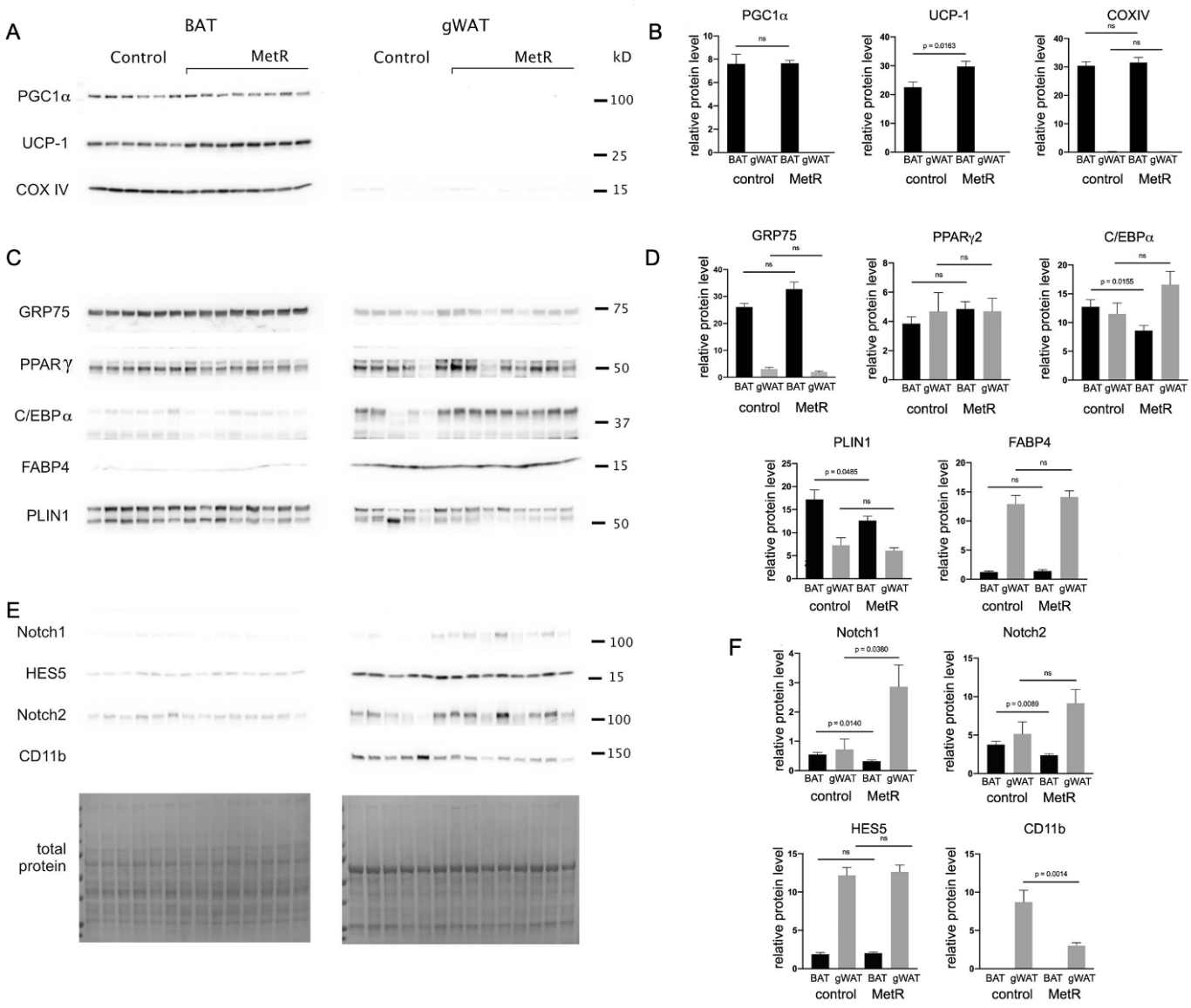

Figure 3.4. Early Initiation of Long-Term Methionine Restriction in Young Mice Increases Mitochondrial Protein Abundance in Brown Adipose Tissue (A, C, E) Immunoblot analysis was performed using brown adipose tissue (BAT) and perigonadal white adipose tissue (gWAT) from the young cohort fed control or MR diet for 1 year (n = 8/diet). Representative samples from each experimental group are shown. Band signals were normalized to total protein, and relative differences for each adipose tissue and each protein are shown in panels B, D, and F. Graphed are mean ± SEM. P values for comparisons are shown for group values that were significantly different. ns, not significant. C/EBPα, CCAAT/enhancer-binding protein alpha; CoxIV, cytochrome c oxidase subunit IV; FABP4, fatty acid-binding protein 4; GRP75, glucose-related protein 75; HES5, hes family bHLH transcription factor 5; PGC1α, peroxisome proliferator-activated receptor gamma coactivator 1-alpha; PLIN1, perilipin-1; PPARγ, peroxisome proliferator-activated receptor gamma; UCP-1, uncoupling protein 1

3.5. Long-Term Methionine Restriction Prevents Lipid Accumulation in Perivascular Adipose Tissue in Young, Middle, and Old Age

The normal process of aging increases lipid accumulation in adipose tissue, including PVAT. We have reported that amount of lipid that accumulated in the PVAT ranges from ~50%-56% in 12–14-week-old C57Bl/6J mice fed a standard diet [358]. Here we show that one-year-old mice on the control diet have PVAT with ~57%-62% lipid (Figure 3.5A,C).

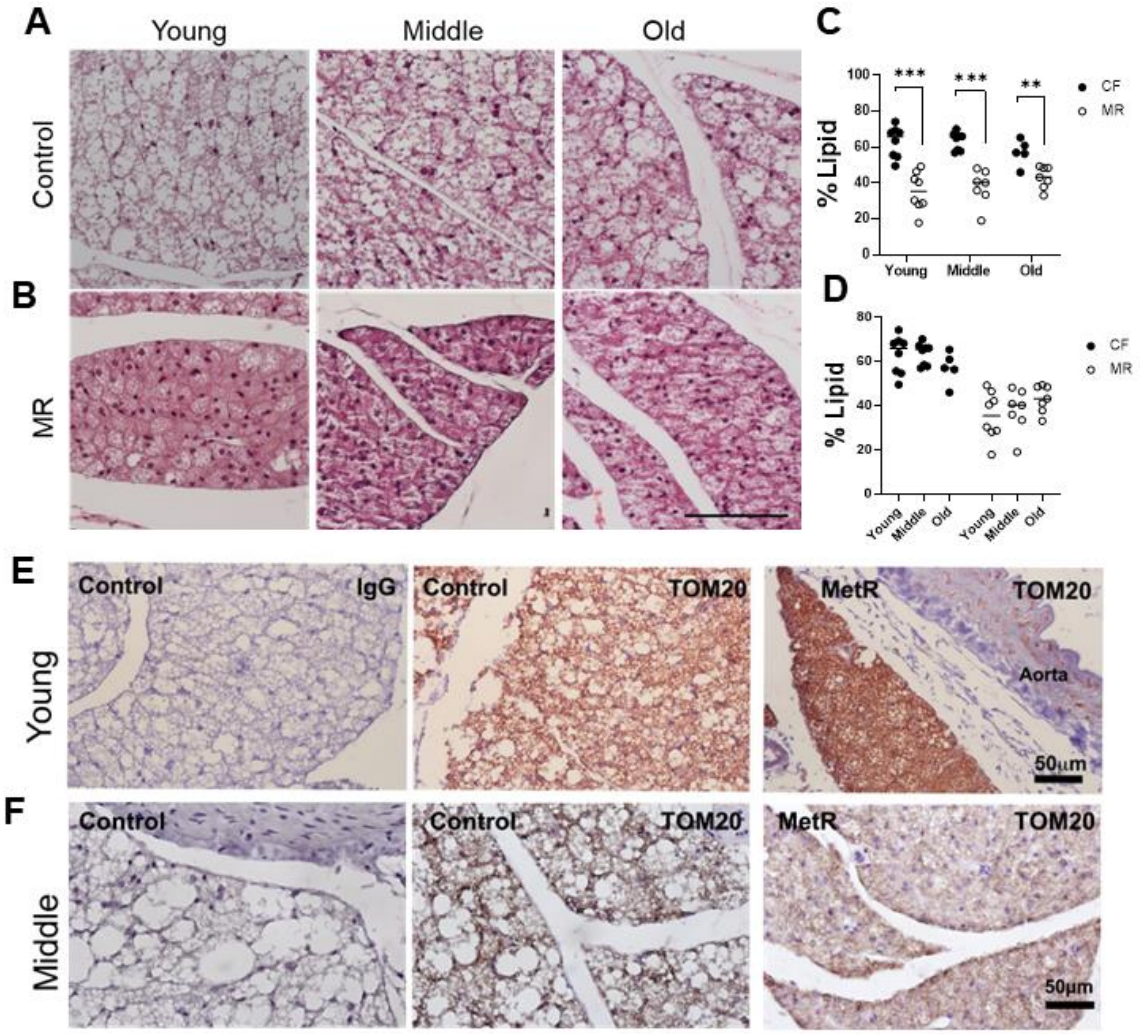

Figure 3.5. Long-Term Methionine Restriction Prevents Lipid Accumulation in Young, Middle, and Old Age Representative hematoxylin and eosin stains show PVAT morphology in A.) control mice and B.) MR mice for the different age cohorts. Scale bar (100 μm) represents all images. The relative amount of lipid region in PVAT was quantified, shown as a percentage. C.) Diet group comparisons and D.) age group comparisons are shown. E.) PVAT sections from the young cohort at 60 weeks of age or F.) middle-aged cohort at 104 weeks of age were immunostained to detect the mitochondrial marker TOM20. Scale bar = 50 μm. TOM20, translocase of outer mitochondrial membrane 20. Mean values shown are mean, with only significant p values indicated as * = $p < 0.05$, ** = $p < 0.005$, *** = $p < 0.0001$

This demonstrates that between the ages of ~12 weeks to 52 weeks, there is an increase in PVAT lipid, similar to the weight gain experienced in this age group regardless of control or MR diet. While the trend is not significant, PVAT does not continue to increase the amount of lipid accumulation as age increases into middle and old age, as shown in Figure 3.5D.

Interestingly, while we do not see an increase in PVAT lipid accumulation after one year of age in control fed mice, we do see that the mice fed a MR diet have significantly decreased PVAT lipid accumulation (Figure 3.5B,C). This significant decrease in PVAT lipid accumulation is consistent across young, middle, and old mice (Figure 3.5B,C). Specifically, the mean PVAT lipid content after consuming the MR diet in young mice is decreased by 43% (Figure 3.5C) and the response to MR is consistent in middle (40% decrease) and old age mice (24% decrease).

3.6. Lean Phenotype in Perivascular Adipose Tissue is Associated with Increased Expression of Mitochondrial Proteins in Young Mice

To accompany the lean phenotype observed after MR diets in young, middle-age and old age we evaluated levels of additional mitochondrial proteins, which is a possible explanation for the decrease in lipid accumulation. Increased mitochondrial content was measured by immunostaining of TOM20, translocase of outer mitochondrial membrane 20, and observed to be increased in young animals on MR diet (Figure 3.5E). TOM 20 does not appear to be increased in middle-aged animals on MR diet (Figure 3.5F). When comparing MR animals in the young cohort to the middle cohort, it appears that middle-age had lower levels of TOM20.

This loss of lipid content following MR diet is consistent with immunofluorescence staining of lipid protein, PLIN1, which is decreased in both young and middle-aged mice after MR (Figure 3.6 A,B,C – Perilipin-1). The increase in mitochondrial proteins in young mice

following MR is also consistent in immunofluorescence staining of UCP1, GRP75, and COXIV. All these proteins are increased in young mice after MR; a trend which is lost in middle-aged mice (Figure 3.6 A,B,C – UCP1, COXIV, GRP75). Noteworthy, in young animals after MR there is a decrease in PGC1α, which is indicative of a decrease in mitochondrial biogenesis. This suggests that in response to MR there may not be an increase in the amount of mitochondria, and in comparison to the stark increase in COXIV, that there is potentially an increase in mitochondrial respiratory activity. Due to the decrease in lipid content that is accompanied by increase in mitochondrial markers, young animals on MR diet can be associated with an increased thermogenic phenotype. While the decrease in lipid content also occurs in middle age, there is a decrease in mitochondrial markers, which suggests that decrease in lipid content is due to a process that is mitochondrial independent.

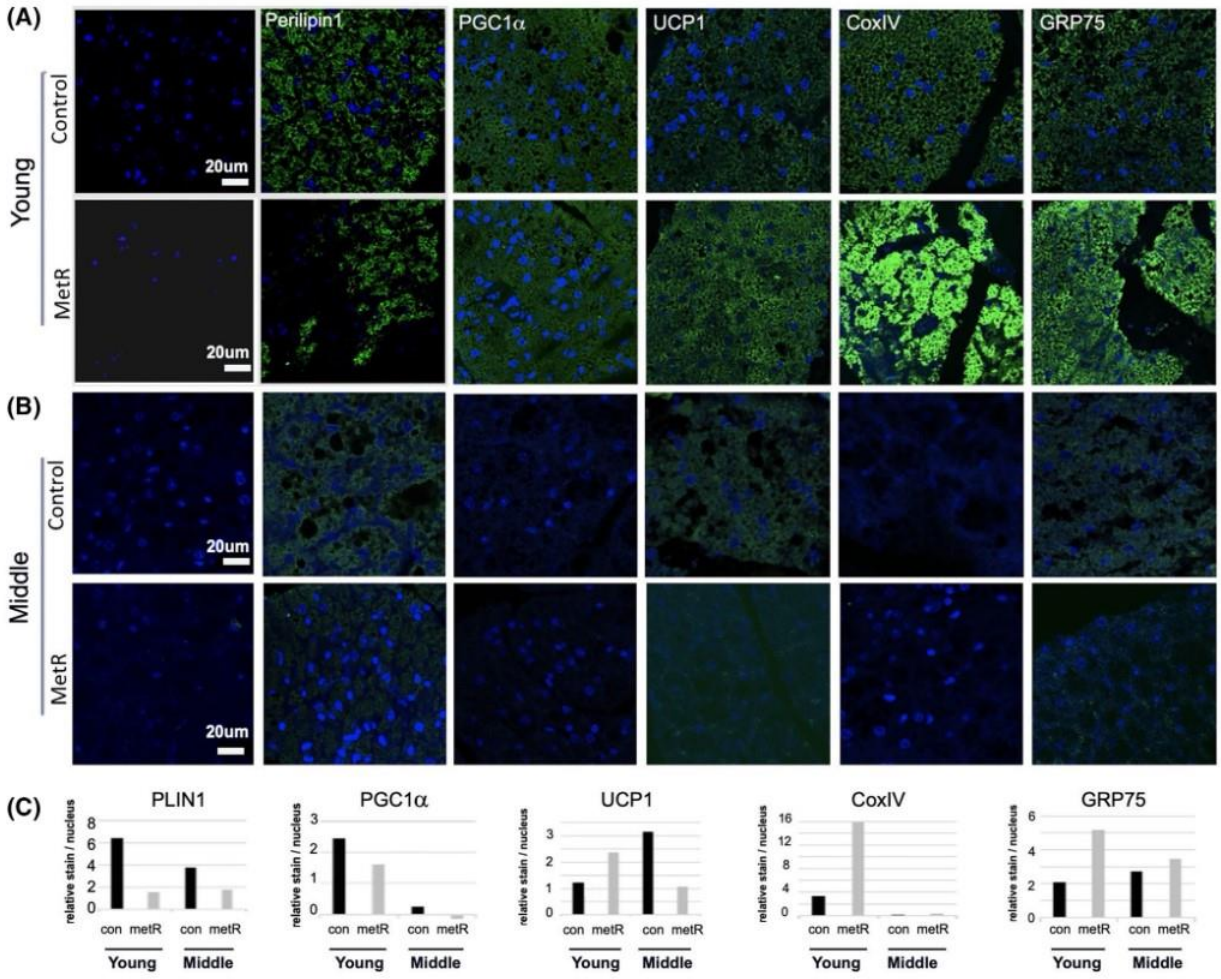

Figure 3.6. Early Initiation of Long-Term Methionine Restriction Affects Thermogenic Phenotype of Perivascular Adipose Tissue Immunofluorescence staining of adipocyte and thermogenic markers. Representative images of PVAT of mice A.) Young cohort at 60 weeks of age and B.) from the middle-aged cohort at 104 weeks of age C.) Quantification of fluorescence; y-axis is normalized relative abundance (raw density of fluorescence divided by number of DAPI stained nuclei). Far left image is control IgG image in which relative abundance of specific antigens were normalized. Scale bar = 20 μm. CoxIV, cytochrome c oxidase subunit IV; GRP75, glucose-related protein 75; PGC1α, peroxisome proliferator-activated receptor gamma coactivator 1-alpha; PLIN1, perilipin-1; UCP1, uncoupling protein 1

3.7. Long-Term MR does not Influence Vascular Morphology

Since we observed a stark lean phenotypic conversion of PVAT in response to MR, we also evaluated the effect of MR on thoracic aorta morphology. We measured the total vessel area, as well as lumen area and then subtracted the lumen from the total to acquire the medial area. While we did not observe any significant differences between any of the age groups or upon MR intervention, there is a downward trend in middle and old groups upon MR. Interestingly, vessel area in young mice does not have this downward trend in response to MR. These results may be influenced by the dramatic loss of weight in response to MR, and vessel size may be due to the smaller overall body size of mice fed long-term MR.

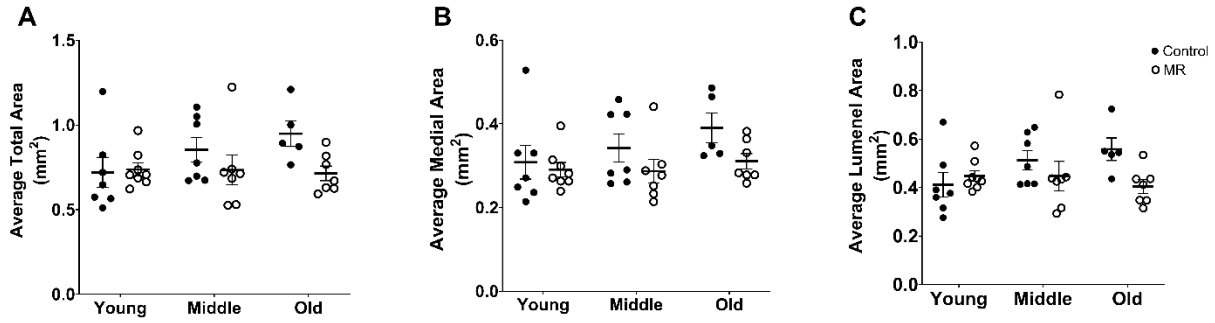

Figure 3.7. Long-Term Methionine Restriction Does Not Influence Thoracic Aorta Morphology Quantification of aortic morphology are shown as A.) total area B.) medial area, and C.) lumenal area. Values shown are mean ± SEM, with only significant p values indicated

3.8. Conclusions

As described in detail in section 1.9-1.14, methionine restriction has been shown to improve health span of mice by lowering weight gain and adiposity, increasing insulin sensitivity, decreasing accumulation of homocysteine, which collectively ultimately decrease the risk of cardiovascular and cardiometabolic disease. With this study, we expanded our understanding of how far the benefits of MR range in aging mice using young, middle, and old aged mice. We show that age-related weight gain is decreased by long-term MR diet, and this

benefit is extended to important cardiometabolic parameters that determine cardiovascular disease risk. The reduction in fasting blood glucose and plasma insulin are consistently improved in all age groups and are further supported by improved HOMA-IR ratio that is used clinically to assess insulin resistance. Secretion of hepatokines and adipokines are improved and correlate with MR-induced weight loss. MR displayed adipose depot specific effects, with iWAT and BAT experiencing increased browning, and iWAT and rpWAT experiencing decreased protection from lipolysis.

We demonstrated that MR prevents age-related weight gain and lipid accumulation in PVAT from the thoracic aorta while improving physiological health at three different age phases in the mouse: mature young adult, middle-aged adult, and old adult. These data show that, whereas the lipid content of PVAT was correlated with body weight and markers of metabolic health, the MR-induced increase in thermogenic markers was seen in PVAT only from the young cohort, not the middle-aged cohort. The primary finding from this study is that the largest effects of MR on PVAT occur when the diet is initiated in young adult mice. We also measured thoracic aorta morphology in response to MR and did not observe any significant changes in total area, medial area or lumenal area. The change in body size may not result in significant differences in vessel morphology, however this may be influencing PVAT through changes in mechanical force and cytoskeleton tensions [359, 360].

3.9. Study Limitations

The use of only males in this study is a very important limiting factor in the translational impact of this work and will be further discussed in section 6.7.1.

The lack of body composition data, like magnetic resonance imaging (MRI) or dual-energy x-ray absorptiometry (DEXA) scans, hinders the ability to assess whole body

composition. Loss of lean mass or prevention of growth has been observed with 80% MR[293] and could be a major factor in dramatic weight loss; however, this cannot be evaluated with the data collected. There was no assessment of adipose tissue mass as they were dissected, which could have been used as a proxy to estimate the amount of weight loss that was due to loss of adiposity.

Several adipose tissues, rpWAT, iWAT, BAT, and gWAT, that were assessed in the young cohort were not collected from the middle-aged and old mice to compare other adipose depot specific effects. This is limiting the ability to make conclusions on adipose depot-specific age-related responses to MR.

The amount of PVAT that can be collected from mice is limited for downstream analyses. This was especially limited following long-term MR due to tissue size. Figures 3.5 and 3.6 are data generated from fixed PVAT of all the animals, and due to different tissue preservation techniques required for different analytical endpoints, only one preservation technique is possible with the small tissue size of PVAT. Examples of other analyses that could have been performed if there were more tissue available or more animals included in the study are RT-qPCR for gene expression, Western Blots for protein abundance, conditioned media from whole tissue for adipokine secretion. It is important to note that our findings are limited to PVAT of thoracic aorta since there are known phenotypic differences in PVAT based on anatomical location as discussed in section 1.5.4.3.

The lack of functional data impedes making conclusions on if MR results in true functional differences in systemic or tissue specific function. Functional studies like Seahorse Flux assay for cellular bioenergetics or indirect calorimetry to assess if mitochondrial function is

changed by MR in different age groups within PVAT and thoracic aorta cells are relevant to this work.

3.10. Future Directions

Determining if MR alters depot-specific secretion of adipokines would contribute substantially to understanding the effects of MR on adipose tissue. This could be done by dissecting whole tissues and assessing the secretion of adiponectin or leptin from conditioned media or performing proteomics on the secretome of whole tissue. Mature adipocytes or adipose progenitor cells can be isolated directly from tissue of mice fed MR to test gene expression. Another direction that is necessary to uplift the body of MR research is understanding the effects of MR on vascular physiology in different ages. While we did not observe any morphological changes in thoracic aorta by measuring the vessel area, other techniques could be applied to assess the effect of MR on vessel function. This could be done using wire myography to measure vessel contractile or dilative capacity, or by assessing organization of smooth muscle cells through staining or visualization of different molecular markers important for vascular structure such as smooth muscle actin or filamin A. Furthermore, isolating aortic vascular smooth muscle cells and measuring rates of proliferation in different age groups could be implemented in the future to understand vascular smooth muscle response to MR at different age phases.

3.11. Elucidating Early Mechanisms of Methionine Restriction in Perivascular Adipose Tissue

The estimated requirement for dietary methionine intake is age-dependent [147] and with the data collected, we have concluded that young animals have the most robust response to MR. This effect may be due to the young animals having the highest requirement for methionine as they are still in a growth phase. Illuminating early mechanisms of MR in PVAT could be

targeted pharmaceutically and used to initiate beneficial effects without the use of dietary intervention and impacting developmental pathways that are methionine dependent.

CHAPTER 4
SHORT-TERM METHIONINE RESTRICTION COUNTERACTS ADVERSE CARDIOMETABOLIC EFFECTS OF DIET-INDUCED OBESITY IN MALE MICE

4.1. Overview

Obesity is acknowledged as a risk factor for cardiovascular and cardiometabolic disease as discussed in section 1.2.4. Methionine restriction (MR) has been shown to improve cardiometabolic health, reduce body weight, by specifically targeting adiposity, as discussed in section 1.11. Previously, we showed the benefits that occur with long-term MR in C57Bl/6J male mice, however few studies look at short-term MR diet. As described in section 1.14, most described as "short-term" durations of MR are within 8-14 weeks [361-363]. Here, we consider "short-term" 10 days or less of MR diet. *The data presented within Chapter 4 are from a manuscript that will be submitted to Elsevier journal, Molecular Metabolism in May 2024.*

To determine if a short-term MR diet affects obesity and improves cardiometabolic health and perivascular adipose tissue (PVAT) phenotype during diet-induced obesity, we studied 4 cohorts of C57BL/6 male mice fed a 60% high fat diet (HFD) till they were obese (>45g), and then kept one cohort on the HFD diet that contains 0.86% methionine diet and the other 3 cohorts on a HFD that contains 0.12% methionine diet (HFD-MR) for 3, 5, or 10 days. The experimental timeline is depicted in Figure 4.1A.

4.2. Short-Term Methionine Restriction Results in Weight-Loss in Obese Male Mice Without Calorie Restriction

To assess if a short-term MR diet can effectively improve cardiometabolic health and decrease body weight during diet-induced obesity, we fed male C57BL/6J mice a MR diet for 3, 5, and 10 days. Despite 60% HFD-induced obesity and continuing to consume HFD, immediate weight loss occurred upon initiation of MR diet and was continuous throughout the study (Figure

4.1C). Significant weight loss was observed by day 10 of MR diet compared to HFD-control (p=0.002). Obese mice lost an average of 3.1% (1.4g±0.2, p=0.001) of their total body weight in 3 days of MR, 7.5% (3.3g±0.3, p<0.0001) in 5 days of MR, and 15.5% (7.0g±0.9, p<0.0001) in 10 days of MR, while the group that continued standard HFD gained 3.9% (1.7g±0.4) in total body weight (Figure 4.1D).

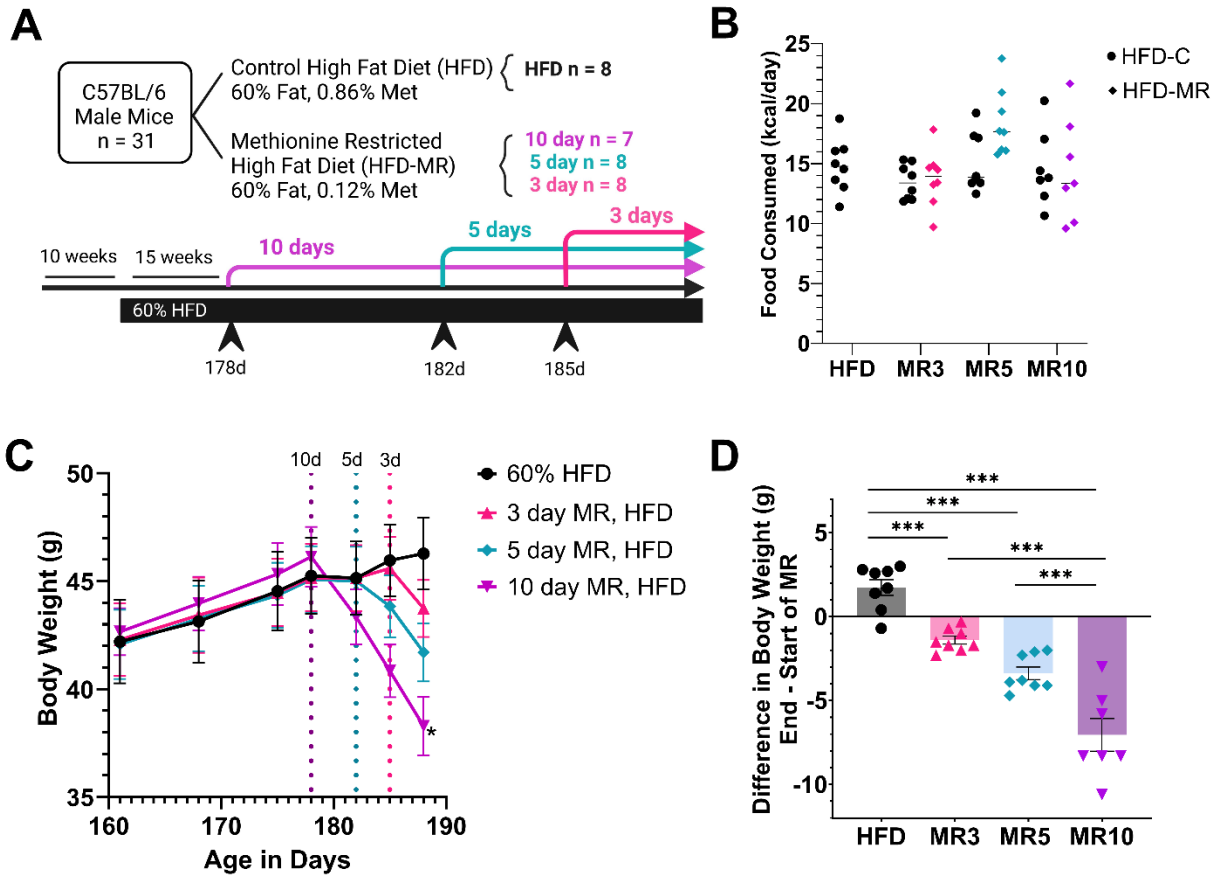

Figure 4.1. Short-Term Methionine Restriction Results in Weight-Loss in Obese Male Mice Without Calorie Restriction A.) Experimental Timeline, control high fat diet (black, n = 8), MR3 (n = 7, pink), MR5 (n = 8, teal), MR10 (n= 7, purple) B.) Food consumption expressed as average kilocalories per day, mean values are shown indicated C.) Total body weights measured longitudinally from 161 days of age to the end of experiment. Dotted lines represent start of methionine restricted diet, Age of animals at start of MR diets; MR10=178 days, MR5=182 days, and MR3=185 days D.) Change in body weight over the course of the dietary intervention. HFD – black circles, MR3 – pink upward triangles, MR5 – teal diamonds, MR10 – purple downward triangles. Values shown are mean ± SEM, with only significant p values indicated as * = p <0.05, ** = p<0.005, *** = p<0.0001

These animals consumed a similar amount of food while on 3, 5, or 10 days of MR (13.7kcal/day±0.8, 18.4kcal/day±0.9, 14.4kcal/day±1.6) as compared to consumption of the standard HFD (13.4kcal/d±0.5, 15.0kcal/day±0.8, 14.5kcal/day±1,1), none of which were statistically significant (Figure 4.1D). Take altogether, even though mice were obese and continuing to consume a 60% HFD, mice fed a MR diet lost a significant amount of weight while their control fed counterparts gained weight. These data show that MR diets are effective at reducing body weight in short durations without reducing calorie consumption.

4.3. Short-Term Methionine Restriction Improves Metabolism Despite Diet-Induced Obesity

To assess if short-term MR affects glucose metabolism, fasting blood glucose and plasma insulin levels were measured. Blood glucose level in HFD control group was elevated from normal in healthy mice [364] (157mg/dL±8.3) and when comparing to HFD control there was a significant decrease of 25% in MR3 (117mg/dL±3.4, $p=0.0004$), 35% in MR5 (102mg/dL±6.4, $p<0.0001$), and 49% in MR10 (80mg/dL±5.1, $p=0.04$) (Figure 4.2A). Plasma insulin levels in animals were significantly reduced by 42% in MR3 (1.9ng/mL±0.3, $p=0.04$), 71% in MR5 (0.9ng/mL±0.1, $p=0.0004$), and 81% in MR10 (0.6ng/mL±0.2, $p=0.001$) when compared to HFD (3.3ng/mL±0.5) (Figure 4.2B). A significant decrease in HOMA-IR was observed within 3 days of MR (10±2.1, $p=0.007$) and continued for 5 days (4±0.8, $p=0.0002$) and 10 days of MR (2.5±1.1, $p=0.0008$), compared to HFD (24.2±4.6). (Figure 4.2C).

To evaluate if short-term MR improves plasma lipid profile, total triglyceride and cholesterol were measured in fasted animals. Plasma triglycerides were significantly reduced after 3 days of MR by 17.9% (64mg/dL±1.2, $p=0.005$), 5 days by 19.2% (63mg/dL±2.6, $p=0.003$) and 10 days by 38.4% (48mg/dL±3.2, $p<0.0001$) compared to HFD (78mg/dL±3.5)

(Figure 4.2D). Total cholesterol in plasma was reduced in MR3 by 15.3% (143mg/dL±11, p=0.155), and this reached significance in MR5 by 26.0% (125mg/dL±6, p=0.005), and MR10 by 46.7% (90mg/dL±6, p<0.0001) compared to HFD (169mg/dL±10) (Figure 4.2E). Common clinical parameters of metabolic health, fasting glucose, insulin, triglycerides, and cholesterol, are all significantly improved within 3-5 days of MR diet, despite continuing HFD.

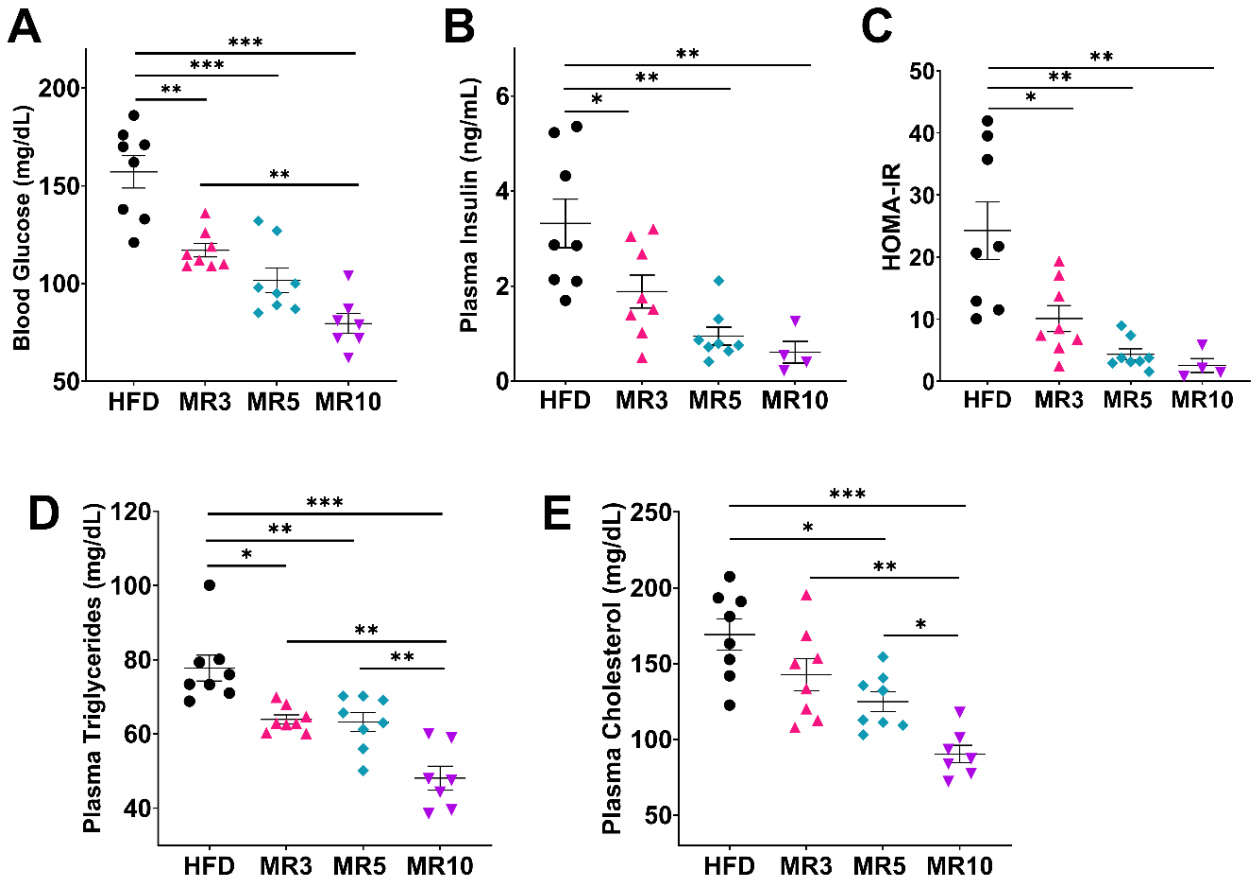

Figure 4.2. Measures of Hyperglycemia, Insulin Resistance and Lipid Profile are Improved After Short-Term Methionine Restriction Plasma collected on day of sacrifice following 4 hours of fasting. A.) Blood Glucose (mg/dL) B.) Plasma Insulin (ng/mL) C.) Homeostasis model for insulin resistance (HOMA-IR) D.) Plasma Triglycerides (mg/dL) E.) Plasma Total Cholesterol (mg/dL). HFD – black circles, MR3 – pink upward triangles, MR5 – teal diamonds, MR10 – purple downward triangles. Values shown are mean ± SEM, with only significant p values indicated as * = p <0.05, ** = p<0.005, *** = p<0.0001

4.4. Short-Term Methionine Restriction Decreases Hepatic Mass and Hepatokine Secretion Without Causing Injury

Since the liver plays a central role in the metabolism of methionine, it is important to assess if there are significant changes to the liver and hepatic functions with short-term MR. Liver mass was significantly reduced by MR by 24% within 3 days (1.32g±0.1, $p=0.01$), 32% within 5 days (1.17g±0.07, $p=0.001$), and 44% within 10 days (0.97g±0.04, $p<0.0001$) compared to HFD (1.74g±0.13) (Figure 4.3A). This significant difference was confirmed with relative liver mass to total body weight (g/g) (Figure 4.3B). Corresponding to the rapid reduction in liver mass, significant changes in levels of circulating hepatokines, IGF-1 and FGF21, were also observed. Changes in IGF-1 have been associated with metabolic syndrome [365-367]. MR significantly decreased plasma levels of IGF-1 by 26.9% within 3 days (307ng/mL±20, $p=0.0005$), 30% in 5 days (294ng/mL±17, $p=0.0001$) and 41.9% in 10 days (244ng/mL±24, $p<0.0001$) compared to HFD (420ng/mL±18) (Figure 4.3C). MR increased plasma levels of FGF21 by 642% within 3 days (5.2ng/mL±0.8, $p=0.057$), by 614% in 5 days (5.0ng/mL±0.7, $p=0.07$), and significantly by 1471% within 10 days (10.6ng/mL±2.3, $p<0.0001$) compared to HFD (0.6ng/mL±0.09) (Figure 4.3D). It has been established that the effects of increased FGF21 to induce increased energy expenditure and remodeling of adipose tissue are due to the influence on the brain rather than directly on adipose tissue [368].

Alterations in methionine intake or metabolism can impact liver health, which indicates a need to assess the impact of MR on liver health by measuring circulating liver-associated enzymes. The most common way to assess liver injury is to measure aspartate aminotransferase (AST) and alanine aminotransferase (ALT) which are liver-associated transaminases and play important roles in amino acid balance [369, 370]. AST is a non-specific

liver marker because it would also increase in other diseases of the heart, skeletal muscle, kidneys, or red blood cells. Plasma AST in HFD-control (12.5mU/mL±0.5) was increased by 0.8% in MR3 (12.6mU/mL±0.4, p=0.99), 1.4% in MR5 (12.7mU/mL±0.2, p=0.98), and decreased by 6% in MR10 (11.7mU/mL±0.3, p=0.57) and none of these differences were significant (Figure 4.3E) and remained non-significant when relative to total body weight (Figure 4.3I). ALT has greater hepatic specificity than AST. ALT levels are low in HFD (14.2mU/mL±3.2) and increased by 67% in MR3 (23.9mU/mL±4.5, p=0.27) and 47% in MR5 (21.1mU/mL±4.3, p=0.56) and decreases by 13% in MR10 (12.3mU/mL±1.3, p=0.98) (Figure 4.3F). While this trend liver-specific enzyme, ALT, none of these changes in absolute values are statistically significant and remain non-significant relative to total body weight (Figure 4.3J). Considering AST and ALT values relative to body weight is not a common practice, but since we had 3-15% difference in body weight in MR animals it is important to bring liver function in context of body composition. Clinicians often normalize these data by using a ratio of AST to ALT, with a value greater than one can be indicative of some form of hepatic injury, such as liver disease, or cirrhosis, while values lower than one are indicative of a healthy liver [371, 372]. The AST/ALT ratio in our study is slightly elevated in HFD control group (1.1±0.1.8) and decreased in MR3 (0.7±0.1, p=0.40), MR5 (0.9±0.2, p=0.85) and MR10 (1.0±0.1, p=0.98), with no significant differences (Figure 4.4G). This suggests that control animals had slightly elevated liver enzymes indicative of hepatic distress, which was improved upon MR. Additionally, we isolated RNA from livers from the animals and measured gene expression of fibrosis markers by RT-qPCR (Figure 4.3K). There were no differences in *Acta2* (alpha smooth muscle actin), *Col1a1* (collagen type 1, alpha 1), and *Col1a2* (collagen type 1, alpha2), which suggests that there were no changes in liver fibrosis. Along with circulating AST/ALT, there were no

indications of liver injury observed with short-term MR. Furthermore, previous studies of MR have seen considerable loss of hepatosteatosis following MR for 14 weeks [275, 288].

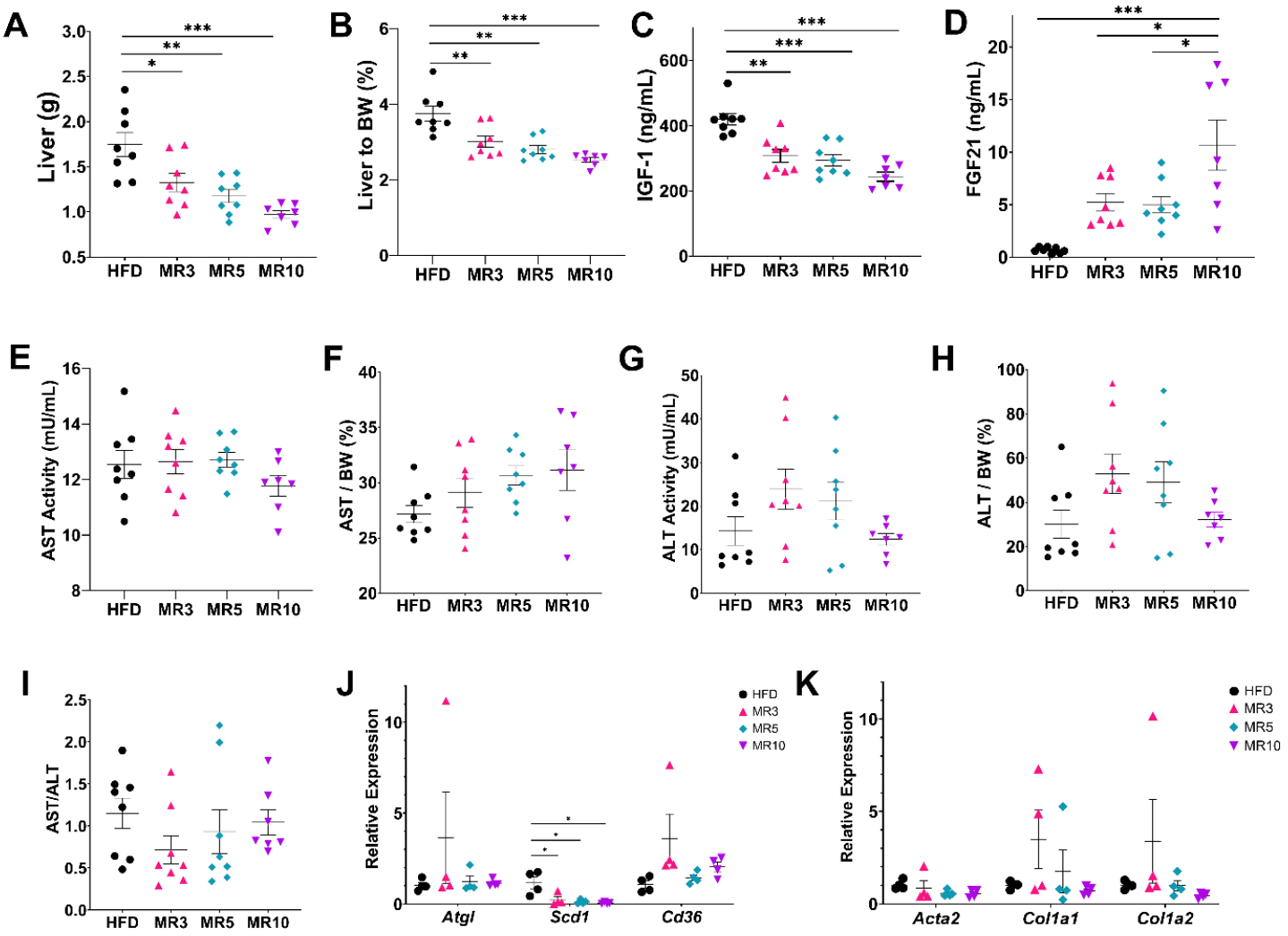

Figure 4.3. A Short-Term Methionine Restriction Decreases Hepatic Mass and Changes Hepatokine Secretion Without Causing Injury A.) Absolute liver mass (g) B.) Liver mass relative to total body weight (%) C.) Plasma Insulin-like growth factor 1 (IGF-1, ng/mL) D.) Plasma Fibroblast growth factor 21 (FGF21, ng/mL) E.) Alanine aminotransferase (AST, mU/mL) F.) AST relative to total body weight (%)G.) Aspartate aminotransferase (ALT, mU/mL) H.) ALT relative to total body weight (%)I.), Ratio of AST to ALT J.) Relative gene expression [ΔΔCq(Fold Change) – relative to actin] of insulin sensitivity markers in liver tissue; *Atgl* – adipose triglyceride lipase, *Scd1* - stearoyl-CoA desaturase 1, *Cd36* – cluster of differentiation K.) Relative gene expression [ΔΔCq(Fold Change) – relative to actin] of fibrosis markers in liver; *Acta2*- alpha skeletal muscle actin, *Col1a1* – collagen type 1, alpha 1, *Col1a2* – collagen type 1, alpha 2. HFD – black circles, MR3 – pink upward triangles, MR5 – teal diamonds, MR10 – purple downward triangles. Values shown are mean ± SEM, with only significant p values indicated as * = p <0.05, ** = p<0.005, *** = p<0.0001

While no histology or lipid analysis was performed on these animals, the significant loss of hepatic mass upon short-term MR could be due to loss of hepatosteatosis. However, there was a significant decrease liver gene expression of *Scd1* (Figure 4.3J) and suggests increased β-oxidation and is consistent with previous studies of MR in rodents [275, 373].

4.5. Short-Term Methionine Restriction Results in Altered Adipokine Secretion Without Significant Changes in Mass of Large Adipose Depots

Obesity is characterized by an increase in circulating leptin and decrease in adiponectin [374]. Measured levels of plasma leptin in obese control animals were exceptionally high (110ng/mL±7.4) and this suggests severe leptin resistance. Upon MR there was significant reductions of 45% within 3 days (80ng/mL±46.2, $p=0.008$), 59% in 5 days (60.4ng/mL±5.2, $p<0.0001$) and 70% in 10 days (32ng/mL±5.0, $p<0.0001$) (Figure 4.4B). Mass of iWAT of obese mice was not significantly impacted by MR for 3 days (1.49g±0.2, $p=0.99$), 5 days (1.36g±0.12, $p=0.86$) or 10 days (1.19g±0.14, $p=0.49$) compared to control mice (1.54g±0.17) (Figure 4.4A). Similarly, the mass of gWAT of obese mice was not dramatically impacted by MR with 3 days (2.46g±0.1, $p=0.84$), 5 days (2.33g±0.13, $p=0.54$) or 10 days (2.20g±0.12, $p=0.27$) compared to control mice (2.65g±0.25). Percent fat mass relative to total body weight remains non-significant. *Adipoq* expression in BAT, iWAT and gWAT are also not significantly different after MR (Figure 4.4D). Despite nonsignificant changes in large adipose depot mass or *Adipoq* expression, plasma adiponectin was increased by 5% within 3 days (8.9mg/mL±0.17, $p=0.47$) and were significantly increased by 11% within 5 days (9.4mg/mL±0.15, $p=0.02$) and 28% within 10 days (10.8mg/mL±0.42, $p<0.0001$) compared to HFD (8.3mg/mL±0.17) (Figure 4.4C).

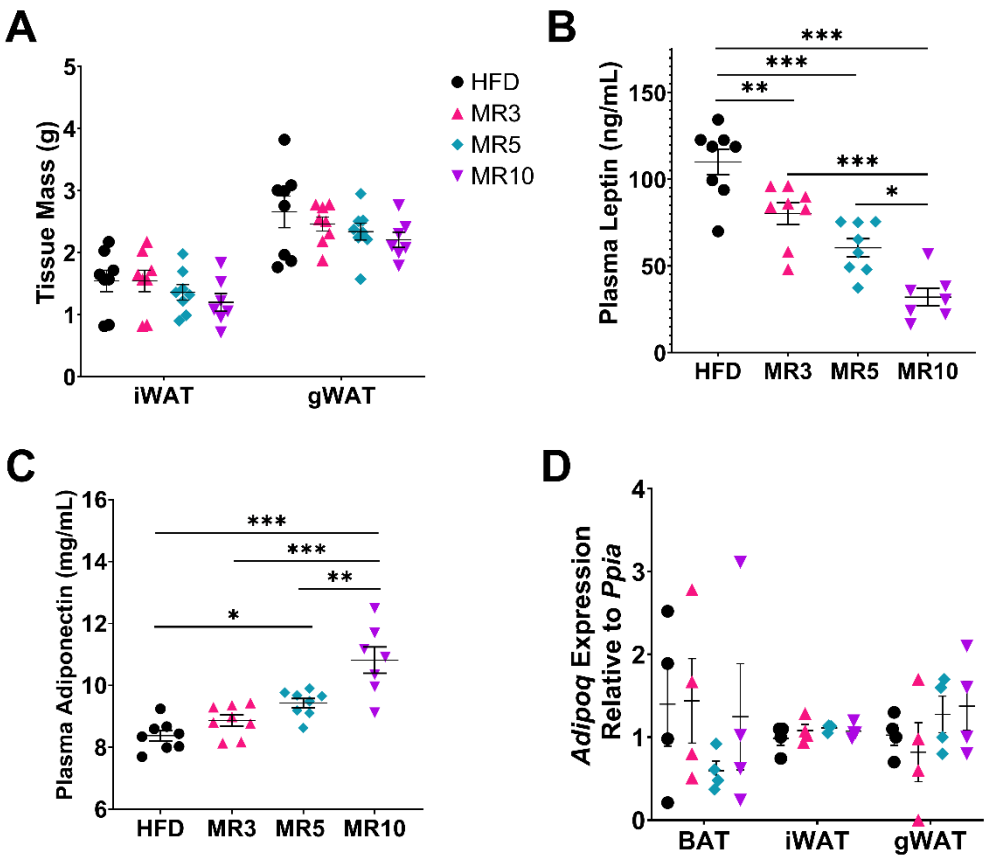

Figure 4.4. Short-Term Methionine Restriction Results in Altered Adipokine Secretion Without Significant Changes in Mass of Large Adipose Depots A.) Tissue mass of inguinal white adipose tissue (iWAT) and perigonadal white adipose tissue (gWAT) B.) Plasma Leptin (ng/mL) C.) Plasma Adiponectin (mg/mL) D.) Relative gene expression of *Adipoq* in brown adipose tissue (BAT), iWAT and gWAT [ΔΔCq(Fold Change) – relative to *Ppia*] HFD – black circles, MR3 – pink upward triangles, MR5 – teal diamonds, MR10 – purple downward triangles. Values shown are mean ± SEM, with only significant p values indicated as * = p <0.05, ** = p<0.005, *** = p<0.0001

4.6. Short-Term Methionine Restriction Has Minimal Effects on Brown and White Adipose Tissues

MR has been shown to reduce adiposity, increase adipose tissue browning, and increase mitochondrial activity in brown adipocytes [368]. Short-term MR does not appear to induce gene expression of mitochondrial markers in WAT (Figure 4.5D) or BAT (Figure 4.5C). Significant decrease in *Fasn* which suggests that there is a decrease in *de novo* lipogenesis in

iWAT, additionally *Pparg*, a nuclear receptor that regulates adipocyte differentiation is increased by MR and significantly by day 10 or MR, iWAT adipocytes might be attempting enhance adipogenesis to increase lipid uptake/storage to account for decreased *de novo* lipogenesis (Figure 4.5B). *Fabp4* is also upregulated in iWAT which participates in intracellular lipid transport. A futile lipid cycle has been observed in MR previously and has been attributed partially to both Adiponectin and FGF21 [281]. Overall, it seems that short-term MR is not adequate to activate BAT, however, there does seem to be modification of adipocyte differentiation and lipid mobilization within iWAT within 3-10 days of MR.

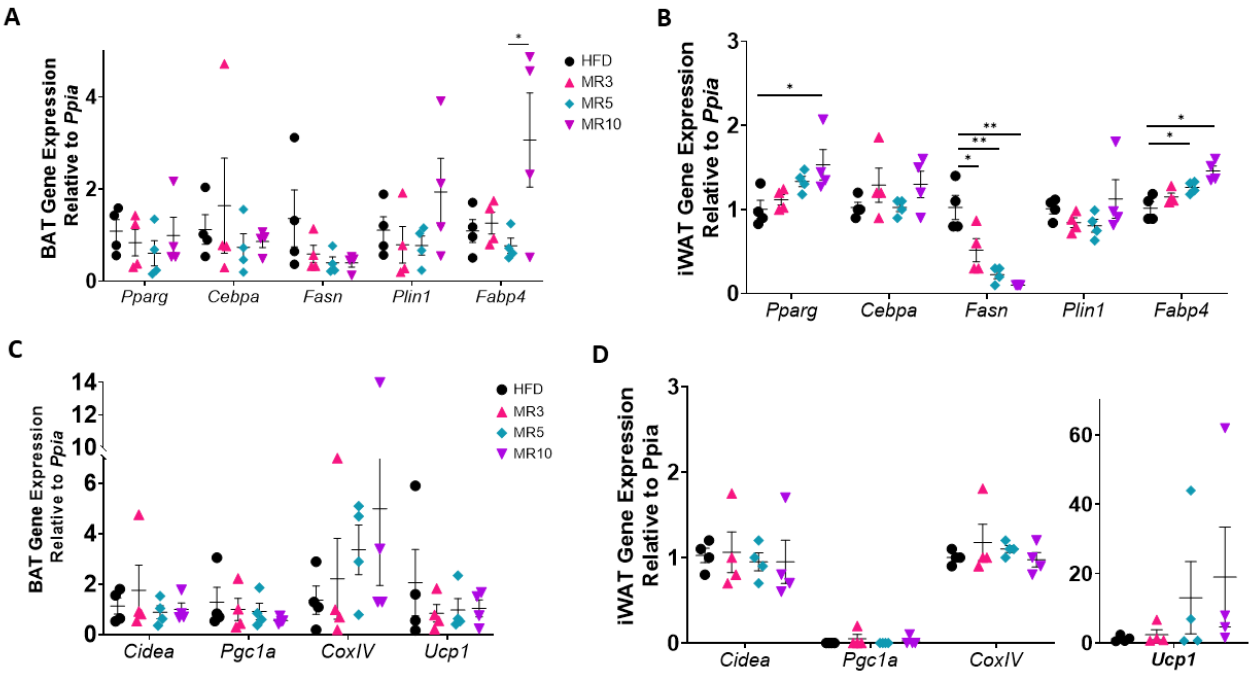

Figure 4.5. Effects of Short-Term Methionine Restriction on BAT and iWAT Gene Expression Relative gene expression in adipose tissues, calculated by [ΔΔCq(Fold Change) – relative to *Ppia*] A.) Adipocyte differentiation markers in BAT B.) and iWAT C.) Mitochondrial markers in BAT D.) and iWAT. *Pparg* – peroxisome proliferator-activated receptor gamma, *Cebpα* - CCAAT enhancer binding protein alpha, *Fasn* – fatty acid synthase, *Plin1* - perilipin-1, *Fabp4* – fatty acid binding protein 4, *Cidea* – cell death inducing DFFA like effector A, *Pgc1α* - PPARG coactivator 1 alpha, *CoxIV* - cytochrome c oxidase subunit IV, *Ucp1* - uncoupling protein 1, HFD – black circles, MR3 – pink upward triangles, MR5 – teal diamonds, MR10 – purple downward triangles. Values shown are mean ± SEM, with only significant p values indicated as * = p <0.05, ** = p<0.005, *** = p<0.0001

4.7. Short-Term Methionine Restriction Counteracts Obesity-Driven Whitening of Thoracic Perivascular Adipose Tissue

Given the proximal location of PVAT to vascular tissue, it is becoming clear that PVAT is pertinent to the development of CVD, as endothelial dysfunction and atherosclerosis are preceded by adventitial inflammation [81]. Due to the dietary response of PVAT to HFD as well as the dramatic response of PVAT to long-term MR shown in chapter 3, characterizing the immediate response of PVAT to short-term MR is our primary objective. Measurement of accumulated lipid in PVAT of animals was significantly reduced by 17.1% after 3 (50.5%±3.4, $p=0.04$), by 36.1%, in 5 days (38.9%±3.2, $p<0.0001$) , and 62.6% in 10 days of MR(22.8%±1.9, $p<0.0001$) compared to HFD (60.9%±1.5) (Figure 4.6A-B). Protein markers of adipogenesis in PVAT peroxisome proliferator-activated receptor (PPARG), which regulated fatty acid storage and glucose metabolism, was significantly decreased in MR 3 and 5 (Figure 4.6E-F). Adipogenesis-related enhancer, CCAAT enhancer binding protein alpha (C/EBPa), was active in HFD control animals and increased in MR3, however, was significantly decreased in MR5. Fatty acid binding protein 4 (FABP4) was not significantly changed in MR3 or MR5, compared to HFD controls (Figure 4.6E-F). Regulator of lipolysis in adipocytes, Perilipin-1 (PLIN1) was temporarily increased in MR3, however was significantly decreased by MR 10. A similar trend of PLIN1 was observed by immunofluorescence in fixed PVAT (Figure 4.6C-D). These data suggest that PVAT that is whitened by 60% HFD has lost over half of its accumulated lipid by day 10 of MR, and that this lean phenotype is mediated both by a reduction of adipocyte differentiation as well as a loss of protection from lipolysis.

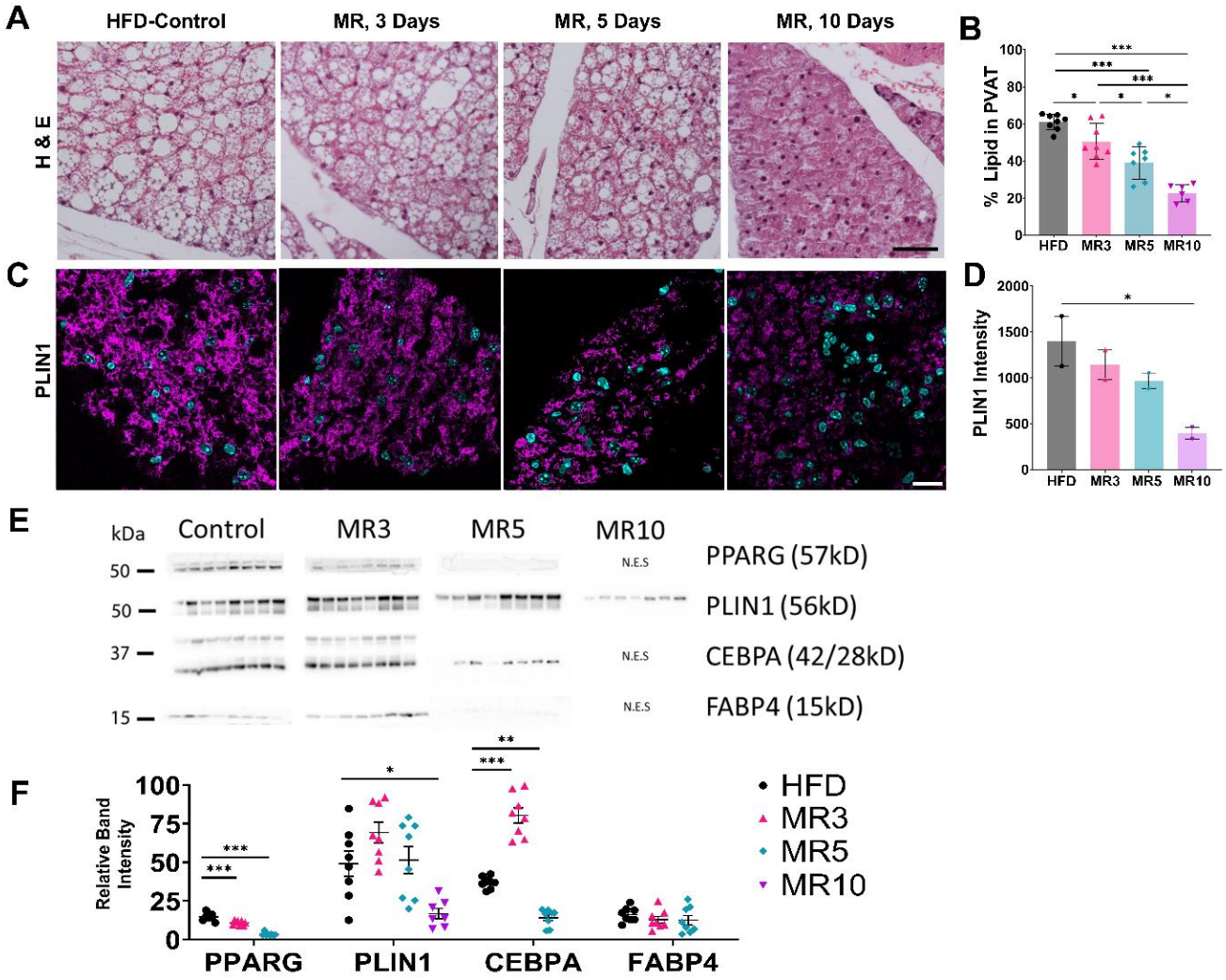

Figure 4.6. Short-Term Methionine Restriction Counteracts Obesity-Driven Whitening of Thoracic Perivascular Adipose Tissue A.) H&E Staining of Thoracic PVAT B.) Quantitation of percent lipid in PVAT Fixed thoracic PVAT was H&E stained and imaged under bright field and B) percent lipid in PVAT was quantified, HFD-control (n= 8), MR10 (n = 7), MR5 (n = 8), MR3 (n = 8), scale bar = 50μm. C.) PLIN1 was detected via immunofluorescent staining in fixed PVAT tissue and relative intensity of fluorescence was quantified, n=2 per group, scale bar = 20μm (pink = PLIN1, teal = nuclei) E.) Western blots of protein expression of adipocyte differentiation in PVAT. Timepoints labeled with N.E.S. indicate that not enough samples were available for this analysis. F.) Quantification of adipogenic proteins in PVAT. PPARG – peroxisome proliferator-activated receptor gamma, CEBPA - CCAAT enhancer binding protein alpha, PLIN1 - perilipin-1, FABP4 – fatty acid binding protein 4. HFD – black circles, MR3 – pink upward triangles, MR5 – teal diamonds, MR10 – purple downward triangles. Values shown are mean ± SEM, with only significant p values indicated as * = $p < 0.05$, ** = $p < 0.005$, *** = $p < 0.0001$

4.8. Short-Term Methionine Restriction Does Not Affect Thermogenic Markers, Decreases Mitochondrial Biogenesis, and Increases Abundance of Electron Transport Chain Subunit

Due to the observed lean phenotype in PVAT, we next assessed the contribution of mitochondrial protein markers in PVAT. Protein markers of browning in PVAT, PPARG coactivator 1 alpha (PGC1a), stimulator of mitochondrial biogenesis and is significantly decreased in PVAT by day 5 and 10 of MR (Figure 4.7). Glucose-regulated protein (GRP75), also known as heat shock protein family A (HSPA9) is trending upwards in MR PVAT but does not reach significance. Uncoupling protein 1 (UCP1) functions to uncouple fatty acid oxidation in the mitochondria, and is unaffected by short-term MR. While these common markers of browning do not suggest increased browning in the PVAT; the terminal enzyme of the mitochondrial respiratory chain, cytochrome c oxidase subunit IV (COXIV) is significantly increased by short-term MR (Figure 4.7). Interestingly, MR has been shown to decrease levels of COXIV in human diploid fibroblasts [375]

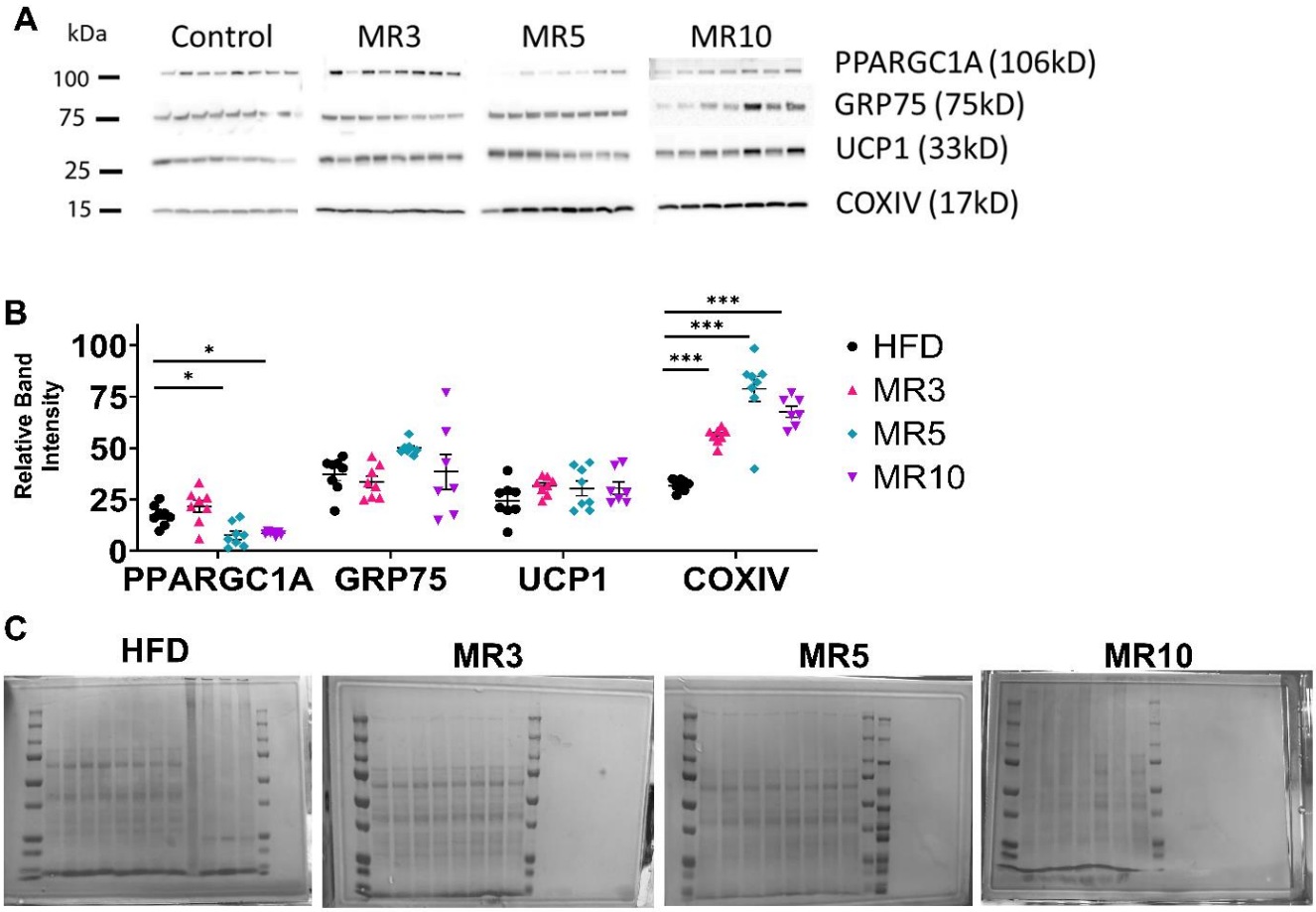

Figure 4.7. Short-Term Methionine Restriction Does Not Affect PVAT Thermogenic Markers, While Increasing Mitochondrial Respiration Marker
A) Immunoblots of PVAT mitochondrial protein expression B) quantification of protein band intensity- relative to total protein C) representative total protein for each group. HFD – black circles, MR3 – pink upward triangles, MR5 – teal diamonds, MR10 – purple downward triangles. Values shown are mean ± SEM, with only significant p values indicated as * = $p < 0.05$, ** = $p < 0.005$, *** = $p < 0.0001$

4.9. Short-Term Methionine Restriction Induces Transient Changes of Global Protein Expression in Thoracic PVAT

To identify molecular mechanisms that mediate the lean PVAT phenotype induced by MR, we performed global proteomics on PVAT from HFD-control, and mice fed MR for 3, 5, and 10 days (n=3 per group). We evaluated the effect of short-term MR during HFD on PVAT protein expression using an unbiased SWATH proteomic approach to characterize the unique

protein signatures. PVAT from three animals from each of the 4 groups were assessed in three technical analytical replicates. When looking at the 1st and 2nd dimensions of variance to assess overall similarity between diet groups, the variation between samples separated the four groups into distinct groups, suggesting that the 3 animals within each group were more similar to each other than other groups (Figure 4.8A). HFD diet group had the highest amount of variation from all other groups, while MR5 and MR10 were the most similar to each other. In total, there were 2878 proteins quantified in each MR group that met the analytical confidence threshold. Short-term MR diet was associated with 118 proteins that were significantly differentially expressed (DE) in the PVAT of these animals. Of all DE proteins in PVAT, 66 were down regulated and 52 were upregulated (Figure 4.8B). A full list of DE proteins is shown in Appendix A. Fifty-three e proteins were unique to MR3, 10 unique to MR5, and 41 unique to MR10 (Figure 4.10A). One upregulated protein, RSSA – small ribosomal subunit protein uS2, was shared between MR3 and MR5. One downregulated protein, STK39 – STE20/SPS1-related proline-alanine-rich protein kinase, was shared between MR3 and MR10. Two downregulated proteins were shared between MR5 and MR10: CO4A3 – collagen alpha-3(IV) chain and SKP1 - S-phase kinase-associated protein 1 (Figure 4.10A).

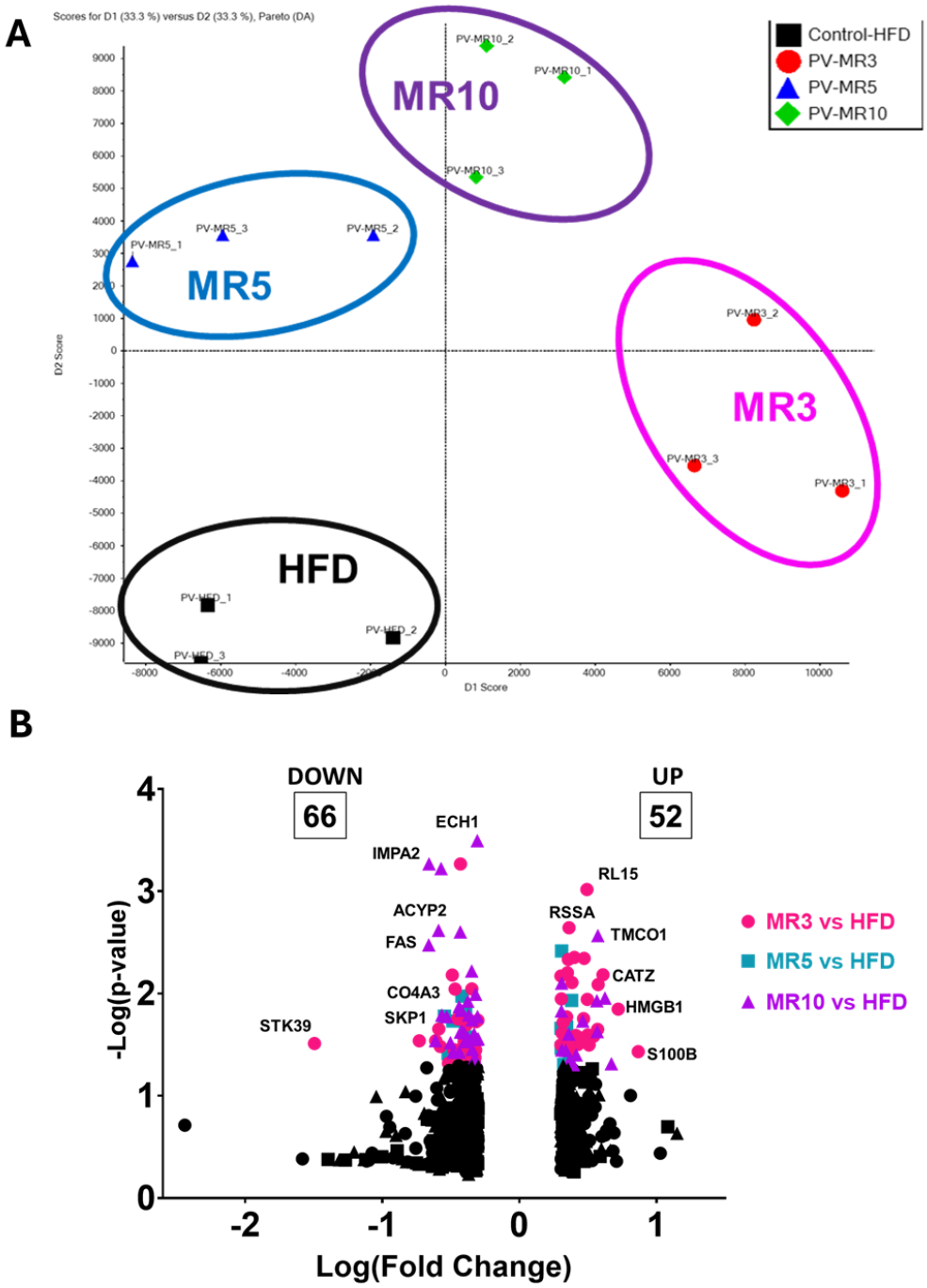

Figure 4.8. Proteomic Analysis of PVAT Reveals Unique Signatures Between 3, 5, and 10 days of MR. A) Principal component analysis (PCA) plot between first and second dimension of variance. Tryptic peptides measured in triplicates (n=3/group) Control HFD (black squares), 3 days of MR (red circles), 5 days of MR (blue triangles), 10 days of MR (green diamonds). B) Volcano plot of relative differential protein expression in MR group compared to HFD. Significant proteins ($p \leq 0.05$ & $FC \geq 2$) are shown in color, 3 days of MR (pink circle), 5 days of MR (teal square), 10 days of MR (purple triangle), non-significant proteins are shown in black.

To understand what is occurring globally to the PVAT proteome upon MR compared to HFD-control, we performed an enrichment of Gene Ontology biological processes [351-353]. Processes were grouped based on semantic similarity, which matches words based on word similarity, and revealed a signature of primarily cellular metabolic process. Many of the individual GO terms that are assigned to the cellular metabolic process GO cluster are related to energy derivation such as the TCA cycle and respiratory electron transport chain (Figure 4.9) and are mostly enriched in MR3. Some proteins that contributed to GO process TCA cycle are NAD/NADP-dependent isocitrate dehydrogenase (IDHC, IDHG1), aconitate hydratase (ACON) which are upregulated, and succinate dehydrogenase (SDHA) which is downregulated. Some proteins related to electron transport chain are several NADH dehydrogenase members (NDUV1, NDUV2, NDUS3) were upregulated in MR3 while dihydrolipoyl dehydrogenase (DLDH) was downregulated. Cytoplasmic glycerol-3-phosphate dehydrogenase (GPDA) was upregulated in MR3 while mitochondrial glycerol-3-phosphate dehydrogenase (GPDM) was downregulated in MR3 and MR10.

Organic acid metabolic process was the most enriched in MR5, in which uronic acid and glucuronate metabolic processes were most significant contributing GO Terms and both utilized sorbitol dehydrogenase (SORD), UDP-glucuronosyltransferase (UD17C), and lambda-crystallin homolog (CRYL1) which were all upregulated. Proteins related to apoptosis were also significantly upregulated in MR3, histone deacetylase 1 (HDAC1), mitochondrial carrier homolog 2 (MTCH2), S100B, and 40S ribosomal protein (RSSA). The next most enriched clusters of GO Terms that are nucleoside phosphate/monophosphate and purine nucleotide biosynthesis were most significantly changed in MR10 (Figure 4.9). Some proteins that contributed to these clusters are ATP synthase subunit e (ATP5I),

phosphoribosylformylglycinamidine synthase (PUR4), and acetyl-CoA carboxylase 2 (ACACB) were downregulated in MR10, while GMP reductase 1 (GMPR1), purine nucleoside phosphorylase (PNPH), inosine-5'-monophosphate dehydrogenase 2 (IMDH2) were upregulated in MR10.

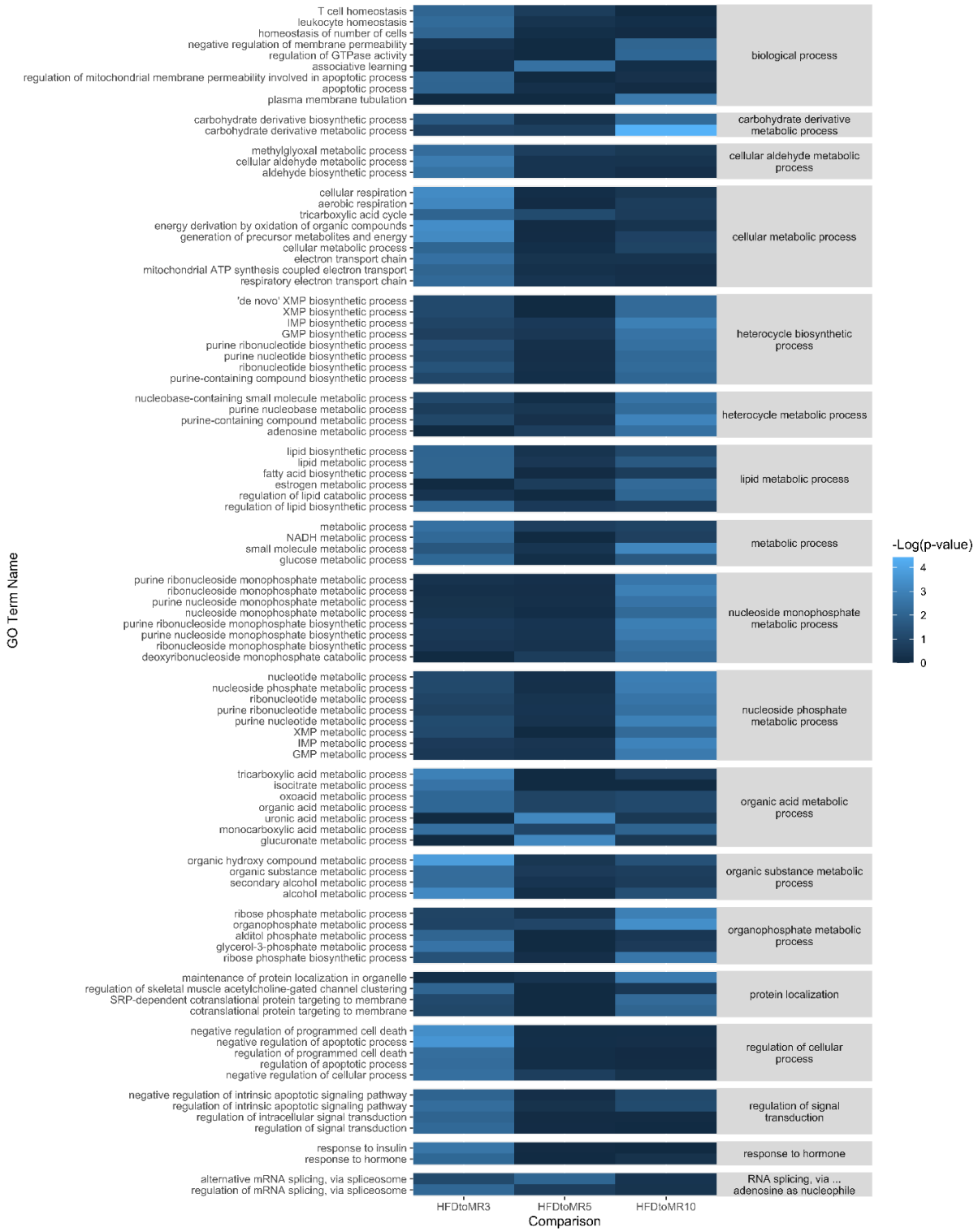

Figure 4.9. Proteomic Analysis Reveals Robust Metabolic Signature Induced by MR in PVAT. Gene Ontology biological processes of significantly differentially expressed proteins grouped into functional clusters. Clusters indicated on the right side in gray column. The heatmap represents significance of enriched terms (shown on left side) in durations of MR (color intensity represents -log(pvalue) of GO term in MR group, light blue = most significant, dark blue= least significant)

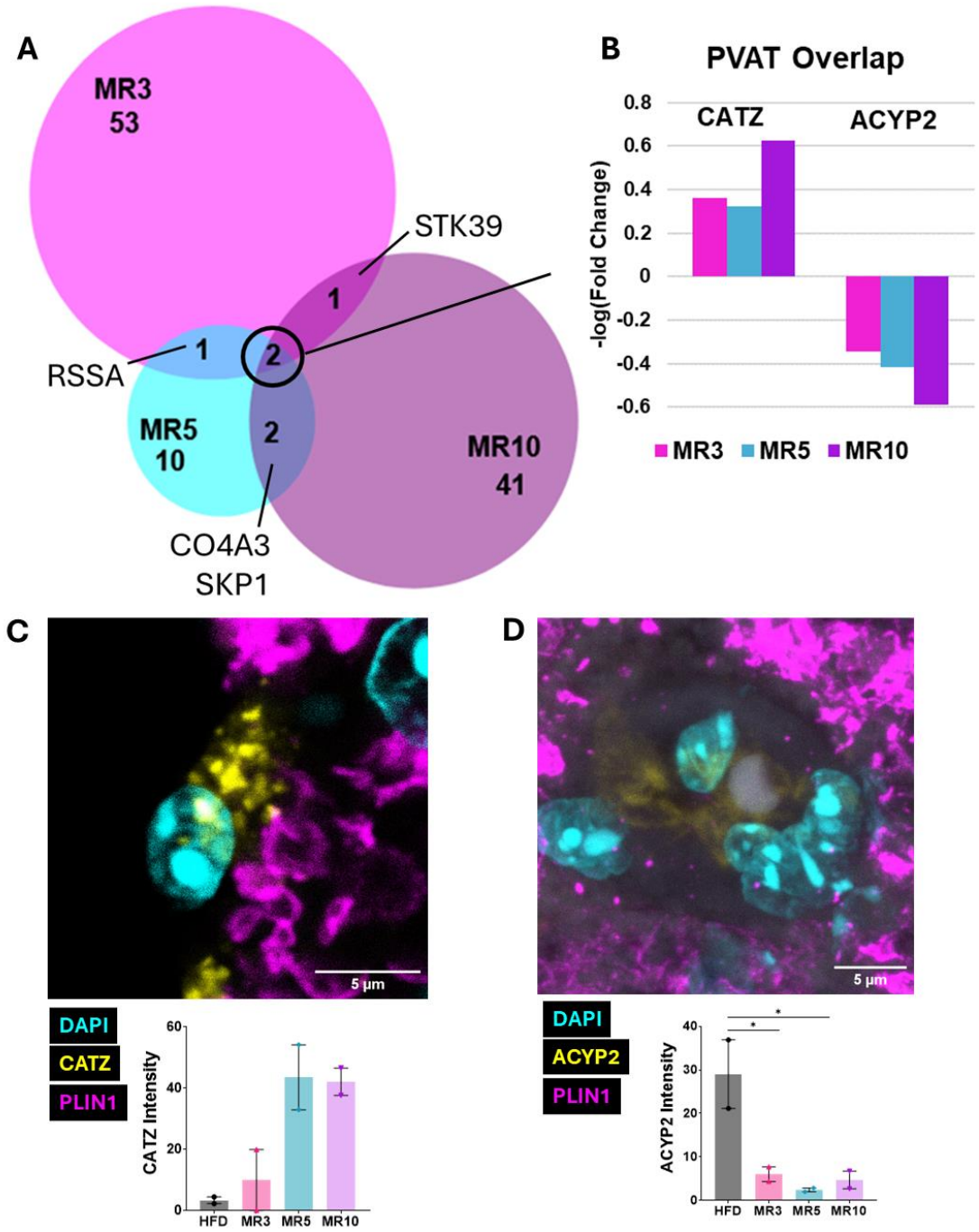

Figure 4.10. Proteomic Analysis Reveals Potential Mediators of MR in PVAT
A) Venn diagram of significant proteins ($p \leq 0.05$ & $FC \geq 2$) from each time point compared to HFD; 3 days of MR (pink), 5 days of MR (blue), 10 days of MR (purple). Proteins shared between 2 out of 3 groups are indicated. Overlap of all three time points circled and expanded in B) -log(Fold Change) of CATZ (Cathepsin Z) and ACYP2 (Acylphosphatase 2) C) Validation of CATZ via immunofluorescent staining in fixed PVAT, quantification of CATZ relative intensity, n=2 per group D) Validation of ACYP2 via immunofluorescent staining in fixed PVAT (z-stack), quantification of ACPY2 relative intensity, n=2

Due to transient nature of the metabolic processes impacted by short-term MR, we compared the DE proteins between each MR group and found that only 2 of DE proteins in PVAT are shared and consistently regulated between all three MR groups, ACYP2 (downregulated) and CATZ (upregulated) (Figure 4.10A-B).

4.9.1. Hydrolytic Enzyme, Acylphosphatase 2, is Consistently Downregulated in PVAT Throughout Short-Term Methionine Restriction

The protein significantly downregulated in PVAT after short-term MR, Acylphosphatase 2 (ACYP2), is encoded by *Acyp2* and is an enzyme that catalyzes the hydrolysis of acylphosphates to carboxylates and inorganic phosphate. Furthermore, ACYP2 is a muscle type isozyme that is most likely localized to mitochondria and catalyzes activity involved in ATP hydrolysis and activation of fatty acids for β-oxidation. ACYP2 is an understudied protein, however downregulation of ACYP2 is also seen in gWAT of obese mice treated with anti-diabetic medication, semaglutide [376]. A subtle presence of ACYP2 was observed by immunofluorescent imaging of fixed PVAT and we were able to validate the downregulation of RAB10 in MR 3, 5, and 10 (Figure 4.10D).

4.9.2. Lysosomal Protease, Cathepsin Z, is Consistently Upregulated in Thoracic PVAT Throughout Short-Term Methionine Restriction

The protein consistently upregulated in PVAT after short-term MR, Cathepsin Z (CATZ) is encoded by *Ctsz* and is a lysosomal cysteine proteinase within the papain family. It is also known as cathepsin X and cathepsin P. Lysosomal cysteine proteases have been shown to be involved in vascular remodeling, a hallmark of atherosclerosis [377] and are also known to process and inactivate leptin [378]. CATZ exhibits both carboxy-monopeptidase and carboxy-dipeptidase activities. Carboxypeptidase activity of CATZ has been shown to modulate immune

response by cleaving C-terminus of regulatory motifs on integrin receptors and enhancing monocyte/macrophage adhesion and phagocytosis [379, 380]. This peptidase activity has also been shown to cause cytoskeleton rearrangements and morphological changes in T-lymphocytes and cancer cells which impacts cell migration and proliferation [379, 381]. CATZ or *Ctsz* has been shown to upregulated in several cancers and neurodegenerative diseases [382-387].

Ctsz is a shared target of PPAR α/γ, and CATZ has been suggested to play a role in BAT thermogenesis as it was found to be necessary in mouse and human brown adipocytes for mitochondrial respiration [388]. We were able to successfully validate the presence of CATZ in fixed PVAT tissue (Figure 4.10C). Increased abundance of CATZ immunofluorescent intensity in MR PVAT was consistent with the proteomics dataset (Figure 4.10B). While there were punctate regions of CATZ in many cells, in multiple instances CATZ was localized primarily in regions that were noticeably lacking adipocyte marker PLIN1 (Figure 4.10C). As previously discussed, PLIN1 coats lipid storage droplets in adipocytes, thereby protecting them until they can be broken down by lipases. Interestingly, the distinct CATZ-positive regions do not appear to colocalize with PLIN1 which could mean that these are adipocytes where PLIN1 has been degraded which means they are no longer protected from lipase activity and subject to lipolysis. Alternatively, these cells could be a type of stromal cell that does not express PLIN1, which is possible because CATZ is expressed in other cell types that are present in PVAT, such as neurons and T-cells. Additional immunofluorescent images are available in Appendix C.

Differences in cathepsins have not been reported to coincide with MR previously, however as described in section 1.5.3.4, lysosomal dysfunction is associated with obesity and metabolic syndrome [70]. While upregulation of other cathepsin family members, L1 and B, have been reported to be upregulated in abdominal subcutaneous adipose tissue of people that are

overweight or obese [72], no studies have indicated CATZ to be related to these changes in body composition. It is possible that MR initiates an upregulation of lysosomal proteolytic activity in PVAT, contributing to altered protein activity, proteolysis and regulation of autophagy and apoptosis in PVAT [389]. Lysine deprivation in undifferentiated and differentiated 3T3-L1 cells has been shown to have alterations in lysosome pathways [390]. Cathepsin Z (CATZ) appears to be a good target, due to being consistently upregulated in MR as well as the body of evidence supporting a role of lysosomal dysfunction in obesity.

4.10. Short-Term MR does not Influences Vascular Morphology

To evaluate vascular response to short-term MR, we measured total vessel area, medial area, and lumenal area of thoracic aorta. Like the long-term study, we did not see any significant differences in any of the measured areas, however that are some trends that emerge. Interestingly, vessel area appears to have a downward trend with 3 and 5 days of MR, and then we see the area increases with 10 days of MR, where the average is the same or slightly higher in 10 days MR than the HFD control group. These findings are interesting, given that we observed such dramatic response in PVAT in both long-term and short-term MR diet.

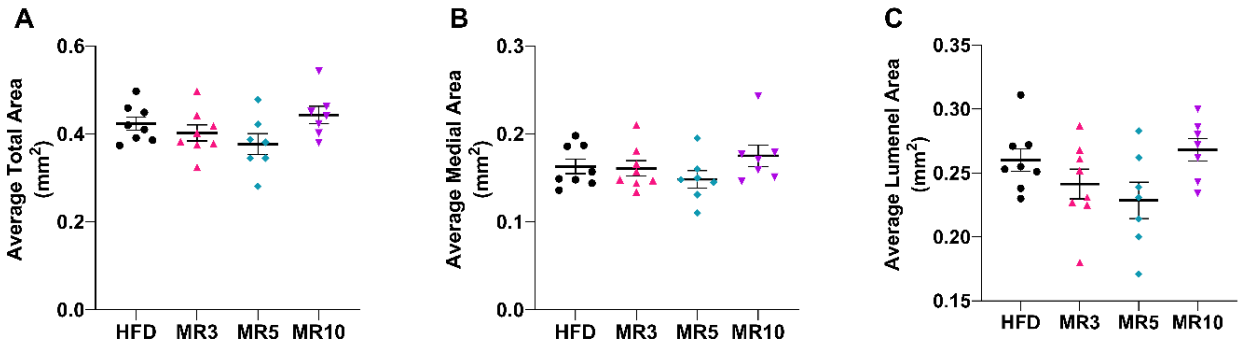

Figure 4.11. Short-Term Methionine Restriction Does Not Influence Thoracic Aorta Morphology Quantification of aortic morphology are shown as A.) total area B.) medial area, and C.) lumenal area. Values shown are mean ± SEM, with only significant p values indicated.

4.11. Short-Term Methionine Restriction Induces Transient Changes of Global Protein Expression in Thoracic Aorta

Due to the expected effects of PVAT on vascular function and no observable differences in vessel area, we evaluated the proteomic profiles of thoracic aorta that the PVAT was directly surrounding to identify molecular pathways that might be altered by MR diet. The aorta dataset was analyzed in the same fashion as the PVAT dataset. When looking at the 1st and 2nd dimensions of variance to assess overall similarity between diet groups, the variation between samples separated the four cohorts into distinct groups, suggesting that the three animals within each group were more similar to each other than other groups (Figure 4.12A). In total, there were 2492 proteins quantified in each MR group that met the analytical confidence threshold.

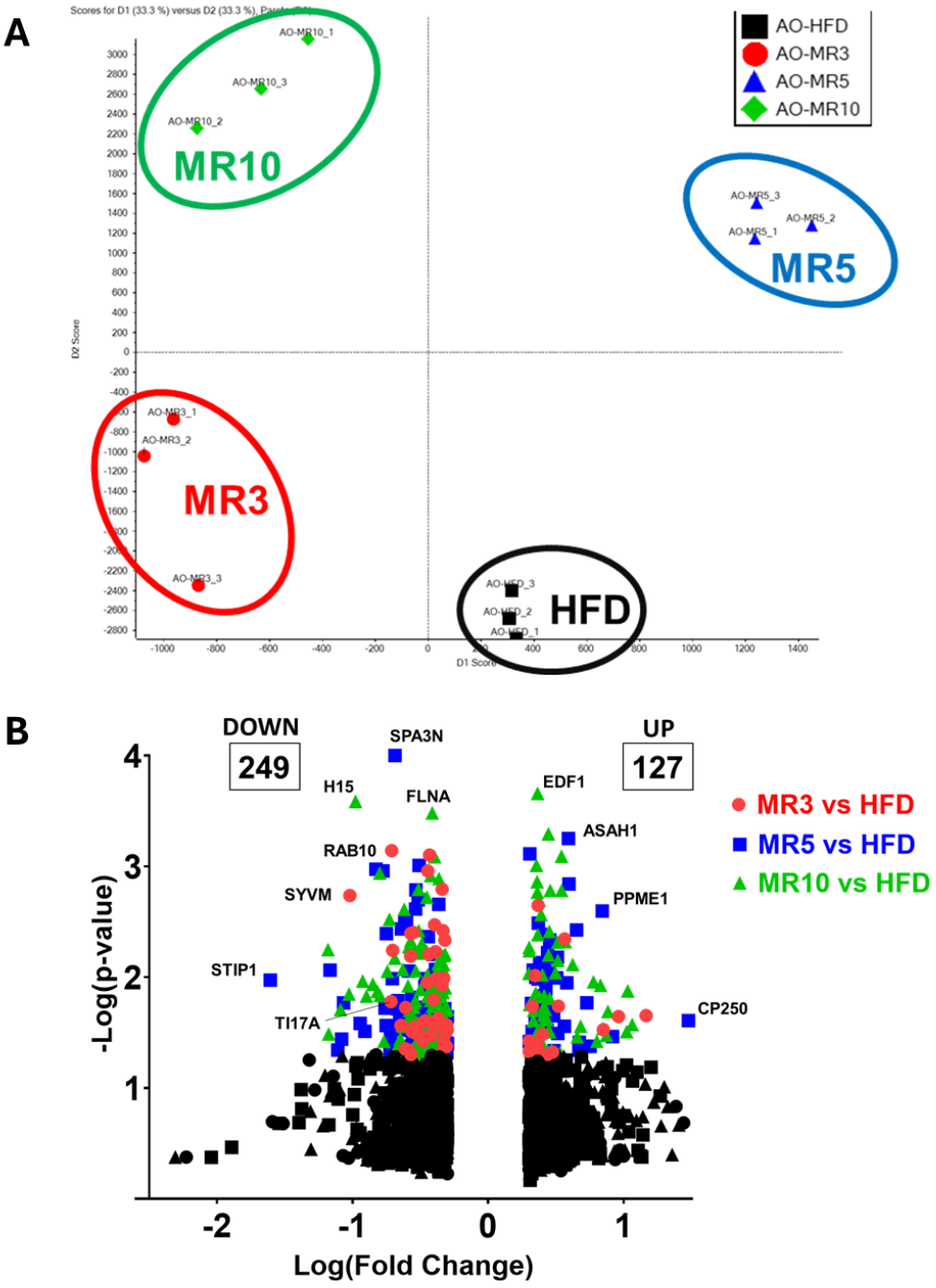

Figure 4.12. Short-Term Methionine Restriction Induces Transient Changes of Global Protein Expression in Thoracic Aorta A) Principal component analysis (PCA) plot between first and second dimension of variance. Tryptic peptides measured in triplicates (n=3/group) Control HFD (black), 3 days of MR (red), 5 days of MR (blue), 10 days of MR (green). B) Volcano plot of relative differential protein expression in MR group compared to HFD. Significant proteins ($p \leq 0.05$ & $FC \geq 2$) are shown in color, 3 days of MR (red circle), 5 days of MR (blue square), 10 days of MR (green triangle), non-significant proteins are shown in black.

Similar to PVAT, we performed an enrichment of Gene Ontology [351-353] biological processes to assess global changes in the aorta proteome upon MR compared to HFD-control. Processes were grouped based on semantic similarity and revealed a signature of primarily anatomical structure development. Many of the individual GO terms that are assigned to the anatomical structure development GO cluster are related to tissue development (Figure 4.13) and are enriched in MR5 and MR10. A small selection of proteins that contributed this GO cluster are integrin-linked protein kinase (ILK), collagen alpha-1(I) chain (CO1A1) which are upregulated, and myosin-11 (MYH11), prostacyclin synthase (PTGIS), fermitin family homolog 2 (FERM2), extracellular matrix protein 1 (ECM1), periostin (POSTN), filamin-A (FLNA), collagen alpha-2(I) chain (CO1A2), collagen alpha-1(XVIII) chain (COlA1), mitogen-activated protein kinase 3 (MK03, MP2K2), neurophilin-1 & 2 (NRP1, NRP2) which are all downregulated. Many of these proteins are related to other organizational processes such as organelle organization. Some proteins related to actin cytoskeleton and supramolecular fiber organization are actin-related protein 2/3 complex subunit 2 (ARPC2), integrin beta-1 (ITB1), tropomyosin (TPM1, TPM2), phosphatase and actin regulator 4 (PHAR4) which are upregulated, and dihydropyrimidinase-related protein 3 (DPYL3), WASH complex subunit 2 (WASC2), serine/threonine-protein kinase (PAK 1) which are downregulated. Protein transport is another highly enriched biological process in MR5 and MR3. Several transmembrane transporter and mitochondrial import proteins that are either upregulated (TIM29, TIM8A) or downregulated (TOM40, TI17A, TIM50, TIM44, TRAM1) in MR compared to HFD-control. Furthermore, some proteins related to protein localization such as Ras-related protein Rab-10 (RAB10) and Peroxisomal targeting signal 1 receptor (PEX5) are downregulated.

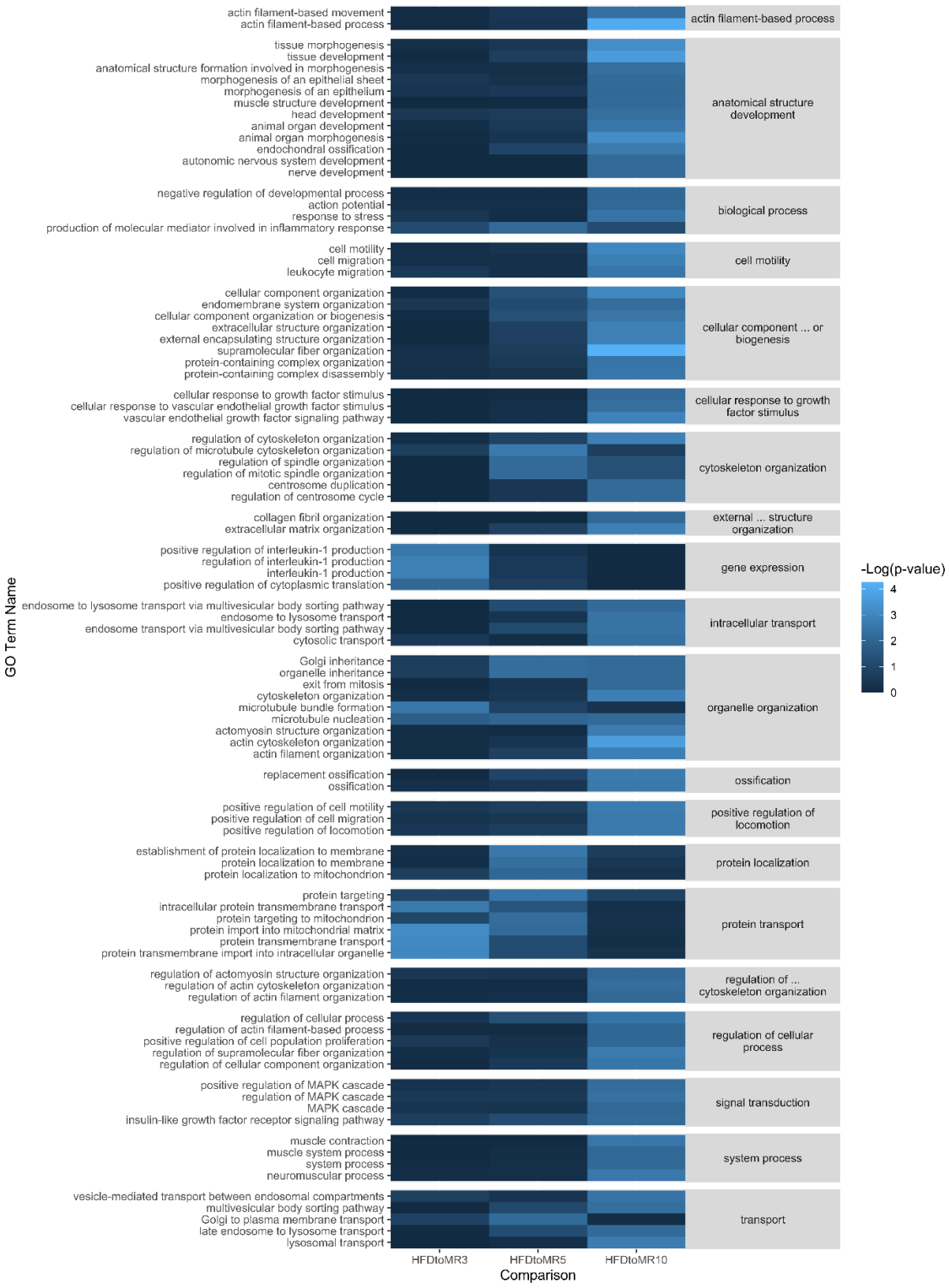

Figure 4.13. Proteomic Analysis Reveals Robust Structural Signature Induced by MR in Thoracic Aorta Gene Ontology biological processes of significantly differentially expressed proteins grouped into functional clusters. Clusters indicated on the right side in gray column. The heatmap represents significance of enriched terms (shown on left side) in durations of MR (color intensity represents -log(pvalue) of GO term in MR group, light blue = most significant, dark blue= least significant)

Short-term MR diet was associated with 376 proteins significantly differentially expressed (DE) in the PVAT of these animals. Of all DE proteins in PVAT, 249 were downregulated and 127 were upregulated (Figure 4.12B). A full list of DE proteins is shown in Appendix B. Thirty were unique to MR3, 81 unique to MR5, and 120 unique to MR10 (Figure 4.14A). Ten proteins were shared between MR3 and MR5 (upregulated - ASAH1, downregulated - HSDL2, TOP1, SHPS1, MYO6, TM20, PSMD9, HP1B3, RHG07, RABE1). Seven proteins were shared between MR3 and MR10 (upregulated - PRDX6, downregulated - CO6A5, SEPT9 D39U1, PAK1, LAD1, WASC2). Thirty-nine were shared between MR5 and MR10 (upregulated - TPM2, PPM1A, DCTN1, QOR, CNN3, downregulated - DD19A, ITPR1, EIF3G, SRP68, EMC10, CHM4B, DDB1, GAPR1, IGG2B, NED4L, THSD4, TXD12, IMPA1, MSTN1, MYO1C, CO7A1, DHDH, AMRP, C163A, NU155, ENAH, NDUB2, ESAM, COFA1, MK03, SEPT4, MEP50, SPA3N, PCNA, HACL2, 1433Z, MICA1, SF3B1, STIP1) (Figure 4.14A)

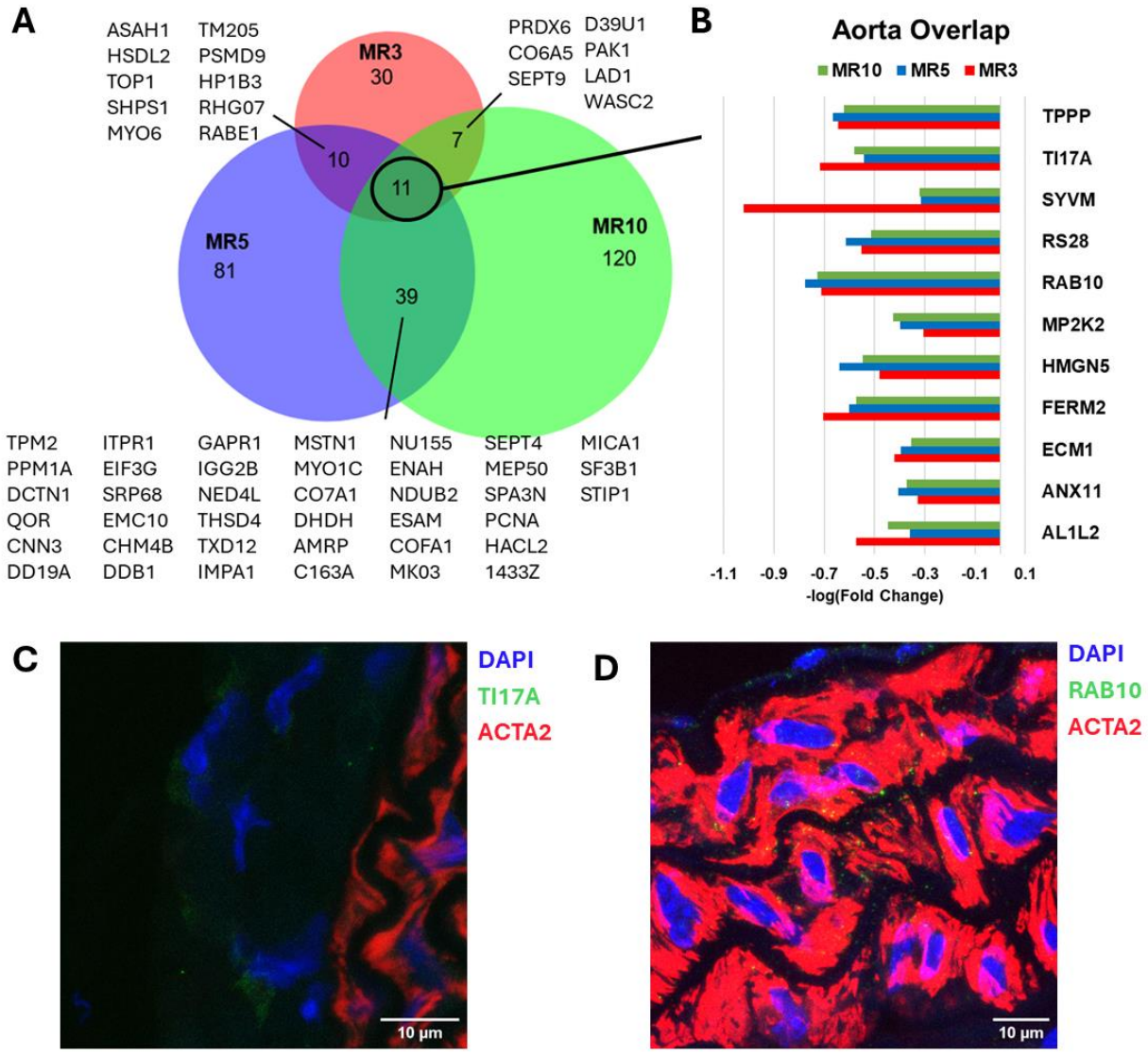

Figure 4.14. Proteomic Analysis Reveals Potential Mediators of MR Thoracic Aorta A) Venn diagram of significant proteins ($p \leq 0.05$ & $FC \geq 2$) from each time point compared to HFD; 3 days of MR (red), 5 days of MR (blue), 10 days of MR (green). Proteins shared between 2 out of 3 groups are indicated. Overlap of all three time points circled and expanded in B) -log(Fold Change) of AL1L2 (Mitochondrial 10-formyltetrahydrofolate dehydrogenase); ANX11 (Annexin A11), ECM1 (Extracellular matrix protein 1), FERM2 (Fermitin family homolog 2), HMGN5 (High mobility group nucleosome-binding domain-containing protein 5), MP2K2 (Dual specificity mitogen-activated protein kinase kinase 2), RAB10 (Ras-related protein Rab-10), RS28 (40S ribosomal protein S28), SYVM (Valine--tRNA ligase), TI17A (Mitochondrial import inner membrane translocase subunit Tim17-A) and TPPP (Tubulin polymerization-promoting protein) from MR3, MR5 and MR10 C) Immunofluorescent staining TI17A in fixed aorta (z-stack) D) Immunofluorescent staining of RAB10 in fixed aorta (z-stack)

4.11.1. Eleven Proteins Consistently Downregulated in Thoracic Aorta Throughout Short-Term Methionine Restriction

Further analysis reveals that 11 of DE proteins in aorta are shared and consistently downregulated in all MR groups, AL1L2, ANX11, ECM1, FERM2, HMGN5, MP2K2, RAB10, RS28, SYVM, TIM17A, and TPPP (Figure 4.14A-B). More details on these markers can be found in Table 4.1. Two downregulated markers were selected for validation, RAB10 (Ras-related protein 10) and TI17A (Mitochondrial import inner membrane translocase subunit 17a).

Ras-related protein RAB10, encoded by *Rab10*, is of the Rab family of GTPases that act as key regulators of intracellular membrane trafficking by formation of transport vesicles to fuse with the membrane and exit the cell [391]. RAB10 has been identified as a major regulator of Collagen IV vesicular trafficking during vascular development, where loss of *Rab10* reduces Collagen IV secretion from the endothelial basement membrane [392]. Immunofluorescent imaging of RAB10 in thoracic aorta from MR animals reveals co-localization of RAB10 with ACTA2, which suggests that vascular smooth muscle cells are utilizing RAB10 (Figure 4.14D, Appendix C). Validating downregulation of RAB10 was not possible as multiple rounds of immunofluorescence did not produce adequate imaging to quantify differences between HFD and MR groups.

Mitochondrial import inner membrane translocase subunit 17a (TI17a), encoded by *Timm17a*, is an essential component of the TIM23 complex which mediates translocation of peptide-containing proteins across the mitochondrial inner membrane. Highly significant GO terms associated with MR3 are protein import into mitochondrial matrix and protein transmembrane transport, which relate the function of TI17A. This protein is of interest to highlight due to most studies of MR exhibiting stimulation of mitochondrial biogenesis [282,

393] and within this study we observe a consistent decrease in mitochondrial proteins. Validating downregulation of TI17A was not possible as multiple rounds of immunofluorescence did not produce adequate imaging to quantify differences between HFD and MR groups. However, a subtle presence of TI17A was observed in the endothelial cells of the thoracic aorta.

Table 4.1: Locations and Functions of Identified Proteomic Targets				
Tissue (Direction of Change)	Protein, Uniprot ID, Gene Name	Full Name	Location	Function
PVAT (UP)	CATZ Q9WUU7 *Ctsz*	Cathepsin Z	cell cortex [GO:0005938]; cell surface [GO:0009986]; collagen-containing extracellular matrix [GO:0062023]; cytoplasmic vesicle [GO:0031410]; endoplasmic reticulum [GO:0005783]; extracellular space [GO:0005615]; growth cone [GO:0030426]; intracellular membrane-bounded organelle [GO:0043231]; lysosome [GO:0005764]	carboxypeptidase activity [GO:0004180]; cysteine-type endopeptidase activity [GO:0004197]
PVAT (DOWN)	ACYP2 P56375 *Acyp2 Acyp*	Acylphosphatase-2	mitochondrion [GO:0005739]	acylphosphatase activity [GO:0003998]; identical protein binding [GO:0042802]
AORTA (DOWN)	AL1L2 Q8K009 *Aldh1l2*	Mitochondrial 10-formyltetrahydrofolate dehydrogenase	mitochondrion [GO:0005739]; nucleoplasm [GO:0005654]	aldehyde dehydrogenase (NAD+) activity [GO:0004029]; formyltetrahydrofolate dehydrogenase activity [GO:0016155]
AORTA (DOWN)	ANX11 P97384 *Anxa11 Anx11*	Annexin A11	azurophil granule [GO:0042582]; collagen-containing extracellular matrix [GO:0062023]; cytoplasm [GO:0005737]; cytosol [GO:0005829]; melanosome [GO:0042470]; midbody [GO:0030496]; nuclear envelope [GO:0005635]; nucleoplasm [GO:0005654]; phagocytic vesicle [GO:0045335]; specific granule [GO:0042581]; spindle [GO:0005819]	calcium ion binding [GO:0005509]; calcium-dependent phospholipid binding [GO:0005544]; calcium-dependent protein binding [GO:0048306]; phosphatidylethanolamine binding [GO:0008429]; S100 protein binding [GO:0044548]
AORTA (DOWN)	ECM1 Q61508 *Ecm1*	Extracellular matrix protein 1	collagen-containing extracellular matrix [GO:0062023]; extracellular space [GO:0005615]	interleukin-2 receptor binding [GO:0005134]; protease binding [GO:0002020]
AORTA (DOWN)	FERM2 Q8CIB5 *Fermt2 Plekhc1*	Fermitin family homolog 2	adherens junction [GO:0005912]; cell cortex [GO:0005938]; cell junction [GO:0030054]; cell surface [GO:0009986]; cytoplasm [GO:0005737]; cytoplasmic side of plasma membrane [GO:0009898]; cytosol [GO:0005829]; extrinsic component of cytoplasmic side of plasma membrane [GO:0031234]; focal adhesion [GO:0005925]; I band [GO:0031674]; lamellipodium membrane [GO:0031258]; nucleoplasm [GO:0005654]; nucleus [GO:0005634]; plasma membrane [GO:0005886]; stress fiber [GO:0001725]	actin binding [GO:0003779]; actin filament binding [GO:0051015]; integrin binding [GO:0005178]; phosphatidylinositol-3,4,5-trisphosphate binding [GO:0005547]; protein kinase binding [GO:0019901]; SMAD binding [GO:0046332]; type I transforming growth factor beta receptor binding [GO:0034713]
AORTA (DOWN)	HMGN5 Q9JL35 *Hmgn5 Garp45 Nsbp1*	High mobility group nucleosome-binding domain-containing protein 5	chromatin [GO:0000785]; mitochondrion [GO:0005739]; nucleoplasm [GO:0005654]; nucleus [GO:0005634]	chromatin binding [GO:0003682]; nucleosomal DNA binding [GO:0031492]
AORTA (DOWN)	MP2K2 Q63932 *Map2k2 Mek2 Mkk2 Prkmk2*	Dual specificity mitogen-activated protein kinase kinase 2	cell cortex [GO:0005938]; cell-cell junction [GO:0005911]; cytoplasm [GO:0005737]; cytoplasmic side of plasma membrane [GO:0009898]; cytosol [GO:0005829]; early endosome [GO:0005769]; endoplasmic reticulum [GO:0005783]; focal adhesion [GO:0005925]; Golgi apparatus [GO:0005794]; late endosome [GO:0005770]; microtubule [GO:0005874]; mitochondrion [GO:0005739]; nucleus [GO:0005634]; perinuclear region of cytoplasm [GO:0048471]	ATP binding [GO:0005524]; MAP kinase kinase activity [GO:0004708]; MAP-kinase scaffold activity [GO:0005078]; metal ion binding [GO:0046872]; molecular adaptor activity [GO:0060090]; PDZ domain binding [GO:0030165]; protein serine kinase activity [GO:0106310]; protein serine/threonine kinase activator activity [GO:0043539]; protein serine/threonine kinase activity [GO:0004674]; protein serine/threonine/tyrosine kinase activity [GO:0004712]; protein tyrosine kinase activity [GO:0004713]; scaffold protein binding [GO:0097110]

Table 4.1: Locations and Functions of Identified Proteomic Targets d (Continued)

Tissue (Direction of Change)	Protein, Uniprot ID, Gene Name	Full Name	Location	Function
AORTA (DOWN)	MP2K2 Q63932 *Map2k2 Mek2 Mkk2 Prkmk2*	Dual specificity mitogen-activated protein kinase kinase 2	cell cortex [GO:0005938]; cell-cell junction [GO:0005911]; cytoplasm [GO:0005737]; cytoplasmic side of plasma membrane [GO:0009898]; cytosol [GO:0005829]; early endosome [GO:0005769]; endoplasmic reticulum [GO:0005783]; focal adhesion [GO:0005925]; Golgi apparatus [GO:0005794]; late endosome [GO:0005770]; microtubule [GO:0005874]; mitochondrion [GO:0005739]; nucleus [GO:0005634]; perinuclear region of cytoplasm [GO:0048471]	ATP binding [GO:0005524]; MAP kinase kinase activity [GO:0004708]; MAP-kinase scaffold activity [GO:0005078]; metal ion binding [GO:0046872]; molecular adaptor activity [GO:0060090]; PDZ domain binding [GO:0030165]; protein serine kinase activity [GO:0106310]; protein serine/threonine kinase activator activity [GO:0043539]; protein serine/threonine kinase activity [GO:0004674]; protein serine/threonine/tyrosine kinase activity [GO:0004712]; protein tyrosine kinase activity [GO:0004713]; scaffold protein binding [GO:0097110]
AORTA (DOWN)	RAB10 P61027 *Rab10*	Ras-related protein Rab-10	cilium [GO:0005929]; cytoplasmic vesicle membrane [GO:0030659]; cytoskeleton [GO:0005856]; endoplasmic reticulum membrane [GO:0005789]; endoplasmic reticulum tubular network [GO:0071782]; endosome [GO:0005768]; endosome membrane [GO:0010008]; exocytic vesicle [GO:0070382]; Golgi apparatus [GO:0005794]; insulin-responsive compartment [GO:0032593]; perinuclear region of cytoplasm [GO:0048471]; phagocytic vesicle membrane [GO:0030670]; plasma membrane [GO:0005886]; recycling endosome [GO:0055037]; recycling endosome membrane [GO:0055038]; synaptic vesicle membrane [GO:0030672]; trans-Golgi network [GO:0005802]	G protein activity [GO:0003925]; GDP binding [GO:0019003]; GDP-dissociation inhibitor binding [GO:0051021]; GTP binding [GO:0005525]; GTPase activity [GO:0003924]; myosin V binding [GO:0031489]
AORTA (DOWN)	RS28 P62858 *Rps28*	40S ribosomal protein S28	cytoplasm [GO:0005737]; cytoplasmic side of rough endoplasmic reticulum membrane [GO:0098556]; cytosol [GO:0005829]; cytosolic small ribosomal subunit [GO:0022627]; nucleolus [GO:0005730]; polysomal ribosome [GO:0042788]; postsynapse [GO:0098794]; presynapse [GO:0098793]; ribosome [GO:0005840]; small-subunit processome [GO:0032040]; synapse [GO:0045202]	structural constituent of ribosome [GO:0003735]
AORTA (DOWN)	SYVM Q3U2A8 *Vars2 Kiaa1885 Vars2l*	Valine--tRNA ligase, mitochondrial	cytosol [GO:0005829]; mitochondrion [GO:0005739]	aminoacyl-tRNA editing activity [GO:0002161]; ATP binding [GO:0005524]; valine-tRNA ligase activity [GO:0004832]
AORTA (DOWN)	TI17A Q9Z0V8 *Timm17a Tim17a*	Mitochondrial import inner membrane translocase subunit Tim17-A	mitochondrial inner membrane [GO:0005743]; mitochondrion [GO:0005739]; nucleoplasm [GO:0005654]; TIM23 mitochondrial import inner membrane translocase complex [GO:0005744]	enzyme binding [GO:0019899]; protein transmembrane transporter activity [GO:0008320]
AORTA (DOWN)	TPPP Q7TQD2 *Tppp*	Tubulin polymerization-promoting protein	cytoplasm [GO:0005737]; cytosol [GO:0005829]; Golgi apparatus [GO:0005794]; microtubule [GO:0005874]; microtubule bundle [GO:0097427]; microtubule organizing center [GO:0005815]; mitochondrion [GO:0005739]; mitotic spindle [GO:0072686]; myelin sheath [GO:0043209]; nucleus [GO:0005634]; perinuclear region of cytoplasm [GO:0048471]; postsynaptic Golgi apparatus [GO:0150051]	GTPase activity [GO:0003924]; magnesium ion binding [GO:0000287]; microtubule binding [GO:0008017]; microtubule nucleator activity [GO:0140490]; protein dimerization activity [GO:0046983]; protein homodimerization activity [GO:0042803]; tubulin binding [GO:0015631]

4.12. Conclusions

The improvements in metabolic parameters observed in chapter 4 suggest that 3-10 days of MR have potential to be a strong metabolic therapy for treatment of cardiometabolic dysfunction and to decrease risk of CVD. We show that diet-induced obesity is decreased by short-term MR diet, and this benefit is extended to important cardiometabolic parameters that determine CVD risk. The reduction in fasting blood glucose and plasma insulin are consistently improved with short-term MR and are supported by improved measure of insulin resistance (HOMA-IR ratio). Secretion of hepatokines and adipokines are improved and correlate well with MR-induced weight loss. MR displayed adipose depot specific effects, with no observable changes in BAT and iWAT experiencing modification of adipocyte differentiation and lipid mobilization.

The primary finding from this study is that MR prevents lipid accumulation in PVAT from the thoracic aorta while improving physiological health with 3-10 days of MR. As a mediator of PVAT lipid accumulation and inflammation in general, MR diets hold promise to counteract diet-related metabolic and vascular dysfunction, as it is clear from these data that MR rapidly changes PVAT phenotype. We demonstrated that MR induces lean phenotype in PVAT very rapidly, and that the lean phenotype appears to be manifested through decreased adipogenesis as well as increased lipolysis. We also identified proteomic targets that have potential to play important roles in early adaptations to MR. Interestingly, this dramatic effect on the PVAT does not translate to changes in vessel area or lumen area.

4.13. Study Limitations

While we have observed that short-term MR diet is a powerful modulator of murine metabolism, the broad translational impact might be limited due to this study performed in only male mice where there are documented sexually dimorphic responses to MR [394]. Additionally,

C57Bl/6J mice represent a narrow genetic background that are responsive to MR diets, however MR has been shown to prevent type 2 diabetes in NZO mice [395]. Another item to take note of is that a 10-day window for mice does not equate to the same time frame for humans and could represent about a year in humans. Furthermore, no functional data was collected to understand if short-term MR influences overall body composition to inform adipose tissue distribution and on an adipose-depot specific level how MR influences mitochondrial energetics, adipokine secretion or glucose uptake.

4.14. Future Directions

Proteomic targets of MR in PVAT and aorta can be tested to determine if changed pathways mediate the response to MR. Human clinical studies of MR experience limitations due to poor palatability of MR diets and subsequent low compliance of participant for 16-week study duration [269] and was improved with 8-week study duration [294] and 4-week duration [291]. Understanding the effects of MR for short durations is needed due to the difficulty of implementing MR diets in human populations. Identified molecular targets of MR in PVAT and aorta have potential to be pursued pharmaceutically and thus expand accessibility of MR to a wider patient population.

CHAPTER 5
IN VITRO EFFECTS OF METHIONINE RESTRICTION ON PERIVASCULAR ADIPOSE TISSUE-DERIVED ADIPOCYTES

5.1. Overview

To test mechanistic targets of MR identified in section 4.9, we developed an *in vitro* model of MR in PVAT-derived adipose progenitor cells (APC). Our primary goal was to characterize cellular effects of MR on PVAT-APC, followed by mimicking the lean PVAT phenotype observed *in vivo* and finally determine if chemical inhibitors targeting proteomic targets would mediate the effects of MR in vitro. *The data presented within Chapter 5 are from a manuscript submitted to Elsevier journal, Molecular Metabolism in May 2024.*

5.2. Spontaneous Immortalization of Primary Cell Line Isolates from PVAT

To address cell specific influences of MR, we collected PVAT from C57Bl/6J male and female mice at 8 weeks of age (n = 3 per sex) and isolated primary APC, as described in section 2.2.1. Primary APCs were expanded clonally and used to practice methodology that was employed in the following *in vitro* experiments. Throughout early testing with PVAT-derived APC, doubling rate was about 3-4 days. Around passage 25, APC had a doubling rate of about 1-2 days. Possible explanations for this increase in doubling rate could be contamination with highly proliferative cells or spontaneous immortalization. Immortalization is a process where cells in culture can divide indefinitely, and typically transpires using retroviral introduction of oncogenes which prevents cells from entering senescence [396], or introduction of telomerase which prevents telomere shortening [397]. Other modes of inducing spontaneous immortalization of primary cells lines are chemical inhibitors [398] or genetic manipulations like CRISPR/Cas9 [399] that alter pathways related to senescence or apoptosis, and finally the use of myeloma cells for the creation of hybridoma technology [400]. In rare occasions, cells can spontaneously immortalize without the

Table 5.1: Cell Line Authentication Via Short Tandem Repeat Profiling. Early and late passages of mouse PVAT APC, along with potential contaminating cell line were sent to ATCC to have 18 mouse loci sequenced. Locus is indicated in the first column, and allele/s for the locus that is present in the sample is indicated.

Locus	PVAT, Mouse, p10	PVAT, Mouse, p40	Thermomouse P7
18-3	16	16	17
4-2	20.3	20.3	19.3
6-7	18	17,18	12
19-2	14	13	12
1-2	19,20	19	13
7-1	27.2	27.2	30
1-1	16	15,16,17	10
3-2	**14**	**14**	**14**
8-1	16	16	15
2-1	16	16	9
15-3	22.3	22.3	20.3
6-4	18	18	15.3
11-2	16	16	15
17-2	16	16	15
12-1	17	17	20
5-5	17	17	14
X-1	27	27,28	26
13-1	17	17,18	15.2

use of retroviruses, chemical and genetic manipulation, and that occurs through random mutations. To test whether our PVAT APC had been contaminated or immortalized, short-tandem repeat profiling was performed by the ATCC Cell Line Authentical Service and compared to potential cell line contaminate, Thermomouse derived APC (JAX#026690). Allelic profiles for 18 loci show both early and late passages of PVAT only share similarity with Thermomouse on one loci (bolded line on Table 5.1), and demonstrates that there was no contamination with highly proliferative Thermomouse cell line. Furthermore, early and late passages of PVAT do differ in 6 loci, while the other 12 loci are identical, which suggests that random mutations have occurred due to passages of cell line over time and have led to the spontaneous immortalization of our cell line. Following cell line authentication, PVAT APCs were used for the following experiments.

5.3. Methionine Restriction Reduces DNA Synthesis in Proliferating PVAT-Derived Preadipocytes

We assessed the individual cellular effects of MR on PVAT-derived APC, starting with cell proliferation. Proliferating APC in methionine/cysteine/cystine deprived conditions for 24 hours results in almost complete loss of living PVAT-APC (Figure 5.1 C-D). Of the surviving

cells, DNA synthesis was still possible, but methionine/cysteine/cystine deprivation resulted in a significant reduction in DNA synthesis. Proliferation in methionine/cysteine/cystine deprived conditions for 2 hours allowed us to measure DNA synthesis with similar number of APC and within 2 hours we observed a significant reduction in DNA synthesis (Figure 5.1 A-B). We also measured the effect of MR on DNA synthesis in proliferating APC with the supplementation of cystine equally to all conditions, in which after 24 hours we observed methionine dose-dependent significant reductions in DNA synthesis (20μM, $p=0.03$; 0μM, $p<0.0001$) compared to control levels of methionine (100μM)(Figure 5.1 E-F). The addition of cystine allowed us to improve cell survival within MR conditions and have similar amounts of proliferating APC to compare. This necessity of cystine/cysteine for the proliferation of APC has been previously established in a study in porcine-derived dorsal subcutaneous APC [401]. As seen by the addition of cystine and increased cell survival in all conditions, including 0μM methionine (Figure 5.1E-F) , the rapid cell death is most likely occurring due to cysteine/cystine deprivation and could be occurring through ferroptosis [402, 403] or autophagy [404].

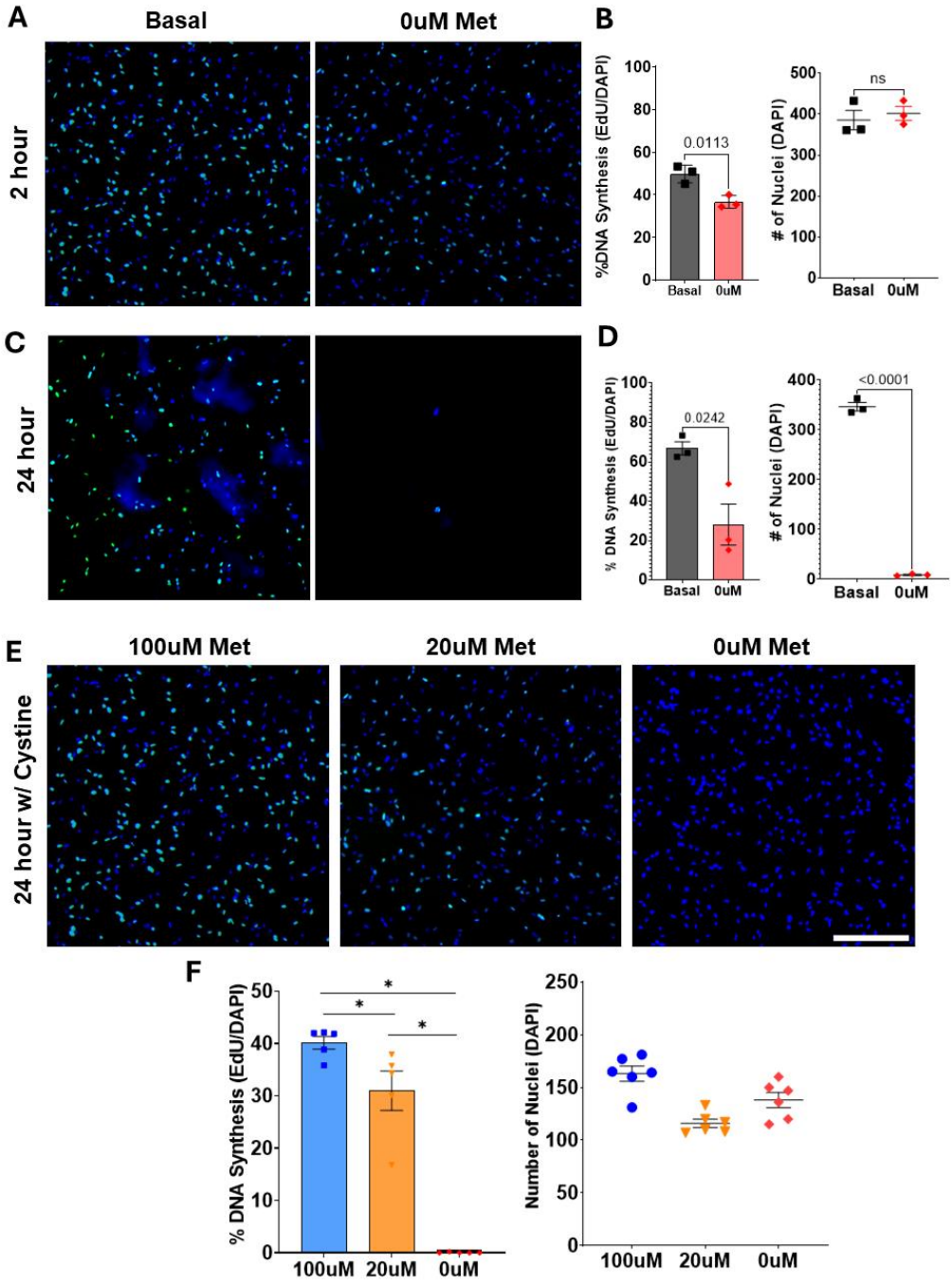

Figure 5.1 Methionine Restriction Reduces DNA Synthesis in Proliferating PVAT-Derived Preadipocytes A.) Fluorescently labeled APC following incubation in basal or methionine depleted conditions for 2 hours B.) Quantification of percent DNA synthesis in cells shown in A, calculated by dividing number of nuclei with recently synthesized DNA (green, EdU labelled APC) by the number of total nuclei (blue, DAPI/Hoechst labelled APC) C.) Fluorescently labeled APC following incubation in basal or methionine depleted conditions for 24 hours D.) Percent DNA synthesis and total cells after 24 hours, shown in C. E.) Images of labeled cells after methionine dose curve (100um, 20um, 0um) with 250uM cystine supplementation in all conditions for 24 hours, scale bar =300μm. F.) Percent DNA synthesis and total cells after 24 hours, cells shown in E.

Due to the significant impact on DNA synthesis in methionine-restricted and depleted conditions, we also asked what phases in cell cycle progression might be impacted during cell proliferation. We have evidence that S phase arrest occurs in 0μM conditions by significant reductions in PCNA (Figure 5.2 C-D), which corroborates our observations of decreased DNA synthesis. We also measured significant increases in p53 which indicates that there is arrest at G1/S and/or G2/M checkpoints (Figure 5.2 B,D). Histone 3 (H3) and phosphorylated H3-Ser10 (pH3), markers of active mitosis were also measured, no changes in H3 were shown (Figure 5.3 A,D). However, to have a complete assessment of the impact on M phase, pH3 would need to be quantified and efforts were unsuccessful. No significant differences in cell cycle markers were seen in 20μM conditions, which suggests that decreased DNA synthesis observed in this condition (Figure 5.1 E-F) is due to alternate mechanism other than arrest in S phase or at G1/S or G2/M checkpoints. Protein translation was also impacted in proliferating APC, where we measured a dose-dependent response in puromycin-incorporation into newly synthesized proteins in conditions supplemented with cystine and either 60μM or 0μM methionine (Figure 5.4A-C).

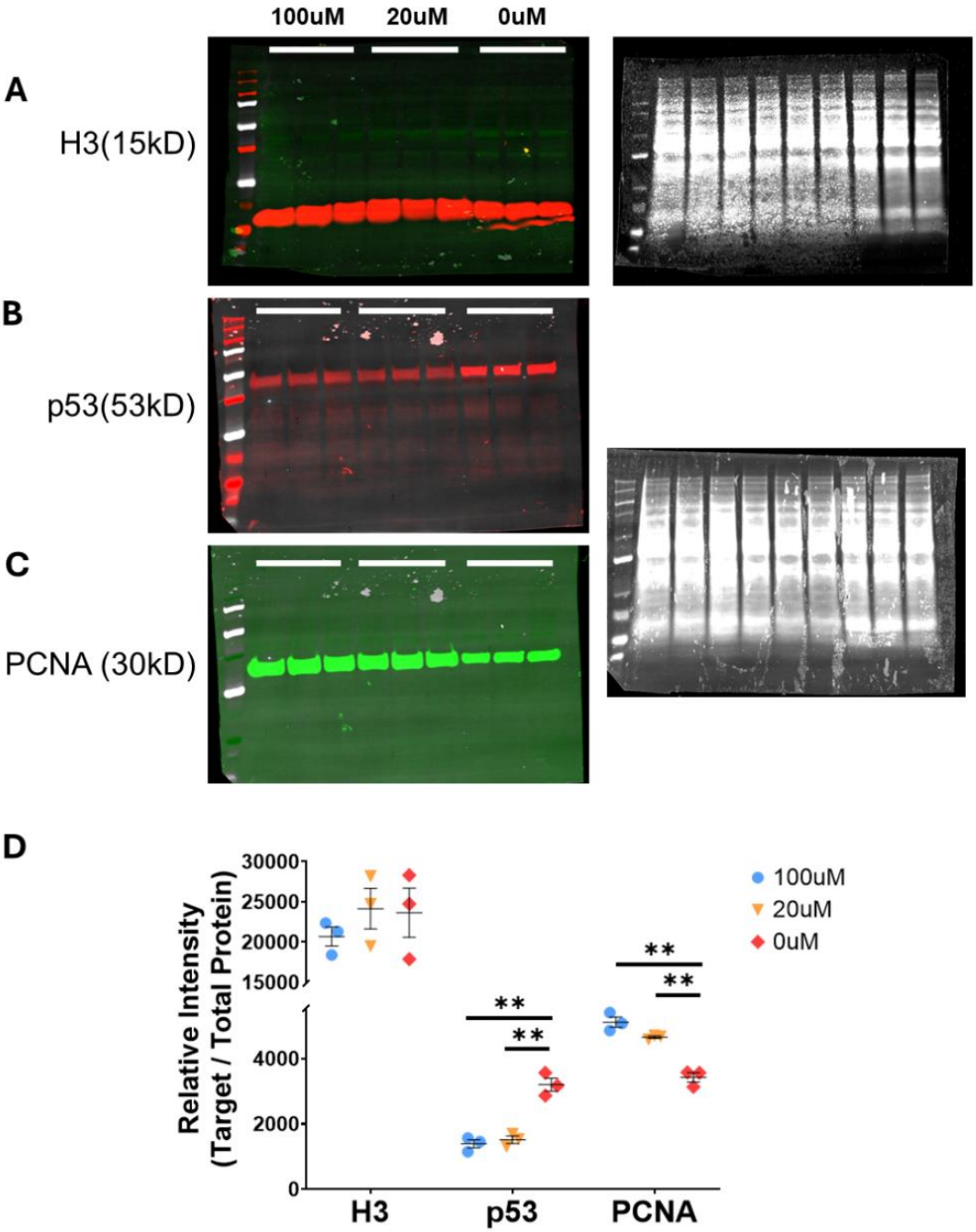

Figure 5.2 Methionine Restriction Suppresses Cell Cycle Progression in Proliferating PVAT Preadipocytes. Proliferating PVAT APC were incubated in methionine dose curve, 100uM, 20uM, 0uM supplemented with 250uM cystine in each condition **A.)** Immunoblot of histone 3, marker of M phase, and total protein. **B.)** Immunoblot of p53, marker of G1/S and G2/M checkpoints, and total protein **C.)** Immunoblot of PCNA, marker of S phase, and shared total protein with p53. Blots utilized fluorescent secondary antibodies and allowed for multiplexed antibodies. **D.)** Quantified protein abundance relative to total protein. 100uM (blue circles), 20uM (orange triangles), 0uM (red diamonds)

5.4. Methionine Restriction Reduces Adipogenesis in PVAT-Derived Adipocytes

To model the lean phenotype observed with MR in mouse PVAT, we induced adipogenic differentiation in PVAT-derived APC. Due to the established effects of MR on proliferating cells, when APC were induced in methionine depleted induction media there was a significant loss of cells (Figure 5.3 A-B). This confounded the ability to effectively compare lipid accumulation between basal and 0μM conditions (Figure 5.3 C-D). For all remaining differentiation experiments we chose to initiate differentiation in induction media containing basal amounts of methionine to ensure the same number of cells were brought into the maintenance phase for all conditions. This was followed by maintenance media made with methionine depleted media (0μM) and L-methionine supplemented to basal levels (100μM) and MR levels (20μM). Induction of APC in basal induction media allowed the same number of cells to survive through induction into the adipogenic process (Figure 5.3 E, G, H). The dose curve of methionine resulted in dose-dependent significant reduction in lipid accumulation in both 20μM ($p=0.007$) and 0μM ($p=0.0006$) conditions compared to 100μM (Figure 5.3 G-H). This dose-dependent trend in adipocyte differentiation independent of cystine supplementation during MR (Figure 5.3 E-F). This *in vitro* model of MR mimics the lean phenotype observed in the *in vivo* study of MR, which suggests that prevention of adipogenesis in perivascular adipocytes is a function of MR *in vivo*. This dose-dependent reduction in adipocyte differentiation has also been observed in porcine-derived dorsal subcutaneous APC [401].

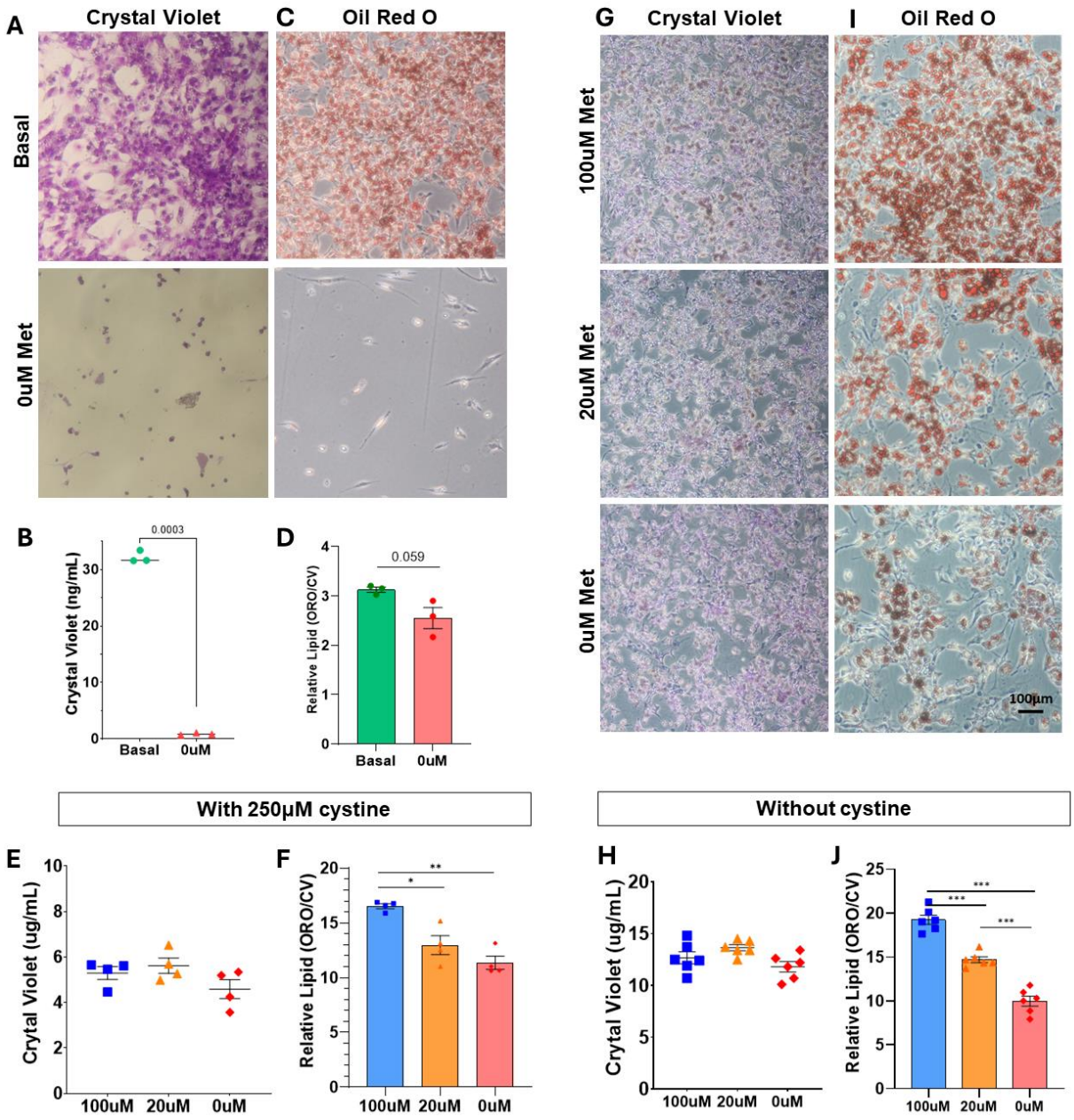

Figure 5.3 M**ethionine Restriction Reduces Differentiation of PVAT-Derived Adipocytes A.)** Bright field images of crystal violet stained APC following induction and maintenance in either basal or methionine depleted conditions **B.)** Quantification of crystal violet stain from cells in A (ng/mL) **C.)** Bright field images of Oil Red O (ORO)-stained lipids in differentiated APC following induction and maintenance either basal or methionine depleted conditions **D.)** Quantification of ORO stain from cells in C, relative to crystal violet in B **E.)** Quantification of crystal violet stain (ng/mL) from APC following methionine dose curve in maintenance phase with 250uM cystine **F.)** Quantification of ORO stain (ng/mL) from methionine dose curve with 250uM cystine, relative to E. **G.)** Bright field images of crystal violet stained APC following methionine dose curve (100um, 20um, 0um) during maintenance phase without cystine **H.)** Quantification of crystal violet stain (ng/mL) from cells in G. **I.)** Bright field images of Oil Red O (ORO)-stained lipids in differentiated APC following methionine dose curve during maintenance phase without cystine **J.)** Quantification of ORO stain from cells in I, relative to crystal violet in H.

5.5. Methionine Restriction Reduces Protein Synthesis in Proliferating Preadipocytes but not in Differentiated Adipocytes from PVAT

Due to methionine being the initiating amino acid in protein synthesis, MR slows protein synthesis in other tissue types [149, 150, 375, 405], it was pertinent to measure the effect of MR on PVAT-APC. As mentioned, protein synthesis is decreased in proliferating APC, however statistics were not possible with only one replicate (Figure 5.4 A-C). Protein synthesis in differentiated adipocytes was not significantly impacted by dose-curve of methionine (Figure 5.4 D-F).

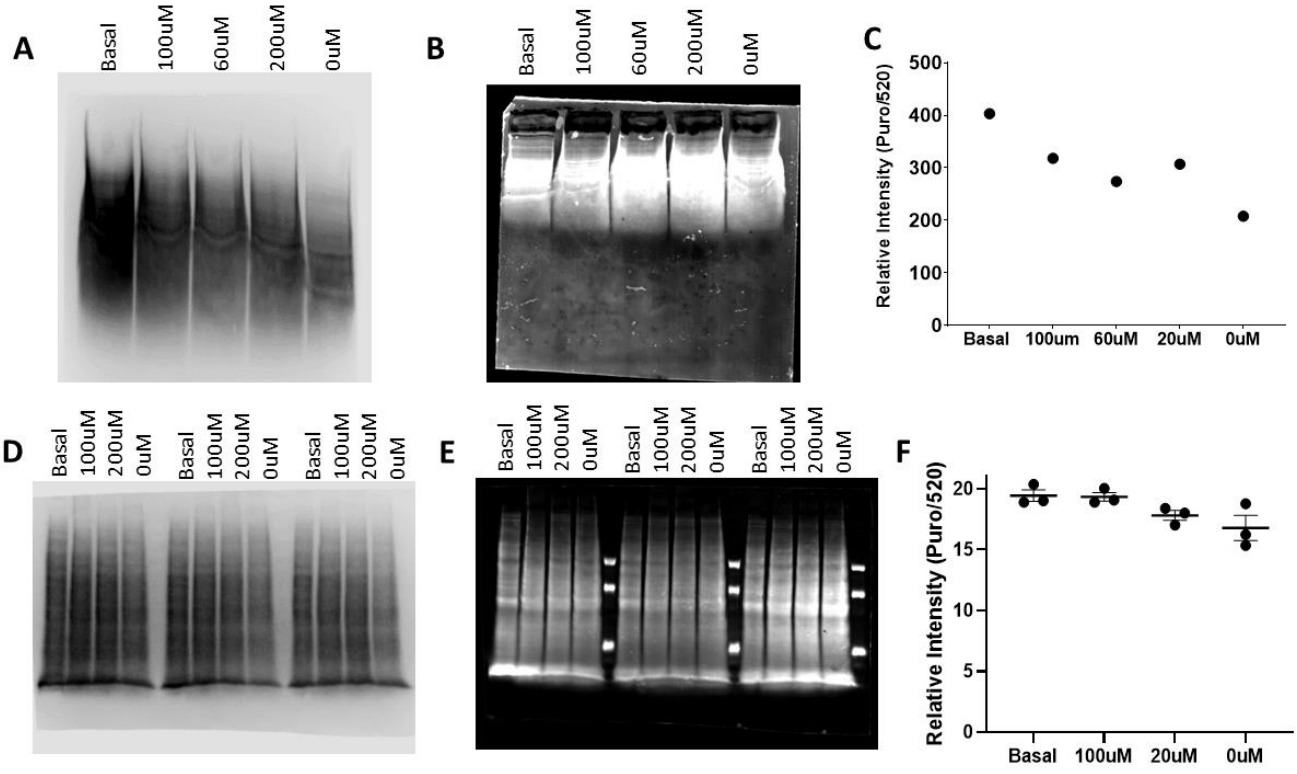

Figure 5.4 Protein Synthesis in Proliferating Preadipocytes and Differentiated Adipocytes
A.) Chemiluminescent exposure of puromycin-incorporations into newly synthesized proteins of PVAT APC during proliferation in methionine dose curve (100uM – 0uM methionine) + 250uM cystine supplemented. B.) Total protein in proliferating APC in methionine dose curve C.) Quantification of relative protein in A-B, puromycin/ total protein D.) Chemiluminescent exposure of puromycin-incorporations into newly synthesized proteins of differentiated PVAT APC in methionine dose curve (100uM – 0uM methionine) E.) Total protein in differentiated APC in methionine dose curve F.) Quantification of relative protein in D-E, puromycin/ total protein

5.6. Inhibition of Cathepsin Z in Differentiating PVAT-Derived Adipocytes

To test proteomic target Cathepsin Z (CATZ) in PVAT, *in vitro* model of PVAT APC differentiation was treated with CATZ inhibitor (CATZi). CATZ was upregulated in MR groups *in vivo,* which led us to hypothesize that if CATZ mediates effects, treatment with CATZi would result in increased lipid accumulation in 20μM methionine group compared to vehicle (DMSO) treated counterpart. Differentiating APC were treated with 10μM CATZi during the maintenance phase of differentiation and resulted in decreased lipid accumulation within the 100μM methionine condition and unaltered lipid accumulation in 20μM and 0μM conditions (Figure 5.5A). The DMSO vehicle control group did not have any change in methionine dose-dependent reductions in lipid accumulation.

Treatment with 20μM CATZi during the induction phase of differentiation did not result in any noticeable differences between treatment and vehicle groups (Figure 5.5B). However, the methionine dose-dependent trend is lost in both vehicle and CATZi groups. This experiment has room to be improved, as the treatment with DMSO during the induction phase has been shown to impact adipocyte contact inhibition of proliferation, a process that is important for adipocyte differentiation [406, 407], and allowed APC to continue proliferation and prevent PVAT-APC differentiation.

Western blot of APC treated with 20μM CATZi during induction shows increase in CATZ protein abundance upon treatment in 100μM Met conditions, however this trend is inversed in 20μM Met conditions (Figure 5.5C), More replicates are needed to confirm these trends. Further studies are needed to determine the effectiveness of CATZi on CATZ function in APC.

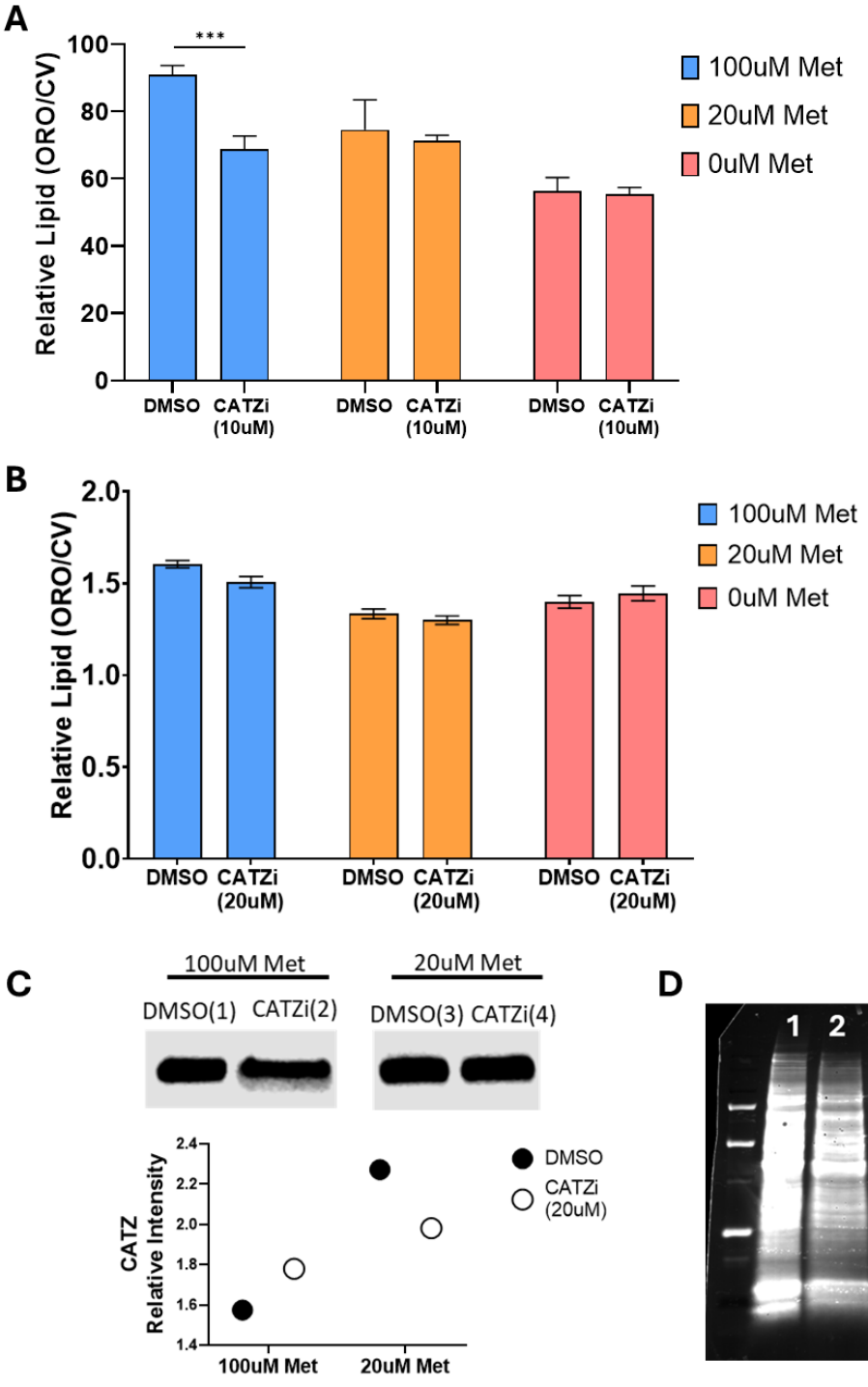

Figure 5.5 Cathepsin Z Inhibitor Studies A.) Relative lipid accumulation in differentiated APC following Cathepsin Z inhibitor (CATZi) treatment during maintenance phase **B.)** Relative lipid accumulation in differentiated APC following CATZi treatment during induction phase **C.)** Western blot of CATZ in differentiated APC following CATZi treatment during maintenance phase, quantification of CATZ abundance **D.)** Total protein of samples in C.

5.7. Conclusions

Methionine is an important precursor to many cellular processes, and these experiments have shown that methionine is essential during PVAT-APC proliferation and differentiation. As described in section 1.6.2, cysteine and cystine, additional amino acids synthesized from methionine, are important for glutathione and redox balance within the cell. From these experiments cystine is a critical factor for the survival of PVAT-derived APC during proliferation. Despite cystine supplementation, we observed a methionine dose-dependent effect reduction in proliferation.

We developed an *in vitro* model of PVAT adipogenesis and successfully replicated the lean phenotype in PVAT that was induced by MR *in vivo*, by significantly reducing adipogenesis in PVAT-APC. Interestingly, this effect is independent of cystine supplementation. Protein synthesis is also dramatically decreased in proliferating APC by MR and minimally in mature adipocytes. Collectively, it appears that MR leads to either quiescence or cell death in preadipocytes and to decreased lipogenesis in mature adipocytes. These effects can reduce both hyperplastic and hypertrophic expansion of PVAT and result in a lean phenotype. A strength of this study that we developed our model using both male and female mice.

We observed in section 4.9 that short-term MR induces upregulation of Cathepsin Z (CATZ) and were able to perform preliminary experiments in PVAT-APC with a CATZ specific inhibitor. We expected to see the methionine dose-dependent decrease in lipid accumulation in differentiating PVAT-APC to be lost if CATZ mediated this effect. However, with these experiments we did not see that effect emerge. It is unclear if this result is due to study design or CATZ not mediating MR-induced lipid accumulation in APC.

5.8. Study Limitations

As mentioned above, our studies on PVAT-APC with CATZ inhibitor are inconclusive, and this is most likely due to study design. In its current form, studying the effects of CATZ inhibition on lipid accumulation in mature adipocytes has room for improvement. The inhibitor was dissolved in DMSO, which has been shown in reduce induction of preadipocyte to differentiate into mature adipocytes [406, 407]. While the amount of DMSO was properly controlled for between vehicle and inhibitor conditions, more care can be given to the amount of DMSO used during these experiments. Furthermore, the hydrophobic qualities of the CATZ inhibitor require solubilization in DMSO, which can complicate the efficacy of the inhibitor in aqueous cell culture conditions. Addition of inhibitor into cell culture medium has potential to precipitate the inhibitor and decrease the ability to traverse cell membranes as well as enter organelles such as endoplasmic reticulum where CATZ is synthesized or in lysosomes where CATZ primarily functions. Study design could also benefit from more robust functional testing of CATZ inhibition and for general impact of MR on lysosomal activity, which will be further discussed in the future directions.

The use of immortalized APC may be limiting to translational impact of this work. Spontaneously immortalized cells have accumulated a number of mutations that impact cellular function. The full impact of these acquired mutations is unknown and most likely influence several relevant cellular processes. While the immortalized cells have been a useful model to study the general effects of MR on PVAT-APC, as they are highly robust, proliferate rapidly and are resistant to cell death, testing these same effects in non-transformed primary cells would be more representative of PVAT biology *in vivo.*

In addition to adipocytes, there are several other types of cells present in PVAT that are most likely impacted by MR as well and are not represented in the *in vitro* model utilized here, such as macrophages, lymphocytes, fibroblasts, endothelial cells, pericytes, neurons and dendritic cells. Three-dimensional *in vitro* models can be used with two or more cell types to improve representative nature of the cell model [408-410].

5.9. Future Directions

Our study lacked confirmation of functional activity of CATZ. Additional studies to understand the role of CATZ in PVAT should be accompanied by measuring activity of CATZ. In the limited literature published on the CATZ inhibitor employed in these studies, functionality was determined by reduced endothelial cell migration with the inhibitor [411, 412]. The molecule operates enzymatically to reduce CATZ activity. In order to determine activity of CATZ, specific activity-based probes have been developed for CATZ [413]. The effect of MR on lysosomal activity should also be performed to understand if CATZ operates through presence in lysosomes or in the cytoplasm. The use of siRNA to silence CATZ may be a more effective strategy to test the role of CATZ in these *in vitro* conditions.

Our experimental scope of CATZ influence on PVAT can be expanded, as CATZ may not be mediating lipid accumulation in mature adipocytes. Since CATZ has broad substrate specificity it could influence several cellular functions such as proliferation, migration, adhesion, and communication in several cell types such as pre-adipocytes, neurons or immune cells. A tissue specific knockout mouse model or siRNA knockout cell model could be used to identify the role of CATZ in MR.

CHAPTER 6

DISCUSSION

6.1. Overview

MR has been shown to extend lifespan and improve healthspan of mice by lowering weight gain, adiposity, and oxidative stress, while increasing mitochondrial activity and insulin sensitivity, which collectively ultimately decrease the risk of cardiovascular and cardiometabolic disease. PVAT has been shown to be both protective from vascular pathology as well as contributing to vascular pathogenesis during injury, aging, and metabolic disorders [81, 358, 414-421]. The primary goal of this project is to determine the effects of MR on PVAT as well as thoracic aorta, and secondary on overall cardiometabolic health.

To investigate our hypothesis, we employed two *in vivo* studies of 80% MR in male mice and developed an *in vitro* model of PVAT-derived adipose progenitor cells (APC) from both male and females. In collaboration with the Orentreich Foundation for the Advancement of Science, the *in vivo* studies allowed us to test long-term MR in three different aged cohorts, as well as short-term MR in diet-induced obesity, on physiological, morphological, and molecular alterations due to an 80% MR diet. The novel *in vitro* model of PVAT-derived APC that we developed allowed us to study the effects of MR on cellular proliferation and differentiation. We were also able to apply this model to a pilot investigation into potential molecular mediators of MR in PVAT.

6.2. Long-Term Methionine Restriction Counteracts Age-Related Metabolic Dysfunctions and Causes Lean Phenotype in Perivascular Adipose Tissue

Within *Chapter 3*, we expanded our understanding of the utility of MR to counteract age-associated metabolic pathology in mice using young, middle, and old aged mice. While many studies have reported effects of MR in diverse age ranges throughout the mouse lifespan [230-232,

266, 267, 280, 344, 422], this is the only study to observe the effects on cardiometabolic health in three age phases simultaneously. We show that long-term MR diet prevents age-related weight gain, and this benefit extends to important cardiometabolic parameters that determine cardiovascular disease risk. Glucose metabolism, cardioprotective hepatokines and adipokines are significantly improved by long-term MR in all age phases, young adults, middle-aged adults, and old adults. Long-term MR reduces body weight in in part by influencing adipose depot adipogenesis, lipolysis, and mitochondrial respiration.

This is also the first study to evaluate the effect of MR on PVAT. While we did not see an age-associated increase in PVAT lipid accumulation, we did observe MR reduce PVAT lipid accumulation in all three age phases in mice. While this study is the first to explore the effect of MR on PVAT, there are several similarities to observed effects of MR on other adipose depots. Specifically, increased mitochondrial proteins, lipolysis, decreased adipocyte differentiation and associated loss of lipid accumulation and tissue mass [264, 281, 286, 293, 357, 363, 393, 423]. Interestingly, while the lipid content of PVAT was correlated with body weight and markers of metabolic health at all three ages, the MR-induced increase in thermogenic markers was seen in PVAT only from the young cohort, not the middle-aged cohort. As the primary finding from this study, it is not entirely surprising that that the largest effects of MR on PVAT occur when the diet is initiated in young adult mice. This is due to the age-associated physiological decline within all organ systems [35], thus it is possible that the difference in mitochondrial response is senescence associated decline. It is also possible that effect may be due to the young animals have the highest requirement for methionine as they are still in a growth phase [147]. Furthermore, aging impacts gastrointestinal motility and slowed food digestion could be another factor in age-related response to MR [424]. Despite these differences in molecular response between young and middle-aged

mice, it is encouraging to see PVAT phenotypic leanness and similar cardiometabolic responses in all ages. This suggests that MR can be implemented in any adult age group and have favorable whole-body metabolic responses as well as influence PVAT phenotype. While this is encouraging, we did not observe any changes in the aortae, thus we have yet to understand if this diet induces any beneficial effects within the aorta. Functional and molecular testing of vessels following MR is pertinent.

Given that the prevalence of metabolic syndrome is highest in old humans, it is promising that MR induces benefits in our middle-age and old mouse cohorts. However, given that prevalence of metabolic syndrome is increasing among adolescents in the United States [17, 18], and CVD risk is greater when the age of onset occurs at a younger age [19], it is encouraging that MR has such a profound impact on metabolic health and PVAT phenotype in young mice. Further understanding of the relationship between MR and PVAT in young mice is pertinent in deploying MR as a therapeutic approach to combat childhood metabolic dysfunction and obesity.

6.2.1. Addressing the Utility of Methionine Restriction in Different Age Groups

Age is an important factor that is often overlooked while conducting biomedical research in rodents. This seemingly simple variable impacts the translation from rodent models to successful clinical outcomes [425]. Studying the effects of MR in three different life stages is meaningful because there are physiological processes that differ based on age. The most commonly used age range in mouse research is 8-12 weeks and a few examples of processes that are still developing during this age are bone mass and structure [426], immune system [427, 428], brain and the central nervous system [429, 430]. Additionally, older adult animals will most likely respond differently than young adults, due to the onset of senescence as well as the dietary requirement for methionine decreases throughout age [147]. Older adults will most likely have

differences in injury recovery [431, 432], nutrient assimilation [433], immune function [434] and drug metabolism [435]. Since most rodent studies on MR are performed in the young adult life stage it is a strength of this study to include mice at three different life stages, however there are some limitations to the translational impact of this work in humans. Considering the age equivalencies between mice and humans, it is important to discuss maturation rates. Between the ages of birth and 1 month of age, mice mature at a rate that is 150 times faster than humans. Between 1 and 6 months of age, mice mature 45 times faster than humans and greater than 6 months that rate decreases to 25 times faster [436]. The age groups that were selected for this study are representative of similar life stages in humans (Table 6.1). However, based on maturation rates the length of the dietary intervention in mice is equivalent to a decade or more in the life of a human. While the physiological benefits of therapeutic MR are robust at all ages, the duration of the diet may be unsustainable in humans, depending on the dietary baseline in which the therapy was initiated and the perceived end goal.

Table 6.1. Age Equivalency Between Mice and Humans. Adapted from Flurkey et al, and the Jackson Laboratory "Life span as a biomarker"

Life Stage	Mouse Age	Human Age
Puberty	1.5-2 months	11-13 years
Adulthood	3-6 months	20-30 years
Middle Age	10-14 months	38-47 years
Old Age	18-24 months	56-69 years

6.3. Short-Term Methionine Restriction Counteracts Diet-Related Metabolic Dysfunctions and Induces Rapid Lean Phenotype in Perivascular Adipose Tissue

Due to the unique response in young mice observed in *chapter 3*, we were motivated to study further explore the response of young mice. Additionally, due to the increase of childhood obesity and metabolic syndrome we were also interested to see if MR could counteract diet-induced obesity in young mice. Furthermore, as described in section 1.14, most mouse studies of

metabolic response to MR used a duration of 14 weeks and the shortest duration was for 6 weeks. The study described in *chapter 4* is a unique study that explores the effect of short-term MR on metabolism and PVAT in young obese mice. With this study we expanded our understanding of the utility of MR to counteract diet-associated metabolic pathology. Implementing the diet for 3-10 days provides many of the same benefits that are commonly reported in moderate to long-term durations of MR, such as weight loss, improved glucose metabolism, cardioprotective hepatokine and adipokine secretion. However, the effects on large adipose tissues do not appear to be as robust as moderate to long-term MR and seem to be depot dependent. WAT has experienced reductions in adipocyte differentiation and lipogenesis, while BAT does not have any recognizable changes in gene expression. The time it takes for large adipose depots to fully adapt to metabolic alterations that occur MR may be longer than the 3-10 days implemented in this study.

Similar to the long-term study, no changes in vessel morphology were observed with short-term MR, however the proteomic analysis of aorta from these animals suggest that there is vascular remodeling occurring in short durations of MR. While there were no changes measured in medial or lumenal area of aorta, there are protein changes that have potential to influence vascular function, thus more research is needed to explore the effects of MR on vessel contractile and dilative capacity.

While a lean PVAT phenotype was observed in the long-term MR study of *chapter 3*, it was still shocking to observe that the lean phenotype occurs so rapidly with short-term MR. This lean phenotype is accompanied by reductions in adipocyte differentiation, lipogenesis, and protection from lipolysis, as well as increased mitochondrial respiration and no change in thermogenic markers. This was contrary to the increased thermogenesis that is typically observed in moderate to long term MR [271, 437]. Increased mitochondrial respiration without increased

mitochondrial biogenesis or thermogenesis in PVAT upon MR suggests that spare respiratory capacity may be initiated to meet cellular energy requirements. This adaptation could also contribute to the increased energy expenditure that occurs with MR [280, 281, 286, 393, 437-439]. This increase in energy expenditure limits fat deposition and coincides with a pronounced expansion of the dynamic range of the respiratory quotient which indicates increased metabolic flexibility and transitioning from glucose utilization and a shift to fat oxidation [280]. Important characteristics of the lean phenotype that we chose to focus on include reductions in adipocyte differentiation as well as cellular proliferation which is very intensely explored in methionine restriction

6.4. Methionine Restriction Reduces PVAT Preadipocyte Proliferation

We developed a novel *in vitro* model of MR that allows us to test the impact of MR on PVAT -preadipocyte functions. Optimization of the model was important as it was clear that complete depletion of methionine and other sulfur amino acids (cystine and cysteine) was inhibitory to PVAT-preadipocyte survival. This was expected considering the highly proliferative state of PVAT-APC employed in these studies and the similarity to uncontrolled proliferation in cancer cells, as described in section 1.10 many studies have observed the cancer cell dependence on methionine and cystine for survival and proliferation [252, 253, 257, 440-445]. Furthermore, methionine and/ or cysteine deprivation sensitizes cancer cells to cell death, primarily by inducing ferroptosis and autophagy [403, 404, 443, 446]. Cellular protection from ferroptosis, iron-dependent necrotic cell death, is reliant on glutathione. As described in section 1.6.2 cysteine is a necessary precursor for glutathione synthesis. Due to the culture medium that is devoid of methionine/cysteine/cystine, cysteine deprivation is occurring in the 0μM methionine conditions, leading to cell death. Supplementing the culture medium with cystine, the oxidized from of

cysteine, prevented cell death in all conditions, and revealed a methionine dose-dependent response in DNA synthesis. We also measured a methionine dose-dependent response in puromycin-incorporation into newly synthesized proteins in conditions supplemented with cystine and either 60μM or 0μM methionine. Considering the reduction in protein synthesis, it is possible that G1 is impacted, and cells have entered a G0 quiescent state [447] instead of continuing through S phase. Reductions in S-adenosyl methionine (SAM) is known to block DNA synthesis and lead to cell cycle arrest at the G1/S transition [145, 158]. Polyamine deprivation is another possibility in which methionine deprivation could be contributing to loss of cell cycle progression from G1 phase [160]. Polyamine supplementation has been shown to reduce DNA damage in adipose stem cells [448]. Mutations in regulatory genes that mediate polyamine synthesis result in S phase and G1/M arrest [161]. PVAT-APC in MR conditions did not have observable change in the tested cell cycle progression markers, which suggests that methionine-dependent decrease in DNA synthesis is due to alternate mechanism other than arrest in S phase or at G1/S or G2/M checkpoints. This is the first study of APC derived from PVAT, however the results are consistent with similar studies performed in porcine-derived dorsal subcutaneous APC [382]. A strength of this model is that the PVAT-APC were derived from both males and females.

6.5. Methionine Restriction Reduces PVAT Adipocyte Differentiation

Our novel *in vitro* model also included a measure of adipogenesis or adipocyte differentiation in PVAT-APC. PVAT-APC experienced methionine-dose dependent reductions in adipogenic capacity, where less lipid was measured in PVAT-APC following maintenance in 4 days in MR conditions. Protein translation in differentiated PVAT-APC was not significantly affected by MR which was interesting considering the dramatic effect observed in proliferating PVAT-APC. This *in vitro* model of MR mimics the lean phenotype observed in the *in vivo* study

of MR, which suggests that prevention of adipogenesis in PVAT adipocytes is a function of MR *in vivo*. This dose-dependent reduction in adipocyte differentiation has also been observed in porcine-derived dorsal subcutaneous APC [382]. Future studies should evaluate if the adipocytes are unable to undergo differentiation or if they are de-differentiating in the presence of MR.

6.5.1. Targeting Cathepsins and Lysosomal Function for Treatment of Obesity and Metabolic Syndrome

Proteomic analysis of PVAT revealed some proteomic targets, and CATZ was selected for downstream testing based it being upregulated upon MR, confidence of validation with immunofluorescent staining and the availability of a molecular inhibitor. While the CATZ inhibitor experiments have room for optimization and no conclusions can be made about the role of CATZ in mediating the lean phenotype induced by MR, it remains a meaningful target due to the well-documented lysosomal dysfunction observed in adipose tissue of obese individuals, discussed in section 1.5.3.4. While it is important to recognize that this proteomic dataset only represents early adaptions to MR diets in mice, the metabolic nature of these adaptations is encouraging that we have identified a relevant window in which MR is operating to induce metabolic changes that could impact metabolic dysfunction within adipose tissue. Lysosomes participate in numerous cell biological processes, such as macromolecular degradation, plasma membrane repair, exosome release, and apoptosis [449], all of which can contribute to obesity pathogenesis. CATZ and fellow members of the cathepsin family can be targeted to modify lysosome function [72, 378, 380, 382, 450, 451]. Furthermore, there are previous studies that have shown cathepsins to be impacted by amino acid deprivation in 3T3-L1 adipocytes [390]. The increase in lysosome might break down unused intracellular protein or damaged organelles to recycle some amino acids, which could provide an extra source of limited methionine for cell survival. Considering the

immunofluorescence images of CATZ within PVAT, we observed CATZ present in punctate regions through PVAT MR, however what was particularly noticeable was the robust expression of CATZ in cellular regions that were negative for PLIN1. There are observations of obesity-associated initiation of lysosomal autophagy in adipocytes, and this caused degradation of PLIN1 [452, 453]. It is possible that in our model of diet-induced obesity, autophagy was triggered by influx of lipid storage in PVAT adipocytes and that upon MR the lysosomal activity was increased to clear out dead or dying adipocytes which contributed to the lean phenotype. This process has been shown to be mediated by mitochondrial dynamics and regulated by B12 metabolism in *C. elegans* [454]. When lysosome dysfunction occurs, this can result in B12 deficiency which affects the reconversion of homocysteine into methionine and can result in increased mitochondrial biogenesis and fragmentation [454]. Lysosome function and CATZ should be further explored as a treatment for obesity and metabolic dysfunction. To the best of our knowledge, this is the first report of MR inducing changes in CATZ.

6.6. Study Limitations

A major limitation to this body of work is the lack of body composition data which would be necessary to understand what types of tissue are being reduced by MR diets. There have been a number of studies that show that about ¼ of the weight lost during MR is lean mass, however the vast majority of weight is lost from fat mass. While it is an important goal of modern obesity treatments to preserve lean mass while attempting to maximize fat loss, it is also important to know that in addition to loss of fat mass there will always be loss of lean mass, as fat mass contains lean mass. It has been established that approximately ¼ of weight loss will be fat-free mass [455, 456], thus the lean mass that is typically lost with MR has potential to be mass that is associated with fat mass without it actually being fat mass. While we cannot make any conclusions

in our studies here without the use of body composition data, it is important to note that we would expect the vast majority of the weight lost with MR to be associated with fat mass.

While these studies are the first to identify impacts of MR on PVAT, they are limited in functional readouts in PVAT. Many of these experimental limitations are due to the small size of PVAT which further shrinks upon MR. Additional molecular pathways could have been measured to explore the lean PVAT phenotype. Lipase expression or direct measurement of lipolysis could have increased confidence in assessing if effects on adipocyte differentiation are only due to lack of differentiation, the onset of de-differentiated or if increased lipolysis occurs. The study of porcine-derived APC measured gene expression of lipoprotein lipase and lipase E which was important to confirm that lipolysis was occurring in their cell model [401]. Another limitation is that no molecular analyses of *in vitro* model were performed to determine if there were any similar changes in differentiation markers in PVAT-APC compared changes observed *in vivo.* Furthermore, functional assays *in vivo* or *in vitro* to measure energy expenditure, maximal mitochondrial respiration, or indirect calorimetry would provide insight into effects of short-term MR. It has been established that MR induces a futile lipid cycle where instead of using glucose for energy production, *de novo* lipogenesis converts glucose to lipid, which is then mobilized and burned for energy production, which collectively prevents the accumulation of adipose tissue [281]. In order to understand if these bioenergetic changes in fuel utilization are unique to adipose tissue, future studies should measure whole body calorimetry vs cellular micro-calorimetry and take into account the contribution of muscle cells vs adipocytes from different adipose depots such as BAT, iWAT, and PVAT. Our in vivo studies were only performed in male mice, which is an important limitation in these studies.

6.6.1. Examining Sex as a Biological Variable

It is well acknowledged that there is a great need to be more inclusive of females in research and to examine sex a biological variable in treatment response. While the *in vivo* studies presented here are only in male mice, it should not detract from the need to study the effects of MR in female mice. There are a few studies that have reported response to MR in both males and females, and the consensus is that both sexes respond favorably to MR. A study of intermittent MR in both male and female mice have shown that both sexes have amelioration of diet-induced blood glucose dysregulation, however they also observed that females lack this response on a continuous MR for 18 weeks [276]. The initiation of dietary MR in young, growing animals has been reported to produce temporal responses in body composition that are sexually dimorphic [394]. Forney et al. observed weight loss of mice on a 0.17% MR diet and reported that males preserve lean tissue at the expense of fat while females preserve fat at the expense of lean tissue [394]. In young females, the increase in energy expenditure develops slower than in age-matched males. Despite these differences in rates of increased energy expenditure, all responses to MR, such as decreases in body weight, decreases in lean mass, and fat mass accumulation, were similar between the sexes after 8 weeks on a MR diet. The differences in energy balance between females and males were only observed when MR was initiated in young mice (MR started at 2 months) and were attributed to a difference in nutrient partitioning from the female having greater energy demands to support reproduction. The effects of MR on energy balance in males and females were comparable when the diet was initiated after attainment of maturity and full body size (MR started at 3 months). Because weight loss was primarily due to changes in adipose tissue in both sexes and, interestingly, the transcriptional responses across target tissues were similarly significantly expressed between control and MR diets (liver: *Fgf21, Asns, Psat1*, and *Scd1*; BAT: *Bmp8b* and *Ucp1*; iWAT: *Cox7a*,

Fatp2, Ucp1, and *Lep*), there is little evidence for sex-specific molecular responses to the diet. Furthermore, study of *Fgf21*-KO and combined *Fgf21/ Adipoq*- KO mice shows that MR response is not dependent on wither FGF21 or Adiponectin in both males and females [281]. The *in vivo* studies presented here focused on male mice because MR initiated in young male mice leads to loss of overall fat mass, which does not occur consistently in young female mice, and MR-induced changes in weight loss and energy balance are comparable between the sexes over time. However, future work on MR should be inclusive of females. To account for the lack of females in our *in vivo* study, we ensured that the *in vitro* study included a mix of male and female. This could have been further improved by performing experiments in the sexes separately to evaluate for sex-specific effects.

6.6.2. Accounting for Differences in the Effects of Methionine Restriction in Animal Studies and Human Clinical Studies

Methionine restriction has been shown in increase lifespan and healthspan in a number of difference species, such yeast, *Drosophila*, *Caenorhabditis elegans*, mice and rats [101, 226-239]. Additionally, MR prevents accelerating aging in progeroid mice [229]. MR occurs naturally in naked mole rats which live remarkably long lives naturally compared to other rodent species has been attributed to low circulating levels of specific amino acids related to the methionine cycle [457]. There are established patents for the use of methionine restricted diets in dogs and cats [249, 250], however there is a lack of studies that test the efficacy of these diets in the intended species.

It is important to acknowledge that there are differences between human and mouse adipose depots that could influence the species-specific response of MR. Anatomical position of adipose depots are unique to the species, however both humans and mice have depots that are either subcutaneous or visceral adipose depots. Some depots have some similarities, however there

have been documented differences in fat deposition and adipose function between humans and mice [458]. While subcutaneous depots can be collected easily, human PVAT can only be collected during invasive surgery, thus tissue inaccessibility is largely limiting to studies accessing the similarities between human and mouse PVAT, however there are efforts to expand this body of research [420].

The current body of research on MR have shown that many of the benefits of MR are translatable between animal models to humans and warrant further clinical development as a strategy for health promotion and disease prevention [291]. There is one important discrepancy between human and rodent studies which is the inclusion of genetic diversity in study design. Only one study has explored expanding genetic diversity by feeding a variety of rat strains (Fisher 344, Brown Norway, Sprague Dawley, and Wistar Hannover) a MR diet, and found that there were strain-dependent extensions in lifespan based on differing pathological profiles in aging [278]. This suggests that MR diet acts by altering the rate of aging and not correcting a single strain-specific pathology. Another way to account for human genetic diversity is to use diversity outbred mice [459].

It is estimated that the average amount of methionine consumed in the typical balanced American diet is about 61mg/kg/day for a 70 kg individual and the current RDA for methionine is about 15 mg/kg/day for the same weight individual [143, 207, 291]. Additionally there have been reports that there can be adverse effects of methionine supplementation beyond 46 mg/kg/day [221]. Collectively, this suggests that even in a typical American diet that is balanced, there is an excess of methionine and could possibly be contributing to adverse health effects. If we were to translate the 80% reduction in methionine used in these mouse studies to the typical amount of methionine consumed in a balanced American diet, it would fall around 12 mg/kg/day which is

below the RDA of 15 mg/kg/day, however this is an estimation of consumption across population data. Additionally, 80% MR is the most stringent application of MR that shows success in mouse models, and as we established there are differences between mice and humans. This suggests that 80% MR may not be necessary to gain beneficial effects of methionine in humans. This has been corroborated in clinical studies of healthy individuals where low levels of MR (70%) and high levels of MR (90%) were implemented [291].

6.7. Important Considerations for Future Studies

Implementing MR during young adulthood could help reduce the early onset of metabolic syndrome in humans, and thus reduce cardiovascular disease risk later in life. Further research is needed to support this hypothesis. Specifically, studies that implement MR in young adulthood and then measure the duration of metabolic benefits after cessation of MR diet. It is possible that metabolic benefits of MR are short lived and to continue reaping these benefits, MR must be implemented regularly.

6.7.1. Alternative Measures to Assess the Effects of Methionine Restriction on PVAT and Vascular Function

Additional research is needed to support the hypothesis that phenotypic changes in PVAT by MR are beneficial to the vasculature. While we did not observe changes in vessel morphology, this does not represent functional capacity of the vessel in question. Mechanical wire myography should be used to measure vessel contraction and relaxation following MR diet, and the effect of PVAT could be tested by keeping the PVAT intact or removal during analysis [460, 461]. Additionally, the impacts on endothelial cells and vascular smooth muscle cells should be evaluated utilizing molecular techniques such as single cell transcriptomics to identify clusters of cell types and associated changes in gene expression upon MR. It has been established that

endothelial cells are influenced by production of hydrogen sulfide [462, 463] which we know to be produced through the methionine cycle and that different epithelial layers of the intestines and colon have altered tight junction barriers and permeability in response to MR [464-466]. Taken together, it is likely that endothelial cells within the vasculature are influenced by MR and future work should evaluate vascular permeability *in vivo* using 2D imaging methods [467].

Adipose-specific knockouts of key methionine cycle enzymes or methyltransferases would be useful to tease out effects of methionine that are unique to adipose tissue. Addition of conditioned media from removed PVAT could also applied to stripped vessel to test the effect of signaling factor secreted from PVAT. Considering that hydrogen sulfide is a downstream metabolite of methionine, reported to be upregulated in liver of MR animals, as well as be an important signaling vasodilative molecule released from PVAT, it is be pertinent to test if hydrogen sulfide production is changed in PVAT and associated secretome in MR conditions [146, 151, 468].

6.7.2. Effects of Methionine Restriction on Other Organ Systems

Since this is a dietary intervention, MR is impacting the entire system, and the physiological effects depend on the system in question. As described in section 1.9-1.13, there are well documented effects on several relevant pathologies, however there are a number of systems that are impacted by MR that the connection with adiposity is not as clear. MR influences the brain and cognition as well as obesity, [114, 246], and thus the effect on adiposity could be occurring indirectly. MR also influences the gastrointestinal tract by influencing the microbiome and tightening intestinal junctions which alters gut barrier function and potentially reduces nutrient absorption [208, 465, 466, 469].

6.8. Establishing the Human Connection

Dietary MR has potential to induce physiological changes that will benefit the diverse range of root causes for metabolic dysfunction. There is a wide breadth of phenotypic variability in obesity, which challenges selection of targeted anti-obesity medications [470]. MR can be used to generally to reduce obesity- and age-related metabolic complications instead of untargeted prescriptions that do not match an individual's sub-phenotype. Given the dramatic effect of MR on obesity, MR will be useful in obesity-related metabolic dysfunctions, however as mentioned previously there are several other organ systems that are influenced by MR as well as several pathologies in which MR can be utilized therapeutically. Depending on the degree and duration of MR, this diet can be leveraged to reduce unwanted weight, improve metabolic function, or reduce overall effect of age. Recombinant methioninase could also be utilized to implement MR in clinical settings to treat metabolic dysfunction and obesity. There have only been studies of administration of recombinant methioninase to healthy individuals, which have shown that the treatment is safe. Future studies should include patients with metabolic dysfunction and obesity to understand if there is efficacy to reduce these risk factors for cardiovascular disease. The use of probiotics engineered to produce methioninase has major potential to increase accessibility and compliance to MR, which are ongoing challenges with implementing MR diets. Overall, methionine restriction has promise as a metabolic therapy for decreased risk and prevalence of cardiovascular pathologies, however there are many future research directions that need to be explored before it is implemented in regular clinical practice for this purpose.

REFERENCES

1. WHO. *Cardiovascular Diseases*. 2021 [cited 2024; Available from: https://www.who.int/news-room/fact-sheets/detail/cardiovascular-diseases-(cvds).

2. Clinic, C. *Cardiovascular Disease*. 2022 [cited 2024; Available from: https://my.clevelandclinic.org/health/diseases/21493-cardiovascular-disease.

3. Grundy, S.M., et al., *Diagnosis and management of the metabolic syndrome: an American Heart Association/National Heart, Lung, and Blood Institute Scientific Statement.* Circulation, 2005. **112**(17): p. 2735-52 https://doi.org/10.1161/circulationaha.105.169404.

4. Tran, V., et al., *The Vascular Consequences of Metabolic Syndrome: Rodent Models, Endothelial Dysfunction, and Current Therapies.* Front Pharmacol, 2020. **11**: p. 148 https://doi.org/10.3389/fphar.2020.00148.

5. Martin, S.S., et al., *2024 Heart Disease and Stroke Statistics: A Report of US and Global Data From the American Heart Association.* Circulation, 2024. **149**(8): p. e347-e913 https://doi.org/10.1161/cir.0000000000001209.

6. (CDC), C.f.D.C.a.P., *Decline in deaths from heart disease and stroke--United States, 1900-1999.* MMWR Morb Mortal Wkly Rep, 1999. **48**(30): p. 649-56

7. *National Health and Nutrition Examination Survey 2020*, NCHS, Editor. 2020.

8. Messerli, F.H., B. Williams, and E. Ritz, *Essential hypertension.* Lancet, 2007. **370**(9587): p. 591-603 https://doi.org/10.1016/s0140-6736(07)61299-9.

9. Zhou, M., et al., *Wall shear stress and its role in atherosclerosis.* Front Cardiovasc Med, 2023. **10**: p. 1083547 https://doi.org/10.3389/fcvm.2023.1083547.

10. A, O.L.E.B.B.J., ed. *Cardiovascular Disease*. StatPearls [Internet]. 2023, StatPearls Publishing Treasure Island (FL).

11. Libby, P., P.M. Ridker, and G.K. Hansson, *Progress and challenges in translating the biology of atherosclerosis.* Nature, 2011. **473**(7347): p. 317-25 https://doi.org/10.1038/nature10146.

12. Gimbrone, M.A., Jr. and G. García-Cardeña, *Endothelial Cell Dysfunction and the Pathobiology of Atherosclerosis.* Circ Res, 2016. **118**(4): p. 620-36 https://doi.org/10.1161/circresaha.115.306301.

13. Gusev, E. and A. Sarapultsev, *Atherosclerosis and Inflammation: Insights from the Theory of General Pathological Processes.* Int J Mol Sci, 2023. **24**(9) https://doi.org/10.3390/ijms24097910.

14. El Hadri, K., et al., *Inflammation, Oxidative Stress, Senescence in Atherosclerosis: Thioredoxine-1 as an Emerging Therapeutic Target.* Int J Mol Sci, 2021. **23**(1) https://doi.org/10.3390/ijms23010077.

15. Liang, X., et al., *Prevalence of metabolic syndrome in the United States National Health and Nutrition Examination Survey 2011–18.* Postgraduate Medical Journal, 2023. **99**(1175): p. 985-992 https://doi.org/10.1093/postmj/qgad008.

16. Moore, J.X., N. Chaudhary, and T. Akinyemiju, *Metabolic Syndrome Prevalence by Race/Ethnicity and Sex in the United States, National Health and Nutrition Examination Survey, 1988-2012.* Prev Chronic Dis, 2017. **14**: p. E24 https://doi.org/10.5888/pcd14.160287.

17. Gaston, S.A., N.S. Tulve, and T.F. Ferguson, *Abdominal obesity, metabolic dysfunction, and metabolic syndrome in U.S. adolescents: National Health and Nutrition Examination Survey 2011-2016.* Ann Epidemiol, 2019. **30**: p. 30-36 https://doi.org/10.1016/j.annepidem.2018.11.009.

18. Messiah, S.E., et al., *Prevalence of the metabolic syndrome by household food insecurity status in the United States adolescent population, 2001-2020: a cross-sectional study.* Am J Clin Nutr, 2024. **119**(2): p. 354-361 https://doi.org/10.1016/j.ajcnut.2023.11.014.

19. Huang, Z., et al., *Association of Age of Metabolic Syndrome Onset With Cardiovascular Diseases: The Kailuan Study.* Front Endocrinol (Lausanne), 2022. **13**: p. 857985 https://doi.org/10.3389/fendo.2022.857985.

20. Manna, P. and S.K. Jain, *Obesity, Oxidative Stress, Adipose Tissue Dysfunction, and the Associated Health Risks: Causes and Therapeutic Strategies.* Metab Syndr Relat Disord, 2015. **13**(10): p. 423-44 https://doi.org/10.1089/met.2015.0095.

21. Schrauwen, P. and K.R. Westerterp, *The role of high-fat diets and physical activity in the regulation of body weight.* Br J Nutr, 2000. **84**(4): p. 417-27 https://doi.org/10.1017/s0007114500001720.

22. O'Donovan, G., et al., *Association of "Weekend Warrior" and Other Leisure Time Physical Activity Patterns With Risks for All-Cause, Cardiovascular Disease, and Cancer Mortality.* JAMA Intern Med, 2017. **177**(3): p. 335-342 https://doi.org/10.1001/jamainternmed.2016.8014.

23. Balhara, Y.P., *Tobacco and metabolic syndrome.* Indian J Endocrinol Metab, 2012. **16**(1): p. 81-7 https://doi.org/10.4103/2230-8210.91197.

24. *Heart Disease and Stroke* 2020 [cited 2024; Available from: https://www.cdc.gov/tobacco/basic_information/health_effects/heart_disease/index.htm.

25. Schultz, W.M., et al., *Socioeconomic Status and Cardiovascular Outcomes: Challenges and Interventions.* Circulation, 2018. **137**(20): p. 2166-2178 https://doi.org/10.1161/circulationaha.117.029652.

26. Minhas, A.M.K., et al., *Family income and cardiovascular disease risk in American adults.* Scientific Reports, 2023. **13**(1): p. 279 https://doi.org/10.1038/s41598-023-27474-x.

27. Guo, F., et al., *Obesogenic environments and cardiovascular disease: a path analysis using US nationally representative data.* BMC Public Health, 2022. **22**(1): p. 703 https://doi.org/10.1186/s12889-022-13100-4.

28. Lake, A. and T. Townshend, *Obesogenic environments: exploring the built and food environments.* J R Soc Promot Health, 2006. **126**(6): p. 262-7 https://doi.org/10.1177/1466424006070487.

29. Sol, J., et al., *Human lifespan and sex-specific patterns of resilience to disease: a retrospective population-wide cohort study.* BMC Med, 2024. **22**(1): p. 17 https://doi.org/10.1186/s12916-023-03206-w.

30. Collins, P., *Risk factors for cardiovascular disease and hormone therapy in women.* Heart, 2006. **92 Suppl 3**(Suppl 3): p. iii24-8 https://doi.org/10.1136/hrt.2005.071787.

31. Mårin, P., et al., *Assimilation of triglycerides in subcutaneous and intraabdominal adipose tissues in vivo in men: effects of testosterone.* J Clin Endocrinol Metab, 1996. **81**(3): p. 1018-22 https://doi.org/10.1210/jcem.81.3.8772568.

32. *National Health and Nutrition Examination Survey 2017*, NCHS, Editor. 2017-2018.

33. Niccoli, T. and L. Partridge, *Ageing as a risk factor for disease.* Curr Biol, 2012. **22**(17): p. R741-52 https://doi.org/10.1016/j.cub.2012.07.024.

34. *Menopause*. 2023; Available from: https://www.mayoclinic.org/diseases-conditions/menopause/symptoms-causes/syc-20353397.

35. Boss, G.R. and J.E. Seegmiller, *Age-related physiological changes and their clinical significance.* West J Med, 1981. **135**(6): p. 434-40

36. Chistiakov, D.A., et al., *Mitochondrial aging and age-related dysfunction of mitochondria.* Biomed Res Int, 2014. **2014**: p. 238463 https://doi.org/10.1155/2014/238463.

37. Heindel, J.J., et al., *Obesity II: Establishing causal links between chemical exposures and obesity.* Biochem Pharmacol, 2022. **199**: p. 115015 https://doi.org/10.1016/j.bcp.2022.115015.

38. Haslam, D.W. and W.P. James, *Obesity.* Lancet, 2005. **366**(9492): p. 1197-209 https://doi.org/10.1016/s0140-6736(05)67483-1.

39. Jura, M. and L.P. Kozak, *Obesity and related consequences to ageing.* Age (Dordr), 2016. **38**(1): p. 23 https://doi.org/10.1007/s11357-016-9884-3.

40. Lloyd-Jones, D.M., et al., *Life's essential 8: updating and enhancing the American Heart Association's construct of cardiovascular health: a presidential advisory from the American Heart Association.* Circulation, 2022. **146**(5): p. e18-e43

41. Berkowitz, S.A., et al., *Association Between Receipt of a Medically Tailored Meal Program and Health Care Use.* JAMA Internal Medicine, 2019. **179**(6): p. 786-793 https://doi.org/10.1001/jamainternmed.2019.0198.

42. Blüher, M., *Obesity: global epidemiology and pathogenesis.* Nat Rev Endocrinol, 2019. **15**(5): p. 288-298 https://doi.org/10.1038/s41574-019-0176-8.

43. WHO. *Obesity and Overweight* 2024 [cited 2024; Available from: https://www.who.int/news-room/fact-sheets/detail/obesity-and-overweight.

44. Kusminski, C.M., P.E. Bickel, and P.E. Scherer, *Targeting adipose tissue in the treatment of obesity-associated diabetes.* Nature Reviews Drug Discovery, 2016. **15**(9): p. 639-660 https://doi.org/10.1038/nrd.2016.75.

45. Lepper, C. and C.M. Fan, *Inducible lineage tracing of Pax7-descendant cells reveals embryonic origin of adult satellite cells.* Genesis, 2010. **48**(7): p. 424-36 https://doi.org/10.1002/dvg.20630.

46. Lynes, M.D. and Y.H. Tseng, *The Thermogenic Circuit: Regulators of Thermogenic Competency and Differentiation.* Genes Dis, 2015. **2**(2): p. 164-172 https://doi.org/10.1016/j.gendis.2015.03.001.

47. Seale, P., et al., *PRDM16 controls a brown fat/skeletal muscle switch.* Nature, 2008. **454**(7207): p. 961-967 https://doi.org/10.1038/nature07182.

48. Rajakumari, S., et al., *EBF2 Determines and Maintains Brown Adipocyte Identity.* Cell Metabolism, 2013. **17**(4): p. 562-574 https://doi.org/https://doi.org/10.1016/j.cmet.2013.01.015.

49. Sanchez-Gurmaches, J. and D.A. Guertin, *Adipocytes arise from multiple lineages that are heterogeneously and dynamically distributed.* Nature Communications, 2014. **5**(1): p. 4099 https://doi.org/10.1038/ncomms5099.

50. Tontonoz, P., E. Hu, and B.M. Spiegelman, *Regulation of adipocyte gene expression and differentiation by peroxisome proliferator activated receptor γ.* Current Opinion in Genetics & Development, 1995. **5**(5): p. 571-576 https://doi.org/https://doi.org/10.1016/0959-437X(95)80025-5.

51. Richard, A.J., et al., *Adipose Tissue: Physiology to Metabolic Dysfunction*, in *Endotext*, K.R. Feingold, et al., Editors. 2000, MDText.com, Inc.Copyright © 2000-2024, MDText.com, Inc.: South Dartmouth (MA).

52. Sztalryd, C. and D.L. Brasaemle, *The perilipin family of lipid droplet proteins: Gatekeepers of intracellular lipolysis.* Biochim Biophys Acta Mol Cell Biol Lipids, 2017. **1862**(10 Pt B): p. 1221-1232 https://doi.org/10.1016/j.bbalip.2017.07.009.

53. Ghorbani, M., T.H. Claus, and J. Himms-Hagen, *Hypertrophy of brown adipocytes in brown and white adipose tissues and reversal of diet-induced obesity in rats treated with a beta3-adrenoceptor agonist.* Biochem Pharmacol, 1997. **54**(1): p. 121-31 https://doi.org/10.1016/s0006-2952(97)00162-7.

54. Smorlesi, A., et al., *The adipose organ: white-brown adipocyte plasticity and metabolic inflammation.* Obes Rev, 2012. **13 Suppl 2**: p. 83-96 https://doi.org/10.1111/j.1467-789X.2012.01039.x.

55. Barbatelli, G., et al., *The emergence of cold-induced brown adipocytes in mouse white fat depots is determined predominantly by white to brown adipocyte transdifferentiation.* Am J Physiol Endocrinol Metab, 2010. **298**(6): p. E1244-53 https://doi.org/10.1152/ajpendo.00600.2009.

56. Tang, Q.Q. and M.D. Lane, *Adipogenesis: from stem cell to adipocyte.* Annu Rev Biochem, 2012. **81**: p. 715-36 https://doi.org/10.1146/annurev-biochem-052110-115718.

57. Lee, M.J., Y. Wu, and S.K. Fried, *Adipose tissue heterogeneity: implication of depot differences in adipose tissue for obesity complications.* Mol Aspects Med, 2013. **34**(1): p. 1-11 https://doi.org/10.1016/j.mam.2012.10.001.

58. Schleh, M.W., et al., *Metabolic dysfunction in obesity is related to impaired suppression of fatty acid release from adipose tissue by insulin.* Obesity (Silver Spring), 2023. **31**(5): p. 1347-1361 https://doi.org/10.1002/oby.23734.

59. Roh, E. and H.J. Yoo, *The Role of Adipose Tissue Lipolysis in Diet-Induced Obesity: Focus on Vimentin.* Diabetes Metab J, 2021. **45**(1): p. 43-45 https://doi.org/10.4093/dmj.2020.0293.

60. Jocken, J.W. and E.E. Blaak, *Catecholamine-induced lipolysis in adipose tissue and skeletal muscle in obesity.* Physiol Behav, 2008. **94**(2): p. 219-30 https://doi.org/10.1016/j.physbeh.2008.01.002.

61. Jung, R.T., et al., *Reduced thermogenesis in obesity.* Nature, 1979. **279**(5711): p. 322-323 https://doi.org/10.1038/279322a0.

62. Amitani, M., et al., *The role of leptin in the control of insulin-glucose axis.* Front Neurosci, 2013. **7**: p. 51 https://doi.org/10.3389/fnins.2013.00051.

63. Lekva, T., et al., *Leptin and adiponectin as predictors of cardiovascular risk after gestational diabetes mellitus.* Cardiovasc Diabetol, 2017. **16**(1): p. 5 https://doi.org/10.1186/s12933-016-0492-4.

64. Abdella, N.A., et al., *Plasma leptin concentration in patients with Type 2 diabetes: relationship to cardiovascular disease risk factors and insulin resistance.* Diabet Med, 2005. **22**(3): p. 278-85 https://doi.org/10.1111/j.1464-5491.2004.01405.x.

65. Redinger, R.N., *The pathophysiology of obesity and its clinical manifestations.* Gastroenterol Hepatol (N Y), 2007. **3**(11): p. 856-63

66. Hu, E., P. Liang, and B.M. Spiegelman, *AdipoQ is a novel adipose-specific gene dysregulated in obesity.* J Biol Chem, 1996. **271**(18): p. 10697-703 https://doi.org/10.1074/jbc.271.18.10697.

67. Krause, M.P., K.J. Milne, and T.J. Hawke, *Adiponectin-Consideration for its Role in Skeletal Muscle Health.* Int J Mol Sci, 2019. **20**(7) https://doi.org/10.3390/ijms20071528.

68. Ouchi, N., R. Shibata, and K. Walsh, *Cardioprotection by adiponectin.* Trends Cardiovasc Med, 2006. **16**(5): p. 141-6 https://doi.org/10.1016/j.tcm.2006.03.001.

69. Lee, M.J., Y. Wu, and S.K. Fried, *Adipose tissue remodeling in pathophysiology of obesity.* Curr Opin Clin Nutr Metab Care, 2010. **13**(4): p. 371-6 https://doi.org/10.1097/MCO.0b013e32833aabef.

70. Mizunoe, Y., et al., *Association between Lysosomal Dysfunction and Obesity-Related Pathology: A Key Knowledge to Prevent Metabolic Syndrome.* Int J Mol Sci, 2019. **20**(15) https://doi.org/10.3390/ijms20153688.

71. Wang, B., et al., *Uncovering impaired mitochondrial and lysosomal function in adipose-derived stem cells from obese individuals with altered biological activity.* Stem Cell Research & Therapy, 2024. **15**(1): p. 12 https://doi.org/10.1186/s13287-023-03625-9.

72. Xu, Q., et al., *Cathepsin gene expression in abdominal subcutaneous adipose tissue of obese/overweight humans.* Adipocyte, 2020. **9**(1): p. 246-252 https://doi.org/10.1080/21623945.2020.1775035.

73. Sam, S., *Differential effect of subcutaneous abdominal and visceral adipose tissue on cardiometabolic risk.* Horm Mol Biol Clin Investig, 2018. **33**(1) https://doi.org/10.1515/hmbci-2018-0014.

74. Liu, W., et al., *Age-adjusted visceral adiposity index (VAI) is superior to VAI for predicting mortality among US adults: an analysis of the NHANES 2011-2014.* Aging Clin Exp Res, 2024. **36**(1): p. 24 https://doi.org/10.1007/s40520-023-02660-z.

75. St-Pierre, J., et al., *Relation of the "hypertriglyceridemic waist" phenotype to earlier manifestations of coronary artery disease in patients with glucose intolerance and type 2 diabetes mellitus.* Am J Cardiol, 2007. **99**(3): p. 369-73 https://doi.org/10.1016/j.amjcard.2006.08.041.

76. de Graaf, F.R., et al., *Usefulness of hypertriglyceridemic waist phenotype in type 2 diabetes mellitus to predict the presence of coronary artery disease as assessed by computed tomographic coronary angiography.* Am J Cardiol, 2010. **106**(12): p. 1747-53 https://doi.org/10.1016/j.amjcard.2010.08.015.

77. Lemieux, I., et al., *Hypertriglyceridemic waist: A marker of the atherogenic metabolic triad (hyperinsulinemia; hyperapolipoprotein B; small, dense LDL) in men?* Circulation, 2000. **102**(2): p. 179-84 https://doi.org/10.1161/01.cir.102.2.179.

78. Tchernof, A. and E.T. Poehlman, *Effects of the menopause transition on body fatness and body fat distribution.* Obes Res, 1998. **6**(3): p. 246-54 https://doi.org/10.1002/j.1550-8528.1998.tb00344.x.

79. Snijder, M.B., et al., *Low subcutaneous thigh fat is a risk factor for unfavourable glucose and lipid levels, independently of high abdominal fat. The Health ABC Study.* Diabetologia, 2005. **48**(2): p. 301-8 https://doi.org/10.1007/s00125-004-1637-7.

80. Goodpaster, B.H., et al., *Subcutaneous abdominal fat and thigh muscle composition predict insulin sensitivity independently of visceral fat.* Diabetes, 1997. **46**(10): p. 1579-85 https://doi.org/10.2337/diacare.46.10.1579.

81. Qi, X.-Y., et al., *Perivascular adipose tissue (PVAT) in atherosclerosis: a double-edged sword.* Cardiovascular Diabetology, 2018. **17**(1): p. 134 https://doi.org/10.1186/s12933-018-0777-x.

82. McNeill, B.T., K.J. Suchacki, and R.H. Stimson, *MECHANISMS IN ENDOCRINOLOGY: Human brown adipose tissue as a therapeutic target: warming up or cooling down?* European Journal of Endocrinology, 2021. **184**(6): p. R243-R259 https://doi.org/10.1530/eje-20-1439.

83. Cheng, L., et al., *Brown and beige adipose tissue: a novel therapeutic strategy for obesity and type 2 diabetes mellitus.* Adipocyte, 2021. **10**(1): p. 48-65 https://doi.org/10.1080/21623945.2020.1870060.

84. Peres Valgas da Silva, C., et al., *Cold and Exercise: Therapeutic Tools to Activate Brown Adipose Tissue and Combat Obesity.* Biology (Basel), 2019. **8**(1) https://doi.org/10.3390/biology8010009.

85. Peres Valgas da Silva, C., et al., *Cold and Exercise: Therapeutic Tools to Activate Brown Adipose Tissue and Combat Obesity.* Biology, 2019. **8**(1): p. 9

86. Puigserver, P., et al., *A cold-inducible coactivator of nuclear receptors linked to adaptive thermogenesis.* Cell, 1998. **92**(6): p. 829-39 https://doi.org/10.1016/s0092-8674(00)81410-5.

87. Cero, C., et al., *β3-Adrenergic receptors regulate human brown/beige adipocyte lipolysis and thermogenesis.* JCI Insight, 2021. **6**(11) https://doi.org/10.1172/jci.insight.139160.

88. Wang, L., et al., *Olodaterol promotes thermogenesis in brown adipocytes via regulation of the β2-AR/cAMP/PKA signaling pathway.* Biochem Biophys Res Commun, 2024. **703**: p. 149689 https://doi.org/10.1016/j.bbrc.2024.149689.

89. Michel, L.Y.M., C. Farah, and J.L. Balligand, *The Beta3 Adrenergic Receptor in Healthy and Pathological Cardiovascular Tissues.* Cells, 2020. **9**(12) https://doi.org/10.3390/cells9122584.

90. Belfort, R., et al., *A placebo-controlled trial of pioglitazone in subjects with nonalcoholic steatohepatitis.* New England Journal of Medicine, 2006. **355**(22): p. 2297-2307

91. Hammarstedt, A., et al., *Improved insulin sensitivity and adipose tissue dysregulation after short-term treatment with pioglitazone in non-diabetic, insulin-resistant subjects.* Diabetologia, 2005. **48**: p. 96-104

92. Kubota, N., et al., *Pioglitazone ameliorates insulin resistance and diabetes by both adiponectin-dependent and -independent pathways.* J Biol Chem, 2006. **281**(13): p. 8748-55 https://doi.org/10.1074/jbc.M505649200.

93. Yu, J.G., et al., *The effect of thiazolidinediones on plasma adiponectin levels in normal, obese, and type 2 diabetic subjects.* Diabetes, 2002. **51**(10): p. 2968-74 https://doi.org/10.2337/diabetes.51.10.2968.

94. Tchernof, A. and J.P. Després, *Pathophysiology of human visceral obesity: an update.* Physiol Rev, 2013. **93**(1): p. 359-404 https://doi.org/10.1152/physrev.00033.2011.

95. Bonam, S.R., F. Wang, and S. Muller, *Lysosomes as a therapeutic target.* Nature Reviews Drug Discovery, 2019. **18**(12): p. 923-948 https://doi.org/10.1038/s41573-019-0036-1.

96. Lizcano, F., *The Beige Adipocyte as a Therapy for Metabolic Diseases.* Int J Mol Sci, 2019. **20**(20) https://doi.org/10.3390/ijms20205058.

97. Chaston, T.B. and J.B. Dixon, *Factors associated with percent change in visceral versus subcutaneous abdominal fat during weight loss: findings from a systematic review.* Int J Obes (Lond), 2008. **32**(4): p. 619-28 https://doi.org/10.1038/sj.ijo.0803761.

98. Carbone, J.W. and S.M. Pasiakos, *Dietary Protein and Muscle Mass: Translating Science to Application and Health Benefit.* Nutrients, 2019. **11**(5) https://doi.org/10.3390/nu11051136.

99. Cava, E., N.C. Yeat, and B. Mittendorfer, *Preserving Healthy Muscle during Weight Loss.* Adv Nutr, 2017. **8**(3): p. 511-519 https://doi.org/10.3945/an.116.014506.

100. Trautman, M.E., et al., *Resistance exercise protects mice from protein-induced fat accretion.* Elife, 2023. **12** https://doi.org/10.7554/eLife.91007.

101. Babygirija, R. and D.W. Lamming, *The regulation of healthspan and lifespan by dietary amino acids.* Transl Med Aging, 2021. **5**: p. 17-30 https://doi.org/10.1016/j.tma.2021.05.001.

102. Trautman, M.E., N.E. Richardson, and D.W. Lamming, *Protein restriction and branched-chain amino acid restriction promote geroprotective shifts in metabolism.* Aging Cell, 2022. **21**(6): p. e13626 https://doi.org/10.1111/acel.13626.

103. Babygirija, R., et al., *Protein restriction slows the development and progression of Alzheimer's disease in mice.* Res Sq, 2023 https://doi.org/10.21203/rs.3.rs-3342413/v1.

104. Richardson, N.E., et al., *Lifelong restriction of dietary branched-chain amino acids has sex-specific benefits for frailty and lifespan in mice.* Nat Aging, 2021. **1**(1): p. 73-86 https://doi.org/10.1038/s43587-020-00006-2.

105. Ferraz-Bannitz, R., et al., *Dietary Protein Restriction Improves Metabolic Dysfunction in Patients with Metabolic Syndrome in a Randomized, Controlled Trial.* Nutrients, 2022. **14**(13) https://doi.org/10.3390/nu14132670.

106. Bessesen, D.H., *The Role of Carbohydrates in Insulin Resistance.* The Journal of Nutrition, 2001. **131**(10): p. 2782S-2786S https://doi.org/https://doi.org/10.1093/jn/131.10.2782S.

107. Foley, P.J., *Effect of low carbohydrate diets on insulin resistance and the metabolic syndrome.* Curr Opin Endocrinol Diabetes Obes, 2021. **28**(5): p. 463-468 https://doi.org/10.1097/med.0000000000000659.

108. O'Neill, B.J., *Effect of low-carbohydrate diets on cardiometabolic risk, insulin resistance, and metabolic syndrome.* Curr Opin Endocrinol Diabetes Obes, 2020. **27**(5): p. 301-307 https://doi.org/10.1097/med.0000000000000569.

109. Goldenberg, J.Z., et al., *Efficacy and safety of low and very low carbohydrate diets for type 2 diabetes remission: systematic review and meta-analysis of published and unpublished randomized trial data.* Bmj, 2021. **372**: p. m4743 https://doi.org/10.1136/bmj.m4743.

110. Al-Reshed, F., et al., *Low carbohydrate intake correlates with trends of insulin resistance and metabolic acidosis in healthy lean individuals.* Front Public Health, 2023. **11**: p. 1115333 https://doi.org/10.3389/fpubh.2023.1115333.

111. Mooradian, A.D., *The Merits and the Pitfalls of Low Carbohydrate Diet: A Concise Review.* J Nutr Health Aging, 2020. **24**(7): p. 805-808 https://doi.org/10.1007/s12603-020-1417-1.

112. Wali, J.A., et al., *Cardio-Metabolic Effects of High-Fat Diets and Their Underlying Mechanisms-A Narrative Review.* Nutrients, 2020. **12**(5) https://doi.org/10.3390/nu12051505.

113. Ledreux, A., et al., *Detrimental effects of a high fat/high cholesterol diet on memory and hippocampal markers in aged rats.* Behav Brain Res, 2016. **312**: p. 294-304 https://doi.org/10.1016/j.bbr.2016.06.012.

114. Freeman, L.R., et al., *Damaging effects of a high-fat diet to the brain and cognition: a review of proposed mechanisms.* Nutr Neurosci, 2014. **17**(6): p. 241-51 https://doi.org/10.1179/1476830513y.0000000092.

115. Holloway, C.J., et al., *A high-fat diet impairs cardiac high-energy phosphate metabolism and cognitive function in healthy human subjects.* The American Journal of Clinical Nutrition, 2011. **93**(4): p. 748-755 https://doi.org/https://doi.org/10.3945/ajcn.110.002758.

116. Mdaki, K.S., et al., *Maternal high-fat diet impairs cardiac function in offspring of diabetic pregnancy through metabolic stress and mitochondrial dysfunction.* Am J Physiol Heart Circ Physiol, 2016. **310**(6): p. H681-92 https://doi.org/10.1152/ajpheart.00795.2015.

117. Chen, D., et al., *A high-fat diet impairs mitochondrial biogenesis, mitochondrial dynamics, and the respiratory chain complex in rat myocardial tissues.* J Cell Biochem, 2018. **119**(11): p. 9602 https://doi.org/10.1002/jcb.27068.

118. Zeng, H., et al., *High-fat diet induces cardiac remodelling and dysfunction: assessment of the role played by SIRT3 loss.* J Cell Mol Med, 2015. **19**(8): p. 1847-56 https://doi.org/10.1111/jcmm.12556.

119. La Berge, A.F., *How the Ideology of Low Fat Conquered America.* Journal of the History of Medicine and Allied Sciences, 2008. **63**(2): p. 139-177 https://doi.org/10.1093/jhmas/jrn001.

120. Cipryan, L., et al., *Very Low-Carbohydrate High-Fat Diet Improves Risk Markers for Cardiometabolic Health More Than Exercise in Men and Women With Overfat Constitution: Secondary Analysis of a Randomized Controlled Clinical Trial.* Frontiers in Nutrition, 2022. **9** https://doi.org/10.3389/fnut.2022.867690.

121. Phinney, S.D., et al., *Capacity for moderate exercise in obese subjects after adaptation to a hypocaloric, ketogenic diet.* J Clin Invest, 1980. **66**(5): p. 1152-61 https://doi.org/10.1172/jci109945.

122. Ting, R., et al., *Ketogenic diet for weight loss.* Can Fam Physician, 2018. **64**(12): p. 906

123. Araya-Quintanilla, F., et al., *[Effectiveness of a ketogenic diet in children with refractory epilepsy: a systematic review].* Rev Neurol, 2016. **62**(10): p. 439-48

124. Hall, K.D., et al., *Energy expenditure and body composition changes after an isocaloric ketogenic diet in overweight and obese men.* Am J Clin Nutr, 2016. **104**(2): p. 324-33 https://doi.org/10.3945/ajcn.116.133561.

125. Yubero-Serrano, E.M., et al., *Insulin resistance determines a differential response to changes in dietary fat modification on metabolic syndrome risk factors: the LIPGENE study.* Am J Clin Nutr, 2015. **102**(6): p. 1509-17 https://doi.org/10.3945/ajcn.115.111286.

126. An, P., et al., *Micronutrient Supplementation to Reduce Cardiovascular Risk.* J Am Coll Cardiol, 2022. **80**(24): p. 2269-2285 https://doi.org/10.1016/j.jacc.2022.09.048.

127. Abdelhamid, A.S., et al., *Omega-3 fatty acids for the primary and secondary prevention of cardiovascular disease.* Cochrane Database Syst Rev, 2018. **7**(7): p. Cd003177 https://doi.org/10.1002/14651858.CD003177.pub3.

128. Maugeri, A. and M. Vinciguerra, *The Effects of Meal Timing and Frequency, Caloric Restriction, and Fasting on Cardiovascular Health: an Overview.* J Lipid Atheroscler, 2020. **9**(1): p. 140-152 https://doi.org/10.12997/jla.2020.9.1.140.

129. DeBlauw, J.A., et al., *The effects of short-term caloric restriction on cardiometabolic health in overweight/obese men and women: A single-arm trial.* Physiol Rep, 2023. **11**(22): p. e15856 https://doi.org/10.14814/phy2.15856.

130. Wang, Y. and R. Wu, *The Effect of Fasting on Human Metabolism and Psychological Health.* Dis Markers, 2022. **2022**: p. 5653739 https://doi.org/10.1155/2022/5653739.

131. Appleton, K.M. and S. Baker, *Distraction, not hunger, is associated with lower mood and lower perceived work performance on fast compared to non-fast days during intermittent fasting.* J Health Psychol, 2015. **20**(6): p. 702-11 https://doi.org/10.1177/1359105315573430.

132. Moreno-Domínguez, S., et al., *Impact of fasting on food craving, mood and consumption in bulimia nervosa and healthy women participants.* Eur Eat Disord Rev, 2012. **20**(6): p. 461-7 https://doi.org/10.1002/erv.2187.

133. Solianik, R., et al., *Effect of 48 h Fasting on Autonomic Function, Brain Activity, Cognition, and Mood in Amateur Weight Lifters.* Biomed Res Int, 2016. **2016**: p. 1503956 https://doi.org/10.1155/2016/1503956.

134. Watkins, E. and L. Serpell, *The Psychological Effects of Short-Term Fasting in Healthy Women.* Front Nutr, 2016. **3**: p. 27 https://doi.org/10.3389/fnut.2016.00027.

135. Hofer, S.J., et al., *The ups and downs of caloric restriction and fasting: from molecular effects to clinical application.* EMBO Mol Med, 2022. **14**(1): p. e14418 https://doi.org/10.15252/emmm.202114418.

136. Wei, M., et al., *Fasting-mimicking diet and markers/risk factors for aging, diabetes, cancer, and cardiovascular disease.* Sci Transl Med, 2017. **9**(377) https://doi.org/10.1126/scitranslmed.aai8700.

137. Martel, J., et al., *Recent advances in the field of caloric restriction mimetics and anti-aging molecules.* Ageing Research Reviews, 2021. **66**: p. 101240 https://doi.org/https://doi.org/10.1016/j.arr.2020.101240.

138. Lee, S.H. and K.J. Min, *Caloric restriction and its mimetics.* BMB Rep, 2013. **46**(4): p. 181-7 https://doi.org/10.5483/bmbrep.2013.46.4.033.

139. Blättler, S.M., et al., *Yin Yang 1 deficiency in skeletal muscle protects against rapamycin-induced diabetic-like symptoms through activation of insulin/IGF signaling.* Cell Metab, 2012. **15**(4): p. 505-17 https://doi.org/10.1016/j.cmet.2012.03.008.

140. Madeo, F., et al., *Caloric Restriction Mimetics against Age-Associated Disease: Targets, Mechanisms, and Therapeutic Potential.* Cell Metabolism, 2019. **29**(3): p. 592-610 https://doi.org/https://doi.org/10.1016/j.cmet.2019.01.018.

141. Mishra, A., et al., *Fasting-mimicking diet prevents high-fat diet effect on cardiometabolic risk and lifespan.* Nat Metab, 2021. **3**(10): p. 1342-1356 https://doi.org/10.1038/s42255-021-00469-6.

142. Brandhorst, S., et al., *A Periodic Diet that Mimics Fasting Promotes Multi-System Regeneration, Enhanced Cognitive Performance, and Healthspan.* Cell Metab, 2015. **22**(1): p. 86-99 https://doi.org/10.1016/j.cmet.2015.05.012.

143. Nimni, M.E., B. Han, and F. Cordoba, *Are we getting enough sulfur in our diet?* Nutr Metab (Lond), 2007. **4**: p. 24 https://doi.org/10.1186/1743-7075-4-24.

144. Townsend, D.M., K.D. Tew, and H. Tapiero, *Sulfur containing amino acids and human disease.* Biomed Pharmacother, 2004. **58**(1): p. 47-55 https://doi.org/10.1016/j.biopha.2003.11.005.

145. Lauinger, L. and P. Kaiser, *Sensing and Signaling of Methionine Metabolism.* Metabolites, 2021. **11**(2) https://doi.org/10.3390/metabo11020083.

146. Kimura, H., *Production and physiological effects of hydrogen sulfide.* Antioxid Redox Signal, 2014. **20**(5): p. 783-93 https://doi.org/10.1089/ars.2013.5309.

147. Sanderson, S.M., et al., *Methionine metabolism in health and cancer: a nexus of diet and precision medicine.* Nature Reviews Cancer, 2019. **19**(11): p. 625-637 https://doi.org/10.1038/s41568-019-0187-8.

148. Brosnan, J.T. and M.E. Brosnan, *The sulfur-containing amino acids: an overview.* J Nutr, 2006. **136**(6 Suppl): p. 1636s-1640s https://doi.org/10.1093/jn/136.6.1636S.

149. Pettit, A.P., et al., *Dietary Methionine Restriction Regulates Liver Protein Synthesis and Gene Expression Independently of Eukaryotic Initiation Factor 2 Phosphorylation in Mice.* J Nutr, 2017. **147**(6): p. 1031-1040 https://doi.org/10.3945/jn.116.246710.

150. Nichenametla, S.N., et al., *Sulfur amino acid restriction-induced changes in redox-sensitive proteins are associated with slow protein synthesis rates.* Ann N Y Acad Sci, 2018. **1418**(1): p. 80-94 https://doi.org/10.1111/nyas.13556.

151. Kolluru, G.K., et al., *Sulfide regulation of cardiovascular function in health and disease.* Nature Reviews Cardiology, 2023. **20**(2): p. 109-125 https://doi.org/10.1038/s41569-022-00741-6.

152. Labarrere, C.A. and G.S. Kassab, *Glutathione: A Samsonian life-sustaining small molecule that protects against oxidative stress, ageing and damaging inflammation.* Front Nutr, 2022. **9**: p. 1007816 https://doi.org/10.3389/fnut.2022.1007816.

153. Kwon, D.H., et al., *Protective Effect of Glutathione against Oxidative Stress-induced Cytotoxicity in RAW 264.7 Macrophages through Activating the Nuclear Factor Erythroid 2-Related Factor-2/Heme Oxygenase-1 Pathway.* Antioxidants (Basel), 2019. **8**(4) https://doi.org/10.3390/antiox8040082.

154. Zamek-Gliszczynski, M.J., et al., *Integration of hepatic drug transporters and phase II metabolizing enzymes: mechanisms of hepatic excretion of sulfate, glucuronide, and glutathione metabolites.* Eur J Pharm Sci, 2006. **27**(5): p. 447-86 https://doi.org/10.1016/j.ejps.2005.12.007.

155. Serpa, J., *Cysteine as a Carbon Source, a Hot Spot in Cancer Cells Survival.* Front Oncol, 2020. **10**: p. 947 https://doi.org/10.3389/fonc.2020.00947.

156. Moffatt, B.A. and H. Ashihara, *Purine and pyrimidine nucleotide synthesis and metabolism.* Arabidopsis Book, 2002. **1**: p. e0018 https://doi.org/10.1199/tab.0018.

157. Annibal, A., et al., *Regulation of the one carbon folate cycle as a shared metabolic signature of longevity.* Nature Communications, 2021. **12**(1): p. 3486 https://doi.org/10.1038/s41467-021-23856-9.

158. Booher, K., et al., *Downregulation of Cdc6 and pre-replication complexes in response to methionine stress in breast cancer cells.* Cell Cycle, 2012. **11**(23): p. 4414-23 https://doi.org/10.4161/cc.22767.

159. Usami, M., et al., *Effect of methionine-deprived nutrition on cell growth and cell kinetics in cell cultures and experimental tumors.* JPEN J Parenter Enteral Nutr, 1991. **15**(5): p. 540-5 https://doi.org/10.1177/0148607191015005540.

160. Koza, R.A. and E.J. Herbst, *Deficiencies in DNA replication and cell-cycle progression in polyamine-depleted HeLa cells.* Biochem J, 1992. **281 (Pt 1)**(Pt 1): p. 87-93 https://doi.org/10.1042/bj2810087.

161. Scorcioni, F., et al., *Manipulation of the expression of regulatory genes of polyamine metabolism results in specific alterations of the cell-cycle progression.* Biochem J, 2001. **354**(Pt 1): p. 217-23 https://doi.org/10.1042/0264-6021:3540217.

162. Barić, I., *Inherited disorders in the conversion of methionine to homocysteine.* J Inherit Metab Dis, 2009. **32**(4): p. 459-71 https://doi.org/10.1007/s10545-009-1146-4.

163. Barić, I., et al., *Consensus recommendations for the diagnosis, treatment and follow-up of inherited methylation disorders.* J Inherit Metab Dis, 2017. **40**(1): p. 5-20 https://doi.org/10.1007/s10545-016-9972-7.

164. Chamberlin, M.E., et al., *Methionine adenosyltransferase I/III deficiency: novel mutations and clinical variations.* Am J Hum Genet, 2000. **66**(2): p. 347-55 https://doi.org/10.1086/302752.

165. Baric, I., et al., *S-adenosylhomocysteine hydrolase deficiency in a human: a genetic disorder of methionine metabolism.* Proc Natl Acad Sci U S A, 2004. **101**(12): p. 4234-9 https://doi.org/10.1073/pnas.0400658101.

166. Ramani, K. and S.C. Lu, *Methionine adenosyltransferases in liver health and diseases.* Liver Res, 2017. **1**(2): p. 103-111 https://doi.org/10.1016/j.livres.2017.07.002.

167. Chen, P.-M., et al., *Downregulation of Methionine Cycle Genes MAT1A and GNMT Enriches Protein-Associated Translation Process and Worsens Hepatocellular Carcinoma Prognosis.* International Journal of Molecular Sciences, 2022. **23**(1): p. 481

168. (HRSA), H.R.S.A. *Hypermethioninemia*. 2023 2024]; Available from: https://newbornscreening.hrsa.gov/conditions/hypermethioninemia.

169. Alkaissi, H. and S.I. McFarlane, *Hyperhomocysteinemia and Accelerated Aging: The Pathogenic Role of Increased Homocysteine in Atherosclerosis, Osteoporosis, and Neurodegeneration.* Cureus, 2023. **15**(7): p. e42259 https://doi.org/10.7759/cureus.42259.

170. Stanger, O., et al., *Clinical use and rational management of homocysteine, folic acid, and B vitamins in cardiovascular and thrombotic diseases.* Z Kardiol, 2004. **93**(6): p. 439-53 https://doi.org/10.1007/s00392-004-0075-3.

171. Boushey, C.J., et al., *A quantitative assessment of plasma homocysteine as a risk factor for vascular disease. Probable benefits of increasing folic acid intakes.* Jama, 1995. **274**(13): p. 1049-57 https://doi.org/10.1001/jama.1995.03530130055028.

172. Alemán, G., A.R. Tovar, and N. Torres, *[Homocysteine metabolism and risk of cardiovascular diseases: importance of the nutritional status on folic acid, vitamins B6 and B12].* Rev Invest Clin, 2001. **53**(2): p. 141-51

173. Clarke, R., et al., *Hyperhomocysteinemia: an independent risk factor for vascular disease.* N Engl J Med, 1991. **324**(17): p. 1149-55 https://doi.org/10.1056/nejm199104253241701.

174. Ganguly, P. and S.F. Alam, *Role of homocysteine in the development of cardiovascular disease.* Nutr J, 2015. **14**: p. 6 https://doi.org/10.1186/1475-2891-14-6.

175. Guéant, J.L., et al., *Hyperhomocysteinemia in Cardiovascular Diseases: Revisiting Observational Studies and Clinical Trials.* Thromb Haemost, 2023. **123**(3): p. 270-282 https://doi.org/10.1055/a-1952-1946.

176. Refsum, H., et al., *Homocysteine and cardiovascular disease.* Annu Rev Med, 1998. **49**: p. 31-62 https://doi.org/10.1146/annurev.med.49.1.31.

177. Yang, Y., et al., *Dietary methionine restriction improves the gut microbiota and reduces intestinal permeability and inflammation in high-fat-fed mice.* Food Funct, 2019. **10**(9): p. 5952-5968 https://doi.org/10.1039/c9fo00766k.

178. van Dijk, S.C., et al., *Homocysteine level is associated with aortic stiffness in elderly: cross-sectional results from the B-PROOF study.* J Hypertens, 2013. **31**(5): p. 952-9 https://doi.org/10.1097/HJH.0b013e32835eb6b9.

179. Momin, M., et al., *Associations of plasma homocysteine levels with peripheral systolic blood pressure and noninvasive central systolic blood pressure in a community-based Chinese population.* Sci Rep, 2017. **7**(1): p. 6316 https://doi.org/10.1038/s41598-017-06611-3.

180. Wang, X.N., et al., *Plasma Homocysteine is a Predictive Factor for Arterial Stiffness: A Community-Based 4.8-Year Prospective Study.* J Clin Hypertens (Greenwich), 2015. **17**(8): p. 594-600 https://doi.org/10.1111/jch.12555.

181. Poddar, R., *Hyperhomocysteinemia is an emerging comorbidity in ischemic stroke.* Exp Neurol, 2021. **336**: p. 113541 https://doi.org/10.1016/j.expneurol.2020.113541.

182. Austin, R.C., S.R. Lentz, and G.H. Werstuck, *Role of hyperhomocysteinemia in endothelial dysfunction and atherothrombotic disease.* Cell Death Differ, 2004. **11 Suppl 1**: p. S56-64 https://doi.org/10.1038/sj.cdd.4401451.

183. Stühlinger, M.C. and O. Stanger, *Asymmetric dimethyl-L-arginine (ADMA): a possible link between homocyst(e)ine and endothelial dysfunction.* Curr Drug Metab, 2005. **6**(1): p. 3-14 https://doi.org/10.2174/1389200052997393.

184. Upchurch, G.R., Jr., et al., *Homocyst(e)ine decreases bioavailable nitric oxide by a mechanism involving glutathione peroxidase.* J Biol Chem, 1997. **272**(27): p. 17012-7 https://doi.org/10.1074/jbc.272.27.17012.

185. Ungvari, Z., et al., *Increased superoxide production in coronary arteries in hyperhomocysteinemia: role of tumor necrosis factor-alpha, NAD(P)H oxidase, and inducible nitric oxide synthase.* Arterioscler Thromb Vasc Biol, 2003. **23**(3): p. 418-24 https://doi.org/10.1161/01.Atv.0000061735.85377.40.

186. Ungvari, Z., et al., *Dysfunction of nitric oxide mediation in isolated rat arterioles with methionine diet-induced hyperhomocysteinemia.* Arterioscler Thromb Vasc Biol, 1999. **19**(8): p. 1899-904 https://doi.org/10.1161/01.atv.19.8.1899.

187. Böger, R.H., et al., *Plasma concentration of asymmetric dimethylarginine, an endogenous inhibitor of nitric oxide synthase, is elevated in monkeys with hyperhomocyst(e)inemia or hypercholesterolemia.* Arterioscler Thromb Vasc Biol, 2000. **20**(6): p. 1557-64 https://doi.org/10.1161/01.atv.20.6.1557.

188. Böger, R.H., et al., *Elevation of asymmetrical dimethylarginine may mediate endothelial dysfunction during experimental hyperhomocyst(e)inaemia in humans.* Clin Sci (Lond), 2001. **100**(2): p. 161-7

189. Vayá, A., et al., *Homocysteine levels in morbidly obese patients: its association with waist circumference and insulin resistance.* Clin Hemorheol Microcirc, 2012. **52**(1): p. 49-56 https://doi.org/10.3233/ch-2012-1544.

190. Wang, Y., et al., *Central But Not General Obesity Is Positively Associated with the Risk of Hyperhomocysteinemia in Middle-Aged Women.* Nutrients, 2019. **11**(7) https://doi.org/10.3390/nu11071614.

191. Liu, C., et al., *Hyperhomocysteinemia Increases Risk of Metabolic Syndrome and Cardiovascular Death in an Elderly Chinese Community Population of a 7-Year Follow-Up Study*. Front Cardiovasc Med, 2021. **8**: p. 811670 https://doi.org/10.3389/fcvm.2021.811670.

192. Zhang, Z., et al., *Homocysteine and the Risk of Cardiovascular Events and All-Cause Death in Elderly Population: A Community-Based Prospective Cohort Study.* Ther Clin Risk Manag, 2020. **16**: p. 471-481 https://doi.org/10.2147/tcrm.S239496.

193. Park, S.B. and A. Georgiades, *Changes in body composition predict homocysteine changes and hyperhomocysteinemia in Korea.* J Korean Med Sci, 2013. **28**(7): p. 1015-20 https://doi.org/10.3346/jkms.2013.28.7.1015.

194. Tatsumi, Y., et al., *Risk for metabolic diseases in normal weight individuals with visceral fat accumulation: a cross-sectional study in Japan.* BMJ Open, 2017. **7**(1): p. e013831 https://doi.org/10.1136/bmjopen-2016-013831.

195. Mudd, S.H., et al., *The natural history of homocystinuria due to cystathionine beta-synthase deficiency.* Am J Hum Genet, 1985. **37**(1): p. 1-31

196. Brenton, D.P., *Skeletal abnormalities in homocystinuria.* Postgrad Med J, 1977. **53**(622): p. 488-94; discussion 95-6 https://doi.org/10.1136/pgmj.53.622.488.

197. Brenton, D.P., et al., *Homocystinuria and Marfan's syndrome. A comparison.* J Bone Joint Surg Br, 1972. **54**(2): p. 277-98

198. Wilcken, D.E. and B. Wilcken, *The pathogenesis of coronary artery disease. A possible role for methionine metabolism.* J Clin Invest, 1976. **57**(4): p. 1079-82 https://doi.org/10.1172/jci108350.

199. Poloni, S., et al., *Body composition in patients with classical homocystinuria: body mass relates to homocysteine and choline metabolism.* Gene, 2014. **546**(2): p. 443-7 https://doi.org/10.1016/j.gene.2014.05.015.

200. Kraus, J.P., et al., *Cystathionine gamma-lyase: Clinical, metabolic, genetic, and structural studies.* Mol Genet Metab, 2009. **97**(4): p. 250-9 https://doi.org/10.1016/j.ymgme.2009.04.001.

201. Martell, H.J., et al., *Associating mutations causing cystinuria with disease severity with the aim of providing precision medicine.* BMC Genomics, 2017. **18**(5): p. 550 https://doi.org/10.1186/s12864-017-3913-1.

202. Gillion, V., et al., *Extremely rapid stone formation in cystinuria: look out for dietary supplements!* Clinical Kidney Journal, 2021. **14**(6): p. 1694-1696 https://doi.org/10.1093/ckj/sfab013.

203. Błaszczyk, I., et al., *Influence of Methionine upon the Concentration of Malondialdehyde in the Tissues and Blood of Rats Exposed to Sodium Fluoride.* Biological Trace Element Research, 2009. **129**(1): p. 229-238 https://doi.org/10.1007/s12011-008-8308-3.

204. Navik, U., et al., *Methionine as a double-edged sword in health and disease: Current perspective and future challenges.* Ageing Res Rev, 2021. **72**: p. 101500 https://doi.org/10.1016/j.arr.2021.101500.

205. Li, Z., et al., *Methionine metabolism in chronic liver diseases: an update on molecular mechanism and therapeutic implication.* Signal Transduct Target Ther, 2020. **5**(1): p. 280 https://doi.org/10.1038/s41392-020-00349-7.

206. Milani, M. and F. Colombo, *Efficacy and tolerability of an oral supplement containing amino acids, iron, selenium, and marine hydrolyzed collagen in subjects with hair loss (androgenetic alopecia, AGA or FAGA or telogen effluvium). A prospective, randomized, 3-month, controlled, assessor-blinded study.* Skin Res Technol, 2023. **29**(6): p. e13381 https://doi.org/10.1111/srt.13381.

207. Academies, T.N., *DRI Values for Indepensable Amino Acids by Life Stage and Gender Group*, in *Dietary Reference Intakes: The Essential Guide to Nutrient Requirements*, J.P.H. Jennifer J. Otten, and Linda D. Meyers, Editor. 2006, Institute of Medicine of the National Academies. p. 459-465.

208. Miousse, I.R., et al., *Short-term dietary methionine supplementation affects one-carbon metabolism and DNA methylation in the mouse gut and leads to altered microbiome profiles, barrier function, gene expression and histomorphology.* Genes Nutr, 2017. **12**: p. 22 https://doi.org/10.1186/s12263-017-0576-0.

209. Weaver, I.C., et al., *Reversal of maternal programming of stress responses in adult offspring through methyl supplementation: altering epigenetic marking later in life.* J Neurosci, 2005. **25**(47): p. 11045-54 https://doi.org/10.1523/jneurosci.3652-05.2005.

210. Tripodi, F., et al., *Methionine supplementation stimulates mitochondrial respiration.* Biochimica et Biophysica Acta (BBA) - Molecular Cell Research, 2018. **1865**(12): p. 1901-1913 https://doi.org/https://doi.org/10.1016/j.bbamcr.2018.09.007.

211. McCampbell, A., et al., *Induction of Alzheimer's-like changes in brain of mice expressing mutant APP fed excess methionine.* J Neurochem, 2011. **116**(1): p. 82-92 https://doi.org/10.1111/j.1471-4159.2010.07087.x.

212. Ewing, L.E., et al., *Dietary Methionine Supplementation Exacerbates Gastrointestinal Toxicity in a Mouse Model of Abdominal Irradiation.* Int J Radiat Oncol Biol Phys, 2021. **109**(2): p. 581-593 https://doi.org/10.1016/j.ijrobp.2020.09.042.

213. Puddu, P., *Homocysteine and risk for atherothrombotic events.* Cardiologia, 1999. **44**(7): p. 627-31

214. Zhou, J., et al., *Dietary supplementation with methionine and homocysteine promotes early atherosclerosis but not plaque rupture in ApoE-deficient mice.* Arterioscler Thromb Vasc Biol, 2001. **21**(9): p. 1470-6 https://doi.org/10.1161/hq0901.096582.

215. Ai, Y., et al., *Homocysteine Induces Hepatic Steatosis Involving ER Stress Response in High Methionine Diet-Fed Mice.* Nutrients, 2017. **9**(4): p. 346

216. Alzoubi, K.H., Z.O. Aburashed, and F. Mayyas, *Edaravone protects from memory impairment induced by chronic L-methionine administration.* Naunyn-Schmiedeberg's Archives of Pharmacology, 2020. **393**(7): p. 1221-1228 https://doi.org/10.1007/s00210-020-01827-z.

217. El-Dessouki, A.M., et al., *Neuroprotective Effects of Simvastatin and Cilostazol in l-Methionine-Induced Vascular Dementia in Rats.* Molecular Neurobiology, 2017. **54**(7): p. 5074-5084 https://doi.org/10.1007/s12035-016-0051-8.

218. Fayez, A.M., et al., *Neuroprotective effects of zafirlukast, piracetam and their combination on L-Methionine-induced vascular dementia in rats.* Fundam Clin Pharmacol, 2019. **33**(6): p. 634-648 https://doi.org/10.1111/fcp.12473.

219. Yang, Y., et al., *High dietary methionine intake may contribute to the risk of nonalcoholic fatty liver disease by inhibiting hepatic H(2)S production.* Food Res Int, 2022. **158**: p. 111507 https://doi.org/10.1016/j.foodres.2022.111507.

220. Chaturvedi, P., et al., *High Methionine Diet Poses Cardiac Threat: A Molecular Insight.* J Cell Physiol, 2016. **231**(7): p. 1554-61 https://doi.org/10.1002/jcp.25247.

221. Cynober, L., et al., *Proposals for Upper Limits of Safe Intake for Methionine, Histidine, and Lysine in Healthy Humans.* The Journal of Nutrition, 2020. **150**: p. 2606S-2608S https://doi.org/https://doi.org/10.1093/jn/nxaa231.

222. Ferla, M.P.P., W.M., *Bacterial methionine biosynthesis* Microbiology, 2014. **160**(8)

223. Chu, P.H., et al., *Starch extracted from pineapple (Ananas comosus) plant stem as a source for amino acids production.* Chemical and Biological Technologies in Agriculture, 2021. **8**(1): p. 29 https://doi.org/10.1186/s40538-021-00227-6.

224. Neubauer, C. and H. Landecker, *A planetary health perspective on synthetic methionine.* Lancet Planet Health, 2021. **5**(8): p. e560-e569 https://doi.org/10.1016/s2542-5196(21)00138-8.

225. Allaway, D., et al., *Adaptations Supporting Plasma Methionine on a Limited-Methionine, High-Cystine Diet Alter the Canine Plasma Metabolome Consistent with Interventions that Extend Life Span in Other Species.* The Journal of Nutrition, 2021. **151**(10): p. 3125-3136 https://doi.org/https://doi.org/10.1093/jn/nxab204.

226. Lee, B.C., et al., *Methionine restriction extends lifespan of Drosophila melanogaster under conditions of low amino-acid status.* Nat Commun, 2014. **5**: p. 3592 https://doi.org/10.1038/ncomms4592.

227. Grandison, R.C., M.D.W. Piper, and L. Partridge, *Amino-acid imbalance explains extension of lifespan by dietary restriction in Drosophila.* Nature, 2009. **462**(7276): p. 1061-1064 https://doi.org/10.1038/nature08619.

228. Wang, S.-Y., et al., *Methionine restriction delays senescence and suppresses the senescence-associated secretory phenotype in the kidney through endogenous hydrogen sulfide.* Cell Cycle, 2019. **18**(14): p. 1573-1587 https://doi.org/10.1080/15384101.2019.1618124.

229. Bárcena, C., et al., *Methionine Restriction Extends Lifespan in Progeroid Mice and Alters Lipid and Bile Acid Metabolism.* Cell Reports, 2018. **24**(9): p. 2392-2403 https://doi.org/https://doi.org/10.1016/j.celrep.2018.07.089.

230. Orentreich, N., et al., *Low methionine ingestion by rats extends life span.* J Nutr, 1993. **123**(2): p. 269-74 https://doi.org/10.1093/jn/123.2.269.

231. Bárcena, C., et al., *Methionine Restriction Extends Lifespan in Progeroid Mice and Alters Lipid and Bile Acid Metabolism.* Cell Rep, 2018. **24**(9): p. 2392-2403 https://doi.org/10.1016/j.celrep.2018.07.089.

232. Miller, R.A., et al., *Methionine-deficient diet extends mouse lifespan, slows immune and lens aging, alters glucose, T4, IGF-I and insulin levels, and increases hepatocyte MIF levels and stress resistance.* Aging Cell, 2005. **4**(3): p. 119-25 https://doi.org/10.1111/j.1474-9726.2005.00152.x.

233. Perrone, C.E., et al., *Metabolic adaptations to methionine restriction that benefit health and lifespan in rodents.* Exp Gerontol, 2013. **48**(7): p. 654-60 https://doi.org/10.1016/j.exger.2012.07.005.

234. Lee, B.C., A. Kaya, and V.N. Gladyshev, *Methionine restriction and life-span control.* Ann N Y Acad Sci, 2016. **1363**: p. 116-24 https://doi.org/10.1111/nyas.12973.

235. Plummer, J.D. and J.E. Johnson, *Extension of Cellular Lifespan by Methionine Restriction Involves Alterations in Central Carbon Metabolism and Is Mitophagy-Dependent.* Front Cell Dev Biol, 2019. **7**: p. 301 https://doi.org/10.3389/fcell.2019.00301.

236. Parkhitko, A.A., et al., *Methionine metabolism and methyltransferases in the regulation of aging and lifespan extension across species.* Aging Cell, 2019. **18**(6): p. e13034 https://doi.org/10.1111/acel.13034.

237. Ruckenstuhl, C., et al., *Lifespan extension by methionine restriction requires autophagy-dependent vacuolar acidification.* PLoS Genet, 2014. **10**(5): p. e1004347 https://doi.org/10.1371/journal.pgen.1004347.

238. Cabreiro, F., et al., *Metformin retards aging in C. elegans by altering microbial folate and methionine metabolism.* Cell, 2013. **153**(1): p. 228-39 https://doi.org/10.1016/j.cell.2013.02.035.

239. Richie, J.P., Jr., et al., *Methionine restriction increases blood glutathione and longevity in F344 rats.* Faseb j, 1994. **8**(15): p. 1302-7 https://doi.org/10.1096/fasebj.8.15.8001743.

240. Wang, S.Y., et al., *Methionine restriction delays senescence and suppresses the senescence-associated secretory phenotype in the kidney through endogenous hydrogen sulfide.* Cell Cycle, 2019. **18**(14): p. 1573-1587 https://doi.org/10.1080/15384101.2019.1618124.

241. Wang, L., et al., *Methionine Restriction Regulates Cognitive Function in High-Fat Diet-Fed Mice: Roles of Diurnal Rhythms of SCFAs Producing- and Inflammation-Related Microbes.* Mol Nutr Food Res, 2020. **64**(17): p. e2000190 https://doi.org/10.1002/mnfr.202000190.

242. Lail, H., et al., *Effects of Dietary Methionine Restriction on Cognition in Mice.* Nutrients, 2023. **15**(23) https://doi.org/10.3390/nu15234950.

243. Xu, Y., et al., *Dietary methionine restriction ameliorates the impairment of learning and memory function induced by obesity in mice.* Food Funct, 2019. **10**(3): p. 1411-1425 https://doi.org/10.1039/c8fo01922c.

244. Xi, Y., et al., *Effects of methionine intake on cognitive function in mild cognitive impairment patients and APP/PS1 Alzheimer's Disease model mice: Role of the cystathionine-β-synthase/H(2)S pathway.* Redox Biol, 2023. **59**: p. 102595 https://doi.org/10.1016/j.redox.2022.102595.

245. Feng, C., et al., *Methionine Restriction Improves Cognitive Ability by Alleviating Hippocampal Neuronal Apoptosis through H19 in Middle-Aged Insulin-Resistant Mice.* Nutrients, 2022. **14**(21) https://doi.org/10.3390/nu14214503.

246. Lail, H., et al., *Effects of Dietary Methionine Restriction on Cognition in Mice.* Nutrients, 2023. **15**(23): p. 4950

247. López-Torres, M. and G. Barja, *Lowered methionine ingestion as responsible for the decrease in rodent mitochondrial oxidative stress in protein and dietary restriction: Possible implications for humans.* Biochimica et Biophysica Acta (BBA) - General Subjects, 2008. **1780**(11): p. 1337-1347 https://doi.org/https://doi.org/10.1016/j.bbagen.2008.01.007.

248. Kitada, M., et al., *Effect of Methionine Restriction on Aging: Its Relationship to Oxidative Stress.* Biomedicines, 2021. **9**(2) https://doi.org/10.3390/biomedicines9020130.

249. Allaway, D.H., M.J.; Gray, K.; Colyer, A., *Reduced Methionine Diet for Dogs*. 2019, MARS, INCORPORATED.

250. Finley, J.W; Gettys, T.; Greenway F.L., *Palatable foods for a methionine-restricted diet* 2014.

251. Kaiser, P., *Methionine Dependence of Cancer.* Biomolecules, 2020. **10**(4) https://doi.org/10.3390/biom10040568.

252. Sedillo, J.C. and V.L. Cryns, *Targeting the methionine addiction of cancer.* Am J Cancer Res, 2022. **12**(5): p. 2249-2276

253. Pokrovsky, V.S., et al., *Targeting Methionine Addiction of Cancer Cells with Methioninase.* Biochemistry (Mosc), 2023. **88**(7): p. 944-952 https://doi.org/10.1134/s0006297923070076.

254. Gao, X., et al., *Dietary methionine influences therapy in mouse cancer models and alters human metabolism.* Nature, 2019. **572**(7769): p. 397-401 https://doi.org/10.1038/s41586-019-1437-3.

255. Hu, J. and N.K. Cheung, *Methionine depletion with recombinant methioninase: in vitro and in vivo efficacy against neuroblastoma and its synergism with chemotherapeutic drugs.* Int J Cancer, 2009. **124**(7): p. 1700-6 https://doi.org/10.1002/ijc.24104.

256. Kubota, Y., et al., *Synergy of Combining Methionine Restriction and Chemotherapy: The Disruptive Next Generation of Cancer Treatment.* Cancer Diagn Progn, 2023. **3**(3): p. 272-281 https://doi.org/10.21873/cdp.10212.

257. Cavuoto, P. and M.F. Fenech, *A review of methionine dependency and the role of methionine restriction in cancer growth control and life-span extension.* Cancer Treatment Reviews, 2012. **38**(6): p. 726-736 https://doi.org/https://doi.org/10.1016/j.ctrv.2012.01.004.

258. Kubota, Y., et al., *[(11)C] Methionine-PET Imaging as a Cancer Biomarker for Methionine Addiction and Sensitivity to Methionine-restriction-based Combination Chemotherapy.* In Vivo, 2024. **38**(1): p. 253-258 https://doi.org/10.21873/invivo.13432.

259. Kubota, Y., et al., *Methionine restriction of glioma does not induce MGMT and greatly improves temozolomide efficacy in an orthotopic nude-mouse model: A potential curable approach to a clinically-incurable disease.* Biochemical and Biophysical Research Communications, 2024. **695**: p. 149418 https://doi.org/https://doi.org/10.1016/j.bbrc.2023.149418.

260. Li, Y., et al., *Upregulation of E-cadherin by the combination of methionine restriction and HDAC2 intervention for inhibiting gastric carcinoma metastasis.* Acta Biochim Biophys Sin (Shanghai), 2023. **56**(1): p. 62-70 https://doi.org/10.3724/abbs.2023244.

261. Tripodi, F., et al., *Methionine Supplementation Affects Metabolism and Reduces Tumor Aggressiveness in Liver Cancer Cells.* Cells, 2020. **9**(11) https://doi.org/10.3390/cells9112491.

262. Baliou, S., et al., *Protective role of taurine against oxidative stress (Review).* Mol Med Rep, 2021. **24**(2) https://doi.org/10.3892/mmr.2021.12242.

263. Chen, S., et al., *Associations of serum amino acids with insulin resistance among people with and without overweight or obesity: A prospective study in Japan.* Clin Nutr, 2022. **41**(8): p. 1827-1833 https://doi.org/10.1016/j.clnu.2022.06.039.

264. Wu, G., et al., *Dietary Methionine Restriction Ameliorated Fat Accumulation, Systemic Inflammation, and Increased Energy Metabolism by Altering Gut Microbiota in Middle-Aged Mice Administered Different Fat Diets.* J Agric Food Chem, 2020. **68**(29): p. 7745-7756 https://doi.org/10.1021/acs.jafc.0c02965.

265. Wu, G., et al., *Effect of different levels of dietary methionine restriction on relieving oxidative stress and behavioral deficits in middle-aged mice fed low-, medium-, or high-fat diet.* Journal of Functional Foods, 2020. **65**: p. 103782 https://doi.org/https://doi.org/10.1016/j.jff.2020.103782.

266. Han, L., et al., *Dietary methionine restriction improves the impairment of cardiac function in middle-aged obese mice.* Food Funct, 2020. **11**(2): p. 1764-1778 https://doi.org/10.1039/c9fo02819f.

267. Lees, E.K., et al., *Methionine restriction restores a younger metabolic phenotype in adult mice with alterations in fibroblast growth factor 21.* Aging Cell, 2014. **13**(5): p. 817-27 https://doi.org/10.1111/acel.12238.

268. Tore, E.C., et al., *Associations between plasma sulfur amino acids and specific fat depots in two independent cohorts: CODAM and The Maastricht Study.* Eur J Nutr, 2023. **62**(2): p. 891-904 https://doi.org/10.1007/s00394-022-03041-4.

269. Plaisance, E.P., et al., *Dietary methionine restriction increases fat oxidation in obese adults with metabolic syndrome.* J Clin Endocrinol Metab, 2011. **96**(5): p. E836-40 https://doi.org/10.1210/jc.2010-2493.

270. Ables, G.P., et al., *Dietary methionine restriction in mice elicits an adaptive cardiovascular response to hyperhomocysteinemia.* Sci Rep, 2015. **5**: p. 8886 https://doi.org/10.1038/srep08886.

271. Wanders, D., et al., *FGF21 Mediates the Thermogenic and Insulin-Sensitizing Effects of Dietary Methionine Restriction but Not Its Effects on Hepatic Lipid Metabolism.* Diabetes, 2017. **66**(4): p. 858-867 https://doi.org/10.2337/db16-1212.

272. Fang, H., et al., *Nutritional Regulation of Hepatic FGF21 by Dietary Restriction of Methionine.* Front Endocrinol (Lausanne), 2021. **12**: p. 773975 https://doi.org/10.3389/fendo.2021.773975.

273. Stone, K.P., et al., *Mechanisms of increased in vivo insulin sensitivity by dietary methionine restriction in mice.* Diabetes, 2014. **63**(11): p. 3721-33 https://doi.org/10.2337/db14-0464.

274. Wanders, D., et al., *Role of GCN2-Independent Signaling Through a Noncanonical PERK/NRF2 Pathway in the Physiological Responses to Dietary Methionine Restriction.* Diabetes, 2016. **65**(6): p. 1499-510 https://doi.org/10.2337/db15-1324.

275. Ables, G.P., et al., *Methionine-restricted C57BL/6J mice are resistant to diet-induced obesity and insulin resistance but have low bone density.* PLoS One, 2012. **7**(12): p. e51357 https://doi.org/10.1371/journal.pone.0051357.

276. Plummer, J.D. and J.E. Johnson, *Intermittent methionine restriction reduces IGF-1 levels and produces similar healthspan benefits to continuous methionine restriction.* Aging Cell, 2022. **21**(6): p. e13629 https://doi.org/10.1111/acel.13629.

277. Sonntag, W.E., et al., *Pleiotropic effects of growth hormone and insulin-like growth factor (IGF)-1 on biological aging: inferences from moderate caloric-restricted animals.* J Gerontol A Biol Sci Med Sci, 1999. **54**(12): p. B521-38 https://doi.org/10.1093/gerona/54.12.b521.

278. Zimmerman, J.A., et al., *Nutritional control of aging.* Exp Gerontol, 2003. **38**(1-2): p. 47-52 https://doi.org/10.1016/s0531-5565(02)00149-3.

279. Sanchez-Roman, I. and G. Barja, *Regulation of longevity and oxidative stress by nutritional interventions: Role of methionine restriction.* Experimental Gerontology, 2013. **48**(10): p. 1030-1042 https://doi.org/https://doi.org/10.1016/j.exger.2013.02.021.

280. Hasek, B.E., et al., *Dietary methionine restriction enhances metabolic flexibility and increases uncoupled respiration in both fed and fasted states.* Am J Physiol Regul Integr Comp Physiol, 2010. **299**(3): p. R728-39 https://doi.org/10.1152/ajpregu.00837.2009.

281. Cooke, D., et al., *Weight Loss and Concomitant Adipose Autophagy in Methionine-Restricted Obese Mice is Not Dependent on Adiponectin or FGF21.* Obesity (Silver Spring), 2020. **28**(6): p. 1075-1085 https://doi.org/10.1002/oby.22763.

282. Ren, B.W., L.; Liu, Z.; Liu, X., *Methionine Restriction Alleviates Aging-related Cognitive Dysfunction via Stimulating FGF21-driven Mitochondrial Biogenesis (P14-026-19).*

283. Swaminathan, A., et al., *Methionine restriction plus overload improves skeletal muscle and metabolic health in old mice on a high fat diet.* Scientific Reports, 2021. **11**(1): p. 1260 https://doi.org/10.1038/s41598-021-81037-6.

284. Cooke, D. and G.P. Ables, *Physical activity of mice on dietary sulfur amino acid restriction is influenced by age of diet initiation and biological sex.* Sci Rep, 2023. **13**(1): p. 20609 https://doi.org/10.1038/s41598-023-47676-7.

285. Huang, T.H., et al., *A methionine-restricted diet and endurance exercise decrease bone mass and extrinsic strength but increase intrinsic strength in growing male rats.* J Nutr, 2014. **144**(5): p. 621-30 https://doi.org/10.3945/jn.113.187922.

286. Malloy, V.L., et al., *Methionine restriction decreases visceral fat mass and preserves insulin action in aging male Fischer 344 rats independent of energy restriction.* Aging Cell, 2006. **5**(4): p. 305-14 https://doi.org/10.1111/j.1474-9726.2006.00220.x.

287. McGilvrey, M., et al., *Effects of dietary methionine restriction on age-related changes in perivascular and beiging adipose tissues in the mouse.* Obesity (Silver Spring), 2023. **31**(1): p. 159-170 https://doi.org/10.1002/oby.23583.

288. Malloy, V.L., et al., *Methionine restriction prevents the progression of hepatic steatosis in leptin-deficient obese mice.* Metabolism, 2013. **62**(11): p. 1651-61 https://doi.org/10.1016/j.metabol.2013.06.012.

289. Liu, M.M., Xiaotong; Zong, Yiling; Niu, Xingyu, *Methionine restriction improve insulin resistance by reducing mitochondrial oxidative stress.pdf>.*

290. Plummer, J.D.H., M. C.; Johnson, J. E., *Intermittent Methionine Restriction Reduces Marrow Fat Accumulation and Preserves More Bone Mass than Continuous Methionine Restriction.* AgingBio, 2024(1): p. 1-12 https://doi.org/10.59368/agingbio.20230019.

291. Richie, J.P., Jr., et al., *Dietary Methionine and Total Sulfur Amino Acid Restriction in Healthy Adults.* J Nutr Health Aging, 2023. **27**(2): p. 111-123 https://doi.org/10.1007/s12603-023-1883-3.

292. Olsen, T., et al., *Dietary sulfur amino acid restriction in humans with overweight and obesity: a translational randomized controlled trial.* Journal of Translational Medicine, 2024. **22**(1): p. 40 https://doi.org/10.1186/s12967-023-04833-w.

293. Forney, L.A., et al., *Concentration-dependent linkage of dietary methionine restriction to the components of its metabolic phenotype.* Obesity (Silver Spring), 2017. **25**(4): p. 730-738 https://doi.org/10.1002/oby.21806.

294. Olsen, T., et al., *Effects of dietary methionine and cysteine restriction on plasma biomarkers, serum fibroblast growth factor 21, and adipose tissue gene expression in women with overweight or obesity: a double-blind randomized controlled pilot study.* Journal of Translational Medicine, 2020. **18**(1): p. 122 https://doi.org/10.1186/s12967-020-02288-x.

295. Stolt, E., et al., *Sulfur amino acid restriction, energy metabolism and obesity: a study protocol of an 8-week randomized controlled dietary intervention with whole foods and amino acid supplements.* J Transl Med, 2021. **19**(1): p. 153 https://doi.org/10.1186/s12967-021-02824-3.

296. Fang, H., et al., *Implementation of dietary methionine restriction using casein after selective, oxidative deletion of methionine.* iScience, 2021. **24**(5): p. 102470 https://doi.org/10.1016/j.isci.2021.102470.

297. Agriculture, U.D.o., *USDA National Nutrient Database for Standard Reference, Release 28,* B.H.N.R.C. Nutrient Data Laboratory, ARS, USDA., Editor. 2016.

298. Haytowitz, D.B.A., Jaspreet K.C.; Wu, Xianli; Somanchi, Meena; Nickle, Melissa; Nguyen, Quyen A.; Roseland, Janet M.; Williams, Juhi R.; Patterson, Kristine Y.; Li, Ying; Pehrsson, Pamela R., *USDA National Nutrient Database for Standard Reference, Legacy Release. Dataset.* , B.H.N.R.C. Nutrient Data Laboratory, ARS, USDA., Editor. 2019.

299. Wu, G., et al., *Methionine-Restricted Diet: A Feasible Strategy Against Chronic or Aging-Related Diseases.* J Agric Food Chem, 2023. **71**(1): p. 5-19 https://doi.org/10.1021/acs.jafc.2c05829.

300. McCarty, M.F., J. Barroso-Aranda, and F. Contreras, *The low-methionine content of vegan diets may make methionine restriction feasible as a life extension strategy.* Med Hypotheses, 2009. **72**(2): p. 125-8 https://doi.org/10.1016/j.mehy.2008.07.044.

301. McCarty, M.F., *Vegan proteins may reduce risk of cancer, obesity, and cardiovascular disease by promoting increased glucagon activity.* Med Hypotheses, 1999. **53**(6): p. 459-85 https://doi.org/10.1054/mehy.1999.0784.

302. Krajcovicova-Kudlackova, M., K. Babinska, and M. Valachovicova, *Health benefits and risks of plant proteins.* Bratisl Lek Listy, 2005. **106**(6-7): p. 231-4

303. Abbasi, H., et al., *Dietary total, plant, and animal protein intake in relation to cardiovascular outcomes and inflammatory factors in elderly men: A cross-sectional study.* Food Sci Nutr, 2024. **12**(2): p. 1230-1244 https://doi.org/10.1002/fsn3.3837.

304. Banaszak, M., I. Górna, and J. Przysławski, *Non-Pharmacological Treatments for Insulin Resistance: Effective Intervention of Plant-Based Diets-A Critical Review.* Nutrients, 2022. **14**(7) https://doi.org/10.3390/nu14071400.

305. Key, T.J., K. Papier, and T.Y.N. Tong, *Plant-based diets and long-term health: findings from the EPIC-Oxford study.* Proc Nutr Soc, 2022. **81**(2): p. 190-198 https://doi.org/10.1017/s0029665121003748.

306. Schmidt, J.A., et al., *Metabolic profiles of male meat eaters, fish eaters, vegetarians, and vegans from the EPIC-Oxford cohort.* Am J Clin Nutr, 2015. **102**(6): p. 1518-26 https://doi.org/10.3945/ajcn.115.111989.

307. Schmidt, J.A., et al., *Plasma concentrations and intakes of amino acids in male meat-eaters, fish-eaters, vegetarians and vegans: a cross-sectional analysis in the EPIC-Oxford cohort.* Eur J Clin Nutr, 2016. **70**(3): p. 306-12 https://doi.org/10.1038/ejcn.2015.144.

308. VandenAkker, N.E., et al., *Whole Red Raspberry (Rubus idaeus)-Enriched Diet Is Hepatoprotective in the Obese Zucker Rat, a Model of the Metabolic Syndrome.* J Med Food, 2021. **24**(8): p. 817-824 https://doi.org/10.1089/jmf.2020.0130.

309. Valenzuela, R., et al., *Anti-steatotic effects of an n-3 LCPUFA and extra virgin olive oil mixture in the liver of mice subjected to high-fat diet.* Food Funct, 2016. **7**(1): p. 140-50 https://doi.org/10.1039/c5fo01086a.

310. Valenzuela, R., et al., *Molecular adaptations underlying the beneficial effects of hydroxytyrosol in the pathogenic alterations induced by a high-fat diet in mouse liver: PPAR-α and Nrf2 activation, and NF-κB down-regulation.* Food Funct, 2017. **8**(4): p. 1526-1537 https://doi.org/10.1039/c7fo00090a.

311. Łuszczki, E., et al., *Vegan diet: nutritional components, implementation, and effects on adults' health.* Front Nutr, 2023. **10**: p. 1294497 https://doi.org/10.3389/fnut.2023.1294497.

312. Kniskern, M.A. and C.S. Johnston, *Protein dietary reference intakes may be inadequate for vegetarians if low amounts of animal protein are consumed.* Nutrition, 2011. **27**(6): p. 727-30 https://doi.org/10.1016/j.nut.2010.08.024.

313. Hoffman, J.R. and M.J. Falvo, *Protein - Which is Best?* J Sports Sci Med, 2004. **3**(3): p. 118-30

314. AL, S.A.C., *Wardlaw's Contemporary Nutrition*. 10 ed. 2016: McGraw-Hill Education

315. WC, M.R.M.C.R., *Feeding Experiments with Mixtures of Highyl Purified Amino Acids: Isolation and Identificaion of a New Essential Amino Acid.* Journal of Biological Chemistry, 1935. **112**: p. 283-302 https://doi.org/10.1016/S0021-9258(18)74986-7.

316. Geiger, E., *Experiments with delayed supplementation of incomplete amino acid mixtures.* J Nutr, 1947. **34**(1): p. 97-111 https://doi.org/10.1093/jn/34.1.97.

317. MacArthur, M.R., et al., *Total protein, not amino acid composition, differs in plant-based versus omnivorous dietary patterns and determines metabolic health effects in mice.* Cell Metab, 2021. **33**(9): p. 1808-1819 e2 https://doi.org/10.1016/j.cmet.2021.06.011.

318. Yap, Y.W., et al., *Restriction of essential amino acids dictates the systemic metabolic response to dietary protein dilution.* Nature Communications, 2020. **11**(1): p. 2894 https://doi.org/10.1038/s41467-020-16568-z.

319. Faure, M., et al., *Dietary Threonine Restriction Specifically Reduces Intestinal Mucin Synthesis in Rats.* The Journal of Nutrition, 2005. **135**(3): p. 486-491 https://doi.org/https://doi.org/10.1093/jn/135.3.486.

320. Yoshida, A., K. Ashida, and A.E. Harper, *Prevention of Fatty Liver due to Threonine Deficiency by Moderate Caloric Restriction.* Nature, 1961. **189**(4768): p. 917-918 https://doi.org/10.1038/189917a0.

321. Zapata, R.C., et al., *Dietary Tryptophan Restriction Dose-Dependently Modulates Energy Balance, Gut Hormones, and Microbiota in Obesity-Prone Rats.* Obesity (Silver Spring), 2018. **26**(4): p. 730-739 https://doi.org/10.1002/oby.22136.

322. Zapata, R.C., et al., *Tryptophan restriction partially recapitulates the age-dependent effects of total amino acid restriction on energy balance in diet-induced obese rats.* The Journal of Nutritional Biochemistry, 2019. **65**: p. 115-127 https://doi.org/https://doi.org/10.1016/j.jnutbio.2018.12.006.

323. Green, C.L., et al., *Dietary restriction of isoleucine increases healthspan and lifespan of genetically heterogeneous mice.* Cell Metab, 2023. **35**(11): p. 1976-1995.e6 https://doi.org/10.1016/j.cmet.2023.10.005.

324. Lees, E.K., et al., *Direct comparison of methionine restriction with leucine restriction on the metabolic health of C57BL/6J mice.* Scientific Reports, 2017. **7**(1): p. 9977 https://doi.org/10.1038/s41598-017-10381-3.

325. Wanders, D., et al., *Metabolic responses to dietary leucine restriction involve remodeling of adipose tissue and enhanced hepatic insulin signaling.* Biofactors, 2015. **41**(6): p. 391-402 https://doi.org/10.1002/biof.1240.

326. Zhou, Z., et al., *A fifty percent leucine-restricted diet reduces fat mass and improves glucose regulation.* Nutr Metab (Lond), 2021. **18**(1): p. 34 https://doi.org/10.1186/s12986-021-00564-1.

327. Richardson, N.E., et al., *Lifelong restriction of dietary branched-chain amino acids has sex-specific benefits for frailty and life span in mice.* Nature Aging, 2021. **1**(1): p. 73-86 https://doi.org/10.1038/s43587-020-00006-2.

328. Wang, D., et al., *Dietary protein and amino acid restriction: Roles in metabolic health and aging-related diseases.* Free Radic Biol Med, 2022. **178**: p. 226-242 https://doi.org/10.1016/j.freeradbiomed.2021.12.009.

329. Einarsson, M.J., A; Baek, AM; Jacobsen, C; Pedersen, SA; Samuelsen, TA; Palsson, J; Eliasen, O; Flesland, O, *Nordic Centre of Excellence Network in Fishmeal and Fish Oil*, I.F.a.B. R&D, Editor. 2019, Matis ltd.

330. Tan, Y., et al., *Overexpression and large-scale production of recombinant L-methionine-alpha-deamino-gamma-mercaptomethane-lyase for novel anticancer therapy.* Protein Expr Purif, 1997. **9**(2): p. 233-45 https://doi.org/10.1006/prep.1996.0700.

331. Miyake, K., et al., *Colon-cancer liver metastasis is effectively targeted by recombinant methioninase (rMETase) in an orthotopic mouse model.* Tissue Cell, 2023. **83**: p. 102125 https://doi.org/10.1016/j.tice.2023.102125.

332. Miyake, M., et al., *Synergy of oral recombinant methioninase (rMETase) and 5-fluorouracil on poorly differentiated gastric cancer.* Biochem Biophys Res Commun, 2023. **643**: p. 48-54 https://doi.org/10.1016/j.bbrc.2022.12.062.

333. Park, J.H., et al., *Oral recombinant methioninase combined with oxaliplatinum and 5-fluorouracil regressed a colon cancer growing on the peritoneal surface in a patient-derived orthotopic xenograft mouse model.* Tissue Cell, 2019. **61**: p. 109-114 https://doi.org/10.1016/j.tice.2019.09.006.

334. Kawaguchi, K., et al., *Efficacy of Recombinant Methioninase (rMETase) on Recalcitrant Cancer Patient-Derived Orthotopic Xenograft (PDOX) Mouse Models: A Review.* Cells, 2019. **8**(5) https://doi.org/10.3390/cells8050410.

335. Hoffman, R.M., *Development of recombinant methioninase to target the general cancer-specific metabolic defect of methionine dependence: a 40-year odyssey.* Expert Opin Biol Ther, 2015. **15**(1): p. 21-31 https://doi.org/10.1517/14712598.2015.963050.

336. Hoffman, R.M., et al., *High Efficacy of Recombinant Methioninase on Patient-Derived Orthotopic Xenograft (PDOX) Mouse Models of Cancer.* Methods Mol Biol, 2019. **1866**: p. 149-161 https://doi.org/10.1007/978-1-4939-8796-2_12.

337. Tashiro, Y., et al., *Oral Recombinant Methioninase Prevents Obesity in Mice on a High-fat Diet.* In Vivo, 2020. **34**(2): p. 489-494 https://doi.org/10.21873/invivo.11799.

338. Tashiro, Y., et al., *Oral Recombinant Methioninase Prevents Nonalcoholic Fatty Liver Disease in Mice on a High Fat Diet.* In Vivo, 2020. **34**(3): p. 979-984 https://doi.org/10.21873/invivo.11866.

339. Tashiro, Y., et al., *Oral Recombinant Methioninase Inhibits Diabetes Onset in Mice on a High-fat Diet.* In Vivo, 2020. **34**(3): p. 973-978 https://doi.org/10.21873/invivo.11865.

340. Perreault, M., et al., *The live biotherapeutic SYNB1353 decreases plasma methionine via directed degradation in animal models and healthy volunteers.* Cell Host Microbe, 2024 https://doi.org/10.1016/j.chom.2024.01.005.

341. Puurunen, M.K., et al., *Safety and pharmacodynamics of an engineered E. coli Nissle for the treatment of phenylketonuria: a first-in-human phase 1/2a study.* Nature Metabolism, 2021. **3**(8): p. 1125-1132 https://doi.org/10.1038/s42255-021-00430-7.

342. Isabella, V.M., et al., *Development of a synthetic live bacterial therapeutic for the human metabolic disease phenylketonuria.* Nature Biotechnology, 2018. **36**(9): p. 857-864 https://doi.org/10.1038/nbt.4222.

343. Vockley, J., et al., *Efficacy and safety of a synthetic biotic for treatment of phenylketonuria: a phase 2 clinical trial.* Nature Metabolism, 2023. **5**(10): p. 1685-1690 https://doi.org/10.1038/s42255-023-00897-6.

344. Kubota, Y., et al., *Old-age-induced obesity reversed by a methionine-deficient diet or oral administration of recombinant methioninase-producing Escherichia coli in C57BL/6 mice.* Aging (Albany NY), 2023. **15**(11): p. 4642-4648 https://doi.org/10.18632/aging.204783.

345. Lin, S., et al., *Development of high fat diet-induced obesity and leptin resistance in C57Bl/6J mice.* Int J Obes Relat Metab Disord, 2000. **24**(5): p. 639-46 https://doi.org/10.1038/sj.ijo.0801209.

346. Toye, A.A., et al., *A genetic and physiological study of impaired glucose homeostasis control in C57BL/6J mice.* Diabetologia, 2005. **48**(4): p. 675-86 https://doi.org/10.1007/s00125-005-1680-z.

347. Rydström, J., *Mitochondrial NADPH, transhydrogenase and disease.* Biochim Biophys Acta, 2006. **1757**(5-6): p. 721-6 https://doi.org/10.1016/j.bbabio.2006.03.010.

348. Ghosh, D., K.R. Levault, and G.J. Brewer, *Relative importance of redox buffers GSH and NAD(P)H in age-related neurodegeneration and Alzheimer disease-like mouse neurons.* Aging Cell, 2014. **13**(4): p. 631-40 https://doi.org/10.1111/acel.12216.

349. Livak, K.J. and T.D. Schmittgen, *Analysis of relative gene expression data using real-time quantitative PCR and the 2(-Delta Delta C(T)) Method.* Methods, 2001. **25**(4): p. 402-8 https://doi.org/10.1006/meth.2001.1262.

350. Tero, B.W., et al., *Quantification of Lipid Area within Thermogenic Mouse Perivascular Adipose Tissue Using Standardized Image Analysis in FIJI.* J Vasc Res, 2022. **59**(1): p. 43-49 https://doi.org/10.1159/000517178.

351. Ashburner, M., et al., *Gene Ontology: tool for the unification of biology.* Nature Genetics, 2000. **25**(1): p. 25-29 https://doi.org/10.1038/75556.

352. Brionne, A., A. Juanchich, and C. Hennequet-Antier, *ViSEAGO: a Bioconductor package for clustering biological functions using Gene Ontology and semantic similarity.* BioData Mining, 2019. **12**(1): p. 16 https://doi.org/10.1186/s13040-019-0204-1.

353. Consortium, T.G.O., et al., *The Gene Ontology knowledgebase in 2023.* Genetics, 2023. **224**(1) https://doi.org/10.1093/genetics/iyad031.

354. Tanabe, H., et al., *CELL LINE INDIVIDUALIZATION BY STR MULTIPLEX SYSTEM IN THE CELL BANK FOUND CROSS-CONTAMINATION BETWEEN ECV304 AND EJ-1/T24.* TISSUE CULTURE RESEARCH COMMUNICATIONS, 1999. **18**(4): p. 329-338 https://doi.org/10.11418/jtca1981.18.4_329.

355. Su, S., et al., *A Renewable Source of Human Beige Adipocytes for Development of Therapies to Treat Metabolic Syndrome.* Cell Rep, 2018. **25**(11): p. 3215-3228 e9 https://doi.org/10.1016/j.celrep.2018.11.037.

356. Ravi, V., et al., *Measuring Protein Synthesis in Cultured Cells and Mouse Tissues Using the Non-radioactive SUnSET Assay.* Curr Protoc Mol Biol, 2020. **133**(1): p. e127 https://doi.org/10.1002/cpmb.127.

357. Patil, Y.N., et al., *Cellular and molecular remodeling of inguinal adipose tissue mitochondria by dietary methionine restriction.* J Nutr Biochem, 2015. **26**(11): p. 1235-47 https://doi.org/10.1016/j.jnutbio.2015.05.016.

358. Boucher, J.M., et al., *Pathological Conversion of Mouse Perivascular Adipose Tissue by Notch Activation.* Arterioscler Thromb Vasc Biol, 2020. **40**(9): p. 2227-2243 https://doi.org/10.1161/atvbaha.120.314731.

359. Li, G., et al., *Mechanical compressive force inhibits adipogenesis of adipose stem cells.* Cell Prolif, 2013. **46**(5): p. 586-94 https://doi.org/10.1111/cpr.12053.

360. Yuan, Y., J. Gao, and R. Ogawa, *Mechanobiology and Mechanotherapy of Adipose Tissue-Effect of Mechanical Force on Fat Tissue Engineering.* Plast Reconstr Surg Glob Open, 2015. **3**(12): p. e578 https://doi.org/10.1097/gox.0000000000000564.

361. Mattocks, D.A., et al., *Short term methionine restriction increases hepatic global DNA methylation in adult but not young male C57BL/6J mice.* Exp Gerontol, 2017. **88**: p. 1-8 https://doi.org/10.1016/j.exger.2016.12.003.

362. Tamanna, N., et al., *The effect of short-term methionine restriction on glutathione synthetic capacity and antioxidant responses at the whole tissue and mitochondrial level in the rat liver.* Experimental Gerontology, 2019. **127**: p. 110712 https://doi.org/https://doi.org/10.1016/j.exger.2019.110712.

363. Yu, D., et al., *Short-term methionine deprivation improves metabolic health via sexually dimorphic, mTORC1-independent mechanisms.* Faseb j, 2018. **32**(6): p. 3471-3482 https://doi.org/10.1096/fj.201701211R.

364. Fontaine, D., *5 Common Questions for Diabetic Models*. 2019, The Jackson Laboratory.

365. Aguirre, G.A., et al., *Insulin-like growth factor-1 deficiency and metabolic syndrome.* J Transl Med, 2016. **14**: p. 3 https://doi.org/10.1186/s12967-015-0762-z.

366. Attia, N., et al., *The Metabolic Syndrome and Insulin-Like Growth Factor I Regulation in Adolescent Obesity1.* The Journal of Clinical Endocrinology & Metabolism, 1998. **83**(5): p. 1467-1471 https://doi.org/10.1210/jcem.83.5.4827.

367. Kubo, H., et al., *Insulin-like growth factor-1 levels are associated with high comorbidity of metabolic disorders in obese subjects; a Japanese single-center, retrospective-study.* Scientific Reports, 2022. **12**(1): p. 20130 https://doi.org/10.1038/s41598-022-23521-1.

368. Forney, L.A., et al., *Dietary Methionine Restriction Signals to the Brain Through Fibroblast Growth Factor 21 to Regulate Energy Balance and Remodeling of Adipose Tissue.* Obesity (Silver Spring), 2020. **28**(10): p. 1912-1921 https://doi.org/10.1002/oby.22919.

369. Sherman, K.E., *Alanine aminotransferase in clinical practice. A review.* Arch Intern Med, 1991. **151**(2): p. 260-5

370. Kim, W.R., et al., *Serum activity of alanine aminotransferase (ALT) as an indicator of health and disease.* Hepatology, 2008. **47**(4): p. 1363-70 https://doi.org/10.1002/hep.22109.

371. Giannini, E.G., R. Testa, and V. Savarino, *Liver enzyme alteration: a guide for clinicians.* Cmaj, 2005. **172**(3): p. 367-79 https://doi.org/10.1503/cmaj.1040752.

372. Botros, M. and K.A. Sikaris, *The de ritis ratio: the test of time.* Clin Biochem Rev, 2013. **34**(3): p. 117-30

373. Elshorbagy, A.K., et al., *Cysteine supplementation reverses methionine restriction effects on rat adiposity: significance of stearoyl-coenzyme A desaturase.* J Lipid Res, 2011. **52**(1): p. 104-12 https://doi.org/10.1194/jlr.M010215.

374. Frühbeck, G., et al., *Adiponectin-leptin ratio: A promising index to estimate adipose tissue dysfunction. Relation with obesity-associated cardiometabolic risk.* Adipocyte, 2018. **7**(1): p. 57-62 https://doi.org/10.1080/21623945.2017.1402151.

375. Kozieł, R., et al., *Methionine restriction slows down senescence in human diploid fibroblasts.* Aging Cell, 2014. **13**(6): p. 1038-48 https://doi.org/10.1111/acel.12266.

376. Zhu, R. and S. Chen, *Proteomic analysis reveals semaglutide impacts lipogenic protein expression in epididymal adipose tissue of obese mice.* Front Endocrinol (Lausanne), 2023. **14**: p. 1095432 https://doi.org/10.3389/fendo.2023.1095432.

377. Liu, J., et al., *Lysosomal cysteine proteases in atherosclerosis.* Arterioscler Thromb Vasc Biol, 2004. **24**(8): p. 1359-66 https://doi.org/10.1161/01.Atv.0000134530.27208.41.

378. Oliveira, M., et al., *Cysteine cathepsin S processes leptin, inactivating its biological activity.* J Endocrinol, 2012. **214**(2): p. 217-24 https://doi.org/10.1530/joe-12-0108.

379. Kos, J.J., Zala; Obermajer, Nataša, *The role of cathepsin X in cell signaling.*

380. Obermajer, N., et al., *Cysteine protease cathepsin X modulates immune response via activation of beta2 integrins.* Immunology, 2008. **124**(1): p. 76-88 https://doi.org/10.1111/j.1365-2567.2007.02740.x.

381. Turk, V., J. Kos, and B. Turk, *Cysteine cathepsins (proteases)--on the main stage of cancer?* Cancer Cell, 2004. **5**(5): p. 409-10 https://doi.org/10.1016/s1535-6108(04)00117-5.

382. Wendt, W., et al., *Differential expression of cathepsin X in aging and pathological central nervous system of mice.* Exp Neurol, 2007. **204**(2): p. 525-40 https://doi.org/10.1016/j.expneurol.2007.01.007.

383. Krueger, S., et al., *Up-regulation of cathepsin X in Helicobacter pylori gastritis and gastric cancer.* J Pathol, 2005. **207**(1): p. 32-42 https://doi.org/10.1002/path.1820.

384. Sevenich, L., et al., *Synergistic antitumor effects of combined cathepsin B and cathepsin Z deficiencies on breast cancer progression and metastasis in mice.* Proc Natl Acad Sci U S A, 2010. **107**(6): p. 2497-502 https://doi.org/10.1073/pnas.0907240107.

385. Nägler, D.K., et al., *Up-regulation of cathepsin X in prostate cancer and prostatic intraepithelial neoplasia.* Prostate, 2004. **60**(2): p. 109-19 https://doi.org/10.1002/pros.20046.

386. Joyce, J.A., et al., *Cathepsin cysteine proteases are effectors of invasive growth and angiogenesis during multistage tumorigenesis.* Cancer Cell, 2004. **5**(5): p. 443-53 https://doi.org/10.1016/s1535-6108(04)00111-4.

387. Yujun Hou, X.C., Jae-Hyeon Park, Qing Zhu, Mansoor Hussain, Zhiquan Li, Helena Borland Madsen, Beimeng Yang, Yong Wei, Yue Wang, Evandro F. Fang, Deborah L. Croteau, Vilhelm A. Bohr, *Urolithin A improves Alzheimer's disease cognition and restores mitophagy and lysosomal functions.* bioRxiv, 2024 https://doi.org/10.1101/2024.01.30.577986.

388. Shen, Y., et al., *Shared PPARalpha/gamma Target Genes Regulate Brown Adipocyte Thermogenic Function.* Cell Rep, 2020. **30**(9): p. 3079-3091 e5 https://doi.org/10.1016/j.celrep.2020.02.032.

389. Lalmanach, G., et al., *Regulation of the Proteolytic Activity of Cysteine Cathepsins by Oxidants.* Int J Mol Sci, 2020. **21**(6) https://doi.org/10.3390/ijms21061944.

390. Lee, L.M.-Y., et al., *Lysine Deprivation Suppresses Adipogenesis in 3T3-L1 Cells: A Transcriptome Analysis.* International Journal of Molecular Sciences, 2023. **24**(11): p. 9402

391. Hutagalung, A.H. and P.J. Novick, *Role of Rab GTPases in membrane traffic and cell physiology.* Physiol Rev, 2011. **91**(1): p. 119-49 https://doi.org/10.1152/physrev.00059.2009.

392. Gross, S.J., et al., *Notch regulates vascular collagen IV basement membrane through modulation of lysyl hydroxylase 3 trafficking.* Angiogenesis, 2021. **24**(4): p. 789-805 https://doi.org/10.1007/s10456-021-09791-9.

393. Perrone, C.E., et al., *Methionine restriction effects on mitochondrial biogenesis and aerobic capacity in white adipose tissue, liver, and skeletal muscle of F344 rats.* Metabolism, 2010. **59**(7): p. 1000-11 https://doi.org/10.1016/j.metabol.2009.10.023.

394. Forney, L.A., et al., *Sexually Dimorphic Effects of Dietary Methionine Restriction are Dependent on Age when the Diet is Introduced.* Obesity (Silver Spring), 2020. **28**(3): p. 581-589 https://doi.org/10.1002/oby.22721.

395. Castaño-Martinez, T., et al., *Methionine restriction prevents onset of type 2 diabetes in NZO mice.* Faseb j, 2019. **33**(6): p. 7092-7102 https://doi.org/10.1096/fj.201900150R.

396. Jiang, M., et al., *Spontaneous immortalization of human dermal microvascular endothelial cells.* World J Stem Cells, 2010. **2**(5): p. 114-20 https://doi.org/10.4252/wjsc.v2.i5.114.

397. Forsyth, N.R., et al., *Spontaneous immortalization of clinically normal colon-derived fibroblasts from a familial adenomatous polyposis patient.* Neoplasia, 2004. **6**(3): p. 258-65 https://doi.org/10.1593/neo.4103.

398. Carnero, A., et al., *Disruptive chemicals, senescence and immortality.* Carcinogenesis, 2015. **36 Suppl 1**(Suppl 1): p. S19-37 https://doi.org/10.1093/carcin/bgv029.

399. Jeong, Y.J., et al., *Immortalization of primary marmoset skin fibroblasts by CRISPR-Cas9-mediated gene targeting.* Anim Cells Syst (Seoul), 2022. **26**(6): p. 266-274 https://doi.org/10.1080/19768354.2022.2151509.

400. Pedrioli, A. and A. Oxenius, *Single B cell technologies for monoclonal antibody discovery.* Trends Immunol, 2021. **42**(12): p. 1143-1158 https://doi.org/10.1016/j.it.2021.10.008.

401. Castellano, R., et al., *Methionine and cysteine deficiencies altered proliferation rate and time-course differentiation of porcine preadipose cells.* Amino Acids, 2017. **49**(2): p. 355-366 https://doi.org/10.1007/s00726-016-2369-y.

402. Homma, T., S. Kobayashi, and J. Fujii, *Methionine Deprivation Reveals the Pivotal Roles of Cell Cycle Progression in Ferroptosis That Is Induced by Cysteine Starvation.* Cells, 2022. **11**(10) https://doi.org/10.3390/cells11101603.

403. Upadhyayula, P.S., et al., *Dietary restriction of cysteine and methionine sensitizes gliomas to ferroptosis and induces alterations in energetic metabolism.* Nature Communications, 2023. **14**(1): p. 1187 https://doi.org/10.1038/s41467-023-36630-w.

404. Liu, H., et al., *Methionine and cystine double deprivation stress suppresses glioma proliferation via inducing ROS/autophagy.* Toxicol Lett, 2015. **232**(2): p. 349-55 https://doi.org/10.1016/j.toxlet.2014.11.011.

405. Jonsson, W.O., et al., *Physiologic Responses to Dietary Sulfur Amino Acid Restriction in Mice Are Influenced by Atf4 Status and Biological Sex.* J Nutr, 2021. **151**(4): p. 785-799 https://doi.org/10.1093/jn/nxaa396.

406. Wang, H. and R.E. Scott, *Inhibition of distinct steps in the adipocyte differentiation pathway in 3T3 T mesenchymal stem cells by dimethyl sulphoxide (DMSO).* Cell Prolif, 1993. **26**(1): p. 55-66 https://doi.org/10.1111/j.1365-2184.1993.tb00006.x.

407. Dludla, P.V., et al., *A dose-dependent effect of dimethyl sulfoxide on lipid content, cell viability and oxidative stress in 3T3-L1 adipocytes.* Toxicol Rep, 2018. **5**: p. 1014-1020 https://doi.org/10.1016/j.toxrep.2018.10.002.

408. Abbott, R.D., et al., *Long term perfusion system supporting adipogenesis.* Methods, 2015. **84**: p. 84-9 https://doi.org/10.1016/j.ymeth.2015.03.022.

409. Bellas, E., K.G. Marra, and D.L. Kaplan, *Sustainable three-dimensional tissue model of human adipose tissue.* Tissue Eng Part C Methods, 2013. **19**(10): p. 745-54 https://doi.org/10.1089/ten.TEC.2012.0620.

410. Kang, J.H., J.M. Gimble, and D.L. Kaplan, *In vitro 3D model for human vascularized adipose tissue.* Tissue Eng Part A, 2009. **15**(8): p. 2227-36 https://doi.org/10.1089/ten.tea.2008.0469.

411. Fonović, U.P., et al., *Structure-activity relationships of triazole-benzodioxine inhibitors of cathepsin X*. European Journal of Medicinal Chemistry, 2020. **193**: p. 112218 https://doi.org/https://doi.org/10.1016/j.ejmech.2020.112218.

412. Mitrović, A., et al., *Evaluation of novel cathepsin-X inhibitors in vitro and in vivo and their ability to improve cathepsin-B-directed antitumor therapy.* Cellular and Molecular Life Sciences, 2022. **79**(1): p. 34 https://doi.org/10.1007/s00018-021-04117-w.

413. Paulick, M.G. and M. Bogyo, *Development of activity-based probes for cathepsin X.* ACS Chem Biol, 2011. **6**(6): p. 563-72 https://doi.org/10.1021/cb100392r.

414. Adachi, Y., K. Ueda, and E. Takimoto, *Perivascular adipose tissue in vascular pathologies-a novel therapeutic target for atherosclerotic disease?* Front Cardiovasc Med, 2023. **10**: p. 1151717 https://doi.org/10.3389/fcvm.2023.1151717.

415. Almabrouk, T.A.M., et al., *High Fat Diet Attenuates the Anticontractile Activity of Aortic PVAT via a Mechanism Involving AMPK and Reduced Adiponectin Secretion.* Front Physiol, 2018. **9**: p. 51 https://doi.org/10.3389/fphys.2018.00051.

416. Stanek, A., K. Brożyna-Tkaczyk, and W. Myśliński, *The Role of Obesity-Induced Perivascular Adipose Tissue (PVAT) Dysfunction in Vascular Homeostasis.* Nutrients, 2021. **13**(11) https://doi.org/10.3390/nu13113843.

417. Chang, L., M.T. Garcia-Barrio, and Y.E. Chen, *Perivascular Adipose Tissue Regulates Vascular Function by Targeting Vascular Smooth Muscle Cells.* Arterioscler Thromb Vasc Biol, 2020. **40**(5): p. 1094-1109 https://doi.org/10.1161/atvbaha.120.312464.

418. Xia, N. and H. Li, *The role of perivascular adipose tissue in obesity-induced vascular dysfunction.* Br J Pharmacol, 2017. **174**(20): p. 3425-3442 https://doi.org/10.1111/bph.13650.

419. Zaborska, K.E., et al., *Loss of anti-contractile effect of perivascular adipose tissue in offspring of obese rats.* Int J Obes (Lond), 2016. **40**(8): p. 1205-14 https://doi.org/10.1038/ijo.2016.62.

420. Stieber, C., et al., *Human Perivascular Adipose Tissue as a Regulator of the Vascular Microenvironment and Diseases of the Coronary Artery and Aorta.* J Cardiol Cardiovasc Sci, 2019. **3**(4): p. 10-15 https://doi.org/10.29245/2578-3025/2019/4.1174.

421. Kip, P., et al., *Short-term Pre-operative Methionine Restriction Induces Browning of Perivascular Adipose Tissue and Improves Vein Graft Remodeling in Mice.* bioRxiv, 2023 https://doi.org/10.1101/2023.11.02.565269.

422. Sun, L., et al., *Life-span extension in mice by preweaning food restriction and by methionine restriction in middle age.* J Gerontol A Biol Sci Med Sci, 2009. **64**(7): p. 711-22 https://doi.org/10.1093/gerona/glp051.

423. Hine, C. and J.R. Mitchell, *Calorie restriction and methionine restriction in control of endogenous hydrogen sulfide production by the transsulfuration pathway.* Exp Gerontol, 2015. **68**: p. 26-32 https://doi.org/10.1016/j.exger.2014.12.010.

424. Soenen, S., et al., *The ageing gastrointestinal tract.* Curr Opin Clin Nutr Metab Care, 2016. **19**(1): p. 12-8 https://doi.org/10.1097/mco.0000000000000238.

425. Jackson, S.J., et al., *Does age matter? The impact of rodent age on study outcomes.* Lab Anim, 2017. **51**(2): p. 160-169 https://doi.org/10.1177/0023677216653984.

426. Halloran, B.P., et al., *Changes in bone structure and mass with advancing age in the male C57BL/6J mouse.* J Bone Miner Res, 2002. **17**(6): p. 1044-50 https://doi.org/10.1359/jbmr.2002.17.6.1044.

427. Holladay, S.D. and R.J. Smialowicz, *Development of the murine and human immune system: differential effects of immunotoxicants depend on time of exposure.* Environ Health Perspect, 2000. **108 Suppl 3**(Suppl 3): p. 463-73 https://doi.org/10.1289/ehp.00108s3463.

428. Holsapple, M.P., L.J. West, and K.S. Landreth, *Species comparison of anatomical and functional immune system development.* Birth Defects Res B Dev Reprod Toxicol, 2003. **68**(4): p. 321-34 https://doi.org/10.1002/bdrb.10035.

429. Downes, N. and P. Mullins, *The development of myelin in the brain of the juvenile rat.* Toxicol Pathol, 2014. **42**(5): p. 913-22 https://doi.org/10.1177/0192623313503518.

430. Fu, Y., et al., *Cellular composition characterizing postnatal development and maturation of the mouse brain and spinal cord.* Brain Struct Funct, 2013. **218**(5): p. 1337-54 https://doi.org/10.1007/s00429-012-0462-x.

431. Yager, J.Y. and J.A. Thornhill, *The effect of age on susceptibility to hypoxic-ischemic brain damage.* Neurosci Biobehav Rev, 1997. **21**(2): p. 167-74 https://doi.org/10.1016/s0149-7634(96)00006-1.

432. Brown, A.W., K.J. Marlowe, and B. Bjelke, *Age effect on motor recovery in a post-acute animal stroke model.* Neurobiol Aging, 2003. **24**(4): p. 607-14 https://doi.org/10.1016/s0197-4580(02)00129-x.

433. Ferraris, R.P. and R.R. Vinnakota, *Regulation of intestinal nutrient transport is impaired in aged mice.* J Nutr, 1993. **123**(3): p. 502-11 https://doi.org/10.1093/jn/123.3.502.

434. Vital, M., et al., *Alterations of the Murine Gut Microbiome with Age and Allergic Airway Disease.* J Immunol Res, 2015. **2015**: p. 892568 https://doi.org/10.1155/2015/892568.

435. Mori, K., et al., *Hepatic transcript levels for genes coding for enzymes associated with xenobiotic metabolism are altered with age.* Toxicol Pathol, 2007. **35**(2): p. 242-51 https://doi.org/10.1080/01926230601156286.

436. Flurkey, K.C., JM; Harrison DE, *The-Mouse-in-Biomedical-Research, 2nd ed. Volume 3, Normative Biology, Husbandry, and Models.* Vol. 3. 2007: Elsevier.

437. Plaisance, E.P., et al., *Role of beta-adrenergic receptors in the hyperphagic and hypermetabolic responses to dietary methionine restriction.* Am J Physiol Regul Integr Comp Physiol, 2010. **299**(3): p. R740-50 https://doi.org/10.1152/ajpregu.00838.2009.

438. Spring, S., et al., *Methionine Restriction Partly Recapitulates the Sympathetically Mediated Enhanced Energy Expenditure Induced by Total Amino Acid Restriction in Rats.* Nutrients, 2019. **11**(3) https://doi.org/10.3390/nu11030707.

439. Wanders, D., et al., *UCP1 is an essential mediator of the effects of methionine restriction on energy balance but not insulin sensitivity.* Faseb j, 2015. **29**(6): p. 2603-15 https://doi.org/10.1096/fj.14-270348.

440. Cavuoto, P. and M.F. Fenech, *A review of methionine dependency and the role of methionine restriction in cancer growth control and life-span extension.* Cancer Treat Rev, 2012. **38**(6): p. 726-36 https://doi.org/10.1016/j.ctrv.2012.01.004.

441. Lien, E.C., et al., *Oncogenic PI3K promotes methionine dependency in breast cancer cells through the cystine-glutamate antiporter xCT.* Sci Signal, 2017. **10**(510) https://doi.org/10.1126/scisignal.aao6604.

442. Koppula, P., L. Zhuang, and B. Gan, *Cystine transporter SLC7A11/xCT in cancer: ferroptosis, nutrient dependency, and cancer therapy.* Protein Cell, 2021. **12**(8): p. 599-620 https://doi.org/10.1007/s13238-020-00789-5.

443. Cellarier, E., et al., *Methionine dependency and cancer treatment.* Cancer Treat Rev, 2003. **29**(6): p. 489-99 https://doi.org/10.1016/s0305-7372(03)00118-x.

444. Guo, H.Y., et al., *Expression of the biochemical defect of methionine dependence in fresh patient tumors in primary histoculture.* Cancer Res, 1993. **53**(11): p. 2479-83

445. Mecham, J.O., et al., *The metabolic defect of methionine dependence occurs frequently in human tumor cell lines.* Biochem Biophys Res Commun, 1983. **117**(2): p. 429-34 https://doi.org/10.1016/0006-291x(83)91218-4.

446. Wallis, K.F., et al., *Differences in cell death in methionine versus cysteine depletion.* Environ Mol Mutagen, 2021. **62**(3): p. 216-226 https://doi.org/10.1002/em.22428.

447. Rong, Y., et al., *Cells use multiple mechanisms for cell-cycle arrest upon withdrawal of individual amino acids.* Cell Rep, 2023. **42**(12): p. 113539 https://doi.org/10.1016/j.celrep.2023.113539.

448. Minguzzi, M., et al., *Polyamine supplementation reduces DNA damage in adipose stem cells cultured in 3-D.* Sci Rep, 2019. **9**(1): p. 14269 https://doi.org/10.1038/s41598-019-50543-z.

449. Ballabio, A. and J.S. Bonifacino, *Lysosomes as dynamic regulators of cell and organismal homeostasis.* Nature reviews Molecular cell biology, 2020. **21**(2): p. 101-118

450. Naour, N., et al., *Cathepsins in Human Obesity: Changes in Energy Balance Predominantly Affect Cathepsin S in Adipose Tissue and in Circulation.* The Journal of Clinical Endocrinology & Metabolism, 2010. **95**(4): p. 1861-1868 https://doi.org/10.1210/jc.2009-1894.

451. Naour, N., et al., *Cathepsins in human obesity: changes in energy balance predominantly affect cathepsin s in adipose tissue and in circulation.* J Clin Endocrinol Metab, 2010. **95**(4): p. 1861-8 https://doi.org/10.1210/jc.2009-1894.

452. Ju, L., et al., *Obesity-associated inflammation triggers an autophagy-lysosomal response in adipocytes and causes degradation of perilipin 1.* Cell Death Dis, 2019. **10**(2): p. 121 https://doi.org/10.1038/s41419-019-1393-8.

453. Cinti, S., et al., *Adipocyte death defines macrophage localization and function in adipose tissue of obese mice and humans.* J Lipid Res, 2005. **46**(11): p. 2347-55 https://doi.org/10.1194/jlr.M500294-JLR200.

454. Wei, W. and G. Ruvkun, *Lysosomal activity regulates Caenorhabditis elegans mitochondrial dynamics through vitamin B12 metabolism.* Proc Natl Acad Sci U S A, 2020. **117**(33): p. 19970-19981 https://doi.org/10.1073/pnas.2008021117.

455. Heymsfield, S.B., et al., *Weight loss composition is one-fourth fat-free mass: a critical review and critique of this widely cited rule.* Obes Rev, 2014. **15**(4): p. 310-21 https://doi.org/10.1111/obr.12143.

456. Heymsfield, S.B., et al., *Are methods of estimating fat-free mass loss with energy-restricted diets accurate?* Eur J Clin Nutr, 2023. **77**(5): p. 525-531 https://doi.org/10.1038/s41430-022-01203-5.

457. Lewis, K.N., N.D. Rubinstein, and R. Buffenstein, *A window into extreme longevity; the circulating metabolomic signature of the naked mole-rat, a mammal that shows negligible senescence.* Geroscience, 2018. **40**(2): p. 105-121 https://doi.org/10.1007/s11357-018-0014-2.

458. Chusyd, D.E., et al., *Relationships between Rodent White Adipose Fat Pads and Human White Adipose Fat Depots.* Front Nutr, 2016. **3**: p. 10 https://doi.org/10.3389/fnut.2016.00010.

459. Churchill, G.A., et al., *The Diversity Outbred mouse population.* Mamm Genome, 2012. **23**(9-10): p. 713-8 https://doi.org/10.1007/s00335-012-9414-2.

460. Li, H.-F., et al., *Role of PVAT in obesity-related cardiovascular disease through the buffering activity of ATF3.* iScience, 2022. **25**(12): p. 105631 https://doi.org/https://doi.org/10.1016/j.isci.2022.105631.

461. Watts, S.W., et al., *A New Function for Perivascular Adipose Tissue (PVAT): Assistance of Arterial Stress Relaxation.* Sci Rep, 2020. **10**(1): p. 1807 https://doi.org/10.1038/s41598-020-58368-x.

462. Longchamp, A., et al., *Amino Acid Restriction Triggers Angiogenesis via GCN2/ATF4 Regulation of VEGF and H(2)S Production.* Cell, 2018. **173**(1): p. 117-129.e14 https://doi.org/10.1016/j.cell.2018.03.001.

463. Das, A., et al., *Impairment of an Endothelial NAD(+)-H(2)S Signaling Network Is a Reversible Cause of Vascular Aging.* Cell, 2018. **173**(1): p. 74-89.e20 https://doi.org/10.1016/j.cell.2018.02.008.

464. Wang, X.M., J. M. , *Methionine Restriction and Modification of Epithelial Tight Junction Barrier Function and Permeability.* Journal of Epithelial Biology and Pharmacology, 2012. **5**(39-46)

465. Ramalingam, A., et al., *Dietary methionine restriction improves colon tight junction barrier function and alters claudin expression pattern.* Am J Physiol Cell Physiol, 2010. **299**(5): p. C1028-35 https://doi.org/10.1152/ajpcell.00482.2009.

466. Skrovanek, S., M.C. Valenzano, and J.M. Mullin, *Restriction of sulfur-containing amino acids alters claudin composition and improves tight junction barrier function.* Am J Physiol Regul Integr Comp Physiol, 2007. **293**(3): p. R1046-55 https://doi.org/10.1152/ajpregu.00072.2007.

467. Meijer, E.F., et al., *Measuring Vascular Permeability In Vivo.* Methods Mol Biol, 2016. **1458**: p. 71-85 https://doi.org/10.1007/978-1-4939-3801-8_6.

468. Wu, G., et al., *Dietary Methionine Restriction Upregulates Endogenous H(2) S via miR-328-3p: A Potential Mechanism to Improve Liver Protein Metabolism Efficiency in a Mouse Model of High-fat-diet-induced Obesity.* Mol Nutr Food Res, 2019. **63**(5): p. e1800735 https://doi.org/10.1002/mnfr.201800735.

469. Yang, M., et al., *Dietary Methionine Restriction Improves Gut Health and Alters the Plasma Metabolomic Profile in Rats by Modulating the Composition of the Gut Microbiota.* International Journal of Molecular Sciences, 2024. **25**(7): p. 3657

470. Acosta, A., et al., *Selection of Antiobesity Medications Based on Phenotypes Enhances Weight Loss: A Pragmatic Trial in an Obesity Clinic.* Obesity (Silver Spring), 2021. **29**(4): p. 662-671 https://doi.org/10.1002/oby.23120.

APPENDICES

APPENDIX A: Significantly Differentially Expressed Proteins from PVAT

Comparison	Protein	Uniprot ID	Gene	Full Name	p-value	Mean (HFD)	Mean (MR)	Fold Change	Log(Fold Change)	(-Log(p-value)
MR03 to HFD	S100B	P50114	S100b	Protein S100-B	0.037	24506	179853	7.339	0.866	1.432
MR03 to HFD	HMGB1	P63158	Hmgb1	High mobility group protein B1	0.014	246205	1292104	5.248	0.720	1.848
MR03 to HFD	ABHD5	Q9DBL9	Abhd5	1-acylglycerol-3-phosphate O-acyltransferase ABHD5	0.007	173728	706375	4.066	0.609	2.184
MR03 to HFD	IF4H	Q9WUK2	Eif4h	Eukaryotic translation initiation factor 4H	0.008	10289	38571	3.749	0.574	2.089
MR03 to HFD	RSSA	P14206	Rpsa	40S ribosomal protein SA	0.022	80945	300399	3.711	0.570	1.651
MR03 to HFD	ADT2	P51881	Slc25a5	ADP/ATP translocase 2	0.026	356343	1237070	3.472	0.541	1.582
MR03 to HFD	LRC59	Q922Q8	Lrrc59	Leucine-rich repeat-containing protein 59	0.032	10446	33635	3.220	0.508	1.497
MR03 to HFD	PNKD	Q69ZP3	Pnkd	Probable hydrolase PNKD	0.025	27758	87292	3.145	0.498	1.595
MR03 to HFD	NDUV2	Q9D6J6	Ndufv2	NADH dehydrogenase [ubiquinone] flavoprotein 2, mitochondrial	0.011	684336	2138290	3.125	0.495	1.943
MR03 to HFD	RL15	Q9CZM2	Rpl15	60S ribosomal protein L15	0.001	69772	216626	3.105	0.492	3.018
MR03 to HFD	ADH1	P00329	Adh1	Alcohol dehydrogenase 1	0.005	79878	236498	2.961	0.471	2.344
MR03 to HFD	EDF1	Q9JMG1	Edf1	Endothelial differentiation-related factor 1	0.018	6896	20248	2.936	0.468	1.755
MR03 to HFD	RS6	P62754	Rps6	40S ribosomal protein S6	0.027	168333	453400	2.693	0.430	1.573
MR03 to HFD	RACK1	P68040	Rack1	Receptor of activated protein C kinase 1	0.031	81603	218272	2.675	0.427	1.503
MR03 to HFD	HNRPK	P61979	Hnrnpk	Heterogeneous nuclear ribonucleoprotein K	0.026	334943	863394	2.578	0.411	1.591
MR03 to HFD	VDAC2	Q60930	Vdac2	Voltage-dependent anion-selective channel protein 2	0.004	139746	350989	2.512	0.400	2.354
MR03 to HFD	CO4B	P01029	C4b	Complement C4-B	0.008	112555	271489	2.412	0.382	2.107
MR03 to HFD	MTCH2	Q791V5	Mtch2	Mitochondrial carrier homolog 2	0.036	788730	1846205	2.341	0.369	1.450
MR03 to HFD	CATZ	Q9WUU7	Ctsz	Cathepsin Z	0.027	191482	440911	2.303	0.362	1.573
MR03 to HFD	MMSA	Q9EQ20	Aldh6a1	Methylmalonate-semialdehyde dehydrogenase [acylating], mitochondrial	0.002	1826132	4197464	2.299	0.361	2.644
MR03 to HFD	CATA	P24270	Cat	Catalase	0.005	644314	1464415	2.273	0.357	2.333
MR03 to HFD	1433Z	P63101	Ywhaz	14-3-3 protein zeta/delta	0.006	411221	919678	2.236	0.350	2.203

APPENDIX A: Significantly Differentially Expressed Proteins from PVAT (Continued)

Comparison	Protein	Uniprot ID	Gene	Full Name	p-value	Mean (HFD)	Mean (MR)	Fold Change	Log(Fold Change)	(-Log(p-value)
MR03 to HFD	MIC19	Q9CRB9	Chchd3	MICOS complex subunit Mic19	0.035	561245	1245208	2.219	0.346	1.451
MR03 to HFD	VASP	P70460	Vasp	Vasodilator-stimulated phosphoprotein	0.017	85731	189047	2.205	0.343	1.772
MR03 to HFD	CX7A1	P56392	Cox7a1	Cytochrome c oxidase subunit 7A1, mitochondrial	0.019	419805	874447	2.083	0.319	1.718
MR03 to HFD	BCAT2	O35855	Bcat2	Branched-chain-amino-acid aminotransferase, mitochondrial	0.033	279548	574011	2.053	0.312	1.482
MR03 to HFD	PCYOX	Q9CQF9	Pcyox1	Prenylcysteine oxidase	0.024	326111	668467	2.050	0.312	1.612
MR03 to HFD	SRSF2	Q62093	Srsf2	Serine/arginine-rich splicing factor 2	0.011	60472	122129	2.020	0.305	1.948
MR03 to HFD	AK1CD	Q8VC28	Akr1c13	Aldo-keto reductase family 1 member C13	0.007	7050	14149	2.007	0.303	2.172
MR03 to HFD	OSTF1	Q62422	Ostf1	Osteoclast-stimulating factor 1	0.032	32218	64628	2.006	0.302	1.498
MR03 to HFD	PPP5	Q60676	Ppp5c	Serine/threonine-protein phosphatase 5	0.018	75912	37706	0.497	-0.304	1.739
MR03 to HFD	OTUB1	Q7TQI3	Otub1	Ubiquitin thioesterase OTUB1	0.019	101128	48699	0.482	-0.317	1.725
MR03 to HFD	ERLN2	Q8BFZ9	Erlin2	Erlin-2	0.036	85567	40977	0.479	-0.320	1.447
MR03 to HFD	NISCH	Q80TM9	Nisch	Nischarin	0.042	47643	22534	0.473	-0.325	1.376
MR03 to HFD	A2AP	Q61247	Serpinf2	Alpha-2-antiplasmin	0.046	80707	37873	0.469	-0.329	1.340
MR03 to HFD	K2C1	P04104	Krt1	Keratin, type II cytoskeletal 1	0.032	4961	2310	0.466	-0.332	1.491
MR03 to HFD	ACTB	P60710	Actb	Actin, cytoplasmic 1	0.048	2048527	925580	0.452	-0.345	1.320
MR03 to HFD	ACYP2	P56375	Acyp2	Acylphosphatase-2	0.009	16943	7618	0.450	-0.347	2.045
MR03 to HFD	HMOX1	P14901	Hmox1	Heme oxygenase 1	0.038	25234	11307	0.448	-0.349	1.418
MR03 to HFD	RS9	Q6ZWN5	Rps9	40S ribosomal protein S9	0.036	61391	27342	0.445	-0.351	1.443
MR03 to HFD	MIRO1	Q8BG51	Rhot1	Mitochondrial Rho GTPase 1	0.044	178704	76220	0.427	-0.370	1.362
MR03 to HFD	PTCD3	Q14C51	Ptcd3	Pentatricopeptide repeat domain-containing protein 3, mitochondrial	0.020	60990	24957	0.409	-0.388	1.693
MR03 to HFD	NDUB4	Q9CQC7	Ndufb4	NADH dehydrogenase [ubiquinone] 1 beta subcomplex subunit 4	0.030	1490795	589259	0.395	-0.403	1.529
MR03 to HFD	PI42C	Q91XU3	Pip4k2c	Phosphatidylinositol 5-phosphate 4-kinase type-2 gamma	0.033	14993	5855	0.391	-0.408	1.480
MR03 to HFD	RT23	Q8VE22	Mrps23	28S ribosomal protein S23, mitochondrial	0.018	231465	89522	0.387	-0.413	1.744
MR03 to HFD	QKI	Q9QYS9	Qki	Protein quaking	0.001	22529	8373	0.372	-0.430	3.268
MR03 to HFD	CY1	Q9D0M3	Cyc1	Cytochrome c1, heme protein, mitochondrial	0.045	6162623	2282554	0.370	-0.431	1.345

APPENDIX A: Significantly Differentially Expressed Proteins from PVAT (Continued)

Comparison	Protein	Uniprot ID	Gene	Full Name	p-value	Mean (HFD)	Mean (MR)	Fold Change	Log(Fold Change)	(-Log(p-value)
MR03 to HFD	DDI2	A2ADY9	Ddi2	Protein DDI1 homolog 2	0.018	113048	40156	0.355	-0.450	1.753
MR03 to HFD	HELZ2	E9QAM5	Helz2	Helicase with zinc finger domain 2	0.009	62797	21306	0.339	-0.469	2.043
MR03 to HFD	RAB8A	P55258	Rab8a	Ras-related protein Rab-8A	0.035	41462	13774	0.332	-0.479	1.452
MR03 to HFD	STRN	O55106	Strn	Striatin	0.007	36158	11704	0.324	-0.490	2.180
MR03 to HFD	MARH5	Q3KNM2	Marchf5	E3 ubiquitin-protein ligase MARCHF5	0.048	20894	6345	0.304	-0.518	1.320
MR03 to HFD	MIA2	Q91ZV0	Mia2	Melanoma inhibitory activity protein 2	0.033	71670	18965	0.265	-0.577	1.483
MR03 to HFD	DLDH	O08749	Dld	Dihydrolipoyl dehydrogenase, mitochondrial	0.022	5682335	1465779	0.258	-0.588	1.654
MR03 to HFD	CSN6	O88545	Cops6	COP9 signalosome complex subunit 6	0.029	64733	15874	0.245	-0.610	1.539
MR03 to HFD	ADPGK	Q8VDL4	Adpgk	ADP-dependent glucokinase	0.029	33941	6319	0.186	-0.730	1.537
MR03 to HFD	STK39	Q9Z1W9	Stk39	STE20/SPS1-related proline-alanine-rich protein kinase	0.031	94865	3038	0.032	-1.494	1.512
MR05 to HFD	HPT	Q61646	Hp	Haptoglobin	0.012	39032	93763	2.402	0.381	1.932
MR05 to HFD	HSPB1	P14602	Hspb1	Heat shock protein beta-1	0.037	1119922	2591338	2.314	0.364	1.432
MR05 to HFD	SPS1	Q8BH69	Sephs1	Selenide, water dikinase 1	0.021	74287	163834	2.205	0.343	1.674
MR05 to HFD	DHSO	Q64442	Sord	Sorbitol dehydrogenase	0.049	30653	66747	2.177	0.338	1.308
MR05 to HFD	CATZ	Q9WUU7	Ctsz	Cathepsin Z	0.049	191482	403240	2.106	0.323	1.306
MR05 to HFD	RSSA	P14206	Rpsa	40S ribosomal protein SA	0.004	80945	164375	2.031	0.308	2.417
MR05 to HFD	PSMD9	Q9CR00	Psmd9	26S proteasome non-ATPase regulatory subunit 9	0.034	20186	40697	2.016	0.305	1.466
MR05 to HFD	UD17C	Q6ZQM8	Ugt1a7c	UDP-glucuronosyltransferase 1-7C	0.022	8355	16803	2.011	0.303	1.661
MR05 to HFD	SKP1	Q9WTX5	Skp1	S-phase kinase-associated protein 1	0.027	150218	61257	0.408	-0.390	1.576
MR05 to HFD	IIGP1	Q9QZ85	Iigp1	Interferon-inducible GTPase 1	0.016	12472	5039	0.404	-0.394	1.809
MR05 to HFD	TR150	Q569Z6	Thrap3	Thyroid hormone receptor-associated protein 3	0.036	27162	10613	0.391	-0.408	1.444
MR05 to HFD	ACYP2	P56375	Acyp2	Acylphosphatase-2	0.011	16943	6459	0.381	-0.419	1.974
MR05 to HFD	TMM9B	Q9JJR8	Tmem9b	Transmembrane protein 9B	0.019	39029	12757	0.327	-0.486	1.731
MR05 to HFD	DPY30	Q99LT0	Dpy30	Protein dpy-30 homolog	0.039	34290	10369	0.302	-0.519	1.413
MR05 to HFD	CO4A3	Q9QZS0	Col4a3	Collagen alpha-3(IV) chain	0.017	25758	7313	0.284	-0.547	1.779
MR10 to HFD	GMPR1	Q9DCZ1	Gmpr	GMP reductase 1	0.049	905672	4234898	4.676	0.670	1.313
MR10 to HFD	CATZ	Q9WUU7	Ctsz	Cathepsin Z	0.011	191482	805225	4.205	0.624	1.955

APPENDIX A: Significantly Differentially Expressed Proteins from PVAT (Continued)

Comparison	Protein	Uniprot ID	Gene	Full Name	p-value	Mean (HFD)	Mean (MR)	Fold Change	Log(Fold Change)	(-Log(p-value)
MR10 to HFD	TMCO1	Q921L3	Tmco1	Calcium load-activated calcium channel	0.003	14862	55377	3.726	0.571	2.567
MR10 to HFD	EWS	Q61545	Ewsr1	RNA-binding protein EWS	0.024	57401	211944	3.692	0.567	1.628
MR10 to HFD	KV5A9	P01642	Gm10881	Ig kappa chain V-V region L7 (Fragment)	0.012	14753	54009	3.661	0.564	1.929
MR10 to HFD	HMGB3	O54879	Hmgb3	High mobility group protein B3	0.019	12764	36926	2.893	0.461	1.730
MR10 to HFD	S12A2	P55012	Slc12a2	Solute carrier family 12 member 2	0.040	93793	243031	2.591	0.413	1.400
MR10 to HFD	COXM2	Q8K199	Cmc2	COX assembly mitochondrial protein 2 homolog	0.050	13164	32558	2.473	0.393	1.304
MR10 to HFD	LRC47	Q505F5	Lrrc47	Leucine-rich repeat-containing protein 47	0.044	110535	259099	2.344	0.370	1.360
MR10 to HFD	PRKRA	Q9WTX2	Prkra	Interferon-inducible double-stranded RNA-dependent protein kinase activator A	0.025	10347	23646	2.285	0.359	1.604
MR10 to HFD	SNX9	Q91VH2	Snx9	Sorting nexin-9	0.036	9709	21079	2.171	0.337	1.443
MR10 to HFD	PX11B	Q9Z210	Pex11b	Peroxisomal membrane protein 11B	0.036	8036	16368	2.037	0.309	1.448
MR10 to HFD	IMDH2	P24547	Impdh2	Inosine-5'-monophosphate dehydrogenase 2	0.008	78738	159844	2.030	0.308	2.101
MR10 to HFD	HOGA1	Q9DCU9	Hoga1	4-hydroxy-2-oxoglutarate aldolase, mitochondrial	0.015	5918	11962	2.021	0.306	1.830
MR10 to HFD	FMO5	P97872	Fmo5	Flavin-containing monooxygenase 5	0.028	52375	26175	0.500	-0.301	1.556
MR10 to HFD	PGRC1	O55022	Pgrmc1	Membrane-associated progesterone receptor component 1	0.017	278960	137746	0.494	-0.306	1.774
MR10 to HFD	ECH1	O35459	Ech1	Delta(3,5)-Delta(2,4)-dienoyl-CoA isomerase, mitochondrial	0.000	3656548	1801706	0.493	-0.307	3.495
MR10 to HFD	TMLH	Q91ZE0	Tmlhe	Trimethyllysine dioxygenase, mitochondrial	0.028	43018	21032	0.489	-0.311	1.551
MR10 to HFD	PGK1	P09411	Pgk1	Phosphoglycerate kinase 1	0.010	2262340	1083243	0.479	-0.320	1.993
MR10 to HFD	C2C2L	Q80X80	C2cd2l	Phospholipid transfer protein C2CD2L	0.027	30260	14363	0.475	-0.324	1.566
MR10 to HFD	MLEC	Q6ZQI3	Mlec	Malectin	0.045	131517	62402	0.474	-0.324	1.347
MR10 to HFD	SKP1	Q9WTX5	Skp1	S-phase kinase-associated protein 1	0.042	150218	70864	0.472	-0.326	1.374
MR10 to HFD	ALG2	Q9DBE8	Alg2	Alpha-1,3/1,6-mannosyltransferase ALG2	0.025	15922	7431	0.467	-0.331	1.604
MR10 to HFD	SGCE	O70258	Sgce	Epsilon-sarcoglycan	0.035	39622	17946	0.453	-0.344	1.455
MR10 to HFD	CAVN2	Q63918	Cavin2	Caveolae-associated protein 2	0.018	1167658	526753	0.451	-0.346	1.743
MR10 to HFD	TCTP	P63028	Tpt1	Translationally-controlled tumor protein	0.006	258427	116009	0.449	-0.348	2.220
MR10 to HFD	HERP1	Q9JJK5	Herpud1	Homocysteine-responsive endoplasmic reticulum-resident ubiquitin-like domain member 1 protein	0.016	16728	7132	0.426	-0.370	1.790

APPENDIX A: Significantly Differentially Expressed Proteins from PVAT (Continued)

Comparison	Protein	Uniprot ID	Gene	Full Name	p-value	Mean (HFD)	Mean (MR)	Fold Change	Log(Fold Change)	(-Log(p-value)
MR10 to HFD	ARL2	Q9D0J4	Arl2	ADP-ribosylation factor-like protein 2	0.027	36375	15324	0.421	-0.375	1.564
MR10 to HFD	PYGL	Q9ET01	Pygl	Glycogen phosphorylase, liver form	0.012	484374	203353	0.420	-0.377	1.925
MR10 to HFD	AL1A7	O35945	Aldh1a7	Aldehyde dehydrogenase, cytosolic 1	0.029	234418	93928	0.401	-0.397	1.530
MR10 to HFD	RER1	Q9CQU3	Rer1	Protein RER1	0.024	10375	4092	0.394	-0.404	1.616
MR10 to HFD	MFAP5	Q9QZJ6	Mfap5	Microfibrillar-associated protein 5	0.023	10543	4020	0.381	-0.419	1.631
MR10 to HFD	NU3M	P03899	Mtnd3	NADH-ubiquinone oxidoreductase chain 3	0.015	31889	12035	0.377	-0.423	1.837
MR10 to HFD	ABCD2	Q61285	Abcd2	ATP-binding cassette sub-family D member 2	0.024	151521	56292	0.372	-0.430	1.623
MR10 to HFD	SUN2	Q8BJS4	Sun2	SUN domain-containing protein 2	0.003	107297	39751	0.370	-0.431	2.602
MR10 to HFD	SYIC	Q8BU30	Iars1	Isoleucine--tRNA ligase, cytoplasmic	0.037	148283	54023	0.364	-0.439	1.428
MR10 to HFD	MPCP	Q8VEM8	Slc25a3	Phosphate carrier protein, mitochondrial	0.013	1105870	401998	0.364	-0.439	1.870
MR10 to HFD	ACLY	Q91V92	Acly	ATP-citrate synthase	0.038	2108373	691987	0.328	-0.484	1.425
MR10 to HFD	RS4X	P62702	Rps4x	40S ribosomal protein S4, X isoform	0.030	878590	275623	0.314	-0.503	1.519
MR10 to HFD	MAOX	P06801	Me1	NADP-dependent malic enzyme	0.017	3390145	999942	0.295	-0.530	1.774
MR10 to HFD	CO4A3	Q9QZS0	Col4a3	Collagen alpha-3(IV) chain	0.016	25758	6984	0.271	-0.567	1.788
MR10 to HFD	DPYL4	O35098	Dpysl4	Dihydropyrimidinase-related protein 4	0.001	43318	11611	0.268	-0.572	3.222
MR10 to HFD	ACYP2	P56375	Acyp2	Acylphosphatase-2	0.002	16943	4354	0.257	-0.590	2.618
MR10 to HFD	STK39	Q9Z1W9	Stk39	STE20/SPS1-related proline-alanine-rich protein kinase	0.029	94865	23177	0.244	-0.612	1.539
MR10 to HFD	IMPA2	Q91UZ5	Impa2	Inositol monophosphatase 2	0.001	434517	95338	0.219	-0.659	3.268
MR10 to HFD	FAS	P19096	Fasn	Fatty acid synthase	0.003	3830643	835095	0.218	-0.662	2.475

APPENDIX B: Significantly Differentially Expressed Proteins from Aorta

Comparison	Uniprot ID	Protein	Gene	Full Name	p-value	Mean (HFD)	Mean (MR)	Fold Change	Log(Fold Change)	(-Log(pvalue)
MR03 to HFD	A6X935	ITIH4	Itih4	Inter alpha-trypsin inhibitor, heavy chain 4	0.022	12854	187867	14.615	1.165	1.653
MR03 to HFD	O08709	PRDX6	Prdx6	Peroxiredoxin-6	0.023	8122	74212	9.137	0.961	1.645
MR03 to HFD	Q7TMK9	HNRPQ	Syncrip	Heterogeneous nuclear ribonucleoprotein Q	0.030	7156	50633	7.075	0.850	1.526
MR03 to HFD	Q76LS9	MINY1	Mindy1	Ubiquitin carboxyl-terminal hydrolase MINDY-1	0.005	1026	3762	3.667	0.564	2.346
MR03 to HFD	Q8BMP6	GCP60	Acbd3	Golgi resident protein GCP60	0.018	781	2571	3.294	0.518	1.738
MR03 to HFD	P61924	COPZ1	Copz1	Coatomer subunit zeta-1	0.047	2173	6502	2.993	0.476	1.324
MR03 to HFD	Q8CHT0	AL4A1	Aldh4a1	Delta-1-pyrroline-5-carboxylate dehydrogenase, mitochondrial	0.050	324	888	2.741	0.438	1.303
MR03 to HFD	Q9WV54	ASAH1	Asah1	Acid ceramidase	0.033	693	1740	2.512	0.400	1.483
MR03 to HFD	O09172	GSH0	Gclm	Glutamate--cysteine ligase regulatory subunit	0.047	21208	49696	2.343	0.370	1.328
MR03 to HFD	P97861	KRT86	Krt86	Keratin, type II cuticular Hb6	0.002	22225	51907	2.335	0.368	2.648
MR03 to HFD	Q505F5	LRC47	Lrrc47	Leucine-rich repeat-containing protein 47	0.044	2079	4803	2.310	0.364	1.357
MR03 to HFD	Q9JMD3	STA10	Stard10	START domain-containing protein 10	0.040	1906	4325	2.269	0.356	1.402
MR03 to HFD	P60670	NPL4	Nploc4	Nuclear protein localization protein 4 homolog	0.050	2930	6527	2.228	0.348	1.305
MR03 to HFD	P83917	CBX1	Cbx1	Chromobox protein homolog 1	0.010	1217	2700	2.219	0.346	2.015
MR03 to HFD	Q64133	AOFA	Maoa	Amine oxidase [flavin-containing] A	0.018	3649	7711	2.113	0.325	1.736
MR03 to HFD	Q9Z0F7	SYUG	Sncg	Gamma-synuclein	0.038	3975	7974	2.006	0.302	1.423
MR03 to HFD	Q8BFZ9	ERLN2	Erlin2	Erlin-2	0.047	3116	6246	2.005	0.302	1.330
MR03 to HFD	Q9CQ65	MTAP	Mtap	S-methyl-5'-thioadenosine phosphorylase	0.030	6848	3419	0.499	-0.302	1.524
MR03 to HFD	Q63932	MP2K2	Map2k2	Dual specificity mitogen-activated protein kinase kinase 2	0.027	4600	2273	0.494	-0.306	1.568
MR03 to HFD	Q2TPA8	HSDL2	Hsdl2	Hydroxysteroid dehydrogenase-like protein 2	0.042	11818	5815	0.492	-0.308	1.376
MR03 to HFD	Q04750	TOP1	Top1	DNA topoisomerase 1	0.032	5329	2581	0.484	-0.315	1.495
MR03 to HFD	Q91VD9	NDUS1	Ndufs1	NADH-ubiquinone oxidoreductase 75 kDa subunit, mitochondrial	0.005	4207	2015	0.479	-0.320	2.334
MR03 to HFD	P97384	ANX11	Anxa11	Annexin A11	0.010	26577	12507	0.471	-0.327	1.991
MR03 to HFD	Q61176	ARGI1	Arg1	Arginase-1	0.037	2473	1158	0.468	-0.329	1.427
MR03 to HFD	P97352	S10AD	S100a13	Protein S100-A13	0.043	8953	4186	0.468	-0.330	1.368
MR03 to HFD	P31725	S10A9	S100a9	Protein S100-A9	0.004	7936	3675	0.463	-0.334	2.420
MR03 to HFD	A6H584	CO6A5	Col6a5	Collagen alpha-5(VI) chain	0.002	1528	699	0.458	-0.339	2.793

APPENDIX B: Significantly Differentially Expressed Proteins from Aorta (Continued)										
Comparison	Uniprot ID	Protein	Gene	Full Name	p-value	Mean (HFD)	Mean (MR)	Fold Change	Log(Fold Change)	(-Log(pvalue)
MR03 to HFD	P70290	EM55	Mpp1	55 kDa erythrocyte membrane protein	0.012	5617	2560	0.456	-0.341	1.926
MR03 to HFD	P97797	SHPS1	Sirpa	Tyrosine-protein phosphatase non-receptor type substrate 1	0.023	3048	1300	0.427	-0.370	1.629
MR03 to HFD	Q8BLF1	NCEH1	Nceh1	Neutral cholesterol ester hydrolase 1	0.027	4559	1875	0.411	-0.386	1.563
MR03 to HFD	Q64331	MYO6	Myo6	Unconventional myosin-VI	0.010	17500	7196	0.411	-0.386	1.985
MR03 to HFD	Q91XE8	TM205	Tmem205	Transmembrane protein 205	0.006	4351	1777	0.408	-0.389	2.230
MR03 to HFD	O35286	DHX15	Dhx15	Pre-mRNA-splicing factor ATP-dependent RNA helicase DHX15	0.003	3458	1391	0.402	-0.395	2.472
MR03 to HFD	Q9CR00	PSMD9	Psmd9	26S proteasome non-ATPase regulatory subunit 9	0.016	580	229	0.395	-0.403	1.798
MR03 to HFD	O35409	FOLH1	Folh1	Glutamate carboxypeptidase 2	0.026	1523	584	0.383	-0.416	1.591
MR03 to HFD	Q61508	ECM1	Ecm1	Extracellular matrix protein 1	0.033	17020	6456	0.379	-0.421	1.475
MR03 to HFD	Q80UG5	SEPT9	Septin9	Septin-9	0.001	5843	2159	0.369	-0.432	3.102
MR03 to HFD	Q5M8N4	D39U1	Sdr39u1	Epimerase family protein SDR39U1	0.006	5135	1874	0.365	-0.438	2.207
MR03 to HFD	Q9R1P1	PSB3	Psmb3	Proteasome subunit beta type-3	0.001	3372	1209	0.359	-0.445	2.959
MR03 to HFD	O88643	PAK1	Pak1	Serine/threonine-protein kinase PAK 1	0.011	2528	900	0.356	-0.449	1.949
MR03 to HFD	Q9DCV7	K2C7	Krt7	Keratin, type II cytoskeletal 7	0.025	3406	1152	0.338	-0.471	1.604
MR03 to HFD	Q9JL35	HMGN5	Hmgn5	High mobility group nucleosome-binding domain-containing protein 5	0.038	2052	681	0.332	-0.479	1.425
MR03 to HFD	Q9D7P6	ISCU	Iscu	Iron-sulfur cluster assembly enzyme ISCU, mitochondrial	0.032	7093	2179	0.307	-0.513	1.496
MR03 to HFD	Q99K85	SERC	Psat1	Phosphoserine aminotransferase	0.033	2711	822	0.303	-0.518	1.480
MR03 to HFD	Q8R2K1	FUCM	Fuom	Fucose mutarotase	0.028	439	125	0.285	-0.546	1.555
MR03 to HFD	P62858	RS28	Rps28	40S ribosomal protein S28	0.004	35901	10074	0.281	-0.552	2.402
MR03 to HFD	Q3TEA8	HP1B3	Hp1bp3	Heterochromatin protein 1-binding protein 3	0.031	14733	4046	0.275	-0.561	1.508
MR03 to HFD	Q7TQI3	OTUB1	Otub1	Ubiquitin thioesterase OTUB1	0.050	8074	2169	0.269	-0.571	1.302
MR03 to HFD	Q9R0Z9	RHG07	Dlc1	Rho GTPase-activating protein 7	0.004	1104	296	0.268	-0.571	2.395
MR03 to HFD	Q8K009	AL1L2	Aldh1l2	Mitochondrial 10-formyltetrahydrofolate dehydrogenase	0.006	8829	2365	0.268	-0.572	2.190
MR03 to HFD	P57016	LAD1	Lad1	Ladinin-1	0.046	7990	2081	0.260	-0.584	1.342
MR03 to HFD	O35551	RABE1	Rabep1	Rab GTPase-binding effector protein 1	0.019	18116	4452	0.246	-0.609	1.726
MR03 to HFD	Q6PGL7	WASC2	Washc2	WASH complex subunit 2	0.044	1047	254	0.243	-0.615	1.355
MR03 to HFD	Q7TQD2	TPPP	Tppp	Tubulin polymerization-promoting protein	0.027	4057	921	0.227	-0.644	1.566
MR03 to HFD	Q8CIB5	FERM2	Fermt2	Fermitin family homolog 2	0.006	4873	961	0.197	-0.705	2.243

APPENDIX B: Significantly Differentially Expressed Proteins from Aorta (Continued)										
Comparison	Uniprot ID	Protein	Gene	Full Name	p-value	Mean (HFD)	Mean (MR)	Fold Change	Log(Fold Change)	(-Log(pvalue)
MR03 to HFD	P61027	RAB10	Rab10	Ras-related protein Rab-10	0.001	5228	1014	0.194	-0.712	3.143
MR03 to HFD	Q9Z0V8	TI17A	Timm17a	Mitochondrial import inner membrane translocase subunit Tim17-A	0.017	16259	3121	0.192	-0.717	1.780
MR03 to HFD	Q3U2A8	SYVM	Vars2	Valine--tRNA ligase, mitochondrial	0.002	2367	226	0.095	-1.021	2.738
MR05 to HFD	Q60952	CP250	Cep250	Centrosome-associated protein CEP250	0.025	4615	138435	29.996	1.477	1.608
MR05 to HFD	P70124	SPB5	Serpinb5	Serpin B5	0.034	980	8094	8.264	0.917	1.464
MR05 to HFD	Q8BVQ5	PPME1	Ppme1	Protein phosphatase methylesterase 1	0.003	10519	73077	6.947	0.842	2.597
MR05 to HFD	P58774	TPM2	Tpm2	Tropomyosin beta chain	0.042	79115	446026	5.638	0.751	1.376
MR05 to HFD	Q9WVA2	TIM8A	Timm8a1	Mitochondrial import inner membrane translocase subunit Tim8 A	0.017	3765	20125	5.345	0.728	1.769
MR05 to HFD	Q9DCD0	6PGD	Pgd	6-phosphogluconate dehydrogenase, decarboxylating	0.042	13007	67322	5.176	0.714	1.375
MR05 to HFD	Q9D0W5	PPIL1	Ppil1	Peptidyl-prolyl cis-trans isomerase-like 1	0.039	1981	9299	4.695	0.672	1.412
MR05 to HFD	Q8K3H0	DP13A	Appl1	DCC-interacting protein 13-alpha	0.046	1069	4985	4.664	0.669	1.341
MR05 to HFD	Q9R0Q7	TEBP	Ptges3	Prostaglandin E synthase 3	0.004	3170	14203	4.481	0.651	2.426
MR05 to HFD	P83882	RL36A	Rpl36a	60S ribosomal protein L36a	0.001	5245	20694	3.945	0.596	2.842
MR05 to HFD	Q9WV54	ASAH1	Asah1	Acid ceramidase	0.001	693	2707	3.908	0.592	3.252
MR05 to HFD	O54754	AOXA	Aox1	Aldehyde oxidase 1	0.011	2449	9299	3.797	0.579	1.948
MR05 to HFD	P49443	PPM1A	Ppm1a	Protein phosphatase 1A	0.028	6528	23778	3.643	0.561	1.556
MR05 to HFD	O09118	NET1	Ntn1	Netrin-1	0.032	3508	11434	3.259	0.513	1.492
MR05 to HFD	Q6P9Q6	FKB15	Fkbp15	FK506-binding protein 15	0.007	3060	9917	3.241	0.511	2.181
MR05 to HFD	O08756	HCD2	Hsd17b10	3-hydroxyacyl-CoA dehydrogenase type-2	0.010	8065	25806	3.200	0.505	1.994
MR05 to HFD	Q3UTJ2	SRBS2	Sorbs2	Sorbin and SH3 domain-containing protein 2	0.046	10944	33472	3.059	0.486	1.336
MR05 to HFD	Q05793	PGBM	Hspg2	Basement membrane-specific heparan sulfate proteoglycan core protein	0.022	39332	119596	3.041	0.483	1.653
MR05 to HFD	P11031	TCP4	Sub1	Activated RNA polymerase II transcriptional coactivator p15	0.020	9290	28044	3.019	0.480	1.690
MR05 to HFD	O08529	CAN2	Capn2	Calpain-2 catalytic subunit	0.049	1912	5533	2.893	0.461	1.313
MR05 to HFD	P62315	SMD1	Snrpd1	Small nuclear ribonucleoprotein Sm D1	0.005	1131	3221	2.848	0.454	2.335
MR05 to HFD	Q91WT9	CBS	Cbs	Cystathionine beta-synthase	0.009	1050	2927	2.787	0.445	2.049
MR05 to HFD	Q99JW2	ACY1	Acy1	Aminoacylase-1	0.006	714	1958	2.741	0.438	2.222
MR05 to HFD	P0C0A3	CHMP6	Chmp6	Charged multivesicular body protein 6	0.030	572	1557	2.723	0.435	1.522
MR05 to HFD	Q60649	CLPB	Clpb	Caseinolytic peptidase B protein homolog	0.013	7958	21197	2.663	0.425	1.892

APPENDIX B: Significantly Differentially Expressed Proteins from Aorta (Continued)										
Comparison	Uniprot ID	Protein	Gene	Full Name	p-value	Mean (HFD)	Mean (MR)	Fold Change	Log(Fold Change)	(-Log(pvalue)
MR05 to HFD	Q9JHR7	IDE	Ide	Insulin-degrading enzyme	0.021	2250	5859	2.604	0.416	1.673
MR05 to HFD	P63168	DYL1	Dynll1	Dynein light chain 1, cytoplasmic	0.023	974	2532	2.600	0.415	1.634
MR05 to HFD	P19783	COX41	Cox4i1	Cytochrome c oxidase subunit 4 isoform 1, mitochondrial	0.008	5097	13246	2.599	0.415	2.105
MR05 to HFD	Q8BM55	TM214	Tmem214	Transmembrane protein 214	0.010	3315	8604	2.595	0.414	1.994
MR05 to HFD	Q9CR68	UCRI	Uqcrfs1	Cytochrome b-c1 complex subunit Rieske, mitochondrial	0.004	4343	11189	2.576	0.411	2.386
MR05 to HFD	P29391	FRIL1	Ftl1	Ferritin light chain 1	0.015	4635	11754	2.536	0.404	1.830
MR05 to HFD	P63242	IF5A1	Eif5a	Eukaryotic translation initiation factor 5A-1	0.024	1902	4769	2.508	0.399	1.617
MR05 to HFD	P31786	ACBP	Dbi	Acyl-CoA-binding protein	0.031	4226	10552	2.497	0.397	1.503
MR05 to HFD	P15327	PMGE	Bpgm	Bisphosphoglycerate mutase	0.019	6075	14945	2.460	0.391	1.728
MR05 to HFD	O08788	DCTN1	Dctn1	Dynactin subunit 1	0.030	671	1650	2.457	0.390	1.517
MR05 to HFD	P42932	TCPQ	Cct8	T-complex protein 1 subunit theta	0.007	6706	16105	2.402	0.380	2.131
MR05 to HFD	P47199	QOR	Cryz	Quinone oxidoreductase	0.003	5187	12145	2.341	0.369	2.487
MR05 to HFD	Q9DAW9	CNN3	Cnn3	Calponin-3	0.010	25501	59512	2.334	0.368	1.983
MR05 to HFD	Q05816	FABP5	Fabp5	Fatty acid-binding protein 5	0.047	3010	6865	2.281	0.358	1.330
MR05 to HFD	Q8CGF7	TCRG1	Tcerg1	Transcription elongation regulator 1	0.010	1706	3830	2.245	0.351	2.000
MR05 to HFD	Q9QYA2	TOM40	Tomm40	Mitochondrial import receptor subunit TOM40 homolog	0.026	4830	10807	2.237	0.350	1.587
MR05 to HFD	Q9ESE1	LRBA	Lrba	Lipopolysaccharide-responsive and beige-like anchor protein	0.026	737	1638	2.221	0.347	1.592
MR05 to HFD	Q8BX02	KANK2	Kank2	KN motif and ankyrin repeat domain-containing protein 2	0.034	5723	12452	2.176	0.338	1.465
MR05 to HFD	Q91X52	DCXR	Dcxr	L-xylulose reductase	0.044	4151	9001	2.169	0.336	1.355
MR05 to HFD	Q9QXK3	COPG2	Copg2	Coatomer subunit gamma-2	0.009	1121	2410	2.150	0.332	2.063
MR05 to HFD	Q61316	HSP74	Hspa4	Heat shock 70 kDa protein 4	0.034	3691	7885	2.136	0.330	1.465
MR05 to HFD	B9EJ86	OSBL8	Osbpl8	Oxysterol-binding protein-related protein 8	0.031	1666	3516	2.111	0.324	1.509
MR05 to HFD	O88487	DC1I2	Dync1i2	Cytoplasmic dynein 1 intermediate chain 2	0.017	4129	8616	2.087	0.320	1.762
MR05 to HFD	Q8CD15	RIOX2	Riox2	Ribosomal oxygenase 2	0.041	540	1115	2.065	0.315	1.391
MR05 to HFD	O70503	DHB12	Hsd17b12	Very-long-chain 3-oxoacyl-CoA reductase	0.001	1675	3398	2.028	0.307	3.114
MR05 to HFD	P15508	SPTB1	Sptb	Spectrin beta chain, erythrocytic	0.038	5657	11370	2.010	0.303	1.418
MR05 to HFD	Q3U9G9	LBR	Lbr	Delta(14)-sterol reductase LBR	0.040	1048	525	0.501	-0.300	1.403
MR05 to HFD	Q9D880	TIM50	Timm50	Mitochondrial import inner membrane translocase subunit TIM50	0.023	3711	1855	0.500	-0.301	1.642

APPENDIX B: Significantly Differentially Expressed Proteins from Aorta (Continued)										
Comparison	Uniprot ID	Protein	Gene	Full Name	p-value	Mean (HFD)	Mean (MR)	Fold Change	Log(Fold Change)	(-Log(pvalue)
MR05 to HFD	Q2TPA8	HSDL2	Hsdl2	Hydroxysteroid dehydrogenase-like protein 2	0.048	11818	5853	0.495	-0.305	1.317
MR05 to HFD	Q149B8	PERM1	Perm1	PGC-1 and ERR-induced regulator in muscle protein 1	0.026	1042	507	0.486	-0.313	1.592
MR05 to HFD	Q61655	DD19A	Ddx19a	ATP-dependent RNA helicase DDX19A	0.032	1084	524	0.483	-0.316	1.499
MR05 to HFD	Q3U2A8	SYVM	Vars2	Valine--tRNA ligase, mitochondrial	0.033	2367	1141	0.482	-0.317	1.487
MR05 to HFD	P97823	LYPA1	Lypla1	Acyl-protein thioesterase 1	0.028	3155	1518	0.481	-0.318	1.552
MR05 to HFD	P11881	ITPR1	Itpr1	Inositol 1,4,5-trisphosphate receptor type 1	0.019	6521	3122	0.479	-0.320	1.715
MR05 to HFD	P97797	SHPS1	Sirpa	Tyrosine-protein phosphatase non-receptor type substrate 1	0.030	3048	1439	0.472	-0.326	1.524
MR05 to HFD	Q8BMG7	RBGPR	Rab3gap2	Rab3 GTPase-activating protein non-catalytic subunit	0.032	1076	504	0.469	-0.329	1.495
MR05 to HFD	Q80UU9	PGRC2	Pgrmc2	Membrane-associated progesterone receptor component 2	0.046	7986	3604	0.451	-0.346	1.338
MR05 to HFD	Q9Z1D1	EIF3G	Eif3g	Eukaryotic translation initiation factor 3 subunit G	0.033	2083	931	0.447	-0.350	1.476
MR05 to HFD	Q8BMA6	SRP68	Srp68	Signal recognition particle subunit SRP68	0.035	1809	802	0.443	-0.353	1.450
MR05 to HFD	Q8K009	AL1L2	Aldh1l2	Mitochondrial 10-formyltetrahydrofolate dehydrogenase	0.015	8829	3863	0.438	-0.359	1.817
MR05 to HFD	Q99J99	THTM	Mpst	3-mercaptopyruvate sulfurtransferase	0.024	14974	6520	0.435	-0.361	1.621
MR05 to HFD	Q8JZK9	HMCS1	Hmgcs1	Hydroxymethylglutaryl-CoA synthase, cytoplasmic	0.028	592	257	0.434	-0.363	1.548
MR05 to HFD	Q3TAS6	EMC10	Emc10	ER membrane protein complex subunit 10	0.002	3610	1558	0.431	-0.365	2.658
MR05 to HFD	P97429	ANXA4	Anxa4	Annexin A4	0.045	10737	4558	0.424	-0.372	1.346
MR05 to HFD	Q64331	MYO6	Myo6	Unconventional myosin-VI	0.021	17500	7314	0.418	-0.379	1.669
MR05 to HFD	Q9D8B3	CHM4B	Chmp4b	Charged multivesicular body protein 4b	0.028	1165	485	0.417	-0.380	1.551
MR05 to HFD	Q9R0Z9	RHG07	Dlc1	Rho GTPase-activating protein 7	0.012	1104	457	0.414	-0.383	1.917
MR05 to HFD	Q64433	CH10	Hspe1	10 kDa heat shock protein, mitochondrial	0.009	4776	1955	0.409	-0.388	2.070
MR05 to HFD	O55135	IF6	Eif6	Eukaryotic translation initiation factor 6	0.032	1450	588	0.406	-0.392	1.488
MR05 to HFD	Q9WV32	ARC1B	Arpc1b	Actin-related protein 2/3 complex subunit 1B	0.042	14350	5798	0.404	-0.394	1.380
MR05 to HFD	Q3U1J4	DDB1	Ddb1	DNA damage-binding protein 1	0.024	20229	8165	0.404	-0.394	1.626
MR05 to HFD	Q04750	TOP1	Top1	DNA topoisomerase 1	0.010	5329	2150	0.403	-0.394	2.013
MR05 to HFD	Q61508	ECM1	Ecm1	Extracellular matrix protein 1	0.035	17020	6850	0.402	-0.395	1.460
MR05 to HFD	Q99N85	RT18A	Mrps18a	28S ribosomal protein S18a, mitochondrial	0.039	4432	1781	0.402	-0.396	1.406
MR05 to HFD	Q63932	MP2K2	Map2k2	Dual specificity mitogen-activated protein kinase kinase 2	0.015	4600	1846	0.401	-0.397	1.822
MR05 to HFD	Q3TCJ1	ABRX2	Abraxas2	BRISC complex subunit Abraxas 2	0.029	454	181	0.398	-0.400	1.545

APPENDIX B: Significantly Differentially Expressed Proteins from Aorta (Continued)										
Comparison	Uniprot ID	Protein	Gene	Full Name	p-value	Mean (HFD)	Mean (MR)	Fold Change	Log(Fold Change)	(-Log(pvalue)
MR05 to HFD	P97384	ANX11	Anxa11	Annexin A11	0.006	26577	10422	0.392	-0.407	2.204
MR05 to HFD	Q3U5Q7	CMPK2	Cmpk2	UMP-CMP kinase 2, mitochondrial	0.011	19384	7221	0.373	-0.429	1.978
MR05 to HFD	Q9CYL5	GAPR1	Glipr2	Golgi-associated plant pathogenesis-related protein 1	0.018	729	268	0.368	-0.435	1.741
MR05 to HFD	P01867	IGG2B	Igh-3	Ig gamma-2B chain C region	0.018	1352	496	0.367	-0.435	1.744
MR05 to HFD	Q9QZD8	DIC	Slc25a10	Mitochondrial dicarboxylate carrier	0.004	5731	2074	0.362	-0.441	2.366
MR05 to HFD	Q791T5	MTCH1	Mtch1	Mitochondrial carrier homolog 1	0.010	655	229	0.349	-0.457	1.986
MR05 to HFD	Q8CFI0	NED4L	Nedd4l	E3 ubiquitin-protein ligase NEDD4-like	0.012	458	156	0.341	-0.467	1.918
MR05 to HFD	Q3UTY6	THSD4	Thsd4	Thrombospondin type-1 domain-containing protein 4	0.025	167980	57007	0.339	-0.469	1.607
MR05 to HFD	Q9CQU0	TXD12	Txndc12	Thioredoxin domain-containing protein 12	0.031	1211	410	0.339	-0.470	1.510
MR05 to HFD	O55023	IMPA1	Impa1	Inositol monophosphatase 1	0.027	3329	1097	0.330	-0.482	1.563
MR05 to HFD	Q99JI1	MSTN1	Mustn1	Musculoskeletal embryonic nuclear protein 1	0.021	39509	12908	0.327	-0.486	1.683
MR05 to HFD	Q9D824	FIP1	Fip1l1	Pre-mRNA 3'-end-processing factor FIP1	0.019	510	166	0.325	-0.488	1.729
MR05 to HFD	Q9WTI7	MYO1C	Myo1c	Unconventional myosin-Ic	0.048	11438	3602	0.315	-0.502	1.319
MR05 to HFD	Q63870	CO7A1	Col7a1	Collagen alpha-1(VII) chain	0.025	37750	11823	0.313	-0.504	1.609
MR05 to HFD	Q9DBB8	DHDH	Dhdh	Trans-1,2-dihydrobenzene-1,2-diol dehydrogenase	0.001	30168	9338	0.310	-0.509	3.009
MR05 to HFD	Q9Z204	HNRPC	Hnrnpc	Heterogeneous nuclear ribonucleoproteins C1/C2	0.045	8160	2519	0.309	-0.511	1.343
MR05 to HFD	P14148	RL7	Rpl7	60S ribosomal protein L7	0.002	6049	1846	0.305	-0.515	2.699
MR05 to HFD	P55302	AMRP	Lrpap1	Alpha-2-macroglobulin receptor-associated protein	0.043	2231	674	0.302	-0.520	1.369
MR05 to HFD	Q2VLH6	C163A	Cd163	Scavenger receptor cysteine-rich type 1 protein M130	0.031	426	126	0.296	-0.529	1.502
MR05 to HFD	Q9CR00	PSMD9	Psmd9	26S proteasome non-ATPase regulatory subunit 9	0.036	580	171	0.295	-0.530	1.445
MR05 to HFD	Q99P88	NU155	Nup155	Nuclear pore complex protein Nup155	0.002	637	187	0.293	-0.533	2.788
MR05 to HFD	Q91XE8	TM205	Tmem205	Transmembrane protein 205	0.002	4351	1269	0.292	-0.535	2.614
MR05 to HFD	Q03173	ENAH	Enah	Protein enabled homolog	0.041	3211	929	0.289	-0.538	1.391
MR05 to HFD	Q9Z0V8	TI17A	Timm17a	Mitochondrial import inner membrane translocase subunit Tim17-A	0.022	16259	4660	0.287	-0.543	1.667
MR05 to HFD	Q9CPU2	NDUB2	Ndufb2	NADH dehydrogenase [ubiquinone] 1 beta subcomplex subunit 2, mitochondrial	0.019	455	130	0.285	-0.545	1.719
MR05 to HFD	Q9Z315	SNUT1	Sart1	U4/U6.U5 tri-snRNP-associated protein 1	0.029	361	103	0.284	-0.547	1.545
MR05 to HFD	Q922J3	CLIP1	Clip1	CAP-Gly domain-containing linker protein 1	0.039	2588	725	0.280	-0.553	1.408
MR05 to HFD	Q925F2	ESAM	Esam	Endothelial cell-selective adhesion molecule	0.039	529	147	0.277	-0.558	1.414

APPENDIX B: Significantly Differentially Expressed Proteins from Aorta (Continued)										
Comparison	Uniprot ID	Protein	Gene	Full Name	p-value	Mean (HFD)	Mean (MR)	Fold Change	Log(Fold Change)	(-Log(pvalue)
MR05 to HFD	Q62000	MIME	Ogn	Mimecan	0.024	599757	163797	0.273	-0.564	1.613
MR05 to HFD	Q8VHY0	CSPG4	Cspg4	Chondroitin sulfate proteoglycan 4	0.015	754	206	0.273	-0.565	1.817
MR05 to HFD	O35206	COFA1	Col15a1	Collagen alpha-1(XV) chain	0.042	147732	40154	0.272	-0.566	1.379
MR05 to HFD	Q3TEA8	HP1B3	Hp1bp3	Heterochromatin protein 1-binding protein 3	0.030	14733	3988	0.271	-0.568	1.517
MR05 to HFD	Q8BYA0	TBCD	Tbcd	Tubulin-specific chaperone D	0.009	1130	292	0.258	-0.588	2.055
MR05 to HFD	O70258	SGCE	Sgce	Epsilon-sarcoglycan	0.049	418	107	0.257	-0.590	1.306
MR05 to HFD	Q63844	MK03	Mapk3	Mitogen-activated protein kinase 3	0.023	1545	389	0.252	-0.599	1.640
MR05 to HFD	Q8CIB5	FERM2	Fermt2	Fermitin family homolog 2	0.003	4873	1219	0.250	-0.602	2.503
MR05 to HFD	P62858	RS28	Rps28	40S ribosomal protein S28	0.003	35901	8705	0.242	-0.615	2.499
MR05 to HFD	Q5ND52	MRM3	Mrm3	rRNA methyltransferase 3, mitochondrial	0.029	350	82	0.234	-0.630	1.540
MR05 to HFD	P28661	SEPT4	Septin4	Septin-4	0.030	727	166	0.229	-0.640	1.524
MR05 to HFD	Q9JL35	HMGN5	Hmgn5	High mobility group nucleosome-binding domain-containing protein 5	0.004	2052	470	0.229	-0.641	2.435
MR05 to HFD	Q69ZR2	HECD1	Hectd1	E3 ubiquitin-protein ligase HECTD1	0.025	447	99	0.222	-0.653	1.610
MR05 to HFD	Q63880	EST3A	Ces3a	Carboxylesterase 3A	0.028	468	101	0.216	-0.666	1.554
MR05 to HFD	Q7TQD2	TPPP	Tppp	Tubulin polymerization-promoting protein	0.016	4057	874	0.215	-0.667	1.788
MR05 to HFD	Q99J09	MEP50	Wdr77	Methylosome protein 50	0.019	308	66	0.214	-0.669	1.716
MR05 to HFD	Q91WP6	SPA3N	Serpina3n	Serine protease inhibitor A3N	0.000	1016	209	0.205	-0.688	4.000
MR05 to HFD	P17918	PCNA	Pcna	Proliferating cell nuclear antigen	0.010	509	100	0.196	-0.707	1.987
MR05 to HFD	Q3V4B5	COMD6	Commd6	COMM domain-containing protein 6	0.035	153	29	0.190	-0.721	1.451
MR05 to HFD	O55137	ACOT1	Acot1	Acyl-coenzyme A thioesterase 1	0.047	3348	632	0.189	-0.724	1.329
MR05 to HFD	Q8BU33	HACL2	Ilvbl	2-hydroxyacyl-CoA lyase 2	0.004	847	150	0.177	-0.751	2.394
MR05 to HFD	P70313	NOS3	Nos3	Nitric oxide synthase, endothelial	0.027	672	119	0.177	-0.753	1.565
MR05 to HFD	P63101	1433Z	Ywhaz	14-3-3 protein zeta/delta	0.019	63972	11083	0.173	-0.761	1.721
MR05 to HFD	P61027	RAB10	Rab10	Ras-related protein Rab-10	0.001	5228	875	0.167	-0.776	2.959
MR05 to HFD	Q8VDP3	MICA1	Mical1	[F-actin]-monooxygenase MICAL1	0.001	4567	679	0.149	-0.828	2.975
MR05 to HFD	Q9QYJ3	DNJB1	Dnajb1	DnaJ homolog subfamily B member 1	0.031	459	57	0.123	-0.910	1.511
MR05 to HFD	O35551	RABE1	Rabep1	Rab GTPase-binding effector protein 1	0.026	18116	2057	0.114	-0.945	1.582
MR05 to HFD	P43275	H11	H1-1	Histone H1.1	0.017	447	38	0.086	-1.067	1.767

APPENDIX B: Significantly Differentially Expressed Proteins from Aorta (Continued)										
Comparison	Uniprot ID	Protein	Gene	Full Name	p-value	Mean (HFD)	Mean (MR)	Fold Change	Log(Fold Change)	(-Log(pvalue)
MR05 to HFD	Q60770	STXB3	Stxbp3	Syntaxin-binding protein 3	0.036	483	40	0.083	-1.082	1.441
MR05 to HFD	P37889	FBLN2	Fbln2	Fibulin-2	0.046	479431	37235	0.078	-1.110	1.342
MR05 to HFD	Q99NB9	SF3B1	Sf3b1	Splicing factor 3B subunit 1	0.009	425	29	0.068	-1.166	2.063
MR05 to HFD	Q60864	STIP1	Stip1	Stress-induced-phosphoprotein 1	0.011	449538	11118	0.025	-1.607	1.973
MR10 to HFD	Q9D2N4	DTNA	Dtna	Dystrobrevin alpha	0.027	1536	17713	11.533	1.062	1.571
MR10 to HFD	O89086	RBM3	Rbm3	RNA-binding protein 3	0.013	2524	27012	10.700	1.029	1.875
MR10 to HFD	Q8R2U0	SEH1	Seh1l	Nucleoporin SEH1	0.031	399	4187	10.493	1.021	1.507
MR10 to HFD	P97371	PSME1	Psme1	Proteasome activator complex subunit 1	0.020	1319	10078	7.639	0.883	1.689
MR10 to HFD	P60229	EIF3E	Eif3e	Eukaryotic translation initiation factor 3 subunit E	0.034	534	3982	7.451	0.872	1.475
MR10 to HFD	P03899	NU3M	Mtnd3	NADH-ubiquinone oxidoreductase chain 3	0.029	1752	12262	6.999	0.845	1.536
MR10 to HFD	Q61879	MYH10	Myh10	Myosin-10	0.012	12335	83085	6.736	0.828	1.926
MR10 to HFD	Q6PB93	GALT2	Galnt2	Polypeptide N-acetylgalactosaminyltransferase 2	0.038	847	5367	6.337	0.802	1.422
MR10 to HFD	P58774	TPM2	Tpm2	Tropomyosin beta chain	0.011	79115	472809	5.976	0.776	1.957
MR10 to HFD	P49443	PPM1A	Ppm1a	Protein phosphatase 1A	0.028	6528	31360	4.804	0.682	1.557
MR10 to HFD	P06151	LDHA	Ldha	L-lactate dehydrogenase A chain	0.035	5488	24893	4.536	0.657	1.462
MR10 to HFD	P02468	LAMC1	Lamc1	Laminin subunit gamma-1	0.008	12187	51146	4.197	0.623	2.114
MR10 to HFD	Q9DB05	SNAA	Napa	Alpha-soluble NSF attachment protein	0.005	7520	27784	3.695	0.568	2.321
MR10 to HFD	P58771	TPM1	Tpm1	Tropomyosin alpha-1 chain	0.002	162672	566213	3.481	0.542	2.783
MR10 to HFD	P62334	PRS10	Psmc6	26S proteasome regulatory subunit 10B	0.001	5878	20434	3.477	0.541	3.092
MR10 to HFD	Q3UJD6	UBP19	Usp19	Ubiquitin carboxyl-terminal hydrolase 19	0.049	1048	3548	3.386	0.530	1.314
MR10 to HFD	Q9CVB6	ARPC2	Arpc2	Actin-related protein 2/3 complex subunit 2	0.007	2506	8180	3.263	0.514	2.151
MR10 to HFD	Q9R0M4	PODXL	Podxl	Podocalyxin	0.005	13024	42315	3.249	0.512	2.315
MR10 to HFD	Q80V42	CBPM	Cpm	Carboxypeptidase M	0.009	2299	7228	3.144	0.497	2.039
MR10 to HFD	O55222	ILK	Ilk	Integrin-linked protein kinase	0.045	29036	85163	2.933	0.467	1.345
MR10 to HFD	Q91X17	UROM	Umod	Uromodulin	0.002	928	2664	2.872	0.458	2.783
MR10 to HFD	Q8BH64	EHD2	Ehd2	EH domain-containing protein 2	0.031	10616	30106	2.836	0.453	1.507
MR10 to HFD	Q6P6L0	FIL1L	Filip1l	Filamin A-interacting protein 1-like	0.016	809	2293	2.836	0.453	1.809
MR10 to HFD	Q61207	SAP	Psap	Prosaposin	0.004	153	432	2.827	0.451	2.412

APPENDIX B: Significantly Differentially Expressed Proteins from Aorta (Continued)										
Comparison	Uniprot ID	Protein	Gene	Full Name	p-value	Mean (HFD)	Mean (MR)	Fold Change	Log(Fold Change)	(-Log(pvalue)
MR10 to HFD	Q9DAW9	CNN3	Cnn3	Calponin-3	0.006	25501	71034	2.786	0.445	2.201
MR10 to HFD	Q9WU84	CCS	Ccs	Copper chaperone for superoxide dismutase	0.031	3948	10986	2.783	0.444	1.510
MR10 to HFD	P49312	ROA1	Hnrnpa1	Heterogeneous nuclear ribonucleoprotein A1	0.001	3005	8352	2.779	0.444	3.292
MR10 to HFD	Q6URW6	MYH14	Myh14	Myosin-14	0.046	16413	44839	2.732	0.436	1.333
MR10 to HFD	O08709	PRDX6	Prdx6	Peroxiredoxin-6	0.024	8122	22061	2.716	0.434	1.618
MR10 to HFD	Q8R1G2	CMBL	Cmbl	Carboxymethylenebutenolidase homolog	0.019	1965	5186	2.640	0.422	1.712
MR10 to HFD	P11087	CO1A1	Col1a1	Collagen alpha-1(I) chain	0.015	534922	######	2.585	0.412	1.833
MR10 to HFD	P70202	LXN	Lxn	Latexin	0.019	577	1479	2.563	0.409	1.731
MR10 to HFD	P47753	CAZA1	Capza1	F-actin-capping protein subunit alpha-1	0.022	44488	113519	2.552	0.407	1.658
MR10 to HFD	Q9DCN2	NB5R3	Cyb5r3	NADH-cytochrome b5 reductase 3	0.049	9195	23384	2.543	0.405	1.310
MR10 to HFD	P34914	HYES	Ephx2	Bifunctional epoxide hydrolase 2	0.010	6730	16865	2.506	0.399	2.021
MR10 to HFD	Q9CPS6	HINT3	Hint3	Histidine triad nucleotide-binding protein 3	0.040	1930	4793	2.484	0.395	1.403
MR10 to HFD	Q6NV83	SR140	U2surp	U2 snRNP-associated SURP motif-containing protein	0.028	2074	5100	2.459	0.391	1.551
MR10 to HFD	Q9DB20	ATPO	Atp5po	ATP synthase subunit O, mitochondrial	0.003	2527	6207	2.456	0.390	2.564
MR10 to HFD	Q9WVK4	EHD1	Ehd1	EH domain-containing protein 1	0.048	3510	8534	2.431	0.386	1.317
MR10 to HFD	Q3UW53	NIBA1	Niban1	Protein Niban 1	0.035	2032	4851	2.387	0.378	1.454
MR10 to HFD	O08788	DCTN1	Dctn1	Dynactin subunit 1	0.015	671	1598	2.381	0.377	1.824
MR10 to HFD	P46656	ADX	Fdx1	Adrenodoxin, mitochondrial	0.002	2956	7027	2.377	0.376	2.695
MR10 to HFD	O89017	LGMN	Lgmn	Legumain	0.038	2021	4784	2.367	0.374	1.418
MR10 to HFD	Q8BTV2	CPSF7	Cpsf7	Cleavage and polyadenylation specificity factor subunit 7	0.046	1069	2503	2.341	0.369	1.340
MR10 to HFD	P62830	RL23	Rpl23	60S ribosomal protein L23	0.049	1932	4509	2.333	0.368	1.312
MR10 to HFD	P09055	ITB1	Itgb1	Integrin beta-1	0.004	11982	27858	2.325	0.366	2.383
MR10 to HFD	Q501J7	PHAR4	Phactr4	Phosphatase and actin regulator 4	0.031	2886	6683	2.316	0.365	1.513
MR10 to HFD	Q9JMG1	EDF1	Edf1	Endothelial differentiation-related factor 1	0.000	1697	3924	2.312	0.364	3.658
MR10 to HFD	Q9D0F9	PGM1	Pgm1	Phosphoglucomutase-1	0.002	3381	7801	2.307	0.363	2.767
MR10 to HFD	P47199	QOR	Cryz	Quinone oxidoreductase	0.001	5187	11916	2.297	0.361	2.860
MR10 to HFD	P97816	S100G	S100g	Protein S100-G	0.001	1037	2357	2.272	0.356	3.009
MR10 to HFD	Q9DBL7	COASY	Coasy	Bifunctional coenzyme A synthase	0.014	6027	13499	2.240	0.350	1.855

APPENDIX B: Significantly Differentially Expressed Proteins from Aorta (Continued)										
Comparison	Uniprot ID	Protein	Gene	Full Name	p-value	Mean (HFD)	Mean (MR)	Fold Change	Log(Fold Change)	(-Log(pvalue)
MR10 to HFD	P56959	FUS	Fus	RNA-binding protein FUS	0.020	2957	6402	2.165	0.335	1.700
MR10 to HFD	Q8BH04	PCKGM	Pck2	Phosphoenolpyruvate carboxykinase [GTP], mitochondrial	0.025	4855	10440	2.150	0.332	1.607
MR10 to HFD	Q9D8U3	ERP27	Erp27	Endoplasmic reticulum resident protein 27	0.046	1903	3877	2.037	0.309	1.335
MR10 to HFD	Q91Y97	ALDOB	Aldob	Fructose-bisphosphate aldolase B	0.018	11524	23284	2.020	0.305	1.753
MR10 to HFD	Q3UHJ8	RNF44	Rnf44	RING finger protein 44	0.006	3042	6118	2.011	0.304	2.239
MR10 to HFD	Q9CR35	CTRB1	Ctrb1	Chymotrypsinogen B	0.005	3806	7642	2.008	0.303	2.268
MR10 to HFD	P10648	GSTA2	Gsta2	Glutathione S-transferase A2	0.009	10645	21255	1.997	0.300	2.034
MR10 to HFD	O55106	STRN	Strn	Striatin	0.019	1483	743	0.501	-0.301	1.712
MR10 to HFD	Q3U1J4	DDB1	Ddb1	DNA damage-binding protein 1	0.026	20229	10020	0.495	-0.305	1.580
MR10 to HFD	O88643	PAK1	Pak1	Serine/threonine-protein kinase PAK 1	0.019	2528	1235	0.488	-0.311	1.727
MR10 to HFD	Q64237	DOPO	Dbh	Dopamine beta-hydroxylase	0.020	767	372	0.485	-0.314	1.704
MR10 to HFD	Q99KI0	ACON	Aco2	Aconitate hydratase, mitochondrial	0.013	10334	4992	0.483	-0.316	1.903
MR10 to HFD	Q8VC30	TKFC	Tkfc	Triokinase/FMN cyclase	0.006	4261	2051	0.481	-0.318	2.207
MR10 to HFD	Q3U2A8	SYVM	Vars2	Valine--tRNA ligase, mitochondrial	0.020	2367	1134	0.479	-0.319	1.698
MR10 to HFD	Q9Z183	PADI4	Padi4	Protein-arginine deiminase type-4	0.020	1310	626	0.478	-0.321	1.707
MR10 to HFD	Q9CYH2	PXL2A	Prxl2a	Peroxiredoxin-like 2A	0.035	22780	10804	0.474	-0.324	1.450
MR10 to HFD	Q3U7R1	ESYT1	Esyt1	Extended synaptotagmin-1	0.006	3740	1760	0.470	-0.327	2.194
MR10 to HFD	Q9Z1P7	KANK3	Kank3	KN motif and ankyrin repeat domain-containing protein 3	0.008	2071	972	0.469	-0.329	2.114
MR10 to HFD	Q8CFI0	NED4L	Nedd4l	E3 ubiquitin-protein ligase NEDD4-like	0.042	458	214	0.468	-0.330	1.377
MR10 to HFD	A6H584	CO6A5	Col6a5	Collagen alpha-5(VI) chain	0.009	1528	713	0.467	-0.331	2.065
MR10 to HFD	Q9D9V3	ECHD1	Echdc1	Ethylmalonyl-CoA decarboxylase	0.029	1261	587	0.465	-0.332	1.539
MR10 to HFD	P01867	IGG2B	Igh-3	Ig gamma-2B chain C region	0.014	1352	629	0.465	-0.333	1.862
MR10 to HFD	P01872	IGHM	Ighm	Immunoglobulin heavy constant mu	0.048	6646	3082	0.464	-0.334	1.320
MR10 to HFD	Q99KV1	DJB11	Dnajb11	DnaJ homolog subfamily B member 11	0.013	7557	3446	0.456	-0.341	1.877
MR10 to HFD	Q5M8N4	D39U1	Sdr39u1	Epimerase family protein SDR39U1	0.012	5135	2334	0.455	-0.342	1.909
MR10 to HFD	A2AN08	UBR4	Ubr4	E3 ubiquitin-protein ligase UBR4	0.021	2314	1049	0.453	-0.343	1.675
MR10 to HFD	Q8C2Q3	RBM14	Rbm14	RNA-binding protein 14	0.020	1574	708	0.450	-0.347	1.689
MR10 to HFD	Q6PDN3	MYLK	Mylk	Myosin light chain kinase, smooth muscle	0.015	323667	145489	0.450	-0.347	1.815

APPENDIX B: Significantly Differentially Expressed Proteins from Aorta (Continued)										
Comparison	Uniprot ID	Protein	Gene	Full Name	p-value	Mean (HFD)	Mean (MR)	Fold Change	Log(Fold Change)	(-Log(pvalue)
MR10 to HFD	Q9ERG2	STRN3	Strn3	Striatin-3	0.030	2808	1261	0.449	-0.348	1.521
MR10 to HFD	Q9QYJ0	DNJA2	Dnaja2	DnaJ homolog subfamily A member 2	0.006	7534	3383	0.449	-0.348	2.205
MR10 to HFD	P11881	ITPR1	Itpr1	Inositol 1,4,5-trisphosphate receptor type 1	0.012	6521	2920	0.448	-0.349	1.930
MR10 to HFD	Q78HU7	GLPC	Gypc	Glycophorin-C	0.010	3404	1518	0.446	-0.351	2.000
MR10 to HFD	Q61508	ECM1	Ecm1	Extracellular matrix protein 1	0.026	17020	7526	0.442	-0.354	1.577
MR10 to HFD	Q99P88	NU155	Nup155	Nuclear pore complex protein Nup155	0.050	637	279	0.438	-0.359	1.301
MR10 to HFD	O09012	PEX5	Pex5	Peroxisomal targeting signal 1 receptor	0.001	1435	621	0.433	-0.364	2.889
MR10 to HFD	O70468	MYPC3	Mybpc3	Myosin-binding protein C, cardiac-type	0.027	1545	668	0.433	-0.364	1.571
MR10 to HFD	Q61655	DD19A	Ddx19a	ATP-dependent RNA helicase DDX19A	0.018	1084	467	0.431	-0.366	1.753
MR10 to HFD	O55028	BCKD	Bckdk	[3-methyl-2-oxobutanoate dehydrogenase [lipoamide]] kinase, mitochondrial	0.013	1020	439	0.430	-0.366	1.872
MR10 to HFD	Q9CQ45	NENF	Nenf	Neudesin	0.037	352	151	0.428	-0.369	1.426
MR10 to HFD	P97384	ANX11	Anxa11	Annexin A11	0.008	26577	11306	0.425	-0.371	2.120
MR10 to HFD	Q63844	MK03	Mapk3	Mitogen-activated protein kinase 3	0.031	1545	654	0.423	-0.374	1.511
MR10 to HFD	Q9D8N2	DEN10	Dennd10	DENN domain-containing protein 10	0.042	398	168	0.421	-0.375	1.372
MR10 to HFD	Q99L43	CDS2	Cds2	Phosphatidate cytidylyltransferase 2	0.009	1227	514	0.419	-0.378	2.052
MR10 to HFD	O88343	S4A4	Slc4a4	Electrogenic sodium bicarbonate cotransporter 1	0.035	6392	2679	0.419	-0.378	1.457
MR10 to HFD	Q9D8B3	CHM4B	Chmp4b	Charged multivesicular body protein 4b	0.036	1165	488	0.419	-0.378	1.439
MR10 to HFD	Q99JP6	HOME3	Homer3	Homer protein homolog 3	0.023	446	182	0.409	-0.389	1.629
MR10 to HFD	Q4VAA2	CDV3	Cdv3	Protein CDV3	0.040	570	232	0.408	-0.389	1.400
MR10 to HFD	Q6P549	SHIP2	Inppl1	Phosphatidylinositol 3,4,5-trisphosphate 5-phosphatase 2	0.013	1095	444	0.405	-0.392	1.891
MR10 to HFD	Q9DBB8	DHDH	Dhdh	Trans-1,2-dihydrobenzene-1,2-diol dehydrogenase	0.001	30168	12155	0.403	-0.395	3.086
MR10 to HFD	Q9CX86	ROA0	Hnrnpa0	Heterogeneous nuclear ribonucleoprotein A0	0.033	4238	1687	0.398	-0.400	1.478
MR10 to HFD	Q00612	G6PD1	G6pdx	Glucose-6-phosphate 1-dehydrogenase X	0.045	17297	6857	0.396	-0.402	1.345
MR10 to HFD	O88207	CO5A1	Col5a1	Collagen alpha-1(V) chain	0.036	17139	6677	0.390	-0.409	1.439
MR10 to HFD	Q920A7	AFG31	Afg3l1	AFG3-like protein 1	0.030	11927	4637	0.389	-0.410	1.530
MR10 to HFD	Q8BTM8	FLNA	Flna	Filamin-A	0.000	######	882905	0.387	-0.412	3.481
MR10 to HFD	Q3TAS6	EMC10	Emc10	ER membrane protein complex subunit 10	0.018	3610	1396	0.387	-0.413	1.737
MR10 to HFD	Q91WP6	SPA3N	Serpina3n	Serine protease inhibitor A3N	0.014	1016	389	0.383	-0.417	1.861

APPENDIX B: Significantly Differentially Expressed Proteins from Aorta (Continued)										
Comparison	Uniprot ID	Protein	Gene	Full Name	p-value	Mean (HFD)	Mean (MR)	Fold Change	Log(Fold Change)	(-Log(pvalue)
MR10 to HFD	P29268	CCN2	Ccn2	CCN family member 2	0.030	22148	8423	0.380	-0.420	1.527
MR10 to HFD	Q61165	SL9A1	Slc9a1	Sodium/hydrogen exchanger 1	0.001	1262	475	0.376	-0.425	2.917
MR10 to HFD	Q60605	MYL6	Myl6	Myosin light polypeptide 6	0.042	######	604933	0.375	-0.425	1.376
MR10 to HFD	Q9CYL5	GAPR1	Glipr2	Golgi-associated plant pathogenesis-related protein 1	0.016	729	274	0.375	-0.426	1.789
MR10 to HFD	Q63932	MP2K2	Map2k2	Dual specificity mitogen-activated protein kinase kinase 2	0.013	4600	1725	0.375	-0.426	1.900
MR10 to HFD	Q9JKF7	RM39	Mrpl39	39S ribosomal protein L39, mitochondrial	0.039	1886	698	0.370	-0.431	1.409
MR10 to HFD	Q8BMA6	SRP68	Srp68	Signal recognition particle subunit SRP68	0.023	1809	666	0.368	-0.434	1.642
MR10 to HFD	Q9Z266	SNAPN	Snapin	SNARE-associated protein Snapin	0.041	3504	1284	0.366	-0.436	1.392
MR10 to HFD	Q08093	CNN2	Cnn2	Calponin-2	0.035	38244	13743	0.359	-0.444	1.451
MR10 to HFD	Q9DB34	CHM2A	Chmp2a	Charged multivesicular body protein 2a	0.010	458	165	0.359	-0.445	1.984
MR10 to HFD	Q99K48	NONO	Nono	Non-POU domain-containing octamer-binding protein	0.015	1539	551	0.358	-0.446	1.828
MR10 to HFD	Q8K009	AL1L2	Aldh1l2	Mitochondrial 10-formyltetrahydrofolate dehydrogenase	0.009	8829	3156	0.357	-0.447	2.023
MR10 to HFD	Q925F2	ESAM	Esam	Endothelial cell-selective adhesion molecule	0.047	529	188	0.355	-0.449	1.328
MR10 to HFD	Q3UVL4	VPS51	Vps51	Vacuolar protein sorting-associated protein 51 homolog	0.002	978	345	0.353	-0.453	2.721
MR10 to HFD	Q3UPL0	SC31A	Sec31a	Protein transport protein Sec31A	0.006	2115	743	0.351	-0.454	2.236
MR10 to HFD	Q91WM2	HDHD5	Hdhd5	Haloacid dehalogenase-like hydrolase domain-containing 5	0.030	501	176	0.350	-0.456	1.524
MR10 to HFD	Q03173	ENAH	Enah	Protein enabled homolog	0.039	3211	1121	0.349	-0.457	1.413
MR10 to HFD	Q8BYM8	SYCM	Cars2	Probable cysteine--tRNA ligase, mitochondrial	0.031	534	186	0.349	-0.457	1.510
MR10 to HFD	O55023	IMPA1	Impa1	Inositol monophosphatase 1	0.024	3329	1136	0.341	-0.467	1.617
MR10 to HFD	Q8BW00	PTH	Ptrh1	Probable peptidyl-tRNA hydrolase	0.036	404	134	0.332	-0.478	1.448
MR10 to HFD	P11531	DMD	Dmd	Dystrophin	0.005	53387	17309	0.324	-0.489	2.304
MR10 to HFD	Q62009	POSTN	Postn	Periostin	0.006	951564	302673	0.318	-0.497	2.217
MR10 to HFD	Q9R1P4	PSA1	Psma1	Proteasome subunit alpha type-1	0.013	14317	4525	0.316	-0.500	1.888
MR10 to HFD	Q9WTI7	MYO1C	Myo1c	Unconventional myosin-Ic	0.049	11438	3575	0.313	-0.505	1.313
MR10 to HFD	Q9CYR0	SSBP	Ssbp1	Single-stranded DNA-binding protein, mitochondrial	0.030	780	243	0.312	-0.506	1.525
MR10 to HFD	Q01149	CO1A2	Col1a2	Collagen alpha-2(I) chain	0.041	629430	196127	0.312	-0.506	1.385
MR10 to HFD	P62858	RS28	Rps28	40S ribosomal protein S28	0.004	35901	11025	0.307	-0.513	2.419
MR10 to HFD	Q80UG5	SEPT9	Septin9	Septin-9	0.002	5843	1788	0.306	-0.514	2.793

APPENDIX B: Significantly Differentially Expressed Proteins from Aorta (Continued)										
Comparison	Uniprot ID	Protein	Gene	Full Name	p-value	Mean (HFD)	Mean (MR)	Fold Change	Log(Fold Change)	(-Log(pvalue)
MR10 to HFD	Q99J09	MEP50	Wdr77	Methylosome protein 50	0.037	308	93	0.302	-0.520	1.437
MR10 to HFD	Q9Z0E0	NCDN	Ncdn	Neurochondrin	0.031	152517	45997	0.302	-0.521	1.507
MR10 to HFD	Q9D4H8	CUL2	Cul2	Cullin-2	0.026	472	142	0.301	-0.522	1.590
MR10 to HFD	P55302	AMRP	Lrpap1	Alpha-2-macroglobulin receptor-associated protein	0.050	2231	669	0.300	-0.523	1.302
MR10 to HFD	O35129	PHB2	Phb2	Prohibitin-2	0.046	233	69	0.297	-0.528	1.342
MR10 to HFD	Q9Z1D1	EIF3G	Eif3g	Eukaryotic translation initiation factor 3 subunit G	0.009	2083	609	0.292	-0.534	2.057
MR10 to HFD	Q99JI1	MSTN1	Mustn1	Musculoskeletal embryonic nuclear protein 1	0.016	39509	11515	0.291	-0.535	1.785
MR10 to HFD	Q62188	DPYL3	Dpysl3	Dihydropyrimidinase-related protein 3	0.017	125730	35696	0.284	-0.547	1.768
MR10 to HFD	Q9JL35	HMGN5	Hmgn5	High mobility group nucleosome-binding domain-containing protein 5	0.006	2052	582	0.284	-0.547	2.258
MR10 to HFD	Q9WVJ9	FBLN4	Efemp2	EGF-containing fibulin-like extracellular matrix protein 2	0.019	40795	11565	0.283	-0.547	1.728
MR10 to HFD	Q2VLH6	C163A	Cd163	Scavenger receptor cysteine-rich type 1 protein M130	0.022	426	118	0.277	-0.558	1.651
MR10 to HFD	Q6PGL7	WASC2	Washc2	WASH complex subunit 2	0.045	1047	289	0.276	-0.559	1.348
MR10 to HFD	P57016	LAD1	Lad1	Ladinin-1	0.048	7990	2193	0.274	-0.562	1.317
MR10 to HFD	Q3UTY6	THSD4	Thsd4	Thrombospondin type-1 domain-containing protein 4	0.005	167980	45022	0.268	-0.572	2.330
MR10 to HFD	Q8CIB5	FERM2	Fermt2	Fermitin family homolog 2	0.005	4873	1305	0.268	-0.572	2.274
MR10 to HFD	Q9Z0V8	TI17A	Timm17a	Mitochondrial import inner membrane translocase subunit Tim17-A	0.020	16259	4274	0.263	-0.580	1.701
MR10 to HFD	Q8BU33	HACL2	Ilvbl	2-hydroxyacyl-CoA lyase 2	0.005	847	220	0.259	-0.586	2.276
MR10 to HFD	Q9CQU0	TXD12	Txndc12	Thioredoxin domain-containing protein 12	0.012	1211	310	0.256	-0.592	1.922
MR10 to HFD	Q01730	RSU1	Rsu1	Ras suppressor protein 1	0.046	202162	51207	0.253	-0.596	1.336
MR10 to HFD	P63101	1433Z	Ywhaz	14-3-3 protein zeta/delta	0.026	63972	16007	0.250	-0.602	1.593
MR10 to HFD	O55003	BNIP3	Bnip3	BCL2/adenovirus E1B 19 kDa protein-interacting protein 3	0.002	770	185	0.240	-0.620	2.613
MR10 to HFD	Q7TQD2	TPPP	Tppp	Tubulin polymerization-promoting protein	0.028	4057	969	0.239	-0.622	1.556
MR10 to HFD	Q8C0Z1	F234A	Fam234a	Protein FAM234A	0.009	588	138	0.234	-0.630	2.069
MR10 to HFD	O35375	NRP2	Nrp2	Neuropilin-2	0.027	909	210	0.231	-0.637	1.565
MR10 to HFD	O35206	COFA1	Col15a1	Collagen alpha-1(XV) chain	0.036	147732	33218	0.225	-0.648	1.446
MR10 to HFD	Q9Z2U1	PSA5	Psma5	Proteasome subunit alpha type-5	0.040	1510	329	0.218	-0.662	1.400
MR10 to HFD	Q9CPU2	NDUB2	Ndufb2	NADH dehydrogenase [ubiquinone] 1 beta subcomplex subunit 2, mitochondrial	0.007	455	93	0.205	-0.689	2.171
MR10 to HFD	P61027	RAB10	Rab10	Ras-related protein Rab-10	0.003	5228	977	0.187	-0.729	2.521

APPENDIX B: Significantly Differentially Expressed Proteins from Aorta (Continued)										
Comparison	Uniprot ID	Protein	Gene	Full Name	p-value	Mean (HFD)	Mean (MR)	Fold Change	Log(Fold Change)	(-Log(pvalue)
MR10 to HFD	Q63870	CO7A1	Col7a1	Collagen alpha-1(VII) chain	0.009	37750	6811	0.180	-0.744	2.053
MR10 to HFD	P24452	CAPG	Capg	Macrophage-capping protein	0.038	407	69	0.170	-0.769	1.420
MR10 to HFD	O70439	STX7	Stx7	Syntaxin-7	0.015	762	121	0.159	-0.798	1.834
MR10 to HFD	Q8VDP3	MICA1	Mical1	[F-actin]-monooxygenase MICAL1	0.001	4567	724	0.158	-0.800	2.939
MR10 to HFD	P56387	DYLT3	Dynlt3	Dynein light chain Tctex-type 3	0.013	263	40	0.152	-0.818	1.873
MR10 to HFD	Q99NB9	SF3B1	Sf3b1	Splicing factor 3B subunit 1	0.012	425	60	0.141	-0.851	1.936
MR10 to HFD	P28661	SEPT4	Septin4	Septin-4	0.015	727	92	0.126	-0.898	1.828
MR10 to HFD	P17918	PCNA	Pcna	Proliferating cell nuclear antigen	0.011	509	60	0.119	-0.926	1.964
MR10 to HFD	P43276	H15	H1-5	Histone H1.5	0.000	349	37	0.105	-0.979	3.585
MR10 to HFD	Q5SWT3	S2535	Slc25a35	Solute carrier family 25 member 35	0.014	426	40	0.094	-1.027	1.847
MR10 to HFD	Q8QZR5	ALAT1	Gpt	Alanine aminotransferase 1	0.020	480	39	0.081	-1.090	1.707
MR10 to HFD	Q3UMR5	MCU	Mcu	Calcium uniporter protein, mitochondrial	0.033	1346	90	0.067	-1.177	1.488
MR10 to HFD	Q60864	STIP1	Stip1	Stress-induced-phosphoprotein 1	0.006	449538	29595	0.066	-1.182	2.249

APPENDIX C: Expanded Immunofluorescence Images

Showing merged and individual images of DAPI, tissue control (PLIN1, ACTA2), Protein of Interest (CATZ, ACYP2, TI17A, RAB10) and negative IgG control.

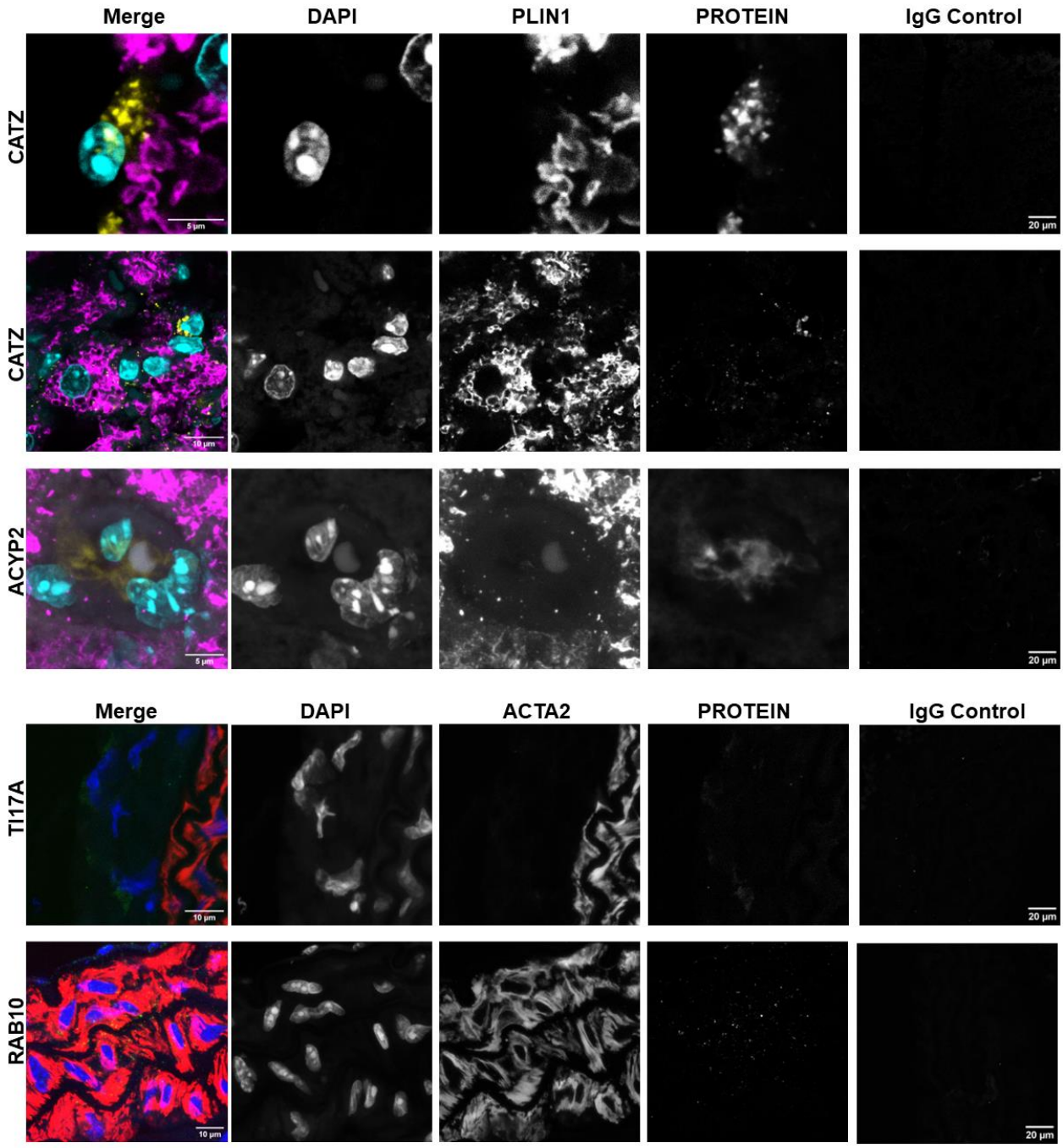

BIOGRAPHY OF THE AUTHOR

Marissa Irene McGilvrey was born in Phoenix, Arizona to Dennis and Beth Saltzman. She earned her high school diploma from Arizona Lutheran Academy. Her bachelor's degree in biomedical science was acquired from Northern Arizona University. During her undergraduate studies, Marissa was first exposed to research within the Center for Microbial Genetics and Genomics in Flagstaff, Arizona, which is now the Pathogen and Microbiome Institute. Marissa worked on microbial pathogen, *Burkholderia pseudomallei*, and developed foundational research skills under Christopher Allender, Dr. Apichai Tuanyok, and Dr. Paul Keim. She continued graduate studies under Dr. Tuanyok at the University of Hawai'i in Manoa. She was employed in Phoenix, Arizona as a Research Associate at the Translational Genomics Research Institute (TGen) in the Collaborative Center for Translational Mass Spectrometry under Dr. Khaytiben Pathak and Dr. Patrick Pirrotte. At TGen, she was strongly encouraged and motivated to pursue a doctoral degree. After joining the Graduate School of Biomedical Science and Engineering at the University of Maine, Marissa studied under the primary mentorship of Dr. Lucy Liaw at the MaineHealth Institute for Research in Scarborough, Maine. She has a strong desire to help improve human health through lifestyle and targeted therapeutics. Marissa is a candidate for the Doctor of Philosophy degree in Biomedical Science at the University of Maine in May 2024.